

1-1-2007

Synthesis and characterization of Ortho phenylene-ethynylne oligomers : a new scaffold for foldamer research.

Ticora V. Jones

University of Massachusetts Amherst

Follow this and additional works at: https://scholarworks.umass.edu/dissertations_1

Recommended Citation

Jones, Ticora V., "Synthesis and characterization of Ortho phenylene-ethynylne oligomers : a new scaffold for foldamer research." (2007). *Doctoral Dissertations 1896 - February 2014*. 1100.
https://scholarworks.umass.edu/dissertations_1/1100

This Open Access Dissertation is brought to you for free and open access by ScholarWorks@UMass Amherst. It has been accepted for inclusion in Doctoral Dissertations 1896 - February 2014 by an authorized administrator of ScholarWorks@UMass Amherst. For more information, please contact scholarworks@library.umass.edu.

★ UMASS/AMHERST ★



312066 0325 0085 6



University of
Massachusetts
Amherst

L I B R A R Y





Digitized by the Internet Archive
in 2015

<https://archive.org/details/synthesischaract00jone>

This is an authorized facsimile, made from the microfilm master copy of the original dissertation or master thesis published by UMI.

The bibliographic information for this thesis is contained in UMI's Dissertation Abstracts database, the only central source for accessing almost every doctoral dissertation accepted in North America since 1861.

UMI[®] Dissertation
Services

From:ProQuest
COMPANY

300 North Zeeb Road
P.O. Box 1346
Ann Arbor, Michigan 48106-1346 USA

800.521.0600 734.761.4700
web www.il.proquest.com

Printed in 2007 by digital xerographic process
on acid-free paper

**SYNTHESIS AND CHARACTERIZATION OF *ORTHO* PHENYLENE-
ETHYNYLENE OLIGOMERS:
A NEW SCAFFOLD FOR FOLDAMER RESEARCH**

A Dissertation Presented

by

TICORA V. JONES

Submitted to the Graduate School of the
University of Massachusetts Amherst in partial fulfillment
of the requirements for the degree of

DOCTOR OF PHILOSOPHY

February 2007

Polymer Science & Engineering

UMI Number: 3254962

INFORMATION TO USERS

The quality of this reproduction is dependent upon the quality of the copy submitted. Broken or indistinct print, colored or poor quality illustrations and photographs, print bleed-through, substandard margins, and improper alignment can adversely affect reproduction.

In the unlikely event that the author did not send a complete manuscript and there are missing pages, these will be noted. Also, if unauthorized copyright material had to be removed, a note will indicate the deletion.

UMI[®]

UMI Microform 3254962

Copyright 2007 by ProQuest Information and Learning Company.

All rights reserved. This microform edition is protected against unauthorized copying under Title 17, United States Code.

ProQuest Information and Learning Company
300 North Zeeb Road
P.O. Box 1346
Ann Arbor, MI 48106-1346

© Copyright by Ticora V. Jones 2007

All Rights Reserved

**SYNTHESIS AND CHARACTERIZATION OF *ORTHO* PHENYLENE-
ETHYNYLENE OLIGOMERS:
A NEW SCAFFOLD FOR FOLDAMER RESEARCH**

A Dissertation Presented

by

TICORA V. JONES

Approved as to style and content by:

Gregory N. Tew, Chair

Murugappan Muthukumar, Member

Dhandapani Venkataraman, Member

Shaw Ling Hsu, Department Head
Polymer Science & Engineering

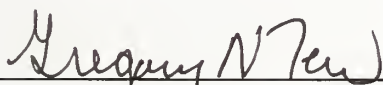
**SYNTHESIS AND CHARACTERIZATION OF *ORTHO* PHENYLENE
ETHYNYLENE OLIGOMERS:
A NEW SCAFFOLD FOR FOLDAMER RESEARCH**

A Dissertation Presented

by

TICORA V. JONES

Approved as to style and content by:



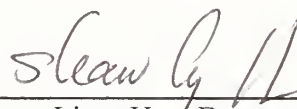
Gregory N. Tew, Chair



Murugappan Muthukumar, Member



Dhandapani Venkataraman, Outside Member



Shaw Ling. Hsu, Department Head
Polymer Science & Engineering

DEDICATION

To my family- those present, and those watching from above

ACKNOWLEDGMENTS

There are so many people to thank, but first I will thank my Lord, my Savior, and my God for bringing me through. It's been a long road, one with many twists and unexpected turns, but You have been faithful through it all, and I thank You for how far you've brought me.

To my wonderful parents- I thank you for instilling within me the drive and determination to pursue my dreams. You've always been there for me, loving me, encouraging me and cheering me from the sidelines, picking me up when I fell, and always expecting great things from me. You taught me to look beyond the surface, to go out into the world, to appreciate the beauty and complexity in things, and to *always* look for goodness in others. I could not ask for anything more. I look forward to more adventures together. I love you!

Grandma and Grandpa- even though you're not here any longer, I know that you continue to watch over me in all that I do. Thank you for your sacrifices. Thank you for instilling in my Mother the drive that she passed on to me. To my Nana- your teacher's spirit is in me, where I'll use it I don't know yet, but I know that you passed that gift to me through my Father. Thank you all for being my angels. I love you, and I hope that I have made you proud.

To my sister and brother, thank you for not taking me too seriously, for making me laugh, and for being the awesome siblings you are. We've got the "Dr." now, Thea,

you get to be the lawyer, and Jonathan- Architect? Engineer? Scholar? Reach for you dreams. I love you both.

To the rest of my family. Aunts, Uncles, cousins, thank all you for your support and encouragement over the years. And yes. I'm finally done with school (I think).

Through it all from high school until now, there have been some friends that have stuck with me, slogging through it, year in, and year out- Amanda (the newly minted Dr. Lawrence) and DeLane. Thank you for being true friends. I still can't believe how long we've known each other, since way back in the day at NCSSM, but I'm so thankful that each of you are in my life, you are both so special to me.

To my St. John's Congregational Church family- words cannot fully express how much I love you, and how much I've appreciated you over these 5 years. You all have become family to me when my blood family was so far away. I didn't now I'd pick up so many extra mothers, aunts, sisters, brothers, and uncles. God's love shines through you, and I thank you for the love you've shown me, for the hugs you give me, and for helping me to find my true self. I'll miss you all, and I love you. Special thanks to my small groups families- Amber, Janice, Reggie, Emily, Babette, Kyle, Sandra, Huon, Francine, Dawn, Dawnelle, Nathan, Tim (lil' bruh!), Nelly, Ramikah, Angela, Jacki, Tehillah. Thank you so much for all of your prayers, your hugs, your love, and your support. And to my Pastor, the Rev. Dr. Howard-John Wesley, thank you for so diligently using your preaching gift.

To my cheerleading sections (and, I'm thankful to have so many)- even when it got tough, you would all check on me to make sure that I was pushing through and holding on. Your words, wisdom, and wit have made the bumps smoother, for that I thank you.

AAAS (I didn't know that you all would stick with me this long! Dr. Shirley Malcom, Crispin Taylor, Ric Weibl, Desiree Atherly, James Austin, Robin Arnette, Joe Perpich, Krystyna Isaacs, Sibrina Collins, & Dr. D Thank you all!

To my MIT cheering section- fellow alums, Kani Udoh (along with Tekah, David and Grace), Gail Lenora Staton, Jolene Saul, Eboney Smith, Wenona Charles, Terraun Jones, Kamla Topsey, Dean Blanche Staton, Christopher Jones, Roy Charles, Ore Adeyemi, and many more, thank you all for your friendship, thank you for being such dynamic and wonderful people, and I'll always remember all those good times back at the Institute.

My NEAGEP family, you are all so wonderful, I promise not to get too far away! Thank you for your encouragement: Sandy Petersen, Ann Lewis, Millicent Jackson, Terry Di Giacomo, Michael Alderman, Barbara Bou, Stephanie Burrell, Catherine Adams, thank you.

To the other UMass folks that have been so encouraging/helpful I thank you as well. Provost Charlena Seymour, Graduate Dean John Mullin, Vice Provost for Research Paul KostECKI, Ms. Marty Martin, Nancy Buffone, Prof. Soren Bisgaard, Alyssa Walder, Josh Kroner. Thank you so much for all of your help and assistance with things for APINE and in general, I hope I have left UMass a little better than when I came in, it is always my goal to do so.

To my Charles Hart Middle School family, thank you for giving me a chance to teach down there in Southeast DC. I've never forgotten the experience, or the lessons I learned. Thank you for welcoming me, even though you knew I was temporary. I know that many of you have retired or moved on from Hart. I hope the years will be kind to you as you gave so much for the kids. Thank you for your encouragement and your love- Desi Mintz, Ann Brogioli, Principal Epps, Mrs. Ethel Rivers, Mrs. Irma Morgan, Mr. Bethea (rest peacefully kind and humble soul), Mr. Carl Grant, Mrs. Felicia Motley, Mrs. Holt, Ms. Janice Waters, and so many others that I cannot name.

Over the years there are many people that have come in, planted seeds of friendship that have grown into beautiful flowers.

To my fellow NEA students, look at us now! Gary, thank you for your thoughtfulness, thank you for being a friend, and thank you for talking me down a number of times in the early days. I can't wait to see where you'll go and what you'll do, all my best to you and Sabine! Colleen, Lillian, Rosa, Vicente, Kathy, Edgardo, Chris, Zuleika, Iris, Destinee, UnJa, Chris Jones (good luck at MIT!), Uche, Uche, Nestor, Jennifer, Lieselle, Rebecca, Kendra, thank you all for your friendship.

To my partner in crime Jessica McCoy. A Ph.D. is Not Enough. Have any truer words been spoken? It has been a pleasure, through the madness, the drama, and all-in-all, trying to make this a better place. I never would've known synergy (and psychosis) if it weren't for you. Don't worry, it'll be over sooner than you think, and thank you, I expect great things from you.

To my other partners in APINE/GECDI crime- Liz, Iris, and Caryl, ladies, thank you so much for taking what Jess and I started and giving it legs to stand on. I can't wait to see what new things await you. I'm proud of you! Thank you for seeing the value in the enterprise. I look forward to where it will all go. And Lizzie – an extra thank you for keeping the chocolate handy, I know you'll make an awesome professor one day. good luck with everything.

To all the little people I've spent time babysitting, you've made life in grad school a little more normal. thanks to you and your parents for letting a grad student hang out with the kiddies. the little Coughlins (Liam "Where's your red truck?" and Louisa) and the little Staudenmeyers (Charlotte and Patrick). and little darlings Tayah and Adrielle. I love you all. thanks for being good kids!

To all the PSE folk-

To Charlie, where would this project have gone without you? I thank you for all of your wisdom, and insight, and for your trust in me with the instrumentation. I know you don't let the 600 keys go to just anybody. I do hope that you're enjoying your much deserved retirement, a little on your own, and a little spoiling the grandkids. I will truly miss our early morning conversations, me bleary-eyed from running the 400 over night, you perky, green tea in hand. You are a zen-master Charlie. I'm so glad to have known you.

To all the office staff, thank you so much for helping to keep everything in order, you all keep us running, and I thank each of you for your help! Eileen, Joann, Sophie, Ann, Anita, and Vivien I wish you well behaved students and faculty (we can hope right?).

To the Tew Group (past and present)-

Erin- You awesome goddess you. thanks for keeping us all straight!

Morris- GWB didn't do it. one day you'll figure out where all your stuff went! I hope that one day you'll find a place of confidence and peace; you are a wonderful human being. don't forget that.

Jason P.- I want my roti! But seriously, thank you for being such a sweetheart. I wish you luck with the project!

Sterling- the abuse is over! Aren't you relieved? (Insert wicked laughter here)

Mac- That little monkey you gave me? He came in handy, thanks!

Abhi- dahling! How I'll miss you!

G- Thank you so much for reading things for me. I appreciate your eye for detail and your commentary. Now about those twinkies....

Lachelle- Cali here I come...

Bob (Roberto)- It folds! It folds!

Jing- Welcome to sugarland, oPE style- I wish you well as the project continues. I'm excited for the direction that it's going.

Khaled- I'll miss talking world politics with you. thank you for being such a wonderful office mate. I wish you well wherever you go. remember to open the steam valve every once in awhile.

Naomi! My little one! You're in charge now dear. keep the boys in-line! Thank you for being a ray of sunshine. good luck with everything.

Raja! Hurry up and get married. I want to go to India! And can we not try to kill me next time? I'm still waiting on flowers from what I'll call the "cashew incident"...

☺

Rich Blatchly and Pat O'Hara, thank you for your enthusiasm about the project and your kindness as well. Vive le France!

And to everyone else in the Tew group, good luck to you all, I wish you well!

To all my undergrads- Jack, Tatyana, Debanti, and the others I occasionally adopted (Dan, Katelyn, Jason R..) good luck with everything in grad school/job/etc., it was such a pleasure to know each of you.

Lunch bunch/gift buddies- thanks for all the chocolate (my thighs don't thank you, but my heart sincerely does)- Julie & Melissa, cume study buddies I guess we'll now be scattered to the winds? Joanna, you gifted sweet spirit, thank you for our conversations on science and spirituality, it's nice to have a kindred spirit around ☺ Donna, you crazy woman you- webmistress for APINE thank you for everything, it wouldn't have happened without you. Matt Misner, Colorado buddy, one of these days we'll compare pictures, frightening that we went to the same elementary school and ended up in PSE together. Jen- you crafty woman you, I envy your quilting/crafting skills. To those that have gone, Gabi (I'm coming back to Europe and I'm going to see you next time, thanks for being a wonderful ear), Constable- maybe I'll make it to Phoenix sooner rather than later!

To my former advisors and mentors- Anne Mayes, Paula Hammond, and Sandy Burkett, thank you for being an inspiration.

To the places where I got my first taste at lab life: Morehouse summer science 1994, Dr. Errol Archibald, Duke university ACS Project SEED & Kenneth Cutler 1995-

1996 in the lab of Dr. Eric Toone with Phaedria St. Hilare and Steven Powell. 1997 at the now defunct Seaford Delaware DuPont plant where I met another inspiration. Dr. Sharon Haynie at the experimental station. 1998 at the Royal Institute of Technology in Stockholm Sweden. Dr. Du Sichen. 1999 IBM Almaden. Dr. Jim Hedrick- what did you all do to me?!?! Just kidding. thank you for the insight and the support though the years.

Professors Crosby, Coughlin, Carter thank you for your support and council through the years.

Now for the money shot- A special thanks to all of the institutions that have taken care of me financially over these last 5 years: The University of Massachusetts Office of Graduate Student Recruitment & Retention fellowship, the Ford Foundation, the NIH NRSA, and MRSEC

To my committee members, DV and Muthu- thank you for your insight and your encouragement. Thank you for taking the time to serve on my committee. I appreciate all of our conversations both on the project as well as on life in science and society.

And finally. to my advisor- Gregory N. Tew. it's been quite a ride. I'm thankful we developed a healthy relationship. I'm still amused by your love for NOBCChE conferences. Even though I can't be here to recruit for you I'll stay on the look-out for prospects. I look forward to your continued success, and I thank you for your council, your enthusiasm, your honesty, and all of your hard work.

And we know that in *all* things God works them together for good according to His purpose Romans 8:28

To who much is given, much is required (Luke 12:48)

It takes a village to raise a child. as you can see by these all of these acknowledgments, there have been a number of villages that I've taken time to visit over the years. I'm not completely grown, but I know I'll never be the same. Each of you has touched my life- I thank you for either passing through or coming to stay.

ABSTRACT

SYNTHESIS AND CHARACTERIZATION OF ORTHO PHENYLENE ETHYNYLENE OLIGOMERS: A NEW SCAFFOLD FOR FOLDAMER RESEARCH

FEBRUARY 2007

TICORA V. JONES S.B., MASSACHUSETTS INSTITUTE OF TECHNOLOGY

M.S., UNIVERSITY OF MASSACHUSETTS AMHERST

Ph.D., UNIVERSITY OF MASSACHUSETTS AMHERST

Directed by: Professor Gregory N. Tew

As a new frontier of foldamer research based on the synthesis and characterization of oligomers programmed to fold and self assemble into secondary structures continues to open, new scaffolds with a variety of dimensions are required. Presented here is the synthesis and characterization of a new *ortho*-Phenylene Ethynylene (*o*-PE) backbone scaffold. This scaffold has been synthesized using Sonogashira methods with a variety of building blocks containing π -rich and π -poor elements substituted with non polar and polar substituents. Solvent induced folding of these short oligomers into well defined helices was confirmed via 1D and 2D NMR methods. Utilizing the electron rich and electron poor phenylene building blocks, variations of these *o*-PE oligomers have been synthesized to determine the folded stability of π -rich vs. π -poor vs. π -poor/rich systems. Variations in temperature offer a route, aside from solvent denaturation, to probe the stability of the folded structures. This is the first report of a highly detailed solution NMR characterization using 1-D and 2-D methods examining the folding of a PE backbone without hydrogen bonds, and the first for an *o*PE system in general.

TABLE OF CONTENTS

	Page
ACKNOWLEDGMENTS	v
ABSTRACT.....	xiv
LIST OF TABLES	xviii
LIST OF FIGURES	xx
CHAPTER	
1. FOLDAMERS- AN OPENING FRONTIER.....	1
1.1 Introduction.....	1
1.1.2 Biologically Inspired Constructs as Foldamers	3
1.1.3 Abiotic Construct Foldamers	5
1.1.3.1 Folding/Unfolding Stimulus: pH	5
1.1.3.2 Folding/Unfolding Stimulus: Metal-Ligand Interaction	6
1.1.3.3 Folding/Unfolding Stimulus: Hydrogen Bonding	7
1.1.3.4 Folding/Unfolding Stimulus: Electrostatic Interactions.....	9
1.1.3.5 Folding/Unfolding Stimulus: Solvent Dependence	10
1.2 <i>ortho</i> Phenylene Ethynylene Oligomers.....	11
1.3 Scope of the Thesis	14
2. SYNTHESIS OF NEW SUBSTITUTED <i>ORTHO</i> PHENYLENE ETHYNYLENES.....	16
2.1 Introduction.....	16
2.2 Synthetic Methodology- Goals and Challenges.....	17
2.3 Synthesis of Non-polar alkoxy-substituted oPEs.....	20
2.4 Synthesis of polar alkoxy substituted oPEs	27
2.5 Synthesis of ester substituted oPE	32
2.6 Mixed alkoxy-ester oPE systems	39
2.7 Conclusions.....	42

3.	CHARACTERIZATION OF CHIRAL ALKOXY NON POLAR OPE	45
	3.1 Introduction.....	45
	3.2 Methods.....	46
	3.3 UV and Fluorescence Studies	47
	3.4 Circular Dichroism.....	52
	3.5 Crystal Structure of hexamer 6	58
	3.6 NMR Studies.....	60
	3.7 Conclusions.....	64
4.	SOLUTION nmr CONFIRMATION OF FOLDING IN SHORT OPE	
	SYSTEMS.....	66
	4.1 Introduction.....	66
	4.2 Methodology	67
	4.3 1-D ¹ H NMR Characterization of Et ₄ , EsEt ₃ , and Es ₄	68
	4.4 2-D NMR Characterization of Et ₄ , EsEt ₃ , and Es ₄	78
	4.5 Temperature study of Et ₄ , EsEt ₃ , and Es ₄	82
	4.6 End group behavior.....	83
	4.7 Conclusions.....	84
5.	CONFIRMING FOLDING IN LONGER OPE SYSTEMS.....	85
	5.1 Introduction.....	85
	5.2 Methodology	85
	5.3 Es ₄ Oligomer Solvent and Temperature Effects	94
	5.4 Es ₅ Oligomer Solvent and Temperature Effects	100
	5.5 Es ₆ Oligomer Solvent and Temperature Effects	106
	5.6 Es ₉ Solvent and Temperature Studies	112
	5.7 2-D NMR studies for Teg-ester oligomers	116
	5.8 Conclusions.....	124
6.	EXPLORING THE INFLUENCE OF BACKBONE ELECTRONICS ON THE	
	Ope SYSTEM.....	125
	6.1 Introduction.....	125
	6.2 Methods.....	126
	6.3 Effect of solvent and temperature on π - π stacking of π -rich, π -	
	poor/rich and π -poor systems.....	126
	6.3.1 Solvent effects.....	126

6.3.2	Temperature studies in CD ₃ CN.....	131
6.3.3	Temperature studies in CDCl ₃	137
6.4	Modeling and the overall impact of solvent and temperature.....	138
6.5	“Breathing” of the oPE system	144
6.6	Conclusions.....	148
7.	MATERIALS AND METHODS.....	149
7.1	Measurements	149
7.2	Materials	149
7.3	General Synthetic Procedures.....	150
7.3.1	General Sonogashira Coupling Procedure	150
7.3.2	General TMS Deprotection Procedure 1 (K ₂ CO ₃).....	151
7.3.3	General TMS Deprotection Procedure 2 (TBAF).....	151
7.3.4	General Sonogashira Coupling Procedure.	152
7.3.5	General Triazene Activation Procedure.....	152
7.3.6	General Microwave Triazene Activation Procedure.....	152
7.4	Synthesis of Non-Polar Alkoxy Compounds.....	153
7.5	Synthesis of Teg Alkoxy Compounds	162
7.6	Synthesis of Teg-Ester Compounds.....	172
7.7	Synthesis of Teg-Alkoxy/Ester Compounds.....	185
	BIBLIOGRAPHY.....	190

LIST OF TABLES

Table	Page
1.1: Biologically Inspired Foldamers.....	4
2.1 Synthesized Non-Polar Alkoxy Oligomers.....	26
2.2: Teg-alkoxy oligomers synthesized	32
2.3 Synthesized TEG-ester oligomers.....	39
2.4 Synthesized Ester-Ether molecules with Teg side-chains	40
2.5: oPE oligomers synthesized for study	43
4.1: Average Δ ppm (CDCl_3 - CD_3CN) shifts for aryl protons for 11, 22, and 17. 75	
4.2 Calculated NOESY distances.	80
5.1 Energies for conformers of hexameric oPE as determined by MMFF in Spartan. The H is the energy of the conformer as given by modeling program while the Δ H is calculated as the difference between the helical and the other conformers.....	91
5.2 Δ ppm and length for folded oPE rings.....	114
5.3 Δ ppm/10°C data for all ester oligomers.....	115
5.4 Calculations comparing ROESY data with model predictions for tetramer 17. The reference peak taken for the calculation is the peak corresponding to protons 2a and 2c which has a calculated distance of 2.44Å	119
5.5: ROESY distance calculations for pentamer 18. The reference peak taken for the calculation is the peak corresponding to protons 3a and 3c which has a calculated distance of 2.44Å.....	120
5.6: ROESY distance calculations for hexamer 19. The reference peak taken for the calculation is the peak corresponding to protons 2a and 2c for the peaks in CD_3CN and 6a to 6c in CDCl_3 which has a calculated distance of 2.44Å.....	122
6.1: Average Δ ppm (CDCl_3 - CD_3CN) shifts for aryl protons of 11, 22, and 17. 126	

6.2: Model Calculations for Tetramers	127
6.3 ΔH_{helix} (kcal/mol) calculations for all oligomers	143

LIST OF FIGURES

Figure	Page
1.1: DNA folding from the base-paired double helix, coiling around histones and ultimately forming the chromosome.	2
1.2: (a) Unsubstituted representative structure for 2,6 disubstituted Pyridine oligomer. (b) Side and top view of crystal structure for single helix oligoamide. Taken from reference (20). (c) Side view of double helix crystal structure. Taken from reference (22).....	6
1.3: (a): Hydrazone linked pyridine oligomer unit. (b) Model of extended hydrazone-pyridine oligomer (c) Helical hydrazone-pyridine oligomer crystal structure with Pb(II) ions embedded in the helix in red. (a-c) taken from reference (23). (d) Pyridine-pyrimidine oligomer basic structure (e) Helical oligomer (f) Extended conformation with Pb(II) ions embedded in dark grey. (d-f) taken from reference (24).	7
1.4: (a) Aromatic δ -peptide with quinoline backbone. (b) Side and top view of crystal structure. Side chains, solvent molecules, and hydrogens were omitted for clarity. Reported structure has 8 repeat units forming a helix with just over 3 turns. Taken from reference (25).....	8
1.5: (a) Aryl oligoamide oligomer unit (b) Side and top view of crystal structure of aryl oligoamide nonamer. Taken from reference (26).....	9
1.6: (a) NDI segment (b) DAN segment (c) Aedamer complex where A [acceptor] represents the NDI segment and D [donor] represents the DAN. Taken from reference (27).....	9
1.7: (a) Basic <i>meta</i> Phenylene Ethynylene (mPE) oligomer unit (b) Extended and folded helical structure of mPE oligomer. Taken from reference (2).....	10
1.8: (a) Basic oPE repeat unit (b) Top and side views of crystal structure of unsubstituted oPE backbone.	11
1.9: Illustration of aspect ratio differences. The radius of the blue figure is equal to the height dimension of the red figure. The radius of the red figure is equal to the height of the blue figure. Given these parameters the surface area of these two figures is equivalent but the aspect ratio of the figures is different.....	13

1.10: (A) Amphiphilic oPE oligomer. Green represents aryl rings that would be substituted with non-polar substituents. Blue aryl rings would be substituted with polar substituents. (B) Lac repressor protein as a self-assembled helical bundle. Non polar Isoleucine groups are pointed towards the center of the structure.	14
2.1 Long chain amphiphilic oPE oligomer and disubstituted oligomer Green = non polar substituents. Blue = polar substituents.	17
2.2 Synthesis scheme for di-substituted alkoxy oPE monomers.	19
2.3: Disubstituted synthesis. mixed products including head-to-head diacetylene coupling.	20
2.4 Synthetic scheme for Non-Polar Monomer	22
2.5: ¹ H NMR spectra for AB monomer 1	23
2.6 Synthetic scheme for Non-Polar oligomer synthesis	25
2.7: Sample NMRs region for oligomers 3, 4, and 6	26
2.8 Synthesis scheme for alkoxy-TEG substituted monomer	28
2.9 ¹ H NMR traces for oligomers 30 through 8-H.....	30
2.10 Synthetic scheme for Teg-alkoxy oligomers	31
2.11 Synthetic scheme for Teg-Ester monomer.....	35
2.12 ¹ H NMR spectra for ester monomer transformation.....	36
2.13: Synthetic scheme for Teg-ester oligomers.....	38
2.14 Synthetic scheme for Teg-ester/ether oligomers.....	41
2.15 ¹ H NMR of the aryl region of hetero oligomer 23 (Es ₂ Et ₃).....	42
2.16: Synthesized oPE backbones. (a) Electron rich ether oligomer Et _n . (c) Electron poor ester oligomer Es _n (c) Sample hetero-oligomer Es _n Et _m . All red rings are electron rich, all blue rings are electron poor. Rings are numbered sequentially from the TMS end of the oligomer to the triazene end.....	44
3.1 Extended and helical conformation of alkoxy substituted nonamer 7.....	45

3.2 (a) NP mPE oligomer (b) UV spectra of increasing oligomer length in heptane. (Taken from ref 30) (c) NP oPE oligomer and macrocycle (d) UV spectra comparing macrocycle to discrete trimer.....	48
3.3 UV spectra of 3-7. (a) Chloroform (b) Heptane (c) Nonamer 7.....	50
3.4 Fluorescence spectra of 3-7 in Chloroform (a) Heptane (b) and a sample fluorescence spectra from a mPE system in CH ₃ CN (c) taken from reference 32.....	51
3.5: CD spectra of tetramer 4, hexamer 6, and nonamer 7 at 0.02mM in at 20°C in chloroform (a) heptane (b).....	53
3.6: Concentration study of nonamer in n-heptane using a 1mm cell (.2mM) and a 1cm cell (.02mM).....	54
3.7 (a) CD spectra of 6 in n-heptane at high concentration. varying temperature (b)7 in n-heptane and chloroform at high concentration varying temperatures.....	56
3.8 Representative CD spectra of apolar mPE oligomers with increasing length in heptane from reference 30.	57
3.9: CD spectra for solution and solid state oPE Macrocycle.....	58
3.10 Crystal structure of hexamer 6 (a) top view (b) and (c) side view.	59
3.11: Expanded aryl region for oligomers 3, 4, and 6 in CDCl ₃	61
3.12: NMR spectra of 4 in Heptane (top) and CDCl ₃ (bottom).....	61
3.13: Aryl region of Nonamer in Chloroform (top) and Heptane (bottom).....	62
3.14: ¹ H Temperature study of oligomer 4 in d-heptane	63
4.1: oPE tetramers 1-3. Electron poor (blue) and electron rich (red) rings are shown. Relevant protons for each tetramer are labeled according to their splitting pattern. Each ring of each oligomer has three protons that are labeled respective to their J-coupling and splitting pattern respectively: a (8.4 Hz, d), b (2.1 Hz, d), and c (8.4 Hz and 2.1 Hz, dd).....	69

4.2: (a) NMR titration curves of 11, 17, and 22 from CDCl ₃ to CD ₃ CN. Upfield shifting of rings 1 and 4 are evident while rings 2 and 3 do not move. (top) 11 Et ₄ , (middle) 22 EsEt ₃ , and (bottom) 17 Es ₄ . (b) Energy minimized (MMFF) conformation of tetramers 1-3 folded into a helix. The Teg side chains are omitted for clarity. Angles indicate the offset between rings 1 and 4 in the helical conformation. Distances given are between the centers of rings 1 and 4.....	72
4.3: (a) NMR traces for each concentration of Acetonitrile (CD ₃ CN) in CDCl ₃ for tetramers 11, 22, and 17 (1.25 mM, 400 MHz, 298 K). Individual signals from rings 1 and 4 have been labeled and were assigned by a combination of COSY and HMBC 2D NMR experiments. Tetramethylsilane is the external reference for the solvent referenced (top) 11 Et ₄ , (middle) 22 EsEt ₃ , (bottom) 17 Es ₄ . (b) Top down views of molecular models.....	77
4.4. Partial NOESY spectra of 22, EsEt ₃ (1.25 mM, 400 MHz, 298 K, mixing time: 0.1 s) for the TMS and aryl region in CDCl ₃ (a) and CD ₃ CN (b). No cross peak is observed in CDCl ₃ while a strong NOE is present in CD ₃ CN. Partial NOESY Spectra of 22 (1.25 mM, 400 MHz, mixing time: 0.1 s) in CD ₃ CN revealing the TMS to aryl interaction at 288K (c) and 310K (d).....	79
4.5: Partial ROESY spectra of 17, Es ₄ (1.25 mM, 600 MHz, 298 K, mixing time: 0.3 s) for the TMS and triazene region in CDCl ₃ (left) and CD ₃ CN (right). No cross peak is observed in CDCl ₃ while a strong NOE is present in CD ₃ CN.....	80
4.6: NMR traces in Acetonitrile (CD ₃ CN) for tetramers 11 Et ₄ (top) 22 EsEt ₃ (middle) and 17 Es ₄ (bottom) at 288K, 299K, and 310K. Downfield shifting is evident as temperature is increased. Tetramethylsilane was used as an external reference for each spectra. Individual signals from rings 1 and 4 have been labeled and were assigned by a combination of COSY and HMBC 2D NMR experiments.....	83
5.1 Comparison of oPE hexamer with two turns (top) and mPE oligomers with one (middle) and two turns (bottom). Bottom two spectra from Jason Nelson's thesis- http://sulfur.uiuc.edu	86
5.2 COSY spectra for Es ₄	87
5.3 HMBC page identifying Es ₄	88
5.4 Assignments and protons for Es ₄ -Es ₆	89

5.5 Potential conformers of oPE hexamer.	90
5.6: Depiction of molecular weight dependence for NOE experiments	93
5.7: Simple relation between intensities and distances for NOESY/ROESY experiments.	94
5.8: (a) Chemical structure and molecular model of tetramer 17 extended and folded. (b) Raw data for solvent titration of 17. (c) Compressed data showing the Δ ppm for each ring.	96
5.9: (a) Molecular model of tetramer 17 folded. (b) Raw data for temperature study of 17 (c) compressed data showing Δ ppm for each ring (R ₁ -R ₄).....	97
5.10: Δ ppm vs. Temperature in CDCl ₃ for tetramer 17	98
5.11: (a) Solvent and temperature plots for rings not involved in folding (R _{2,3}). (b) Solvent and temperature plots for rings involved in folding (R _{1,4}).	99
5.12: (a) Chemical structure of pentamer 18 extended and a folded molecular model. (b) Raw data of solvent titration of 18. (c) Compressed data for solvent titration.....	101
5.13: (a) Molecular model of pentamer 18 and extended chemical structure. (b) Raw data for temperature titration. (c) Compressed data.....	103
5.14: Compressed data for temperature study of pentamer 18 in CDCl ₃	104
5.15: (a) Solvent and temperature plots for rings not involved in folding (R ₃). (b) Solvent and temperature plots for rings involved in folding (R _{1,2,4,5}).....	105
5.16: (a) Chemical structure for the extended hexamer 19 and molecular model of folded structure (b) Raw data for solvent titration (c) Compressed data.	107
5.17: Top down view of a model for hexamer 19.....	108
5.18: (a) Folded molecular model and extended chemical structure of hexamer 19. (b) Raw data for temperature study (c) Compressed data.....	110
5.19: Plot of Δ ppm versus Temperature study of hexamer 19 in CDCl ₃	111

5.20: Solvent and temperature plots for hexamer 19 R ₁₋₆	112
5.21: ¹ H NMR data for nonamer 20 in CDCl ₃ and CD ₃ CN.....	113
5.22: Nonamer 20 solvent and temperature studies (a) Δppm vs. Volume % CD ₃ CN (b) Δppm vs. Temperature in CD ₃ CN (c) Δppm vs. Temperature in CDCl ₃	115
5.23 Solvent and temperature plots for nonamer 20 R ₁₋₉	116
5.24 ROESY spectra and models for tetramer 17 (a) ROESY spectra in CD ₃ CN 270K (b) ROESY spectra in CD ₃ CN 298K (c) Helical model showing TMS to proton 3b interaction (d) Helical model showing TMS to proton 2b interaction (e) and (f) ROESY spectra showing TMS and triazene regions in CDCl ₃ (e) and CD ₃ CN (f). (g) Extended model of tetramer 17.	118
5.25 ROESY spectra and models for pentamer 18 (a) ROESY spectra in CDCl ₃ at 270K (b) ROESY spectra in CD ₃ CN 270K (c) Extended model showing TMS and all potential interactions (d) Helical model showing TMS to proton 2b, 4a, 5b, and 3b interaction with the TMS 'flipping' from one side of the molecule to the other shown.	121
5.26 ROESY spectra and models for hexamer 19 (a) ROESY spectra in CDCl ₃ at 270K (b) ROESY spectra in CD ₃ CN 270K (c) Extended model showing TMS and all potential interactions (d) Helical model showing TMS to proton 2b, and 5b interaction	123
6.1 (a) Δppm vs. Solvent composition and (b) chemical structures for pentamers 12 (π-rich), 23 (π-poor/rich), and 18 (π-poor).....	129
6.2 (a) Δppm vs. Solvent composition and (b) chemical structures for hexamers 13 (π-rich), 24 (π-poor/rich), and 19 (π-poor).....	131
6.3 Δppm vs. Temperature (°C) in CD ₃ CN for tetramers 11, 22, and 17.	133
6.4 Δppm vs. Temperature (°C) in CD ₃ CN for pentamers 12, 23, and 18.	134
6.5 Δppm vs Temperature (°C) in CD ₃ CN for hexamers 13, 24, and 19.....	136
6.6 Δppm vs. Temperature in CD ₃ CN extracting π-rich (a) and π-poor (b) portions of oligomer 24 compared with oligomers 13 and 19.....	136
6.7 Δppm vs Temperature (°C) in CD ₃ CN for the ester rings of 22-24.....	136

6.8 Δ ppm vs Temperature ($^{\circ}$ C) in CDCl_3 for pentamers 18 (a) and 23 (b).	137
6.9 Δ ppm vs Temperature ($^{\circ}$ C) in CDCl_3 for hexamers 24 and 18.	138
6.10: Combined solvent and temperature plots for all pentamers (a) π -rich 12 (b) π -poor/rich 23 (c) π -poor 18.....	139
6.11: Combined solvent and temperature plots for all hexamers. (a) π -rich 13 (b) π -poor/rich 24 (c) π -poor 19.....	140
6.12: MMFF energy minimized models for all pentamers (a) π -rich 12 (b) π - poor/rich 23 (c) π -poor 18.....	141
6.13: MMFF energy minimized models for all hexamer (a) π -rich 13 (b) π - poor/rich 24 (c) π -poor 19.....	142
6.14: Plots of Energy vs. Number of Rings for (a) π -rich and π -poor systems as synthesized and (b) unsubstituted oligomers using MMFF energy minimization.	144
6.15: Plot of Δ ppm ($\text{CD}_3\text{CN} - \text{CDCl}_3$) vs. number of rings for π -rich and π - poor systems.....	144
6.16: Models showing (a) "inside" protons 2a and 3a and (b) "outside" protons 4a and 5a for π -poor hexamer 19.	146
6.17: Plot of ppm vs. Temperature in CD_3CN for "inside" protons 2a and 3a and "outside" protons 4a and 5a.	146
6.18: Representations of (a) breathing, (b) unfolding and (c) twisting for oPE systems.....	147

CHAPTER 1

FOLDAMERS- AN OPENING FRONTIER

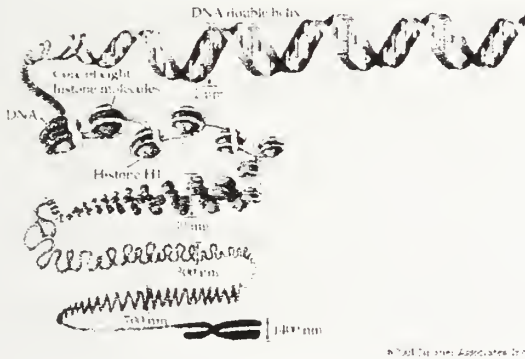
1.1 Introduction

Foldamers are molecular or supramolecular systems that respond to external stimuli and form coherent secondary structures (1-3). Protein folding offers inspiration to the field of foldamers- all secondary structures that are currently sought in the foldamer literature are found in nature. Secondary structures of amino acid sequences- helices, sheets, and turns- associate into tertiary and quaternary protein structures that perform a specific function. For example, a protein functions by binding into a particular receptor to influence the cell cycle, or associating with a bacterial or viral cell membrane to prevent infection. Ultimately this marriage of structure and function is one of the most fundamental aspects of biology.

Scientific understanding of *how* a macromolecule folds into a discrete and functional conformation is still limited. As chemists, we are able to synthesize duplicate amino acid sequences in gram quantities. Science as a whole, however, is still relatively unable to consistently control the formation of "native" protein conformations. Maladies such as mad cow disease and Alzheimer's are attributed to protein *misfolding*, making the quest to understand the subtleties of macromolecular folding and organization more compelling. Exploring the folding of biological and abiological scaffolds through the study of foldamers is essential to gaining more insight and understanding into this problem.

DNA is the ultimate example of macromolecular organization and self assembly to accomplish function (Figure 1). Each cell contains DNA that encodes for every

protein and enzyme necessary for bodily function. Nature has designed a system that uncoils segments of DNA and reads them through transcription and translation. The amino acid sequence translated from the DNA segment encodes for a particular protein and the DNA is folded back into the chromosome.



© Sinauer Associates 2001 taken from <http://distancelearning.ksi.edu/demo/bio378/bio378.htm>

Figure 1.1: DNA folding from the base-paired double helix, coiling around histones and ultimately forming the chromosome.

Foldamers provide a unique opportunity to explore specific non-covalent forces or other stimuli and their propensity to induce secondary structure. These non-covalent forces or external stimuli including metal-ligand interactions, hydrogen bonding, electrostatics or electronics, hydrophobic interactions, pH, solvent and temperature dependence- can be varied utilizing different chemical handles to help us deconvolute the influence of a particular stimuli.

Our understanding of protein folding has been enhanced using a variety of techniques that have also been useful for the study of foldamers. Computer modeling offers a mechanism to attempt to predict folded structure and association.

Unfortunately modeling still can not transform an entire amino acid sequence to the correct native protein structure. X-ray crystal structures show secondary conformations in the solid state. Folded states in solution can be examined by a variety of means that are familiar to chemists: Nuclear Magnetic Resonance (NMR), Circular Dichroism

(CD), and fluorescence. All of these techniques have been useful for characterizing foldamers.

As a field, foldamers have evolved over the last decade. Many groups have utilized built in chemical handles and the external stimuli mentioned above to manipulate and induce secondary structure. Some of these groups have even been able to provoke the formation of tertiary structures. For example, helical bundles of β -peptides and peptoids have been created by specifically programming molecular sequence and structure to incorporate elements to stabilize the tertiary structure (4-7).

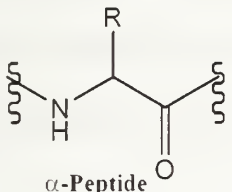
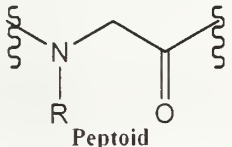
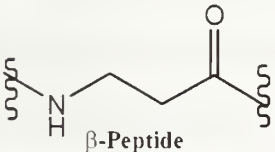
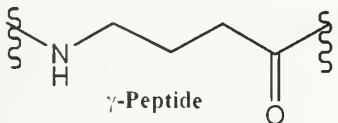
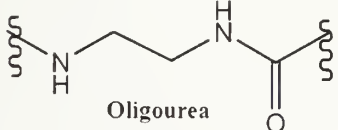
At present, most foldamers are discrete oligomers that offer a stable scaffold or backbone upon which to build or create specific secondary structure. Given this premise, current foldamer scaffolds can be separated into two large groups- Biologically Inspired Constructs (BIC) and Abiological Constructs (AC). A brief review of each will be presented here.

1.1.2 Biologically Inspired Constructs as Foldamers

BIC foldamers are variations of naturally occurring amide backbones. Table 1 gives basic examples for each of these foldamers. These oligomers have been substituted with a variety of side chains: traditional amino acids and their variations, aromatic rings and cycles. The side chain variation within these structures influences the secondary structure of BIC foldamers. These oligomers have been shown to form a variety of helices, sheets, and turns that have been examined by NMR, CD, and fluorescence, and crystallography, the same tools that are used for protein folding. Some BICs have been associated into helical bundles as an example of tertiary structure. These two to six helix bundles have been formed using amphiphilic β -peptide

and peptoid helices (4, 5). β -peptide helices with disulfide linkages (6), and β -peptide helices with nucleobase side chains (7).

Table 1.1: Biologically Inspired Foldamers

Basic Structure	Groups	Secondary structures and tertiary structures Characterization
 <p>α-Peptide</p>	DeGrado. Gellman. Reiser. Balarm	α/β -peptides form 14/15 and 11 helices (8) in CH_3OH . Constrained α/β -peptides form 13-helices (9) in CH_3OH , and β peptides were introduced into α hairpin structure (10). All have been studied by NMR
 <p>Peptoid</p>	Zuckermann. Barron	Peptoids adopt polyproline type I helices in solution and solid state (11). An amphiphilic peptoid helix has been shown to associate in to helical bundles (4).
 <p>β-Peptide</p>	Gellman. Seebach. DeGrado. Schepartz. Sharma. Wang	β -peptides can adopt helices, sheets, and turns as secondary structures. The 14-helix (12-15) has been shown to gradually unfold, suggesting cooperativity (16). Helical bundles have been generated by introducing amphiphlicity (5), di-sulfide linkages (6), and nucleobases on side chains (7). 12-helices, 10-helices, 10/12-helices, and 8-helices have also been formed and studied.
 <p>γ-Peptide</p>	Seebach. Gellman.	γ -peptides can form a 14-helix (17) or strands (18). These conformations have been studied by NMR and crystallography.
 <p>Oligourea</p>	Guichard	Oligoureas (19) form a 14-helix similar to γ -peptides and have been studied by NMR and crystallography.

1.1.3 Abiotic Construct Foldamers

The AC foldamer family contains a variety of aromatically based molecules that fold based on many of the principles that facilitate BIC foldamers secondary structure while using non-covalent interactions. The new *ortho* Phenylene Ethynylene (oPE) backbone that has been synthesized in our group falls into the AC foldamer family. Examples of AC foldamers and the work that has been performed to characterize them are detailed below.

1.1.3.1 Folding/Unfolding Stimulus: pH

Pyridine oligoamide oligomers (Figure 1.2) have been shown to fold into helices in solution and unfold by a reversible protonation process by Lehn (20) and Huc (21). This process unfolds the helical oligomer with the addition of triflic acid, and the proton binds to the pyridine nitrogen. The addition of triethylamine deprotonates the pyridine and reverses the unfolding. Initial work showed that the pyridine oligoamide oligomer can dimerize (22) to form a stable double helix in solution and in the solid state (Figure 1.2c). NMR was used to probe the stability of these systems in solution and monitor helix formation as evidenced by upfield shifts in the aryl region due to π - π stacking. Crystal structures for each system are also shown in Figure 1.2c.

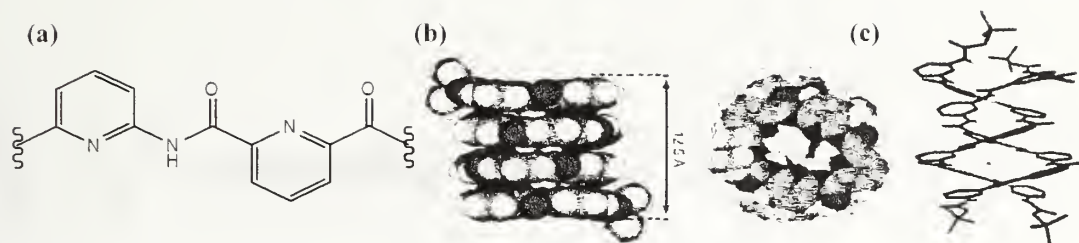


Figure 1.2: (a) Unsubstituted representative structure for 2,6 disubstituted Pyridine oligomer. (b) Side and top view of crystal structure for single helix oligoamide. Taken from reference (20). (c) Side view of double helix crystal structure. Taken from reference (22).

1.1.3.2 Folding/Unfolding Stimulus: Metal-Ligand Interaction

In addition to these pyridine oligoamides, other work from Lehn and coworkers includes molecules that coordinate with metals to control secondary structure (23, 24). The linear ligand hydrazone-linked pyrimidines (23) in Figure 1.3 have been shown to form a helix upon coordination with Pb(II) by X-ray crystallography and can be extended with the introduction of a small Pb-binding ligand. The pyridine-pyrimidine helix (24) can unfold and coordinate with Pb(II) as shown in Figure 1.3 with pH assisted switching, taking helices 10 Å in length and extending them to linear ligands almost 40 Å long. These systems were also studied by NMR and X-ray crystallography to examine ligand binding.

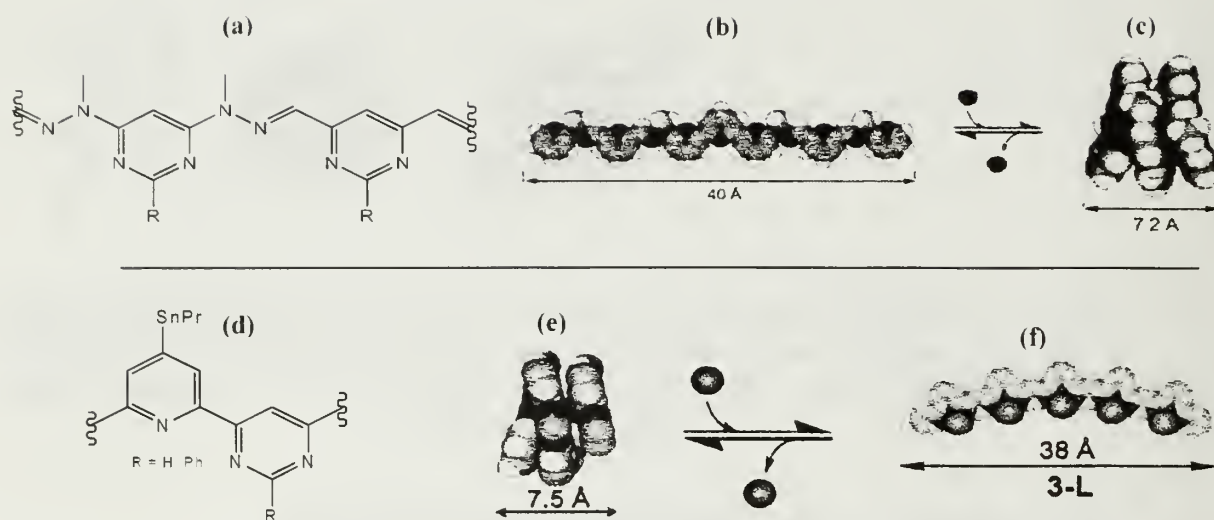


Figure 1.3: (a): Hydrazone linked pyridine oligomer unit. (b) Model of extended hydrazone-pyridine oligomer (c) Helical hydrazone-pyridine oligomer crystal structure with Pb(II) ions embedded in the helix in red. (a-c) taken from reference (23). (d) Pyridine-pyrimidine oligomer basic structure (e) Helical oligomer (f) Extended conformation with Pb(II) ions embedded in dark grey. (d-f) taken from reference (24).

1.1.3.3 Folding/Unfolding Stimulus: Hydrogen Bonding

Huc and coworkers have studied hydrogen bonded aromatic δ -peptides (25) that adopt a stable helical conformation in CDCl_3 and d_6 -DMSO with eight repeat units (Figure 1.4). The helix crystal structure shows a helix with slightly more than three turns without solvent molecules on the interior of the structure (Figure 1.4b). By NMR these helices did not appear to associate into complex aggregates. The stability of these helices was due in part to the hydrogen bonds that are formed between the amide linkages and pyridine nitrogen γ to the amide nitrogen. The helical conformation can also be attributed to the rigidity of the quinoline that forms the aromatic portion of the molecule.



Figure 1.4: (a) Aromatic δ -peptide with quinoline backbone. (b) Side and top view of crystal structure. Side chains, solvent molecules, and hydrogens were omitted for clarity. Reported structure has 8 repeat units forming a helix with just over 3 turns. Taken from reference (25).

Gong and coworkers have also incorporated hydrogen bonding and rigid aryl rings to control the backbone of the folded structure with aryl oligoamides (26). This work centers on the formation of nanocavities in hollow helices with an inner diameters of 10 to 30 Å (Figure 1.5). A strong Nuclear Overhauser Effect (NOE) for a nonamer and 21-mer has been observed for this system. This NOE is indicative of a stable end-to-end distance of less than 5Å through space. The variation of the amide position on the aryl rings of the oligomer allows for the tuning of the cavity size. Intermittently *para* substituted amides allow for longer oligomers with wider cavities, while all *meta* substituted amides shrink the diameter of the cavity and reduce the number of residues necessary for one full turn from 30Å (21-mer) to 10Å (nonamer).

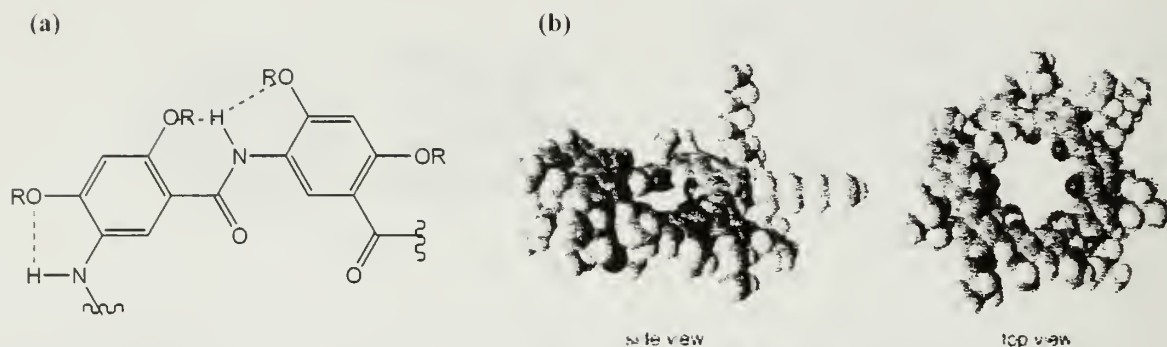


Figure 1.5: (a) Aryl oligoamide oligomer unit (b) Side and top view of crystal structure of aryl oligoamide nonamer. Taken from reference (26).

1.1.3.4 Folding/Unfolding Stimulus: Electrostatic Interactions

Iverson and coworkers have shown the controlled pleating of an oligomeric system through electrostatic interaction (27, 28). The electron poor, 1,4,5,8-Naphthalenetetracarboxylic Diimide (NDI), and electron-rich, 1,5-Dialkoxynaphthalene (DAN) pair were tethered together with a linker designed to allow for free short-range movement to promote the association of these molecules (Figure 1.6). The “Aedamers” (Aromatic Electron Donor-Acceptor) electronic association has been confirmed by UV-Fluorescence, and NMR studies that confirm the presence of the donor-acceptor interaction.

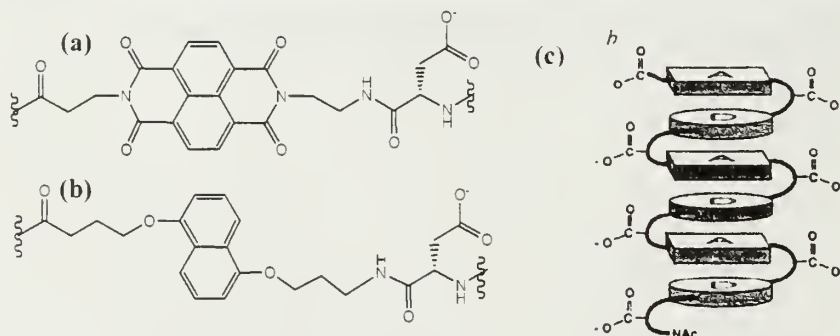


Figure 1.6: (a) NDI segment (b) DAN segment (c) Aedamer complex where A [acceptor] represents the NDI segment and D [donor] represents the DAN. Taken from reference (27).

1.1.3.5 Folding/Unfolding Stimulus: Solvent Dependence

Solvent dependant folding (29) is exhibited by *meta* Phenylene Ethynylene (mPE) oligomers studied by Moore and coworkers (Figure 1.7). These oligomers fold in acetonitrile with a six-ring repeat structure reminiscent of an mPE macrocycle. The helix can be unfolded from the helix to an extended structure in chloroform. This solvent dependant folding has been characterized by CD (30), fluorescence (31, 32), UV-Vis, Electron Paramagnetic Resonance (EPR) (33), and 1-D NMR. Variations of these mPE structures have included oligomers with hydrogen bonds along the outer perimeter, shown to stabilize the helical structure, (34) also shown by Gong and coworkers (35). In addition, water soluble oligomers with hexamethylene glycol side chains have also been formed (36). Backbone modifications of these mPE oligomers have introduced electron poor pyridine rings to the system to modify the basicity of the binding cavity that the mPE oligomer creates (37) allowing for the variation of a host-guest interaction through the center of the helix. Structurally rigid helicenes have also been utilized to bias the oligomer to a particular folding direction (38).

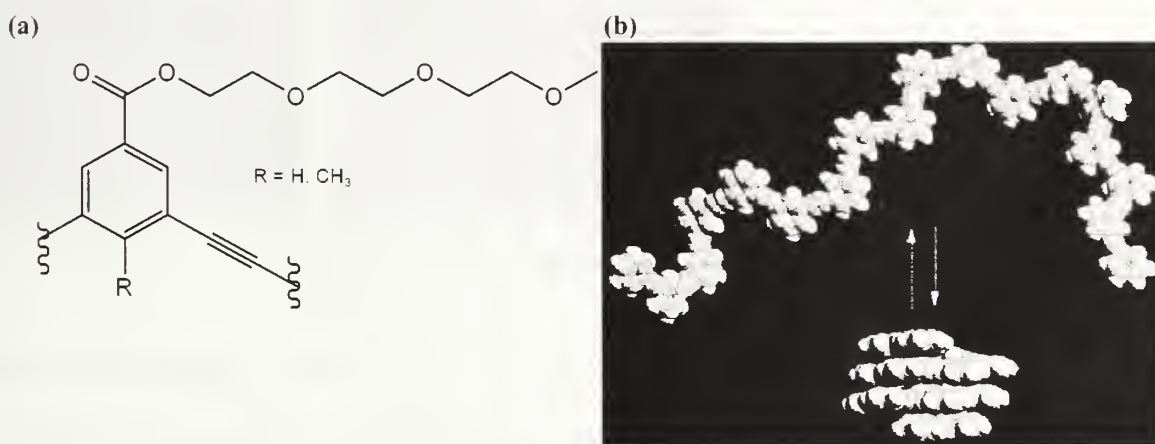


Figure 1.7: (a) Basic *meta* Phenylene Ethynylene (mPE) oligomer unit (b) Extended and folded helical structure of mPE oligomer. Taken from reference (2).

1.2 *ortho* Phenylene Ethynylene Oligomers

We propose the synthesis and characterization of a new backbone to add to the AC family, *ortho* Phenylene Ethynylenes (oPE). These backbones, shown in Figure 1.8, will add to the current work in AC foldamers while offering the opportunity to explore new avenues that examine the nuances of these folding structures that until now, have not been fully characterized.

The crystal structure shown in Figure 1.8 was reported by Grubbs and Kratz in 1993 when they synthesized a series of unsubstituted (oPE) oligomers of lengths three to nine (39). These oligomers were created to 1) study the possible formation of one-dimensional conductors as graphite like strands that would be formed from the cyclization of this system, 2) study possible helical conformations of the system, and 3) use as model compounds to study optical and electroactive properties of the corresponding polymers.

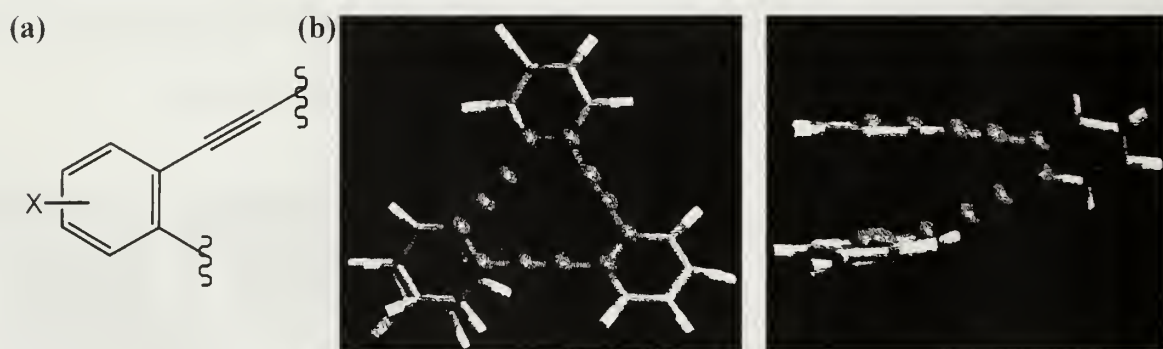


Figure 1.8: (a) Basic oPE repeat unit (b) Top and side views of crystal structure of unsubstituted oPE backbone.

To date there has been very little published work that uses the oPE oligomer as a foldamer in the same manner that mPEs and other foldameric backbones have been used. The early papers that exist containing open oligomeric oPEs did not show regularly substituted aryl rings (40, 41). This could be due in part, to synthetic

constraints. With the advances of the coupling reactions between acetylenes and halogens, we have been able to synthesize a variety of molecules to be assembled into oligomeric structures based on Sonogashira chemistry (42, 43). Other recent work by Bunz and coworkers has shown the synthesis and characterization of a dimethoxy substituted oPE.(44) Crystal structures of this oligomer were flat and extended contrary to findings by Grubbs.(39) A new and very exciting development is a microwave synthesis from Hecht that polymerizes the oPE backbone in situ, showing what appears to be no diyne defects.(45)

New scaffolds are necessary to probe the varying interactions that foldamers can experience. Using different structure isomers allows for the variation of scaffolds to provide the opportunity to create secondary structures with very distinct characteristics. If we examine a hockey puck and a pencil, they are fundamentally the same shape-cylinders. Upon further examination, the characteristics of these secondary structures, though they are the same shape, are vitally different. If we take a ribbon with the same diameter and wrap it around each cylinder as shown in the Figure 1.9, a variety of characteristics would be different depending on the ribbons characteristics or pendants. Host-guest interactions through the center of the wider circumference cylinder would allow for the accommodation of large molecules, possibly aromatic or cyclic structures. Host-guest interactions through the center of the smaller circumference cylinder might be limited, if they even occur at all.

A pencil would allow for a motif to appear a larger number of times concentrated in regions of the outer perimeter of the cylinder. A puck would only allow a motif to appear a few times per region, spreading the motif to a wider circle of targets.

The puck would allow wide unfocused targeting versus the pencil's concentrated or focused targeting. In addition, the conformational limits placed on an oPE may promote helices at much shorter oligomer lengths.

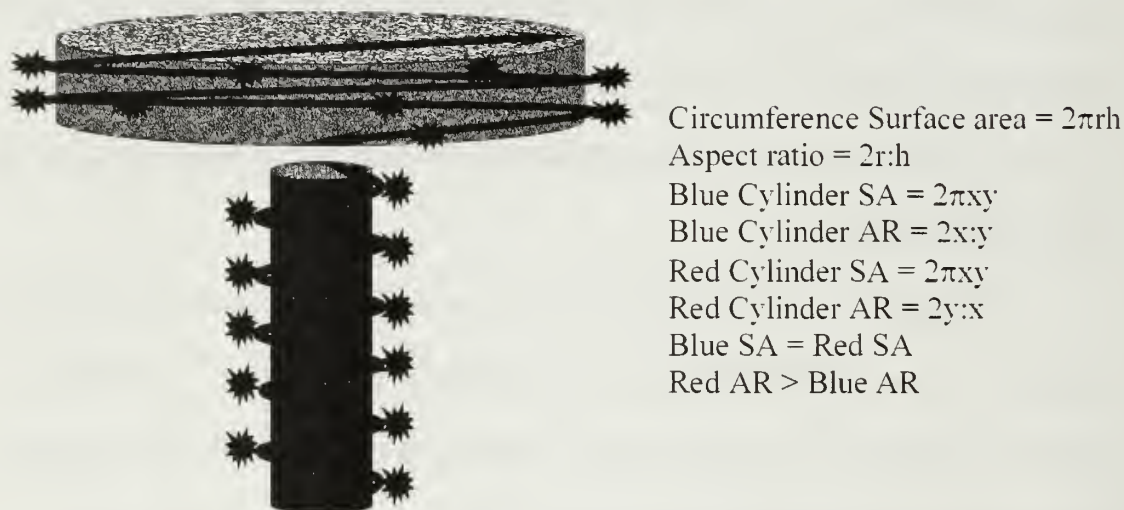


Figure 1.9: Illustration of aspect ratio differences. The radius of the blue figure is equal to the height dimension of the red figure. The radius of the red figure is equal to the height of the blue figure. Given these parameters the surface area of these two figures is equivalent but the aspect ratio of the figures is different.

Finally, our ultimate goal is to be able to pattern these oPE oligomers in a fashion that would allow us to create facially amphiphilic structures and tertiary bundles as shown in Figure 10. If we are successful with this endeavor, this effort would mark the first controlled abiotic assembly of tertiary structure from a discrete macromolecule to a tertiary structure. Though we are pioneering new ground with these scaffolds we believe they will prove to be versatile macromolecules.

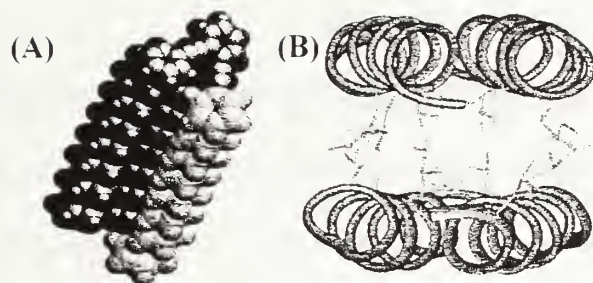


Figure 1.10: (A) Amphiphilic oPE oligomer. Green represents aryl rings that would be substituted with non-polar substituents. Blue aryl rings would be substituted with polar substituents. (B) Lac repressor protein as a self-assembled helical bundle. Non polar Isoleucine groups are pointed towards the center of the structure.

1.3 Scope of the Thesis

The work reported here is an extended exploration into the synthesis of *ortho* Phenylene Ethynylene oligomers and the determination of their propensity for folding into secondary helical structures by varying side chain composition, solvent composition, and temperature variation using a variety of characterization techniques including UV, fluorescence, crystallography, and most prominently, NMR.

As this is the first reported synthesis of long chain substituted oPE oligomers, Chapter 2 will focus on the synthesis of these systems and include a discussion of the challenges related to oPE synthesis. Chapter 3 chronicles the characterization of non polar (NP) oPEs in the quest to observe secondary helical structure as induced through solvophobic interaction. Though there were small successes with the NP systems, a change in approach was made to create a greater contrast between the side chain and the phenyl backbone. The new polar tri ethylene glycol side chain was introduced and

explored in chapters 4-6. Chapter 4 examines solvent induced folding in very short 4 unit oPEs as observed by 1-D and 2-D NMR. The effect of backbone electronics on these very short systems is also observed.

Chapter 5 explores the impact of increasing the length of one set of electron poor oPEs to 9 units and determining whether these structures a) become completely helical, upon solvent change b) are responsive to a wide range of temperatures and c) increase in folded stability as length increases. Chapter 6 returns to the issue of backbone electronics at longer oligomer lengths to determine the folding and stability of π -rich versus π -poor versus π -poor/rich systems. In addition, issues of whether the oPEs completely unfold or simply "breathe" like a macromolecular spring will be discussed. Finally Chapter 7 details all of the synthetic work for the oligomers characterized in this thesis.

CHAPTER 2

SYNTHESIS OF NEW SUBSTITUTED *ORTHO* PHENYLENE ETHYNYLENES

2.1 Introduction

The work presented here represents the first published/known synthesis of substituted *o*PE oligomers in the literature and the elaboration of these oligomers to form a variety of chain lengths, compositions, and side-chain variations.(42, 43, 46, 47). The few known syntheses of open *o*PE oligomers have been unsubstituted and of lengths up to 9 units.(39-41, 44, 48) Side chains have often been added to a variety of PE systems to increase polymerization length or to enhance the properties of the systems for electronic/sensor systems (49, 50).

The reason for this lack of molecules with an *ortho* backbone can be attributed to a number of synthetic challenges that are unique to the *ortho* substitution. The selective reactivity of *ortho* sites and the likelihood that the sites that are orthogonal to one another will prevent or inhibit the transformation of the other sites is a very real possibility. There are a number of reactions published that show the cyclization of groups orthogonal to one another on a benzene ring. Haley and coworkers have shown the formation of 5 unit or 6 unit heterocycles cyclized from a *ortho* triazene and acetylene linkages at high temperatures (51-53), while Tour has shown the formation of polynaphthalenes from *ortho* dialkynylbenzenes.(54) Earlier work with *o*PE oligomers discussed difficulties using Sonogashira methods but the synthetic methodology found here, using tri-substituted aryl rings, takes advantage of known and fairly recently developed chemistry. These methods have been reported in good to excellent yield for a variety of compositions that vary both the electronic composition of the oligomers and

the polarity of the side chains. Though the synthesis of these substituted oPEs was ultimately successful, there were a number of hurdles along the way. Through this synthesis chapter, the synthetic strategy as well as the challenges that were met and overcome will be discussed. Specific synthesis conditions can be found in Chapter 7.

2.2 Synthetic Methodology- Goals and Challenges

The original goal for this project was to build a long chain, amphiphilic, di-substituted oPE moiety like that shown in Figure 2.1. Blue represents rings with charged (preferably cationic) side chains while green represents rings with non-polar substituents. Initially, the target was a di-substituted oligomer like that shown in Figure 2.1b. This molecule would have a variety of substitutions, the most sought after would have cationic groups on two of the rings in the three ring repeat pattern (blue), and a non-polar substituents on the remaining ring (green). Other synthetic work in the group (55, 56) had shown the viability of a Boc-protected amine as a side-chain for mPE oligomers and polymers, the hope was that the same would hold for oPEs.

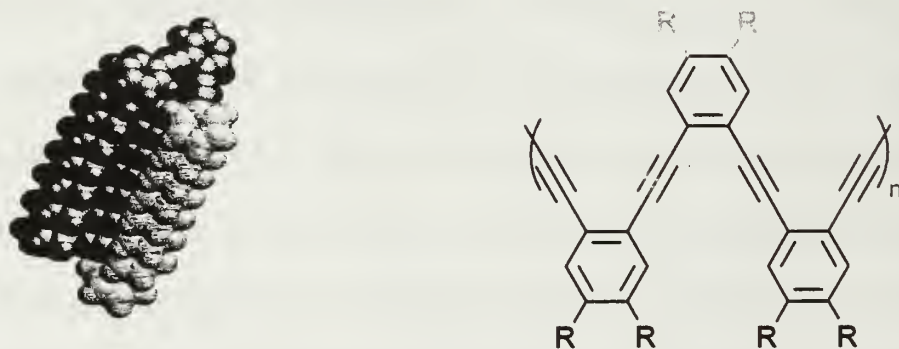


**Figure 2.1 Long chain amphiphilic oPE oligomer and disubstituted oligomer
Green = non polar substituents. Blue = polar substituents.**

The first challenge was in creating a di-substituted oligomer. A simple dialkylation using Mitsunobu condition with the diphenol and a simple alcohol did not

react. Figure 2.2 shows that the final reaction conditions for alkylation of catechol (di-iodo or otherwise) using potassium carbonate (K_2CO_3), dimethyl sulfoxide (DMSO), and a brominated alkyl at $110^\circ C$. While success was found iodinating (and isolating) the di-iodo alkylated (Figure 2.2c) compounds with mercury based conditions, replacing the iodines with trimethylsilyl (TMS) acetylene groups proved to be challenging (Figure 2.2 d1 and d2). Initially the reaction never went to full completion, there was always a mixture of products that included the un-substituted, mono-substituted, and di-substituted products. Adding a large excess of TMS acetylene (4 equivalents) eliminated all of the un-substituted product, but yields for the mono-substituted compounds were never above 40%. The challenge purifying the TMS substituted compounds was due to the minimal polarity difference between the TMS and iodide groups. Differentiating between the un-substituted, mono-substituted, and di-substituted for purification by column chromatography proved to be difficult for the polar versions of these oligomers. To alleviate this difficulty in purification a new acetylene with a hydroxyl group was used, 2-methyl-3-butynyl-2-ol, or mebynol, and provided enough contrast in polarity to purify these compounds. The conditions required for deprotection were potassium hydroxide (KOH) in toluene at $80^\circ C$ for 2 hours. While this reaction worked relatively well, the yield was always below 60%.

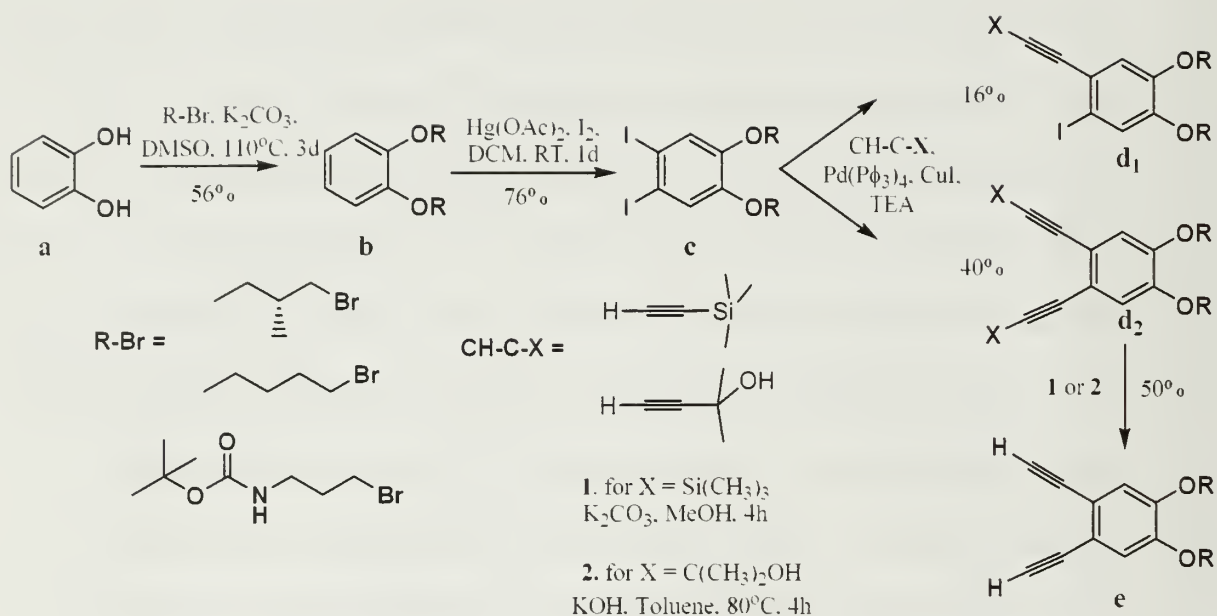


Figure 2.2 Synthesis scheme for di-substituted alkoxy oPE monomers.

Once these compounds were purified and reacted with a terminal iodine in a typical Sonogashira reaction (Figure 2.3), isolation of the desired product (Figure 2.3f) away from the side reactions was also a challenge. This time the additional products came about due to diacetylene head-to-head coupling that could take place as shown in Figure 2.3 (g & h). This challenge will arise again in subsequent syntheses.

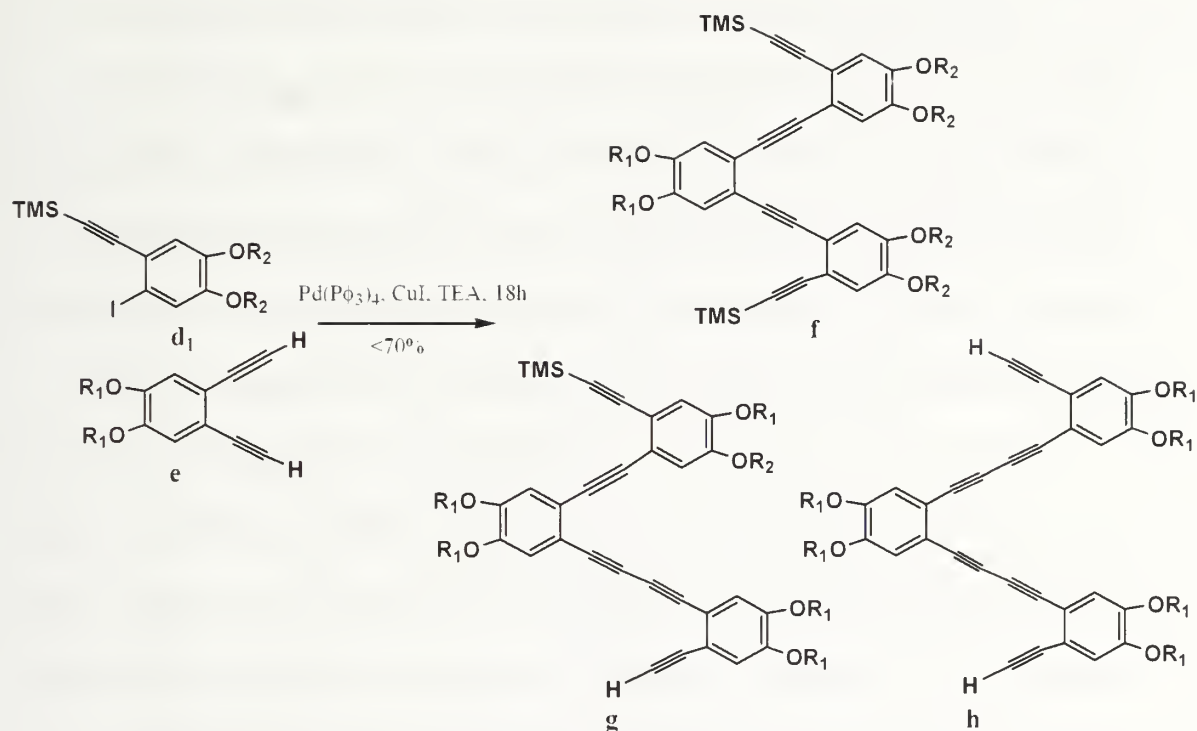


Figure 2.3: Disubstituted synthesis, mixed products including head-to-head diacetylene coupling.

Ultimately the di-substituted synthesis was eliminated as a viable way to build long chain oPE oligomers due to the challenges in purification and synthesis, and low yields. A new synthetic strategy involving mono-substituted oPE was employed.

2.3 Synthesis of Non-polar alkoxy-substituted oPEs

The new synthetic strategy, shown in Figure 2.4, utilized all three reactive handles of a commercially available 3-nitro-4-iodo-phenol to create a mono-substituted, AB protected monomer. This monomer was essential to the oligomer synthesis: from it, activation of the B portion or deprotection of the A portion is possible without altering the other substituents. In addition, to cut costs, the 3-nitro-4-iodo-phenol is synthetically accessible using a Sandmeyer reaction to iodinate the 4 position from a 3-nitro-4-amino-phenol.

The new target molecules incorporated a chiral S-methyl-butoxy group to facilitate the study of potential helical conformations or chiral aggregates of the resulting oligomers. Other abiotic foldameric systems in the literature, especially *meta* Phenylene Ethynylene systems studied by Moore (30) and larger chiral aggregates studied by Meijer (57) utilized chiral side chains to facilitate study of the oligomers by Circular Dichroism spectroscopy; more on this topic will be discussed in Chapter 3.

The synthesis of the monomer **1** is notable for the reduction of the nitro group in the presence of the aryl iodide.(58) In our hands, the traditional method for reducing the nitro compound (SnCl_2) also reduced the aryl iodide, but alternate conditions gave excellent yield. Formation of the triazene from aniline **3** using a modified Sandmeyer reaction to trap the azide with diethylamine requires vigorous mixing and dark conditions to achieve high yield. The orthogonally protected **1** yields the two fundamental starting materials for stepwise oligomer synthesis in separate steps shown in Figure 2.4. Despite the *ortho* proximity of the triazene and acetylene, the overall synthesis of **1** proceeds in moderate yield.(59-62)

It should also be noted that in particular, two products of these reactions should always be used immediately (upon purification) for the next reaction. All anilines and free acetylenes proved to be relatively unstable for long periods of time (more than 1 or 2 days). The anilines are slightly more stable in solution, but will turn to black goo if evaporated and left (even in the refrigerator) for more than 24 hours. The free acetylenes have a tendency to begin head-to-head coupling if left for too long, rendering them useless for the next reaction. Overall, the other products tend to be stable for long periods either refrigerated or at RT under foil.

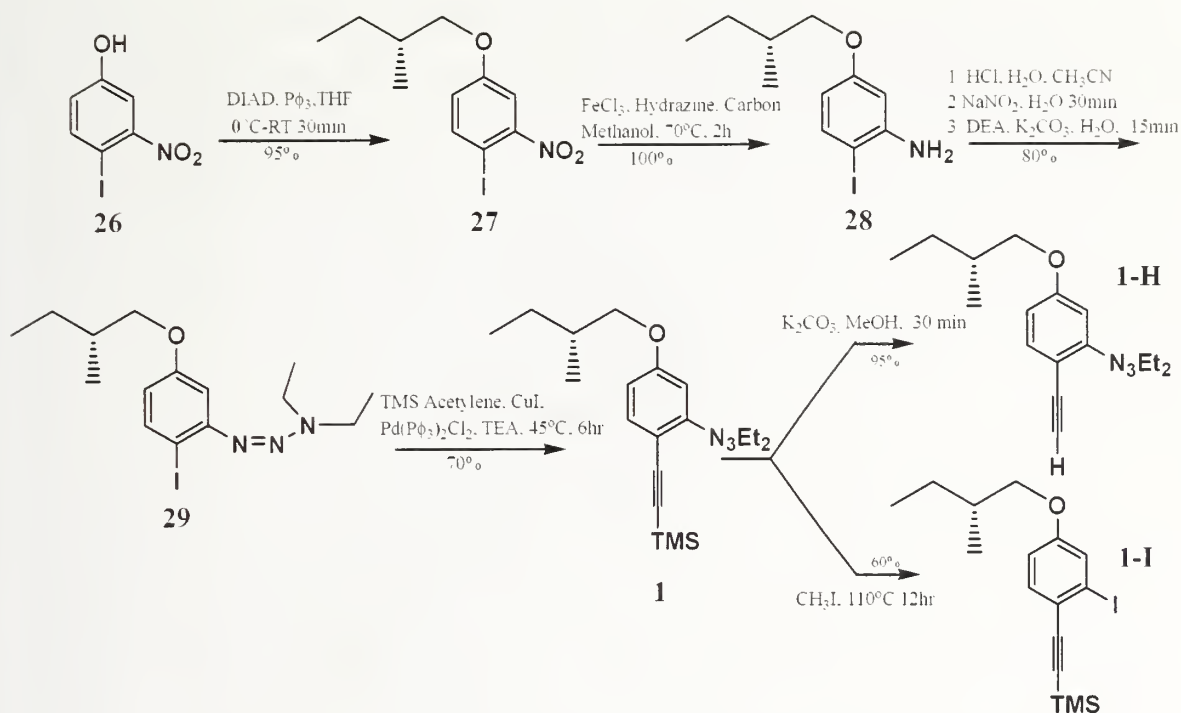


Figure 2.4 Synthetic scheme for Non-Polar Monomer

A labeled ^1H NMR spectrum showing the AB monomer **1** can be found in Figure 2.5. The transformation from **26** to **1** can be followed with relative ease. The protons for the ring are easily assignable based on their characteristic splitting pattern where the *a* proton is split into a wide doublet by the proton *ortho* to it ($J = 8.4$ Hz), the *b* proton is split into a narrow doublet by the proton *meta* to it ($J = 2.2$ Hz), and the *c* proton is split into a doublet of doublets by the *a* and *b* protons that are *ortho* and *meta* to it ($J = 8.4$ Hz and 2.2 Hz). The methyl and methylene protons of the triazene (h and i respectively) group are located directly under the signal for the methylene directly next to the alkoxy group (d) and the signal for the two methyl groups on the alkoxy side chain (f and g). Splitting patterns and integration make these distinguishable from one another.

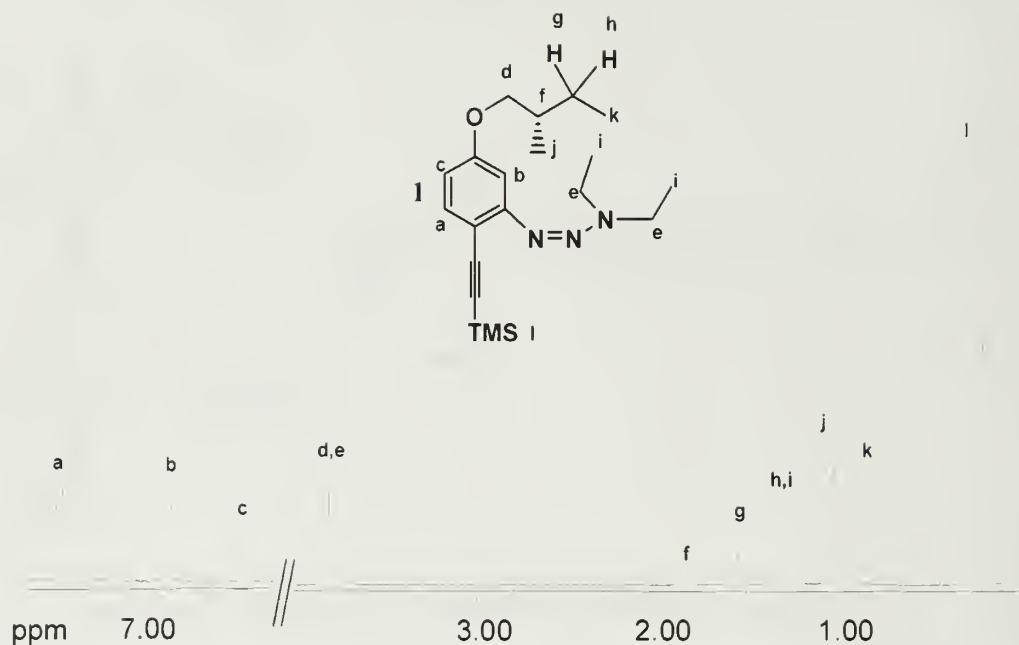


Figure 2.5: ^1H NMR spectra for AB monomer **1**

The oligomer synthesis, after the production of pivotal monomer **1**, follows a cycle of acetylene deprotection, triazene activation, and Sonogashira coupling (Figure 2.5 to produce dimer **2**, trimer **3**, and tetramer **4**. Convergent coupling of appropriate trimer molecules (**3-H** and **3-I**) produces hexamer **6**. Coupling **6-H** with an additional **3-I** yields nonamer **7**. An additional dodecamer was synthesized by convergent coupling of **6-H** and **6-I** (not shown), but due an impurity of head-to-head coupling of **6-H** with **6-H** this compound was not purifiable.

Elaboration of the monomer to produce a series of oligomers was carried out in satisfactory yield. The non-polar ether side chain, *ortho*-acetylene moieties and the TMS protecting group are easily able to withstand the triazene deprotection conditions

which were found to be methyl iodide (CH_3I) at 110°C for 12 h. Moreover, the key deprotection, activation, and coupling steps are not hindered by sterics related to ortho-substitution.

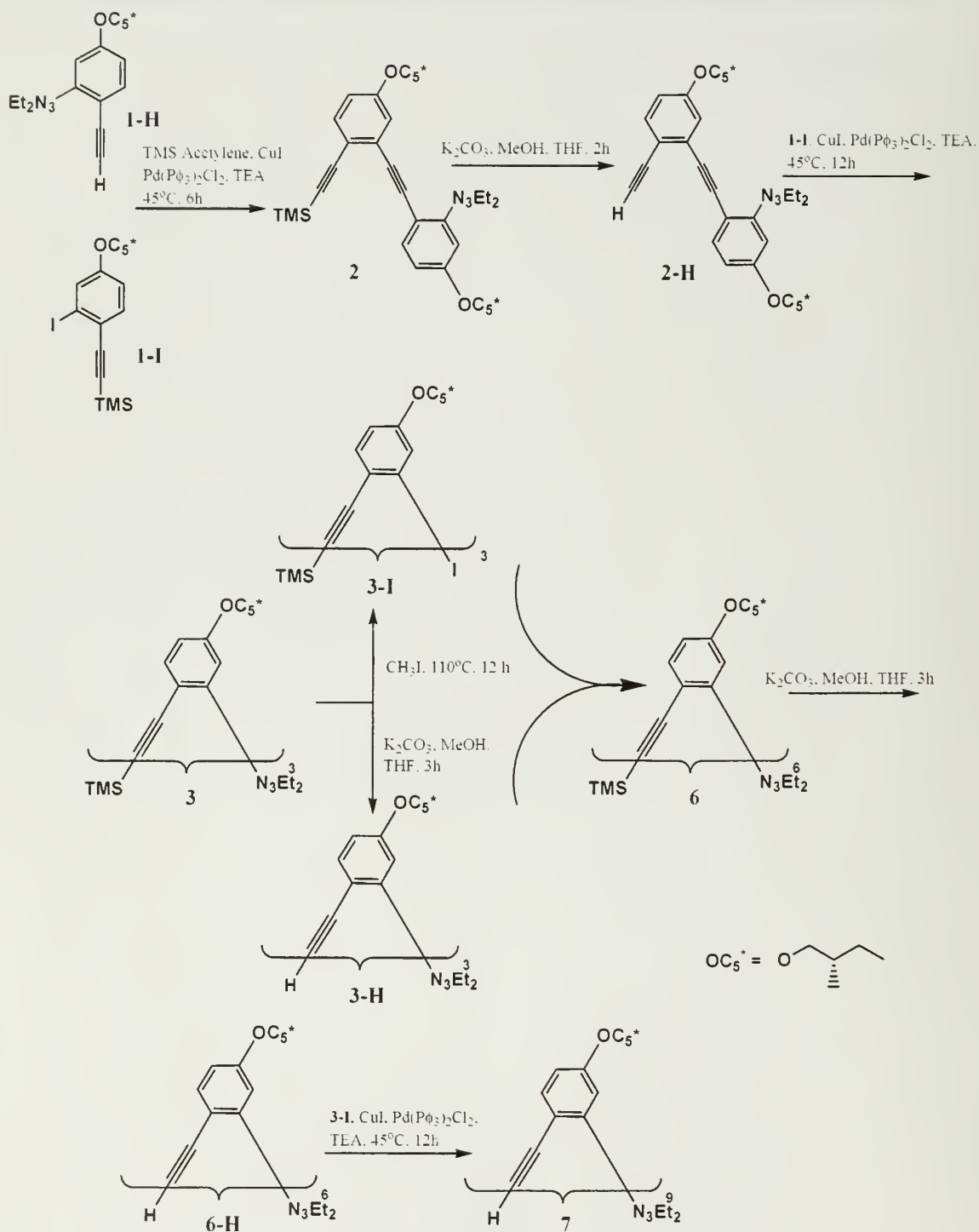


Figure 2.6 Synthetic scheme for Non-Polar oligomer synthesis

All oligomers **1-7**. are soluble in common organic solvents including THF, ethyl acetate, chloroform, and hexanes. ^1H NMR data for compounds **3**, **4**, and **6** show excellent resolution even in the aryl region of the hexamer: all aryl resonances are assignable at 300MHz in chloroform (CHCl_3) (Figure 2.6). This clarity and resolution will be essential to data collection and analysis in subsequent discussions. Table 2.1 shows the oPE oligomers synthesized with the non-polar chiral alkoxy side chain.

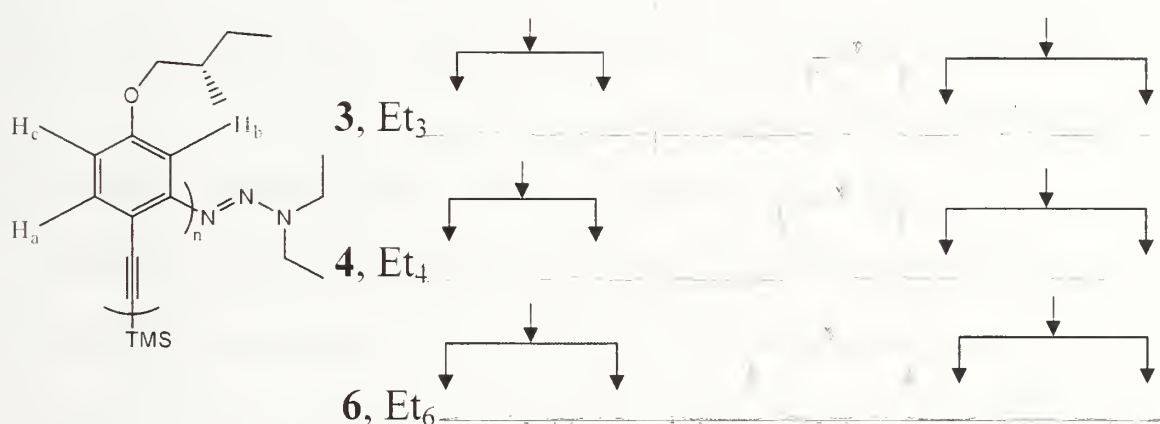


Figure 2.7: Sample NMRs region for oligomers **3**, **4**, and **6**

Table 2.1 Synthesized Non-Polar Alkoxy Oligomers

Non Polar Side-Chains				
#	Backbone	Oligomer Sequence and (Length)	Sidechain	MW
2	Ether	Et ₂ (2)	C5 Chiral	545.83
3	Ether	Et ₃ (3)	C5 Chiral	732.08
4	Ether	Et ₄ (4)	C5 Chiral	918.33
6	Ether	Et ₆ (6)	C5 Chiral	1290.83
7	Ether	Et ₉ (9)	C5 Chiral	1849.58

2.4 Synthesis of polar alkoxy substituted oPEs

There were a number of challenges that came about for the synthesis of polar substituted ether and ester substituted oligomers. The initial hope was to create a polar and cationically charged monomer from a Boc-protected ethyl ether to make create amine functionality on each oligomer. Unfortunately this was not possible due to the harshness of the triazene activation with methyl iodide at 110°C. This reaction produced acidic conditions that (at the very least) deprotected the amine and gave a messy product. Other protecting groups for the amine were attempted but all failed to withstand the methyl iodide reaction.

In place of the charged group, a tri-ethylene glycol monomethyl ether (TEG) polar side chain was utilized (Figure 2.8). This side chain would prove to be most robust and effective for the studies of oPE as a folded compound, due to the contrast in polarity between the side-chain and the backbone. Additional synthetic challenges for this molecule occurred with regard to purification. For purification purposes, the difference between compound **30** and the byproducts of the Mitsunobu reaction (the DIAD adduct and triphenylphosphine-oxide in particular) were a little challenging to remove from the product. Careful column chromatography in 45% EtOAc, 45% Hexanes, 10% DCM was able to isolate the product in relatively high yield.

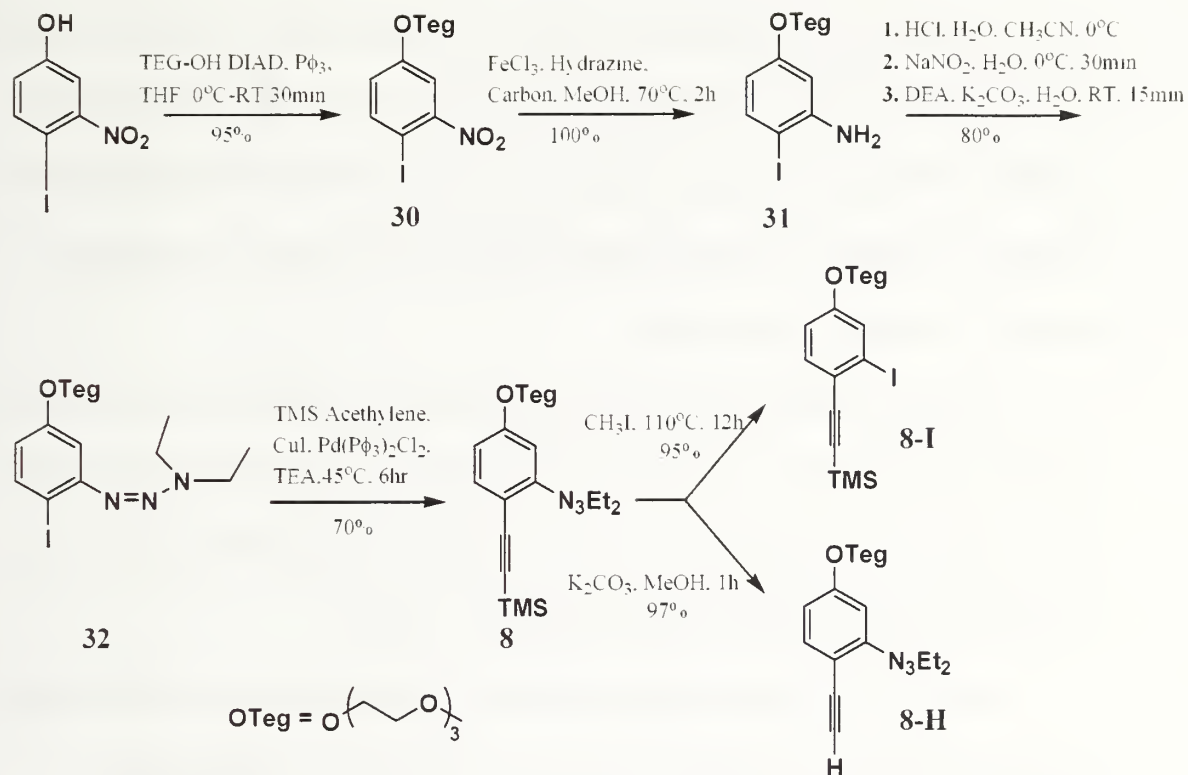


Figure 2.8 Synthesis scheme for alkoxy-TEG substituted monomer

Other challenges with this synthesis included the isolation of compound **8**, the AB protected monomer, from the iodinated precursor, **32**. If the reaction was not pushed to completion, the R_f difference between these two compounds is minimal. The same could be said of compounds **8-H** and **8-I** as compared to compound **8**. Careful co-spotting for reactant and product is not enough to tell the difference between a 100% complete conversion and a 90% conversion, and thus *conversion of reactant to product should be checked by NMR*.

Originally, a hydroxyl substituted acetylene (mebyinol) was used for the creation of monomer **8** to increase the R_f difference between **32** and **8**. Unfortunately this hydroxyl protecting group required harsh deprotection procedures (KOH, Toluene, 90°C, 12h) that would not work for the ester-Teg compounds. Additionally, the

mebynol protected compound did not perform well during the activation of the triazene at 110°C in methyl iodide. The decision was made to return to the TMS protecting group for the acetylene for its ease of synthesis and simple removal with potassium carbonate in methanol. Aside from these challenges, the synthesis of compound **8** proceeds in moderate to good yield.

Labeled ^1H NMR spectra showing the transformation from **30** to **8**, **8-H**, and **8-I** can be found in Figure 2.9. It should be noted that the transformation can be followed with relative ease. The exception is the location of the methylene from the triazene, which is buried under the alkoxy region between 3 – 4ppm

Figure 2.10 shows the synthetic scheme for oligomerization of the TEG alkoxy substituted oligomers. It should be noted that care is taken to evade symmetric couplings to avoid the head-to-head coupling that can occur through the Sonogashira coupling. Symmetric couplings yield compounds that are virtually impossible to separate by column chromatography. Compound **9** is the exception to this argument for avoiding symmetric couplings as it is only achieved by adding **8-H** and **8-I**. Much success was made by rigorous exclusion of oxygen, the freeze-pump-thawing of a stock solvent mixture to be used only for the Sonogashira coupling. Additional challenges for this synthesis include a decrease in solubility in Triethylamine (TEA) as oligomer length increases. To resolve this issue, THF was introduced as a co-solvent typically in a 1:1 ratio. Teg-alkoxy substituted oligomers of up to length $n = 6$ have been synthesized and characterized for further study as folding oligomers. Table 2.2 shows the synthesized oligomers with Teg-alkoxy side chains including their molecular weights.

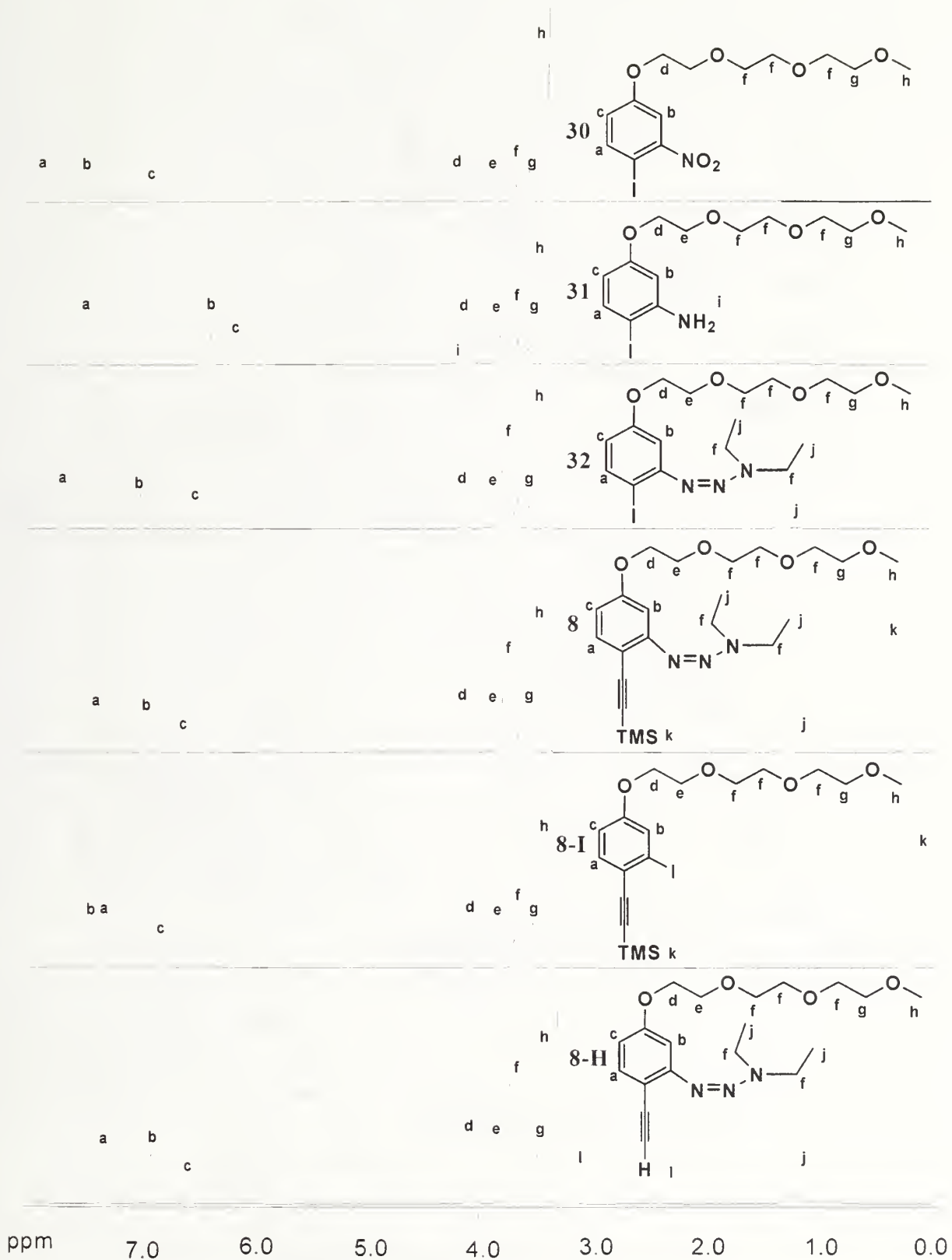


Figure 2.9 ^1H NMR traces for oligomers 30 through 8-H

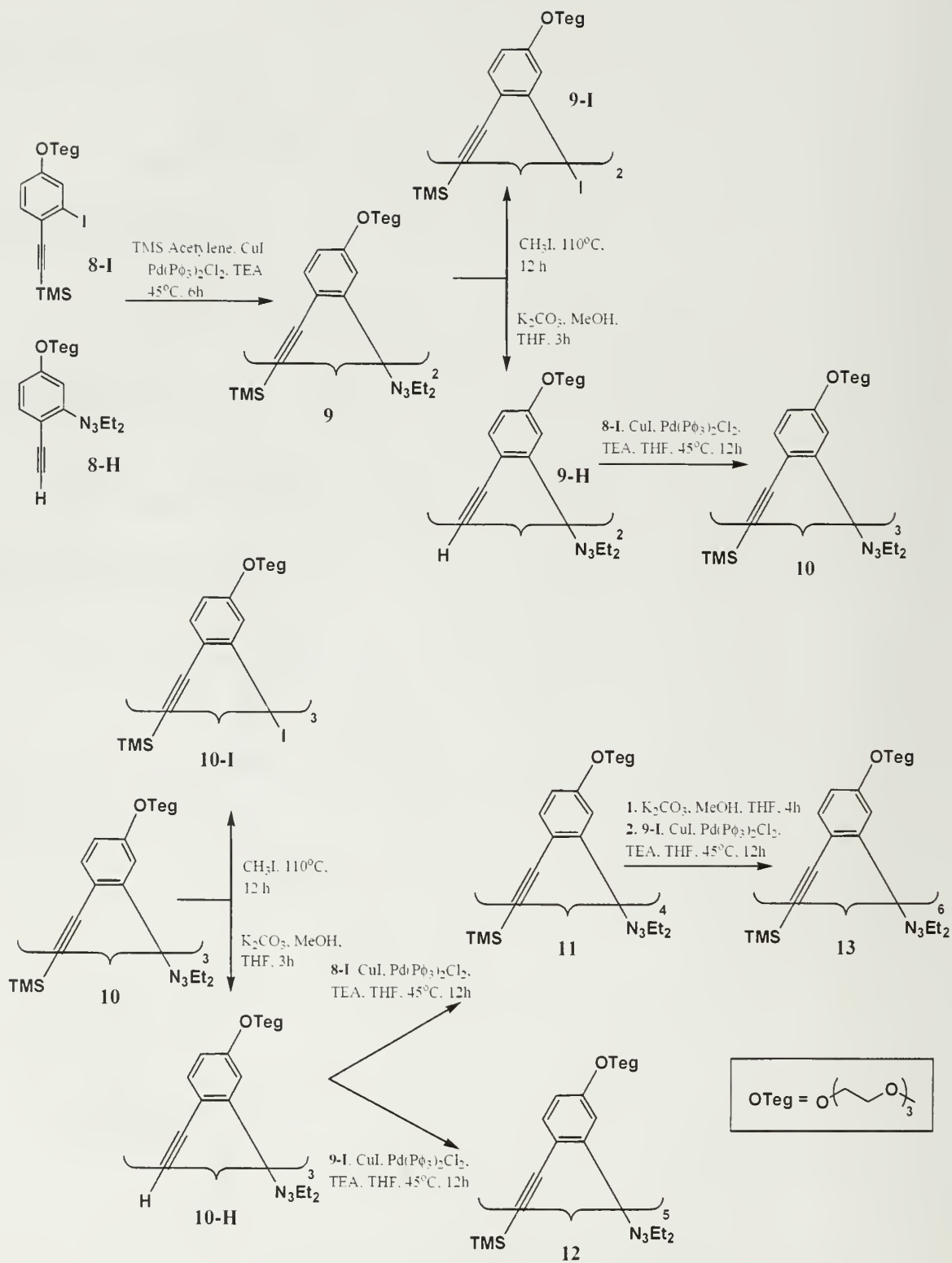


Figure 2.10 Synthetic scheme for Teg-alkoxy oligomers

Table 2.2: Teg-alkoxy oligomers synthesized

Polar Side-Chains				
#	Backbone	Oligomer Sequence and (Length)	Sidechain	MW
9	Ether	Et ₂ (2)	TEG	697.51
10	Ether	Et ₃ (3)	TEG	959.76
11	Ether	Et ₄ (4)	TEG	1222.01
12	Ether	Et ₅ (5)	TEG	1484.26
13	Ether	Et ₆ (6)	TEG	1746.51

2.5 Synthesis of ester substituted oPE

The synthesis of the ester substituted AB monomer **14** in Figure 2.11 proved to be a bit more challenging initially, in part, due to the electron withdrawing nature of the molecule, which made certain transformations at the site para to the ester group for this molecule very slow. Initial attempts with this molecule focused on trying to transesterify the ethyl ester, but this method proved to be slow and inefficient. Distinguishing between the AB monomer **14** and precursor **36** was again difficult due to the minimal polarity difference between TMS and iodide at the same position. This is similar to what occurred with the Teg-alkoxy molecules: the starting material and product smear into one spot on the TLC plate. *¹H NMR is again very useful for distinguishing completion of the reaction.*

An added element of complexity for these systems is the rate at which the transformation from **14** to **14-I** occurs. Our initial attempts at making this molecule with only distilled CH₃I failed to produce a product similar to the product that was obtained with relative ease for compound **8-I**. It was found that the addition of a catalytic amount of I₂ (5%) was required for this reaction to occur, and then, it was still

a matter of a week or more to complete the transformation as it was monitored by NMR. This extended time could be explained by the nature of this system as it compares to the ether substituted system. Here the triazene moiety that we seek to activate is *para* to the electron withdrawing ester group. Basic principles of electrophilic aromatic substitution indicate that substitutions and transformations involving the electron withdrawing groups (in this case, the ester) usually give the highest yields when the transformation site is *meta* to the substituents electron withdrawing group. In this case, the transformation site where we would like to substitute the triazene with an iodine is *para* to the ester. Given that this starting triazene is similar to what is found in a basic Sandmeyer reaction, even though the mechanism is not known, it would be reasonable to think that the transformation is slower in this case due to the presence of the ester in the *para* position. This could account for the extended time required to activate the triazene to an iodide. This timeframe was radically reduced by using microwave assisted synthesis. By adding compound **14** to a reaction mixture including 5-10% I₂, x mol CH₃I and microwaving at 150°C, reaction time was reduced from nearly 1 week to 1 hour in excellent yield. This advancement greatly improved our ability to synthesize longer oligomers with the Teg-ester substitution.

The final challenge with the Teg-ester monomer and oligomers was that of the TMS deprotection. Our initial efforts, using the same conditions for the Teg-alkoxy oligomers (K₂CO₃ in MeOH), gave TLCs with 5 spots of varying R_f when there should have been one. This was duplicated for a number of molecules by a number of different researchers in the group. At present there is no explanation for the catastrophic failure

of this basic reaction. Initial efforts to replace this reaction yielded a procedure that utilized tetra butyl ammonium fluoride (TBAF) in THF. While this reaction was moderately successful, and very fast (5 min) it was difficult to control. Heating the compound to evaporate the THF for purification would often give a colorful mess. While a method that used hexane to dilute the reaction was utilized for a while, and was relatively successful, another method using potassium fluoride (KF-H₂O) in N,N dimethyl formamide (DMF), though slow (overnight) proved to be more reliable. Challenges with this procedure necessitate that all of the fluoride be removed: this appears to be accomplished fairly well with a wash in 5% CaCl₂ in water during the work up. Additionally, the product must be dried overnight to eliminate any residual DMF as this can inhibit the subsequent Sonogashira reaction.

Ultimately this set of oPE molecules has the most potential for relatively easy diversification due to the synthesis of the triazene/iodide/carboxylic acid molecule **35** in high yield. This molecule can then be esterified using EDC and DMAP to substitute at the carboxylic acid site. Labeled ¹H NMR spectra showing the transformation from **33** to **14**, **14-H**, and **14-I** can be found in Figure 2.12. It should be noted that the transformation can be followed with relative ease. The two exceptions are the location of the methylene from the triazene, which is buried under the alkoxy region between 3 – 4ppm, and the acetylene hydrogen of compound **14-H** which can also be hidden in the 3-3.2ppm region.

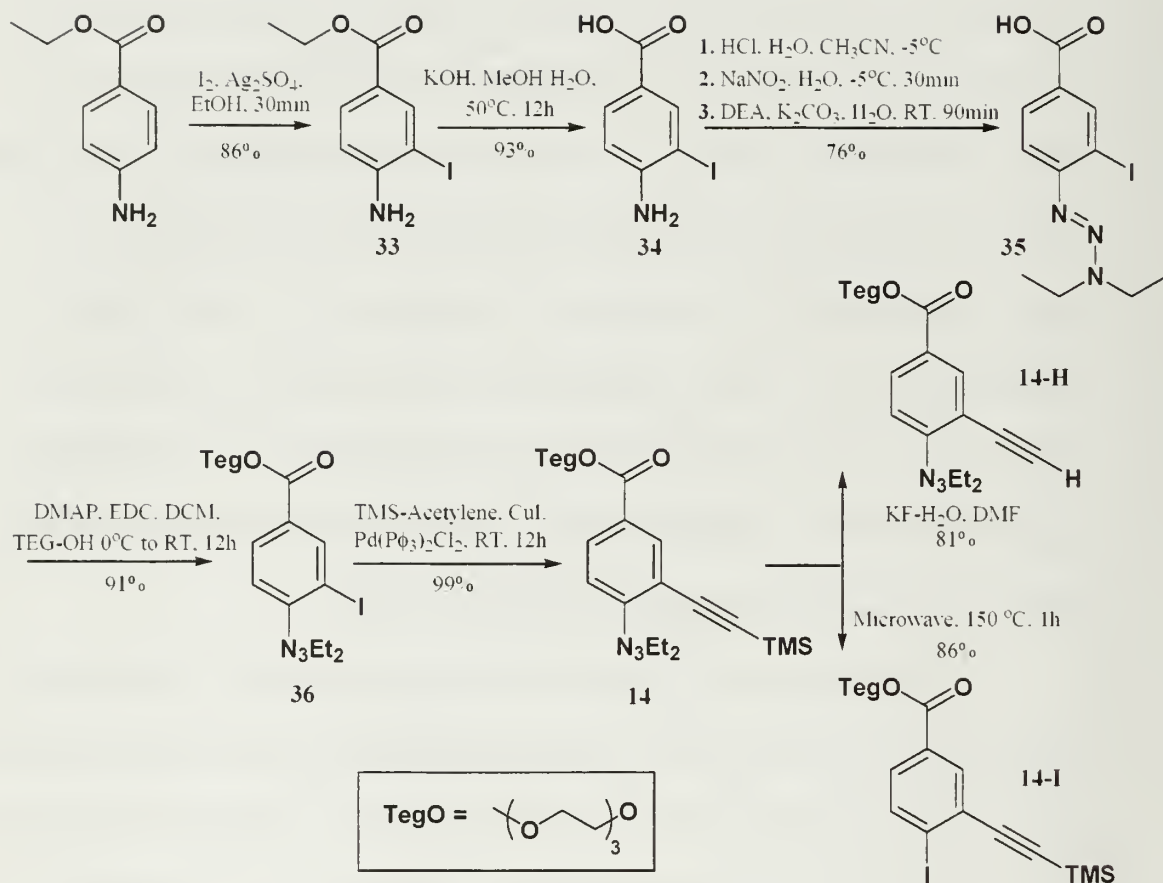


Figure 2.11 Synthetic scheme for Teg-Ester monomer

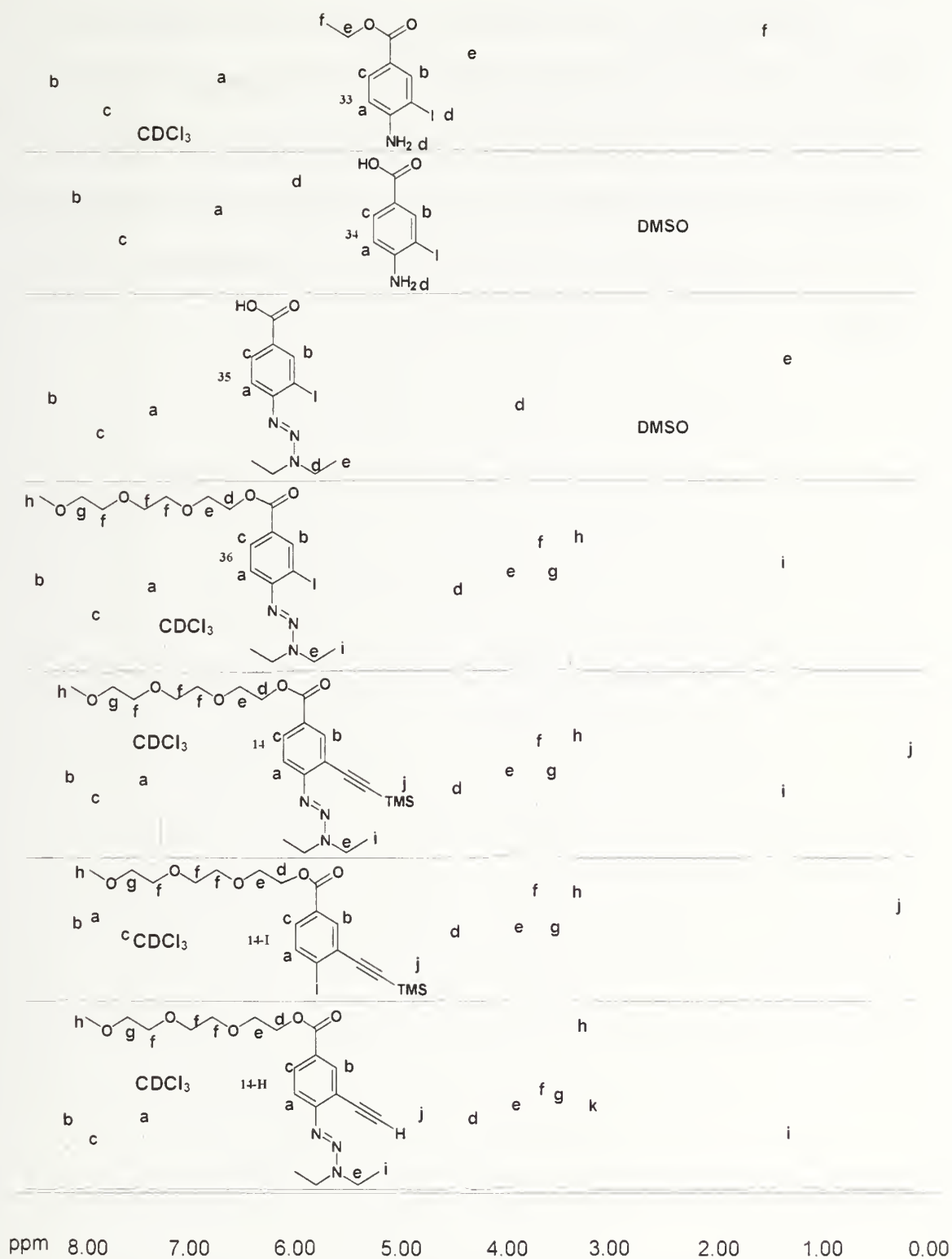


Figure 2.12 ^1H NMR spectra for ester monomer transformation

Oligomer synthesis for the Teg-ester system proceeded in moderate yield. Figure 2.10 shows the synthetic steps taken to lengthen this oligomer to a total of 9 units (molecule **21**). Fortunately the aryl regions of these oligomers proved to be relatively clear and deconvolutable up to 9 units. The ability to deconvolute the aryl regions these oligomers has been essential to the study of these oligomers as folded systems.

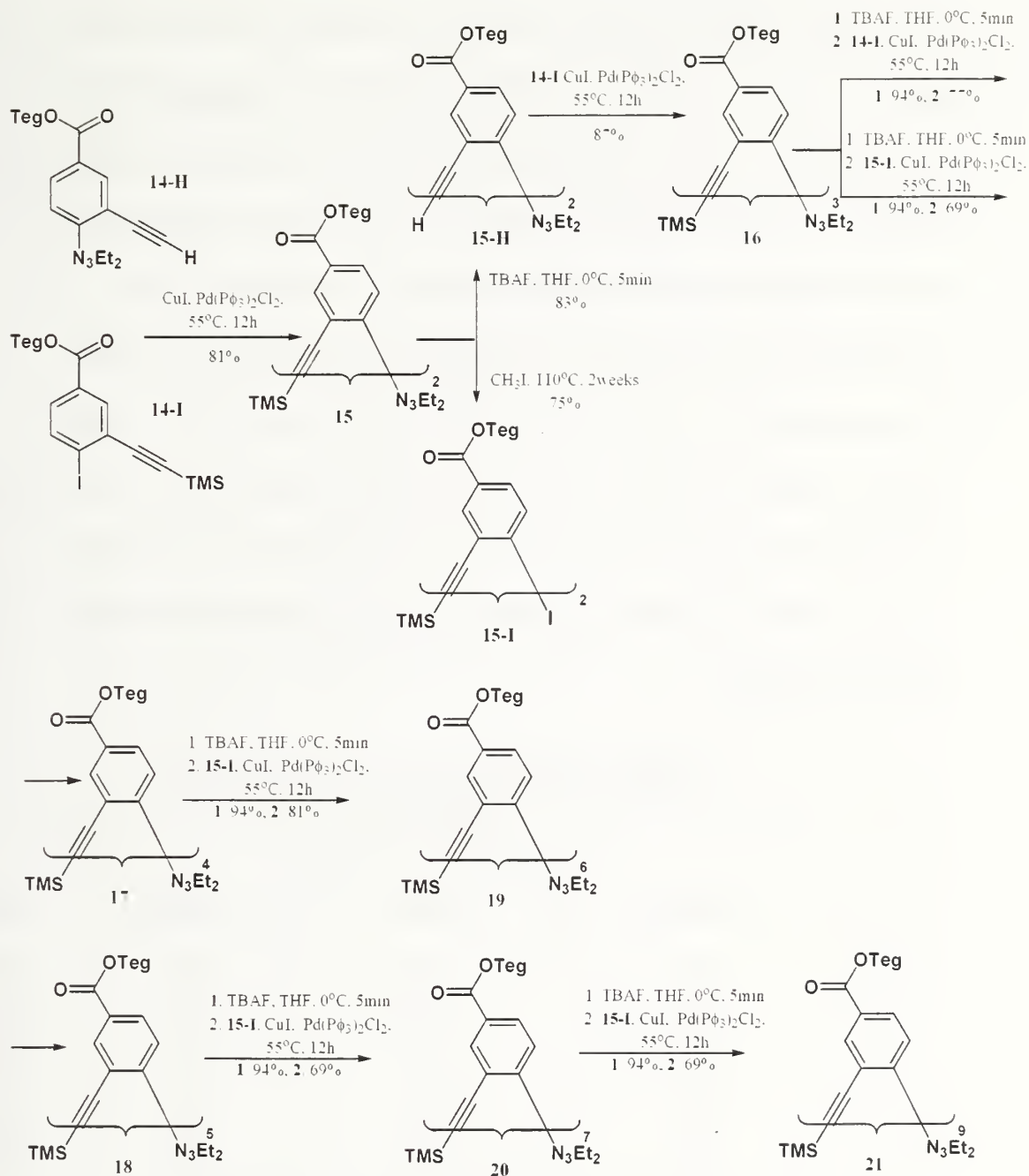


Figure 2.13: Synthetic scheme for Teg-ester oligomers

Our initial hope was to synthesize trimers, iodinate them and couple them with the free acetylene moieties, thus building the oligomers by units of three rather than one or two. The problem is that head to head coupling previously described occurs and thus

why it takes 3 extra steps to get to a hexamer instead of simply adding a trimer free acetylene and a trimer iodide. An additional problem with respect to the lengthening of oligomers for the Teg-ester systems is that the yield for creating the Teg-ester trimer iodide via microwave assisted synthesis gives an extremely low yield (<10%). By schlenk techniques the same yield was obtained over a number of weeks.

Unfortunately, it is not worth the effort to produce the trimer if it will simply decompose/degrade over the course of synthesizing the trimer iodide. Thus, the decision to make only dimer iodides (which proceed in approximately 1 hour with similar yield in microwave assisted reactions) was made, though it extends the synthesis. Table 2.3 shows the Teg-ester oPE oligomers synthesized and their molecular weights.

Table 2.3 Synthesized TEG-ester oligomers

Polar Side-Chains				
#	Backbone	Oligomer Sequence and (Length)	Sidechain	MW
15	Ester	ES ₂ (2)*	TEG	725.52
16	Ester	ES ₃ (3)*	TEG	1015.78
17	Ester	ES ₄ (4)*	TEG	1306.04
18	Ester	ES ₅ (5)*	TEG	1596.30
19	Ester	ES ₆ (6)*	TEG	1886.56
20	Ester	ES ₉ (9)*	TEG	2757.34

* Synthesized with Morris M. Slutsky and Jason Phillips

2.6 Mixed alkoxy-ester oPE systems

Finally, a series of oligomers that included both electron rich and electron poor moieties was synthesized to evaluate the effect of the electronic interactions on the folding and helical nature of the oPE oligomers. These systems build on the same basic

chemistry detailed previously in this chapter to couple electron rich alkoxy (Ether = Et) systems and electron poor ester (Ester = Es) systems as building blocks to create hetero oligomers. Three such systems were created and evaluated, a tetramer, pentamer, and hexamer (Figure 2.14). The effects of electronics on the folding of these systems will be discussed in Chapters 4 and 6.

The ^1H NMR data of the aryl region for these systems was particularly easy to deconvolute as the nature of the ester and ether systems was so radically different. Figure 2.15 shows an example of the aryl region for pentamer **22**. Table 2.4 shows the mixed oPE oligomers synthesized with their molecular weights.

Table 2.4 Synthesized Ester-Ether molecules with Teg side-chains

Polar Side-Chains				
#	Backbone	Oligomer Sequence and (Length)	Sidechain	MW
22	Ester-Ether	Es ₁ Et ₃ (4)	TEG	1022.34
23	Ester-Ether	Es ₂ Et ₃ (5)	TEG	1312.60
24	Ester-Ether	Es ₃ Et ₃ (6)	TEG	1602.86

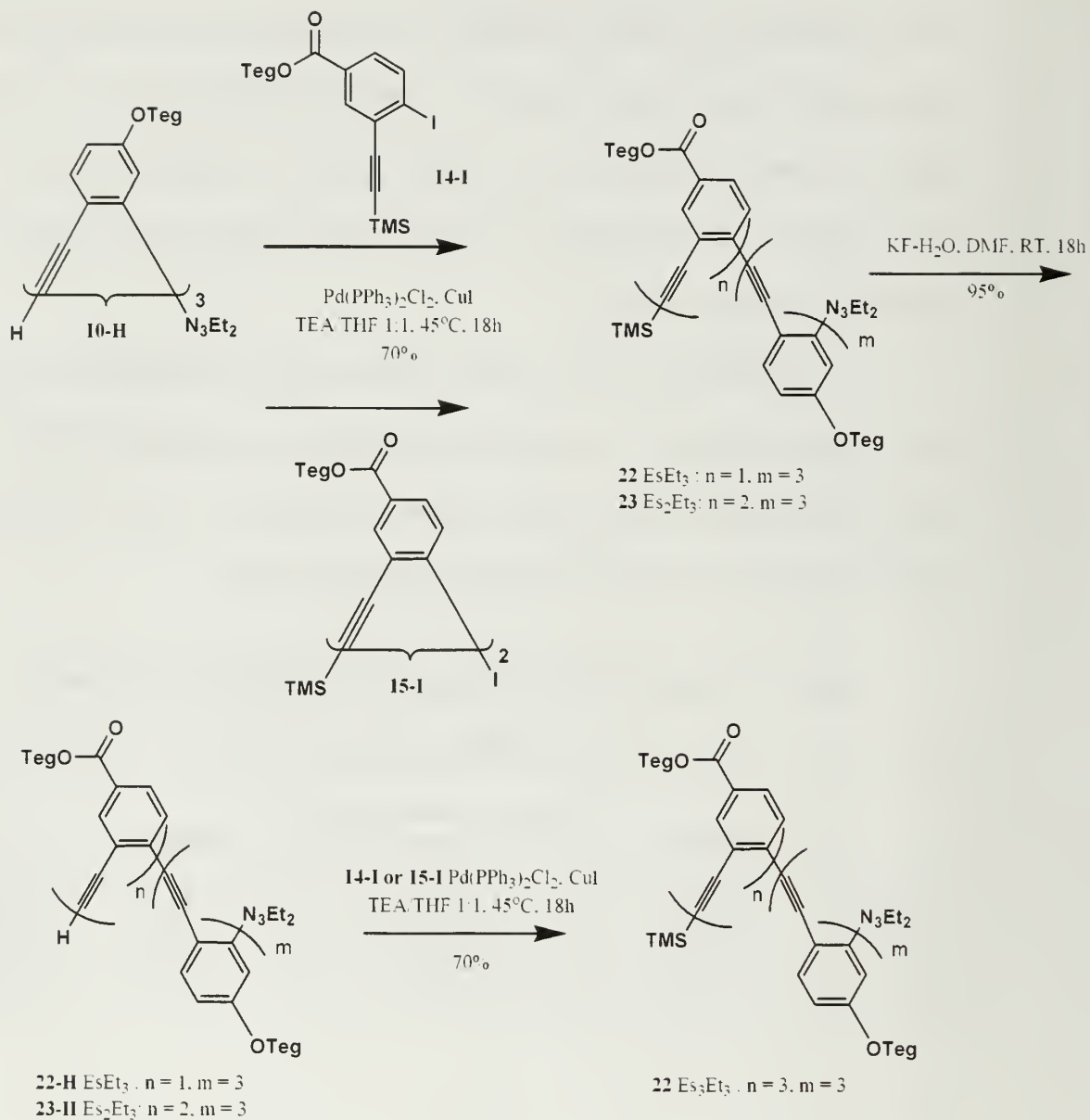


Figure 2.14 Synthetic scheme for Teg-ester/ether oligomers

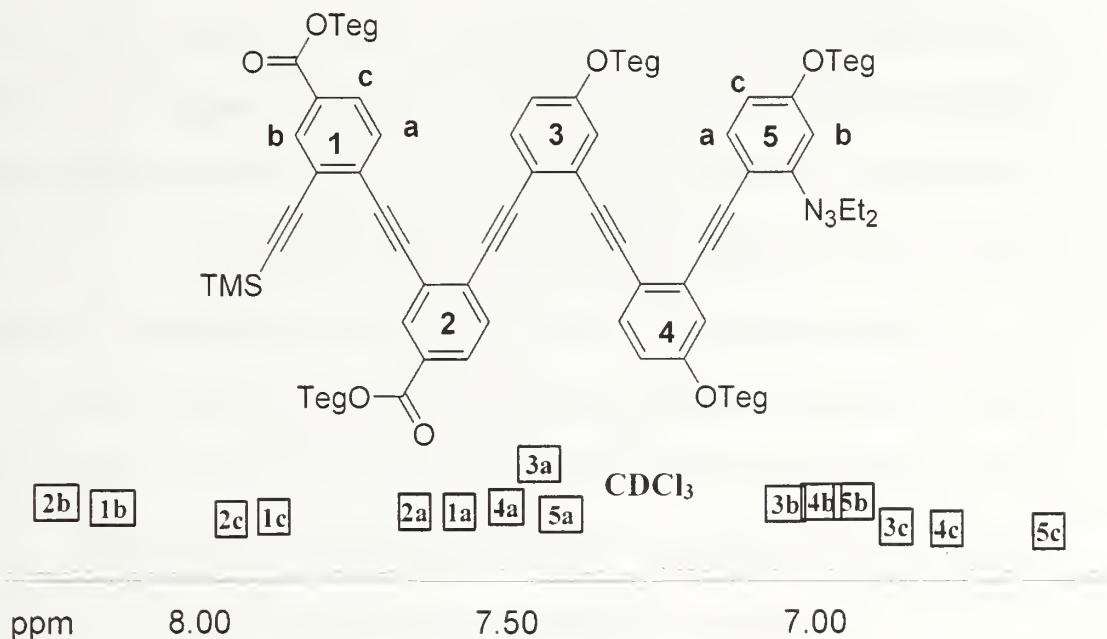


Figure 2.15 ^1H NMR of the aryl region of hetero oligomer 23 (Es_2Et_3)

2.7 Conclusions

A number of alkoxy and ester substituted *ortho* Phenylene Ethynylene oligomers have been synthesized, the first of their kind. Homo-oligomers with either all electron rich or all electron poor aryl rings have been synthesized as well as hetero-oligomers. mixing both the electron rich and electron poor aryl moieties have also been synthesized. Figure 2.15 shows the basic repeat unit for each set of oligomers while Table 2.1 shows the oligomers that have been synthesized to date.

The importance of side-chain variation can not be stressed enough for these oligomeric systems. We hope to exploit the contrast between the side-chain and the backbone to show that folding of these oligomeric systems is solvent induced and can be mediated by π - π stacking of the rings of the oPE system.

The mono substituted aryl side-chains for oPE were varied by polarity to assist us in adjusting the contrast between the synthesized molecules and their surrounding

solvent. Heptane will be used to preferentially solvate the side chains of the molecules containing the chiral C5 side-chains and force the aryl rings to segregate. Acetonitrile will be used to preferentially solvate the side chains of the molecules containing the triethylene glycol side-chains and force the aryl rings to segregate.

At present, there is still an issue of head-to-head coupling for the free acetylene moieties, thus there is always some unreacted iodide left in the reaction mixture. Efforts to eliminate this side reaction through changing the catalyst or eliminating the copper altogether, are on-going with the Venkataraman group in Chemistry.

Table 2.5: oPE oligomers synthesized for study

Non Polar Side-Chains					Polar Side-Chains				
#	Backbone	Oligomer Sequence and (Length)	Sidechain	MW	#	Backbone	Oligomer Sequence and (Length)	Sidechain	MW
2	Ether	Et ₂ (2)	C5 Chiral	545.83	9	Ether	Et ₂ (2)	TEG	697.51
3	Ether	Et ₃ (3)	C5 Chiral	732.08	10	Ether	Et ₃ (3)	TEG	959.76
4	Ether	Et ₄ (4)	C5 Chiral	918.33	11	Ether	Et ₄ (4)	TEG	1222.01
6	Ether	Et ₆ (6)	C5 Chiral	1290.83	12	Ether	Et ₅ (5)	TEG	1484.26
7	Ether	Et ₉ (9)	C5 Chiral	1849.58	13	Ether	Et ₆ (6)	TEG	1746.51
					15	Ester	Es ₂ (2)*	TEG	725.52
					16	Ester	Es ₃ (3)*	TEG	1015.78
					17	Ester	Es ₄ (4)*	TEG	1306.04
					18	Ester	Es ₅ (5)*	TEG	1596.30
					19	Ester	Es ₆ (6)*	TEG	1886.56
					21	Ester	Es ₉ (9)*	TEG	2757.34
					22	Ester-Ether	Es ₁ Et ₃ (4)	TEG	1022.34
					23	Ester-Ether	Es ₂ Et ₃ (5)	TEG	1312.60
					24	Ester-Ether	Es ₃ Et ₃ (6)	TEG	1602.86

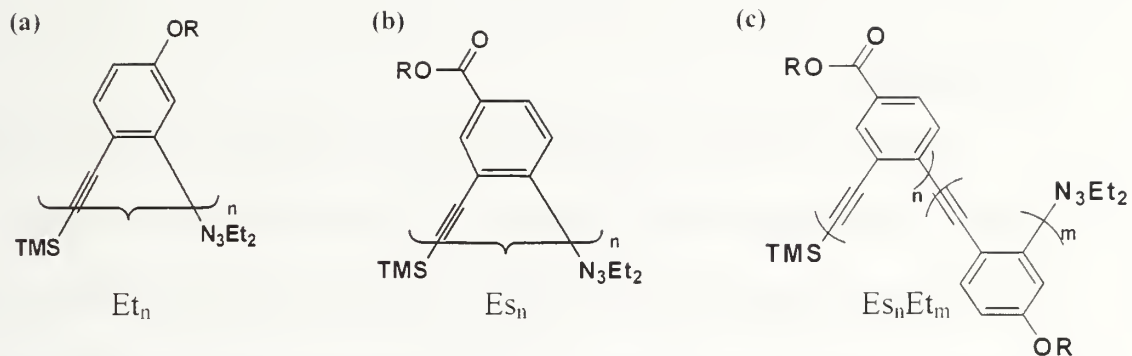


Figure 2.16: Synthesized oPE backbones. (a) Electron rich ether oligomer Et_n . (c) Electron poor ester oligomer Es_n (c) Sample hetero-oligomer Es_nEt_m . All red rings are electron rich, all blue rings are electron poor. Rings are numbered sequentially from the TMS end of the oligomer to the triazene end.

CHAPTER 3

CHARACTERIZATION OF CHIRAL ALKOXY NON POLAR OPE

3.1 Introduction

Chapter 2 detailed the synthesis of these new oPE systems. The next task was to determine the propensity for these oligomers to adopt helical secondary structures. Other oligomeric structures in the literature with non-polar side chains make use of either long chain alkanes as a solvent to preferentially solvate the side chains and force the oligomers into helical structure or use the sidechains to promote solubility. (22, 30, 57, 63, 64) The primary tools for characterizing helix formation are Ultra Violet-Visible (UV-Vis) spectroscopy, Fluorescence spectroscopy, and Circular Dichroism. This chapter investigates the use of these methods with the addition of NMR to characterize whether these alkoxy-NP oligomers form helices in solution. A crystal structure was also obtained and analyzed for helix formation. Oligomers with up to 3 turns are utilized in this study: a trimer **3** (1 turn), tetramer **4** (1 and 1/3 turn), hexamer **6** (two turns), and nonamer **7** (3 turns). Figure 3.1 shows the extended chemical structure and helical conformation of nonamer **7**.

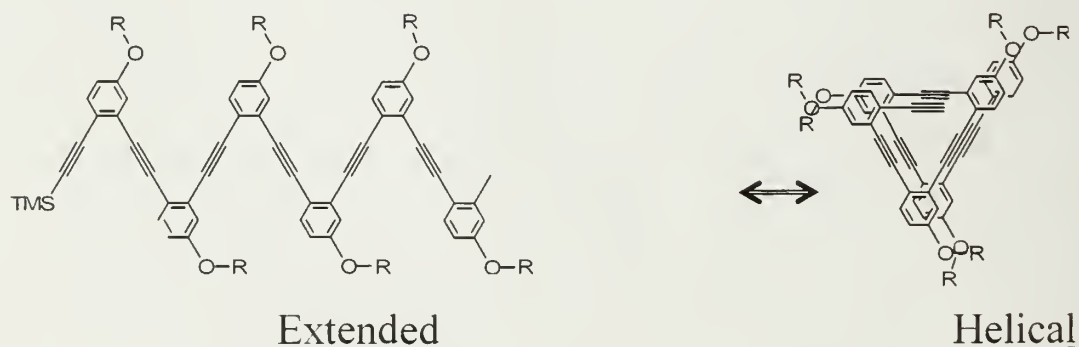


Figure 3.1 Extended and helical conformation of alkoxy substituted nonamer **7**.

3.2 Methods

These materials have been characterized by UV, Fluorescence, NMR, and CD to determine whether the scaffold takes on a helical conformation when placed in a solvent that is better suited to the side chain rather than the backbone of the oligomer. The two solvents used to probe the solution properties of these oligomers are chloroform and n-heptane which was similar to work done by Jeff Moore in 2000 for "Conformational Order of Apolar Chiral *m*-Phenylene Ethynylene Oligomers". UV and Fluorescence data were taken with concentrations similar to those seen in the mPE literature to investigate whether a transition between unfolded and folded would be observed in chloroform (CHCl₃) and n-heptanes, the "unfolded" and "folded" solvents respectively. UV-visible spectra were recorded on a Hewlett-Packard 8453. Emission and excitation spectra were taken on a Perkin-Elmer LS 50B spectrometer with a xenon lamp light source with solution concentrations having an absorbance of less than 0.1.

Fluorescence data was taken with solutions with absorbance of less than 0.1 to eliminate possible long range aggregation. A red shift and broadening would be indicative of π - π aggregation/stacking, and hence confirm folding.

Circular Dichroism (CD) measures the difference between right-handed and left-handed circularly polarized light. The CD signal arises from chromophores that absorb left and right polarized light differently-i.e. non symmetric absorption behavior of chiral chromophores. The nature of the chiral chromophores in 3D, eg helix handedness, is related to the overall 3-dimensional secondary structure, thus this measurement should be influenced by the perturbation or disruption of the structure. CD Spectra were taken

on a JASCO J720 spectrometer in rectangular cuvettes using concentrations of 200 μM or less.

1-D ^1H NMR in CDCl_3 and d-heptane were taken to examine changes in the aryl protons. If these oligomers are folding π - π stacking of the aromatic rings on top of one another would be reflected by upfield shifting in the aryl region of the NMR. 2-D NMR to examine for through space interactions that would exist only in a secondary structure was attempted as well, but proved to be unsuccessful.

Finally a crystal of hexamer **6** was obtained by crystallizing the oligomer from n-heptane and analyzed by X-ray crystallography.

What follows is a discussion of the first attempts to characterize NP alkoxy oPE oligomers as a helically folding system.

3.3 UV and Fluorescence Studies

UV-Vis and fluorescence spectroscopy were initial tools to study and characterize secondary structure formation for these oPEs. Contrary to what is observed with *meta* Phenylene Ethynylene systems as shown in Figure 3.2 (a) and (b), there is no convenient correlation between macrocycles of oPE and the larger open oligomer structures. The 287 nm peak shown in Figure 3.2 (a) for mPE was classified as the cisoid peak which would predominate a helical conformation, making it closely resemble the 6 unit macrocycle. The shoulder peak at 303 nm was classified as the transoid band (29-31). With increasing oligomer lengths in heptane this 303 band decreases and the 287 band increases showing a cooperative transition (30). Unfortunately a corollary for this phenomena is not found for the oPE systems. Figure 3.2 (c) and (d) show the trimer and 3-unit macrocycle. The sharp transitions for the

macrocycle are not characteristics displayed by the 6-unit macrocycles. These transitions could be due to very short conjugation lengths which are absent in the *meta* systems due to the aromaticity of the 6-unit macrocycle.

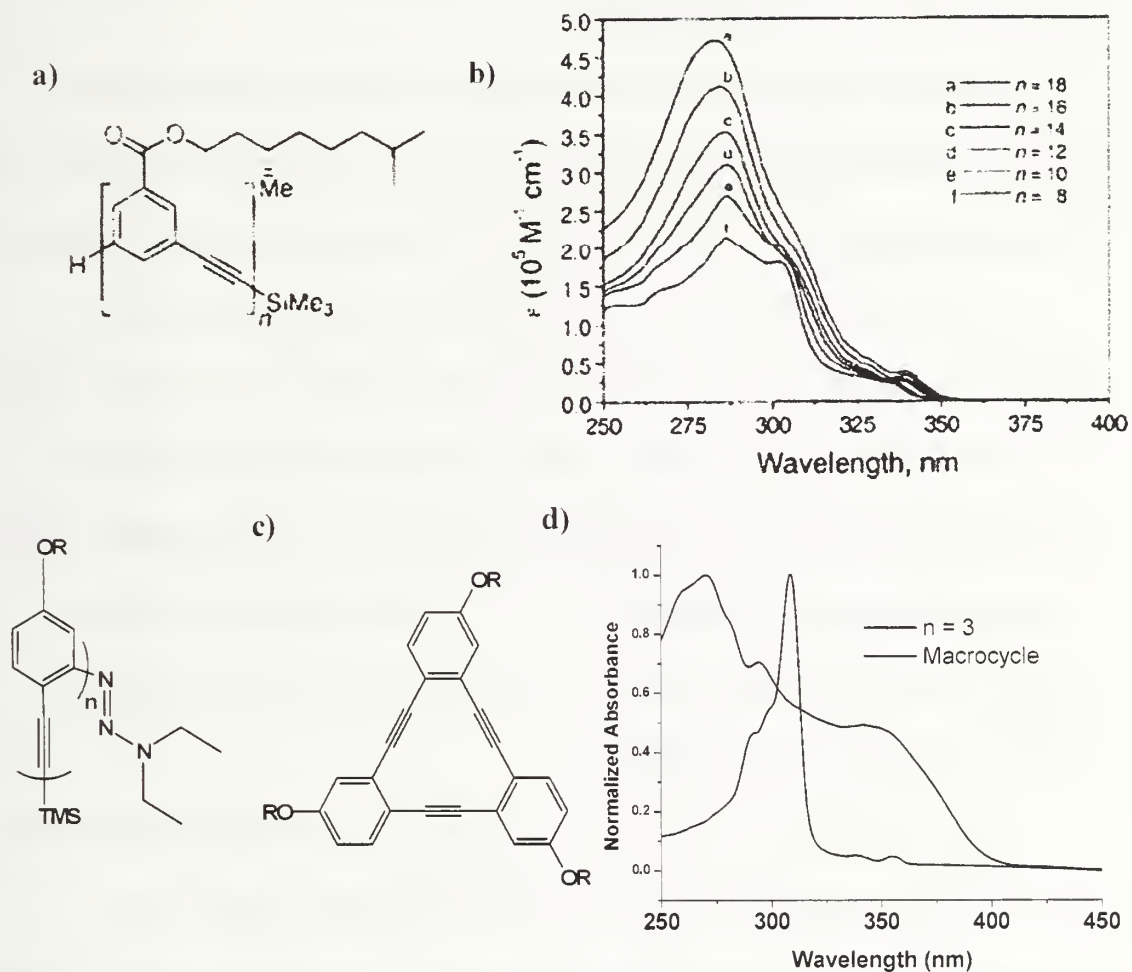


Figure 3.2 (a) NP mPE oligomer (b) UV spectra of increasing oligomer length in heptane. (Taken from ref 30) (c) NP oPE oligomer and macrocycle (d) UV spectra comparing macrocycle to discrete trimer.

Figure 3.3 contains the normalized data for trimer **3**, tetramer **4**, hexamer **6**, and nonamer **7** in chloroform (a), heptane (b) and for nonamer **7** plotted in chloroform and heptane (c). The spectra in these figures are remarkably similar. Further studies performed on model dimers found that the UV spectra observed here can effectively be

divided into discrete units. These units each have very unique absorbance patterns that contain a) the dimeric oPE without the TMS, b) the Dimeric oPE without triazene and c) the dimeric oPE with no end groups. This is in contrast to the very broad patterns observed in the UV for the mPE systems.

As the oPE oligomer increases in length there are subtle changes to the UV spectra. In heptane there is a peak and shoulder at 300 and 290 nm for **3** which increase and red shift as oligomer length increases. But this phenomena happens in chloroform as well. The outer band at 350 nm red shifts from **3** to **7** in both n-heptane and chloroform. Examining **7** in chloroform and heptane in Figure 3.3 (c) there are only a few nm that separate the two spectra, a slightly broader peak at 300 nm between heptane and chloroform, and a final shoulder between 340-415 nm that appears slightly red shifted and reduced in chloroform. By UV we were not able to quantify any definitive changes in structural ordering, as a result, UV was not used to probe secondary structure in future experiments.

Figure 3.4 shows the Fluorescence spectra of **3 -7** in chloroform (a) and heptane (b). This data is normalized to track the red shift of the peak, indicative of π -aggregation. In heptane the peak from the main band does red shift from **3** (375 nm) – **7** (425nm) while in chloroform, the shifting stops with the hexamer at approximate 410nm. The red-shifting observed in mPE systems was much more abrupt as the main band shifts and broadens from ~350nm to 420nm as the system moves from what would be 1 and 2/3 turns (decamer) to 2 turns (dodecamer) for polar folded mPE in acetonitrile as shown in 3.4 (c).

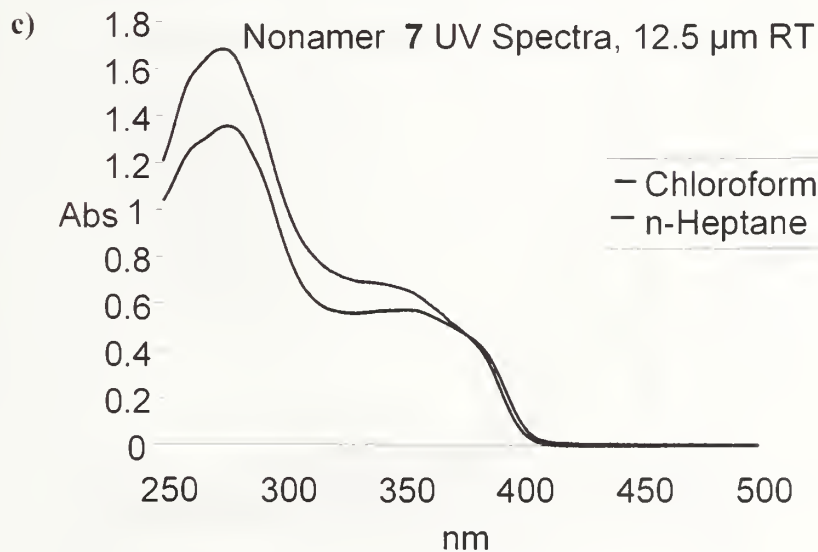
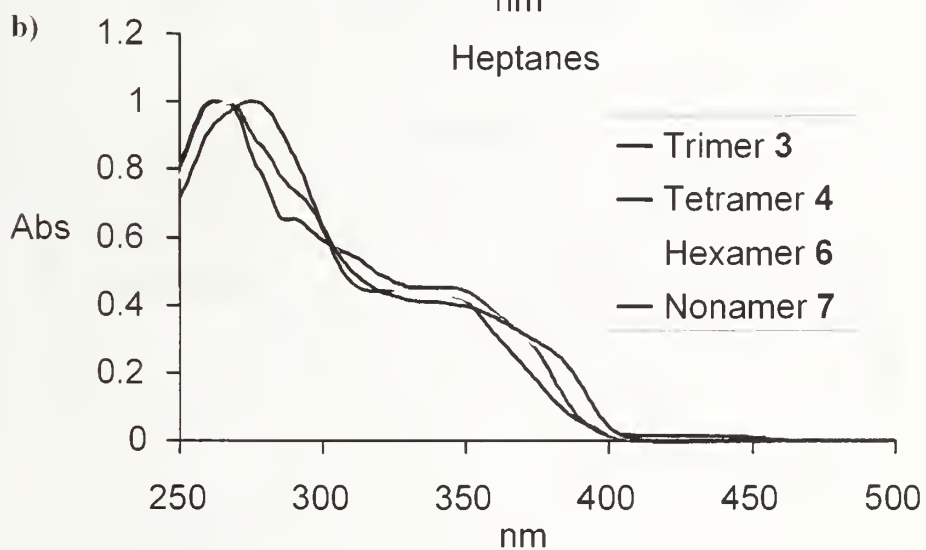
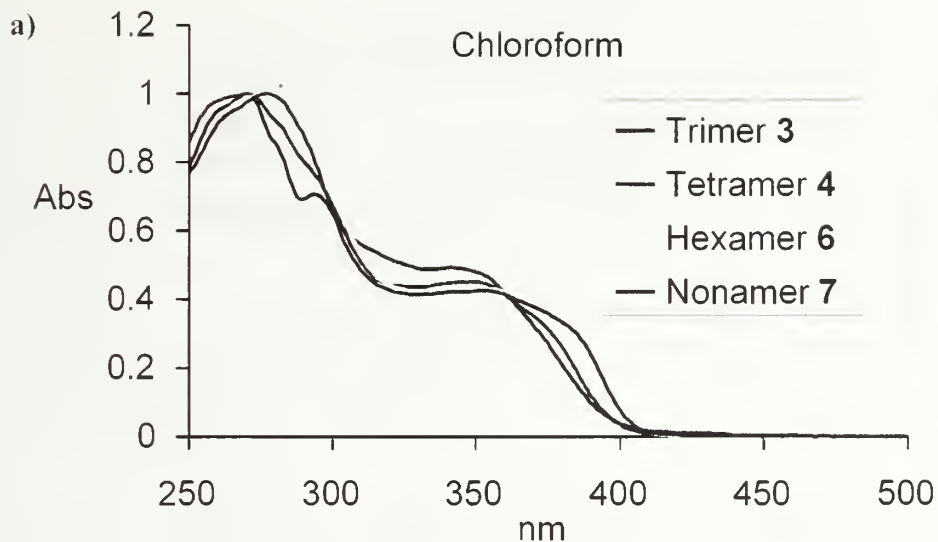


Figure 3.3 UV spectra of 3-7. (a) Chloroform (b) Heptane (c) Nonamer 7.

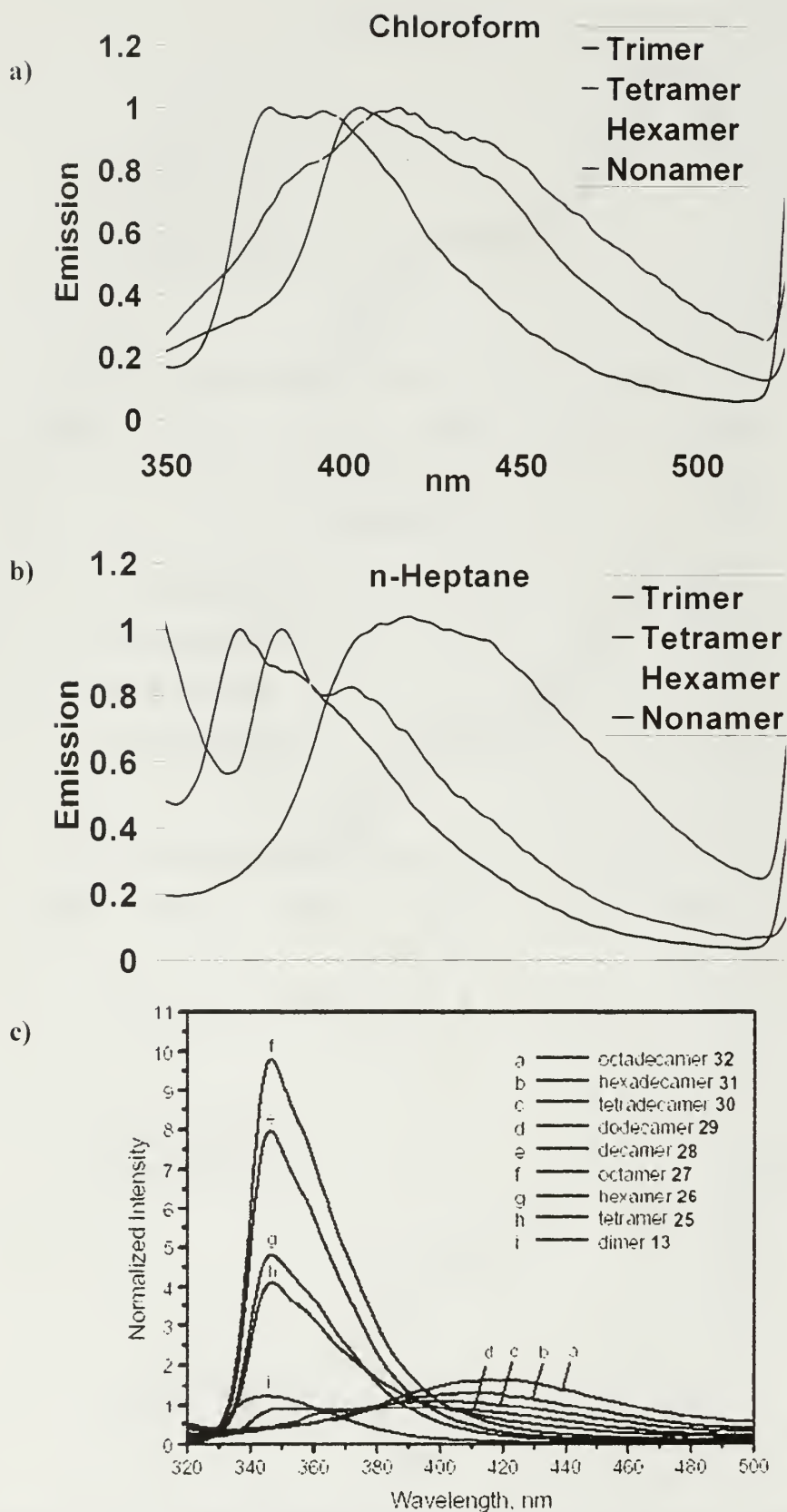


Figure 3.4 Fluorescence spectra of 3-7 in Chloroform (a) Heptane (b) and a sample fluorescence spectra from a mPE system in CH₃CN (c) taken from reference 32.

3.4 Circular Dichroism

Circular Dichroism has been used as a method to examine secondary structures of biological macromolecules and foldameric systems.(12, 65-68) Specific patterns in the CD spectra are correlated with secondary structures like helices, sheets and turns. Chirality is required for contrast to observe the difference between circularly polarized light. The chiral S-methoxy butanol side chain substituents proved to be of some utility.

Initial efforts, using this method to determine whether the oPE oligomers formed helices in solution, examined the difference between tetramer **4**, hexamer **6**, and nonamer **7** in heptane and chloroform. Figure 3.5 (a) shows the lack of coherent signal in chloroform for **4**, **6**, and **7** while (b) shows a small but increasingly well defined signal going from **4** (1 and 1/3 turns) to **6** (2 turns) and finally to **7** (3 turns) at room temperature. While this data was encouraging molar ellipticity ($\Delta\epsilon$) was on the order of 2 magnitudes below what was reported for other systems in the literature.

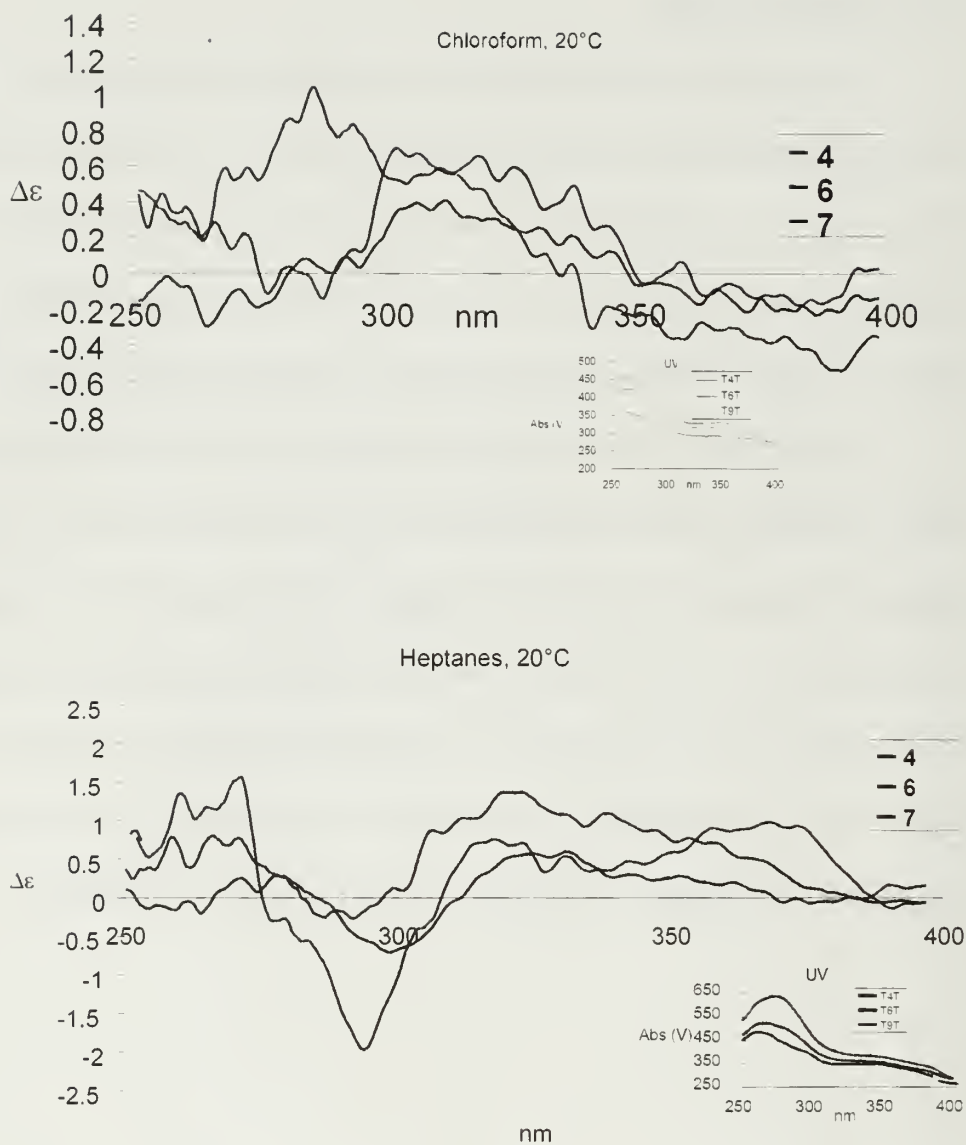


Figure 3.5: CD spectra of tetramer 4, hexamer 6, and nonamer 7 at 0.02mM in at 20°C in chloroform (a) heptane (b).

To determine whether concentration or temperature had an impact on the signal and to determine whether we were observing aggregation effects, two other studies were performed. The first, shown in Figure 3.6 shows the impact of increasing concentration by an order of magnitude while decreasing the path length of the laser by

the same order of magnitude. These two data sets are essentially the same, indicating a lack of large scale aggregation that would create an undefined larger structure.

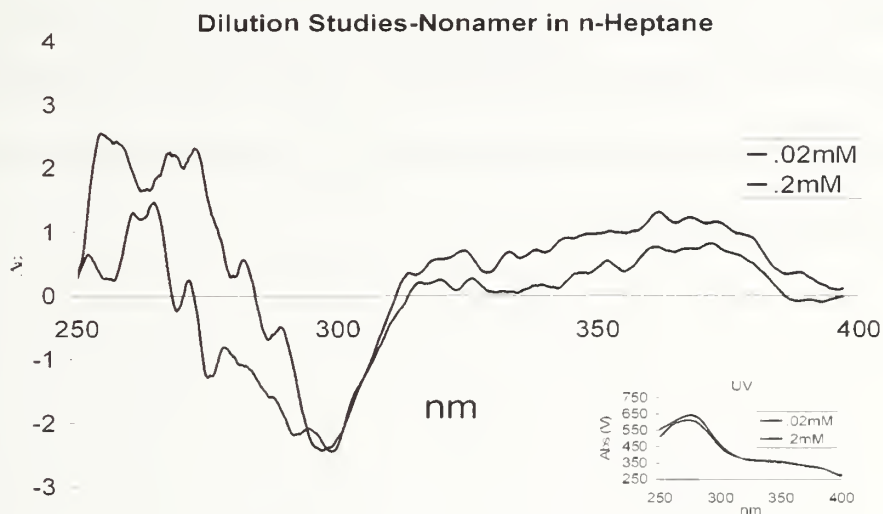


Figure 3.6: Concentration study of nonamer in n-heptane using a 1mm cell (.2mM) and a 1cm cell (.02mM).

Figure 3.7 (a) two shows the CD of the hexamer at relatively high concentration in *n-heptane* (0.167mM) using a 1mm path length cell, at 0, 10, and 20°C. Figure 3.7(b) shows the CD of the nonamer in *chloroform* at higher concentration (0.268mM) at 0°C as well as in *n-heptane* at 0.167mM at 0, 10, and 20°C. Insets of the UV spectra obtained from each run are shown as well. The purpose of this experiment was to determine whether a helical conformation was obtained in *n-heptane* versus an extended conformation in *chloroform*: a decrease in temperature should favor a folded structure. In Figure 3.7, there is little to no CD signal for the nonamer in *chloroform*, even at 0°C while there is a substantial signal for the nonamer in *n-heptane*. The maxima and minima in the UV spectra corresponding to each CD seem to coincide with the inflection points in each CD spectra. In all spectra there appears to be a lopsided Cotton effect but the data shown here does not follow a pattern similar to other literature

accounts that shows a flat baseline before a minimum then maximum. Instead, a positive maximum, a minimum, and finally another maximum were observed in most of the spectra that were obtained. Again, comparing our UV spectra to those obtained for the *m*-phenylene ethynylene systems shown in Figure 3.8 there are much broader less defined peaks in the regions from 345nm-400nm which must contribute to this additional peak in our spectra.

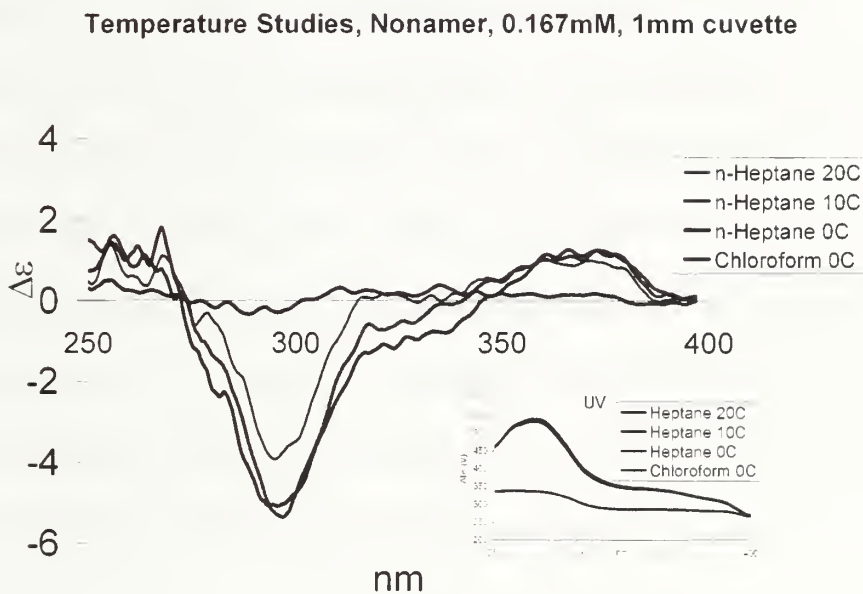
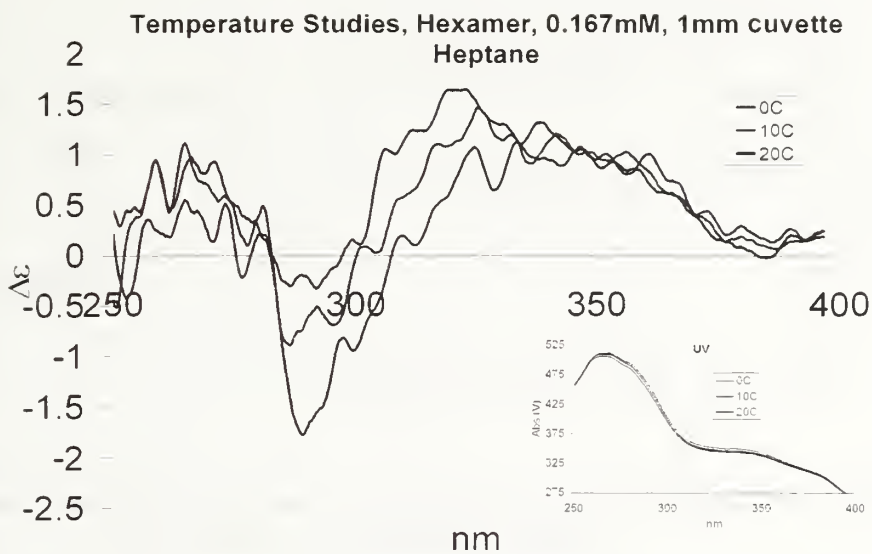


Figure 3.7 (a) CD spectra of 6 in n-heptane at high concentration, varying temperature (b) 7 in n-heptane and chloroform at high concentration varying temperatures.

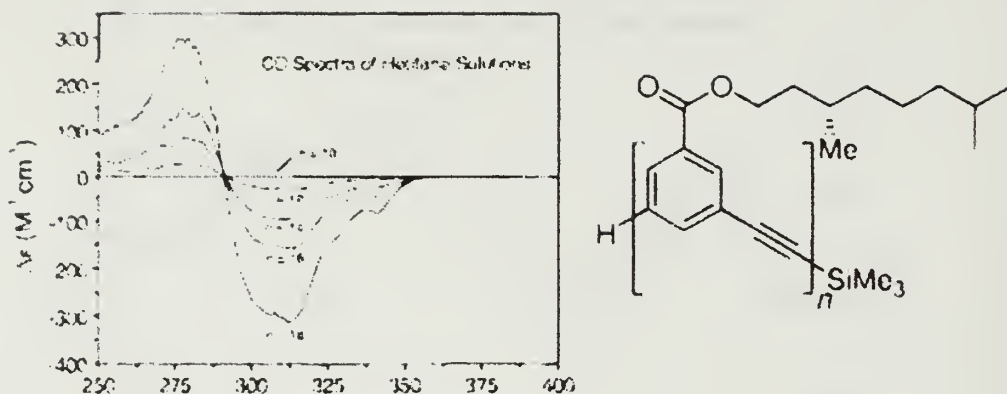


Figure 3.8 Representative CD spectra of apolar mPE oligomers with increasing length in heptane from reference 30.

While it is encouraging that this data does follow the desired trend, increasing signal with supposed addition of helical layers, it does not give us data similar to what is found in other literature accounts. This could simply be attributed to the oPE systems having a lower $\Delta\epsilon$ because each system is different and thus, there are no clean mechanisms for predicting and interpreting CD spectra. Figure 3.9 shows a solution and a solid state CD sample of the alkoxy oPE macrocycle. It is encouraging to note similar $\Delta\epsilon$ values are observed for the solid state macrocycle despite the high concentration. At the same time, the nature of the peak is somewhat different.

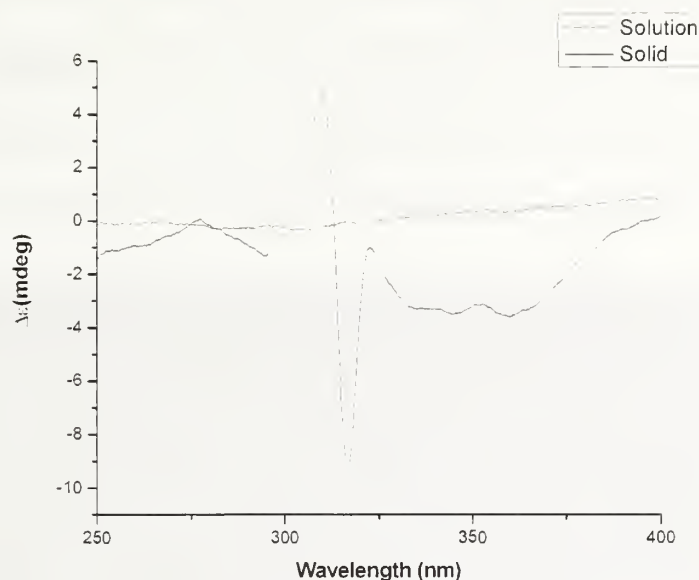


Figure 3.9: CD spectra for solution and solid state oPE Macrocycle.

3.5 Crystal Structure of hexamer 6

A crystal structure was obtained by crystallizing hexamer **6** from n-heptane. Shown in Figure 3.10 are the top (a) and side (b) and (c) views of the solved crystal structure for **6**. Contrary to the helical structure we sought, clearly this is a flat and extended structure in the solid state. In fact the solvent appears to co-crystallize along the acetylenic linkage between rings 2 and 3 shown in (b). Additionally, there appears to be a slight twist to the extended structure as the plane of the oPE backbone moves clockwise as observed by looking down the z axis in (c). Models of these extended oPE systems also show this slight twist. Resolution of this crystal structure is limited as the side chains are not particularly well resolved, but the structure of the backbone is very clear.

Though the crystal structure did not give the desired helical conformer, it is consistent with a recently reported oPE backbone from Bunz showing a flat

interdigitated and slipstacked dimethoxy oPE with pyridine end groups.(44) This crystal structure does show the existence of the planar structure in the solid state. This refutes the possibility that the oPE oligomers exist only in a helical state and are available for folding and manipulation by a change in environmental stimulus.

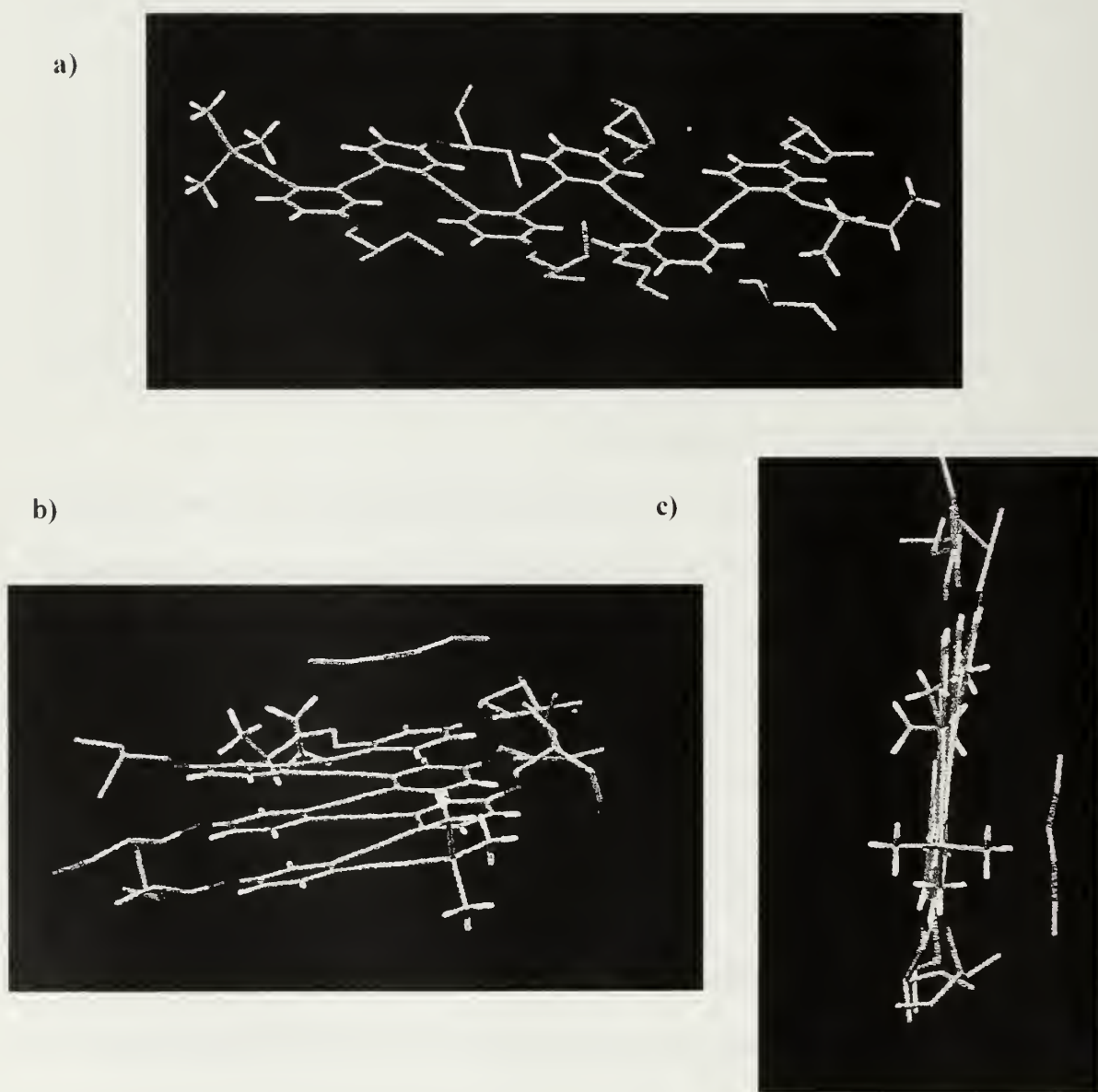


Figure 3.10 Crystal structure of hexamer 6 (a) top view (b) and (c) side view.

3.6 NMR Studies

Moving back to solutions studies of these oPE systems. NMR experiments were attempted to observe and characterize helix formation in nonpolar media.

Unfortunately d-heptane is too prohibitively expensive to conduct extensive experiments involving titrations, but simple studies of what was hoped to be unfolded (CDCl_3) and folded (d-heptane) solvents were possible.

Figure 3.11 shows the aryl regions of **3**, **4**, and **6**, exhibiting dispersion through the region as all 9, 12, and 18 protons can be counted and assigned to specific ring systems in contrast to the mPE systems. Examining Figure 3.12, the CDCl_3 spectra of the aryl region of **4** is on the bottom, d-heptane is on the top. The expected observation is selective upfield shifting for rings 1 and 4 due to π - π stacking. Bringing rings 1 and 4 in close proximity with one another would create a folded and helical structure. What is observed is an upfield shift for ring 1, relative stability of rings 2 and 3, and a downfield shift for ring 4. All of these Δppm values are very small, on the order of 0.02 ppm difference for rings 1 and 4. The alkoxy substituted oPEs tend to have lower Δppm values as shifting is observed in the aryl region. This phenomenon will be discussed extensively in chapter 4.

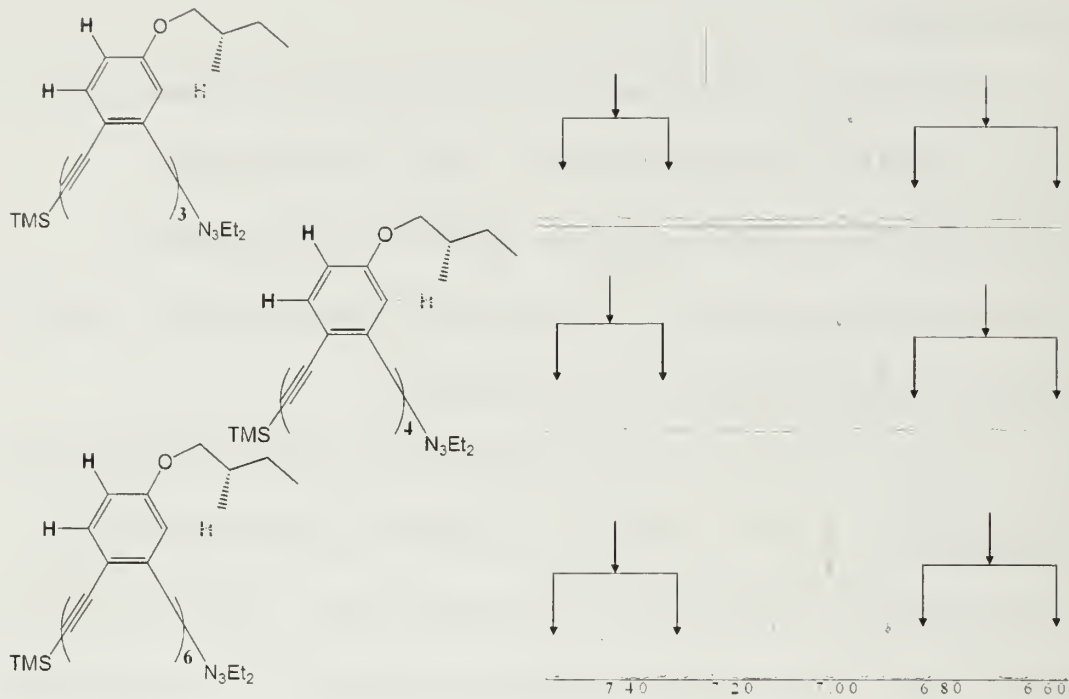


Figure 3.11: Expanded aryl region for oligomers 3, 4, and 6 in CDCl_3 .

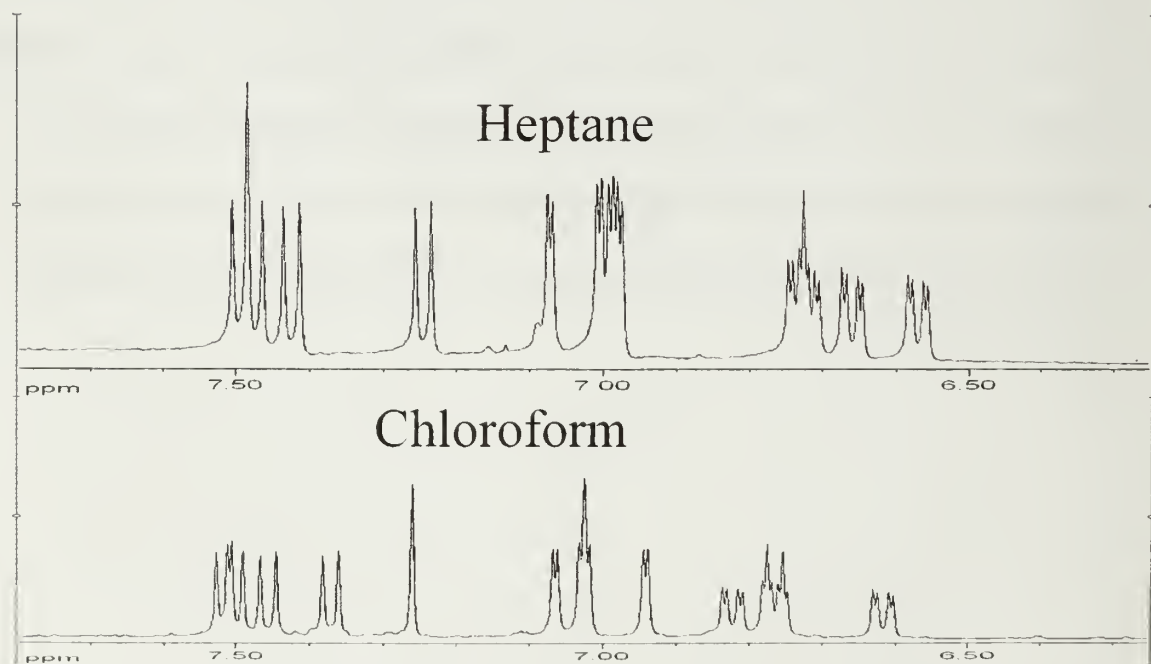


Figure 3.12: NMR spectra of 4 in Heptane (top) and CDCl_3 (bottom).

The NMR data in Figure 3.13 for nonamer **7** was taken at 600MHz in d-heptane (top) and CDCl₃ (bottom). While it is clear in 3.13 that there is a difference in the aryl region between d-heptane and CDCl₃ it appears that the peaks go *downfield* in contrast to the expected upfield shift in the folded solvent, d-heptane. There is still excellent dispersion and so large and uncontrolled aggregation can be ruled out.

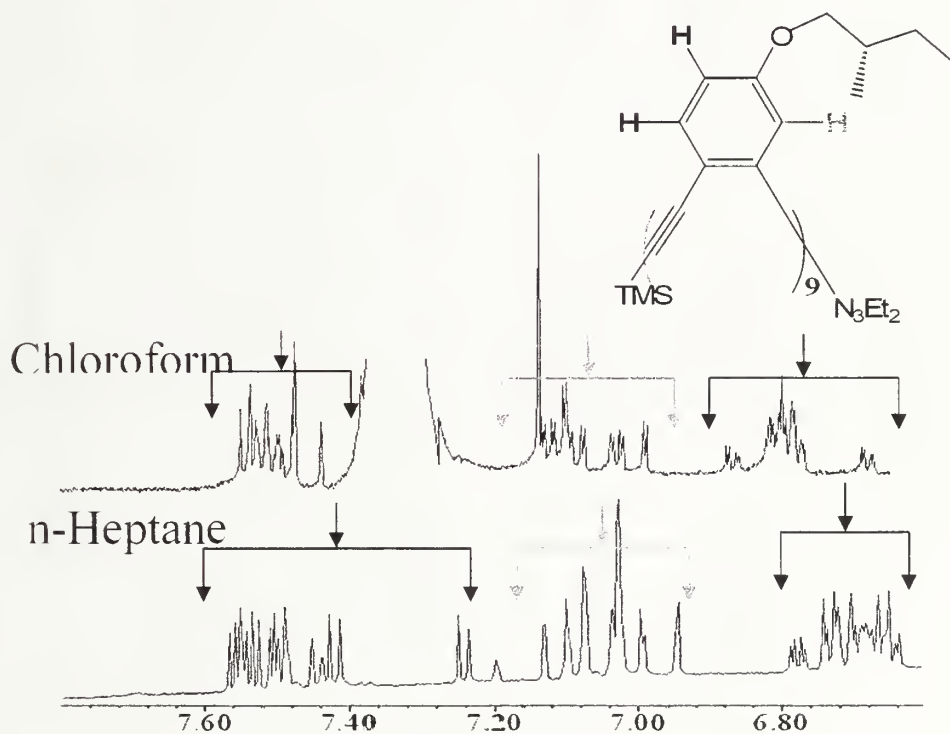


Figure 3.13: Aryl region of Nonamer in Chloroform (top) and Heptane (bottom).

A brief temperature study of tetramer **4** was conducted to determine whether the aryl regions of these oligomers were sensitive to temperature change. Each sample was equilibrated at 4 temperatures and ¹H NMR and COSY data were obtained. The sensitive ring systems are noted with red and blue arrows in Figure 3.14.

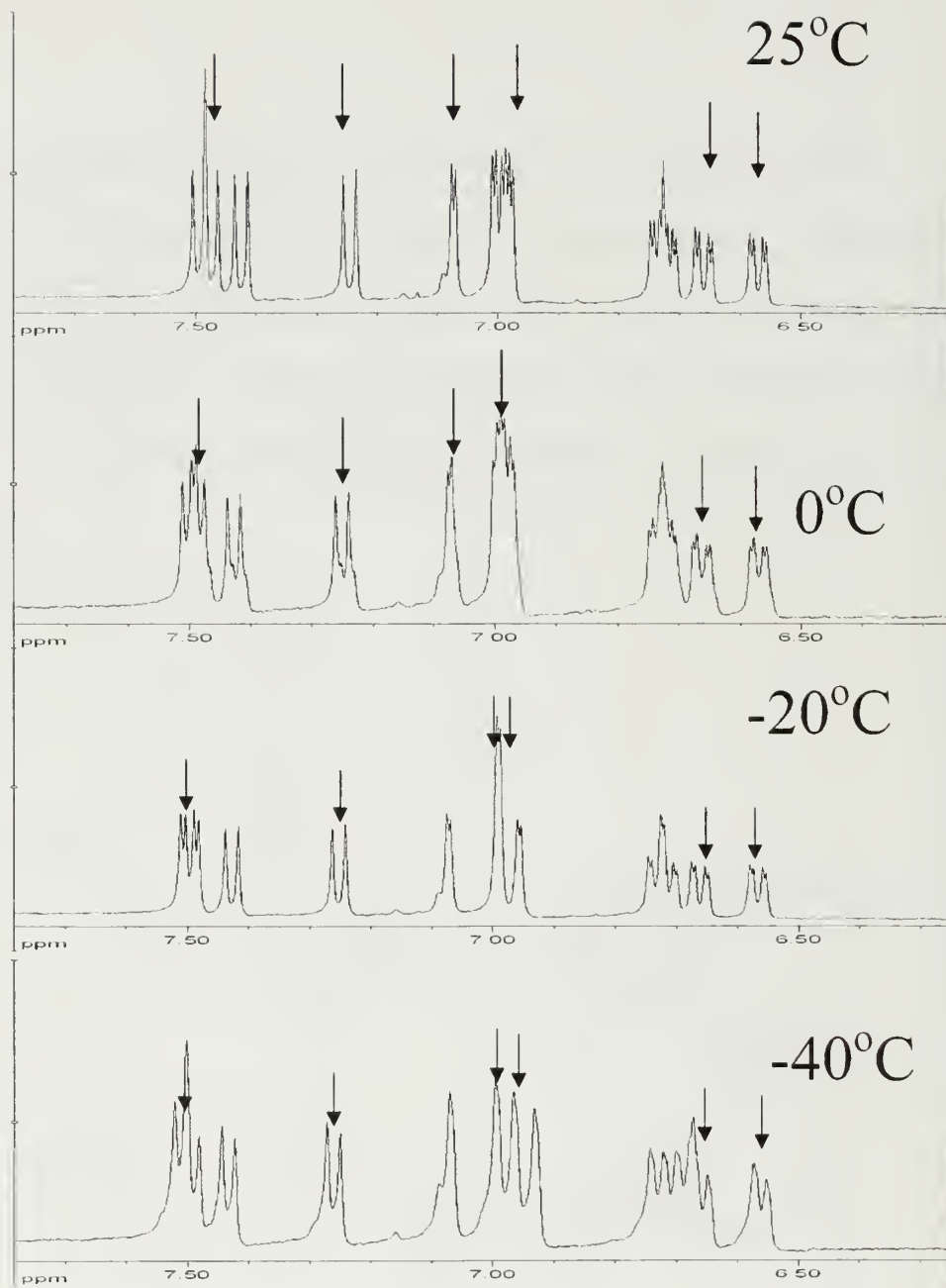


Figure 3.14: ^1H Temperature study of oligomer 4 in d-heptane

2-D NMR studies to investigate space interactions between the aryl protons and the terminal TMS group proved to be challenging and to date unsuccessful for these NP oPE systems.

3.7 Conclusions

The synthesis of non polar oPE systems serves as the first published report of substituted oPEs and established protocols for the continued synthesis and exploration of these systems as foldameric oligomers. Overall, the synthesis of the NP systems proved to be more facile than their polar counterparts. A number of studies were performed in an attempt to try to induce and observe helical secondary structure for alkoxy substituted NP oPEs. Unfortunately, none of these experiments provided definitive proof of a helical structure. UV proved to be too ambiguous to identify dramatic changes with increasing length of the oPE in heptane. Comparing the 3-unit macrocycle to the open oligomer proved to be of little utility, as a correlation between the cisoid structure and a folding oligomer could not be found. Circular Dichroism did exhibit elements of length, solvent, and temperature dependence for the resulting signals of these oPEs. These signals appeared to be strongest for nonamer **7** in n-heptane at 0°C. These signals were 2 orders of magnitude smaller than other reported literature values, but were similar to values found for macrocycles in the solid state. NMR also showed some signs of upfield shifting which would be indicative of π - π stacking and thus folding in these systems. ^1H NMR spectra of tetramer **4** were responsive to temperature, shifting downfield with an increase in temperature. However, the overall Δ ppm values observed with changing solvent were extremely

small and appear to go downfield for nonamer **7** from CDCl_3 to d-heptane. The data suggest a helical structure may be formed from these systems, but it is not definitive.

CHAPTER 4

SOLUTION NMR CONFIRMATION OF FOLDING IN SHORT *o*PE SYSTEMS

4.1 Introduction

Noting the lack of definitive proof of folding for the non-polar *ortho* Phenylene Ethynylene (NP *o*PE) systems in Chapter 3, a new strategy was developed. Encouraging results were obtained from the ^1H NMR studies of NP *o*PE oligomers showing shifting in the aromatic regions which would be indicative of π - π stacking but the desired trend was not apparent. Examining literature accounts of folded mPE systems (^{26, 29, 35, 65, 69}) polar side chains have often been used as substituents for folding oligomeric systems. In this case a Tri-ethylene glycol monomethyl ether (Teg) side chain was chosen as the new polar side chain with which to probe the propensity for folding of these *o*PE systems. The hope was that using solvents with a higher dielectric contrast between the "folded" and "unfolded" solvent would bring about a clearer change in the aromatic protons of these *o*PE systems, proving that they indeed fold, using solution 1-D and 2-D NMR methods.

Additionally, 2-D NMR experiments using the terminal trimethylsilyl (TMS) as a probe to look for Nuclear Overhauser Effect Spectroscopy (NOESY)^(70, 71) type cross peaks signaling intramolecular spacings between protons of less than 5 Å in the NP *o*PEs was greatly hindered by the large *n*-heptane solvent peaks that occurred between 0.9 and 1.4 ppm as discussed in Chapter 3. Thus, a new approach using a polar side chain and a relatively inexpensive deuterium-solvent (acetonitrile, CD_3CN) was taken using NMR as the primary weapon for characterization.

This Chapter focuses on the effort to definitively determine by 1-D and 2-D NMR methods that the oPE system forms a helix even with extremely short tetrameric units with polar substituents.

4.2 Methodology

Synthesis for tetramer **11** (Et₄, electron rich), tetramer **22** (EsEt₃, hetero rich-poor), and tetramer **17** (Es₄, electron poor) are described in Chapter 2 and detailed in Chapter 7. All NMR experiments with the exception of the 2-D ROESY experiment performed on tetramer **17** were taken on a Bruker Avance 400MHz NMR.

Solvent titrations were all performed at a concentration of 1.25 mM in solvent mixtures of 0-100% acetonitrile (CD₃CN) in chloroform (CDCl₃) in increments of 10%. A brief temperature study was undertaken to determine if there was any temperature sensitivity of these oPE systems in CD₃CN in the range of 288-310K (14°C-34°C). A more detailed description of the methods used to deconvolute and assign the 1-D NMR spectra by 2-D J Coupled Correlation Spectroscopy (COSY) and Heteronuclear Multiple Bond Correlation (HMBC) can be found in section 5.2.

¹H, ¹³C NMR, 2D COSY, and NOESY spectra were obtained at 400 MHz with a Bruker DPX-400 NMR spectrometer and analyzed with the Bruker XWIN NMR program. The 400 MHz machine is equipped with a cryogenic probe. [1H,1H]-NOESY spectra of **22** were recorded at a 400 MHz ¹H spectrometer frequency with a mixing time, τ_{mix} , of 100 ms and at *T* (sample) of 14, 24, and 34 °C in CD₃CN at a concentration of 1.25mM.

¹H, and ROESY spectra for **17** was obtained with a Bruker 600MHz spectrometer at a concentration of 1.25mM. The 600 MHz machine is equipped with a

cryogenic probe. [1H,1H]-ROESY spectra of **17** were recorded at a 600 MHz ¹H spectrometer frequency with a mixing time, τ_{mix} , of 300 ms and at T (sample) of 24 °C in CD₃CN and CDCl₃.

What follows is the first attempts at determining whether there is helical character to very short polar substituted oPE oligomers of varying electronic character as induced by solvophobicity.

4.3 1-D ¹H NMR Characterization of Et₄, EsEt₃, and Es₄

The oPE oligomers reported here were synthesized using standard Sonogashira methods reported earlier in good yield to afford three tetramers of different electronic composition. The oligomers shown in Figure 4.1 include an electron rich tetramer **11** (Et₄) where all of the Teg side chains are attached to the oPE backbone through ethers, a mixed system **22**. (EsEt₃) with one electron poor ester ring and three electron rich ether rings, and an electron poor tetramer **17** (Es₄).

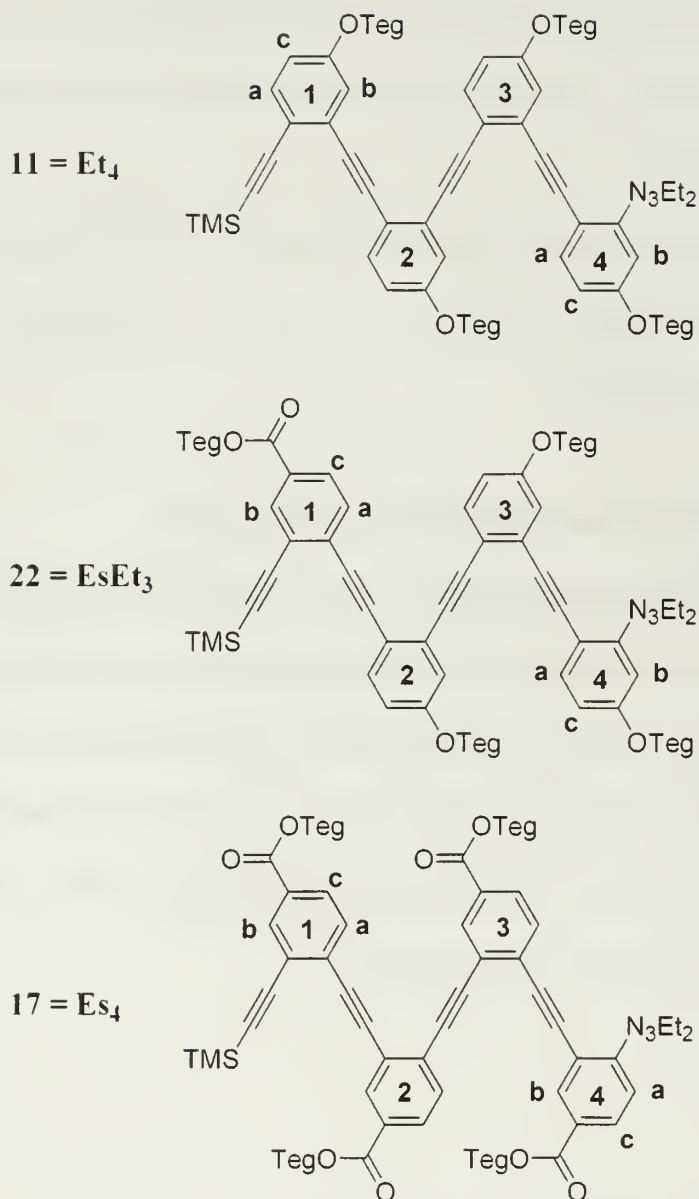


Figure 4.1: oPE tetramers 1-3. Electron poor (blue) and electron rich (red) rings are shown. Relevant protons for each tetramer are labeled according to their splitting pattern. Each ring of each oligomer has three protons that are labeled respective to their J-coupling and splitting pattern respectively: a (8.4 Hz, d), b (2.1 Hz, d), and c (8.4 Hz and 2.1 Hz, dd).

Previous work suggested halogenated solvents would promote a predominantly random conformation (72) while more polar solvents drive a folded structure. If indeed these short tetramers fold in solution, it is well documented that π - π stacking shifts aryl

protons upfield to smaller ppm values.(73) A solvent titration study shown in Figure 4.2a was conducted at constant temperature and concentration to determine the effects of π - π stacking as a function of solvent composition for the three tetramers. Each graph represents a solvent titration series for each of the three tetramers at increments of 10 volume percent acetonitrile (CD_3CN) in Chloroform (CDCl_3) from 0% CD_3CN to 100% CD_3CN ; all data was referenced to the internal standard, tetramethylsilane. The ppm shifts for protons a, b, and c of each ring were averaged to represent a single data point per ring at each measured concentration. The original 0% CD_3CN (or 100% CDCl_3) value was set to zero in order to normalize all of the data and then the change in ppm (Δppm) was plotted as a function of solvent composition.

The Δppm , when the solvent is changed from CDCl_3 to CD_3CN , indicates a clear upfield shift for the aryl protons of rings 1 and 4 predicted to be involved in π - π stacking for all three tetramers **11**, **22**, and **17**. Initial studies were performed to determine the impact of changing dielectric from CDCl_3 to CD_3CN on oPE systems. Using model compounds from monomers to trimers which cannot fold given their short length, the average Δppm was calculated by averaging each signal from the aromatic protons for each compound in CDCl_3 and subtracting that from the same values found for the aromatic protons in CD_3CN . The average ring ppm going from CDCl_3 to CD_3CN is +0.05ppm based on model compounds like the monomers, dimers and trimers, which can not fold.(74) At the same time, the protons expected to experience no π - π stacking interactions (rings 2 and 3) were observed to remain at ≈ 0 Δppm throughout the titration, completely consistent with the expected folded structure.

Further, when comparing all three oligomers the differences in Δppm are also in agreement with expectations. Oligomer **22** is expected to fold better than **11** due to complimentary electrostatics. Rings 1 and 4 of **22** are π -poor and π -rich respectively, while these two rings in **11** are both π -rich. The electron poor system of oligomer **17** has the largest Δppm for rings 1 and 4 suggesting closer stacking interactions, although π -poor systems may be more sensitive spectroscopically.(75)

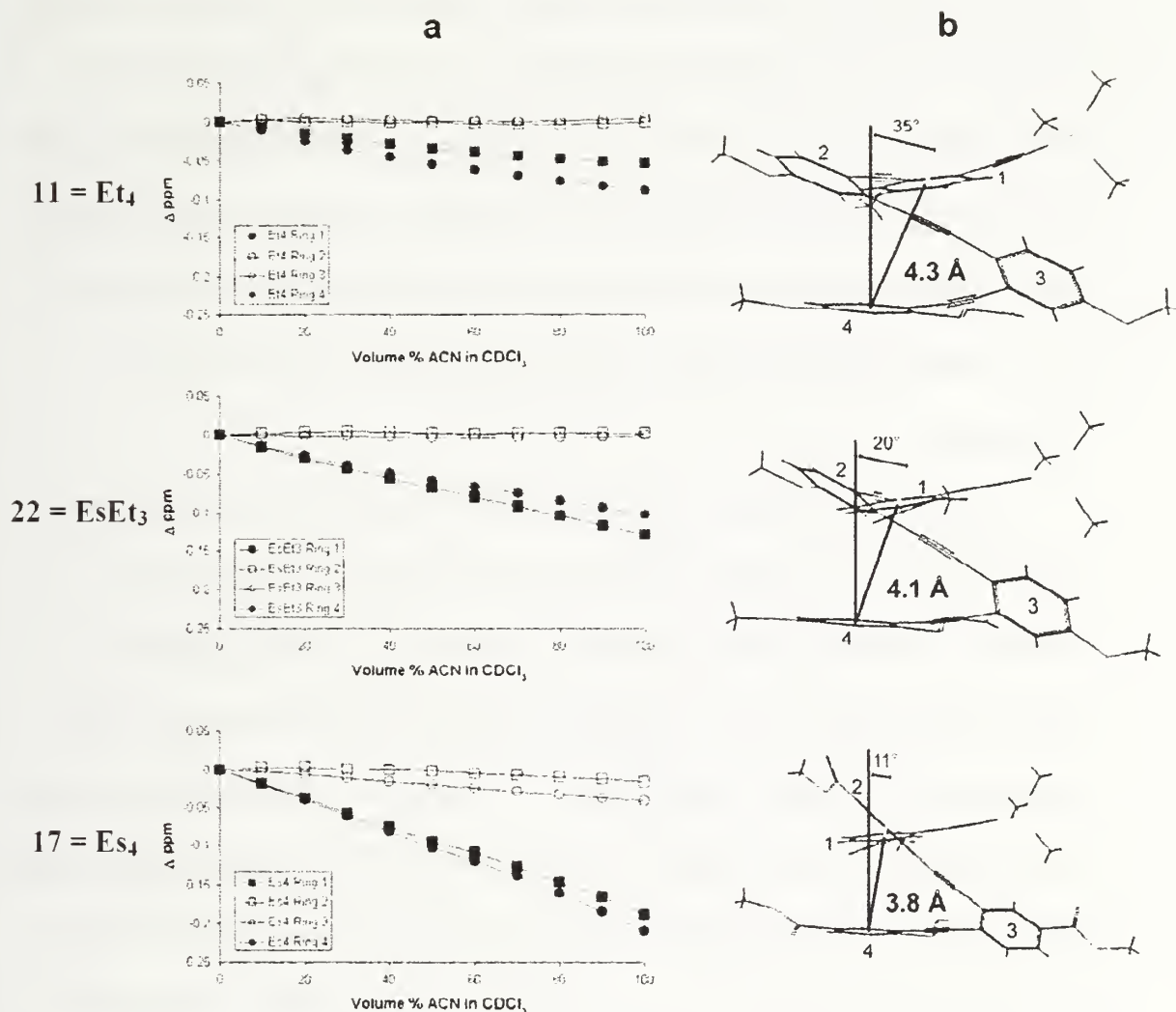


Figure 4.2: (a) NMR titration curves of **11**, **17**, and **22** from CDCl_3 to CD_3CN . Upfield shifting of rings 1 and 4 are evident while rings 2 and 3 do not move. (top) **11** Et_4 , (middle) **22** EsEt_3 , and (bottom) **17** Es_4 . (b) Energy minimized (MMFF) conformation of tetramers 1-3 folded into a helix. The Teg side chains are omitted for clarity. Angles indicate the offset between rings 1 and 4 in the helical conformation. Distances given are between the centers of rings 1 and 4.

The overall upfield shifting (Δ ppm) of the signals corresponding to the protons on rings 1 and 4 in tetramer **11** are relatively small; however, it is clear that the signals from the protons on rings 2 and 3 are not affected by a change in solvent as evidenced in the top graph of Figure 4.2a. When the data for tetramer **22** is examined (middle graph of Figure 4.2a), it is again very clear that the signals from the protons on rings 2

and 3 do not shift upfield upon solvent change, indicating no conformation change that moves them to within proximity of a π -stacking event, which is perfectly consistent with the expected helical structure. The data obtained by solvent titration for tetramer **17** (bottom graph of Figure 4.2a) is even more dramatic. It is clearly evident that the average upfield shifts (Δppm) for the signals corresponding to the protons on rings 1 and 4 are greater than rings 2 and 3, which strongly supports a helical folded conformation.

Helical molecular models shown in Figure 4.2b predict and confirm folded conformations for each tetramer: side chains have been omitted for clarity. The variations in tetramer structures are primarily seen in the slip stacking angle and distance between rings 1 and 4. A vertical line is shown for each molecule which is perpendicular to the plane of ring 4 along with a second line extending from the center of ring 4 through the center of ring 1. The angle between these lines helps approximate the slip-stacking offset while the distances between rings were measured through the center of each ring. Exact face to face stacking of the rings would be indicated by an offset angle of 0° and a distance between rings similar to constrained and π -stacked benzene rings, or 3.4 \AA .⁽⁷⁶⁾ Given the conformational constraints of this oPE system, the electronics and/or dipoles of each ring should have an influence on the details of the geometry of the stacked rings⁽⁷⁷⁾ which in turn impacts the folded conformation. The structures shown in Figure 4.2b are the minimized conformations; however it should be noted that the system is dynamic, so this is really only one snapshot.

The repulsion that might be expected for the electron rich rings of tetramer **11** (Et₄, top of Figure 4.2b) is observed by the 35° slip stack angle between rings 1 and 4.

For tetramers **22** (EsEt₃) and **17** (Es₄) the slip stack angle is approximately 20° and 11° respectively. These predictions fall directly in line with the data shown in Figure 4.2a. The angle of slip-stack or off-set should directly correlate to the degree of π - π stacking experienced by each ring, which would therefore be reflected in the magnitude of upfield shifting experienced by the protons of rings 1 and 4. This is consistent with the observations here in which the system with the smallest angle of off-set (**17**, Es₄), is the system in which the largest degree of upfield shifting occurs.

In terms of the distances that can be measured from the center of ring 1 to the center of ring 4, tetramers **11**, **22**, and **17** are separated by approximately 4.3Å (Et₄), 4.1Å (EsEt₃) and 3.8Å (Es₄) respectively. This again provides evidence to support the data obtained in Figure 4.2a, suggesting that protons of tetramer **17** (Es₄) are most affected in the helical conformation. In addition, the tilt, or face-to-edge stacking, between rings 1 and 4 is very small. The models show a trend in which this small tilt is observed to increase from tetramer **17** to tetramer **11**. Table 4.1 summarizes the ring proton shifts (Δ ppm) for the endpoints of the titrations of tetramers **11**, **22**, and **17** and shows that in all cases rings 1 and 4 shift upfield while rings 2 and 3 move very little, which is perfectly consistent with the expected helical structure.

Table 4.1: Average Δ ppm (CDCl₃-CD₃CN) shifts for aryl protons for **11, **22**, and **17**.**

Ring Number	11 (Et ₄)	22 (EsEt ₃)	17 (Es ₄)
1	-0.09	-0.13	-0.21
2	0.01	0.00	-0.04
3	0.02	0.00	-0.02
4	-0.05	-0.10	-0.19

By examining the 1D NMR traces of all the aromatic protons (Figure 4.3a) and coupling these observations with the molecular models or tetramers **11**, **22**, and **17** (Figure 4.3b), more details about the ppm-shifting of each aryl proton can be found. Ring assignments were made using a combination of J-coupled correlation spectroscopy (COSY) and heteronuclear multiple bond correlation (HMBC) NMR experiments to identify which protons are attached to each ring of the tetramers. For tetramer **11**, the model shown at the top of Figure 4.3b suggests that protons 1a, 4a, and 4b would experience the largest change in chemical environment. The NMR spectra shown alongside the model in Figure 4.3a(top) supports this observation as these three protons experience the largest change from CDCl₃ to CD₃CN. Proton 4b is influenced by the aromatic ring while protons 1a and 4a are influenced by the triazene and acetylene functionality, respectively. At the same time, very little upfield shift is observed for 4c, while 1c actually shifts *downfield*. In general, we observe this small downfield shift for the aromatic protons of model compounds which is most likely due to the change in dielectric constant of the solvent. The internal standard, tetramethylsilane, corrects this shift. At the same time, the inherent downfield shift of the protons going from CDCl₃ to CD₃CN provides further support for π - π stacking of rings 1 and 4 influences and upfield

shifts we observe in CD_3CN . The overall upfield shifts for **11** are the smallest of the three tetramers, again indicating a very weak interaction between rings 1 and 4 overall.

For tetramer **22** (EsEt_3) the model indicates that the protons of rings 1 and 4 which should be most affected by the folded conformation are 1b, 1c, 4a, and 4b. Proton 1b is located under the triazene group, proton 1c is influenced by the ester function, proton 4a is located near the acetylene bond, and 4b is located above ring 1. Interestingly, protons 1b and 4c of tetramer **1** as well as 1a and 4c of tetramer **22** do not experience significant upfield shift. These protons, although labeled differently due to chemical connectivity, are found in the same locations on the two foldamers (see Figure 4.3b, top and middle). The molecular model of tetramer **17** (Es_4) indicates that the rings are nearly on top of one another suggesting that all of the protons on rings 1 and 4 should be affected and all their signals should shift upfield accordingly. Indeed this is what is observed in the NMR spectra at the bottom of Figure 4.3a. In fact, all of the proton signals associated with rings 1 and 4 shift upfield considerably more than tetramers **11** or **22**.

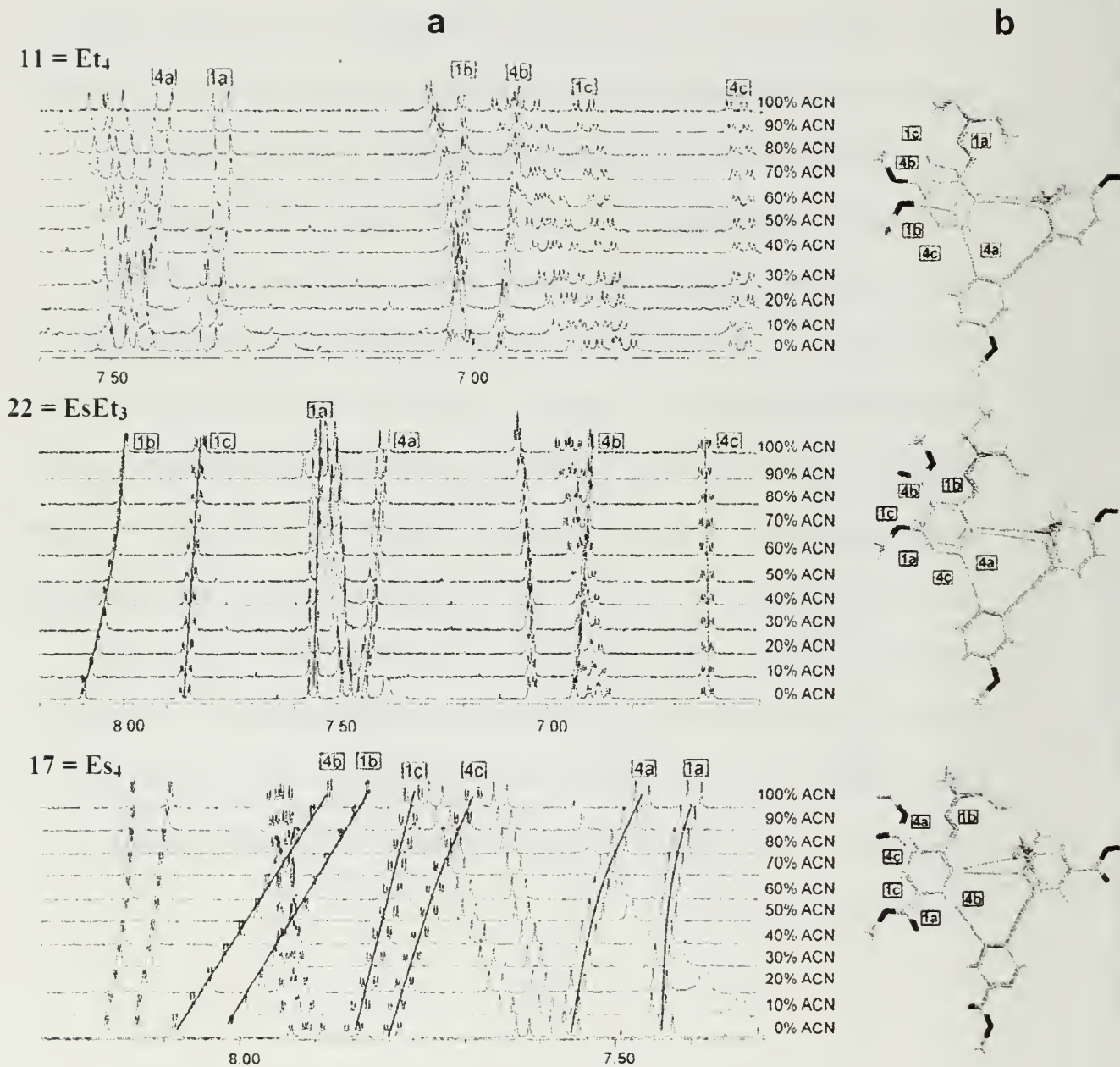


Figure 4.3: (a) NMR traces for each concentration of Acetonitrile (CD₃CN) in CDCl₃ for tetramers 11, 22, and 17 (1.25 mM, 400 MHz, 298 K). Individual signals from rings 1 and 4 have been labeled and were assigned by a combination of COSY and HMBC 2D NMR experiments. Tetramethylsilane is the external reference for the solvent referenced (top) 11 Et₄, (middle) 22 EsEt₃, (bottom) 17 Es₄. (b) Top down views of molecular models.

4.4 2-D NMR Characterization of Et₄, EsEt₃, and Es₄

In addition to the 1D data, we speculated that the terminal TMS group would provide an excellent NMR probe in NOESY experiments for two main reasons. The chemical shift of the TMS falls at a unique region in the spectra (~ 0.2 ppm) compared to the rest of the protons in the molecule and the methyl groups extend beyond the aromatic backbone plane by ~ 2.0 Å. Due to the inherent distance dependence of NOESY, which is typically 4-5 Å, and the likelihood of similar stacking distances, this additional ~ 2.0 Å plays an important role.

Tetramer **22**, EsEt₃, was examined by 2D (NOESY) ¹H NMR studies at room temperature in CDCl₃ and CD₃CN (Figure 4.4a). The TMS peak appears at 0.2 ppm and the aryl peaks corresponding to ring 3 appear at 7.51 ppm (*3a*), 7.07 ppm (*3b*), and 6.96 ppm (*3c*) in CD₃CN. A strong NOE between the TMS protons and proton 3c was observed in CD₃CN but is completely absent in CDCl₃ as shown by the partial NOESY spectra in Figures 4a and 4b. The NOE interactions are consistent with a folded structure in which the electron-poor ring 1 stacks with the electron-rich ring 4 (see Figure 4.3b, middle).

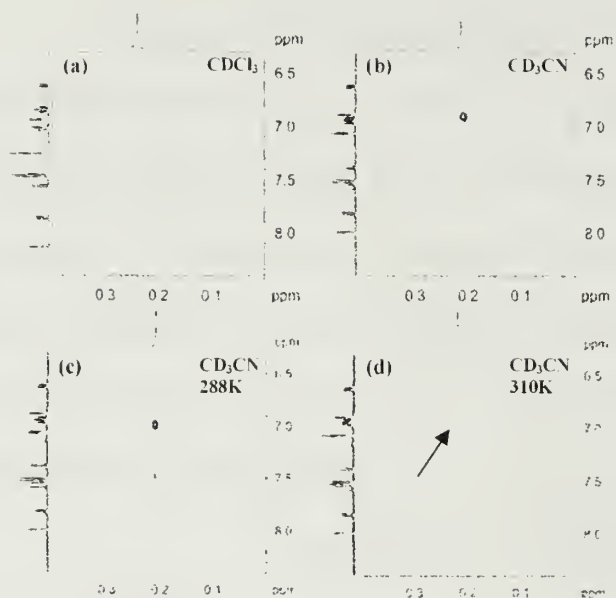


Figure 4.4. Partial NOESY spectra of **22**, EsEt₃ (1.25 mM, 400 MHz, 298 K, mixing time: 0.1 s) for the TMS and aryl region in CDCl₃ (a) and CD₃CN (b). No cross peak is observed in CDCl₃ while a strong NOE is present in CD₃CN. Partial NOESY Spectra of **22** (1.25 mM, 400 MHz, mixing time: 0.1 s) in CD₃CN revealing the TMS to aryl interaction at 288K (c) and 310K (d).

When tetramer **17** was examined by 2D (ROESY) ¹H NMR studies (Figure 4.5) at room temperature in CDCl₃ and CD₃CN, a strong NOE cross peak was observed between the terminal TMS of the molecule and a methyl from the triazene end group of ring 4 *only* in CD₃CN. This cross peak is completely absent in CDCl₃ indicating tetramer **17**, Es₄, folds in CD₃CN but not in CDCl₃. This NOE further indicates the TMS group continues in the progression of the helix, consistent with the NOE observed for **22** in Figure 4.4a, and that rings 1 and 4 are closer to face-to-face stacking than face-to-edge since face-to-edge would most likely move the two end groups (triazene and TMS) away from each other. Extracting distance data based on the normalized integrals (A_N) of the NOESY/ROESY cross peaks (see Table 4.2) confirms the close proximity of the TMS and ring 3 (**22**, EsEt₃) or the TMS and triazene end groups (**17**, Es₄). As the distance r_1 between protons a and c on one ring can be approximated as 2.44 Å, a relation between the observed cross peaks and the distances can be

determined. At room temperature, the TMS is ca. 2.29 Å away from proton 3c of **22** and the triazene is ca. 3.36 Å from the TMS of **17**. Based on the formula presented below, NOESY distances were calculated using the aryl a proton to c proton distance as a standard.

$$\frac{A_1}{A_2} \propto \frac{r_1^6}{r_2^6}$$

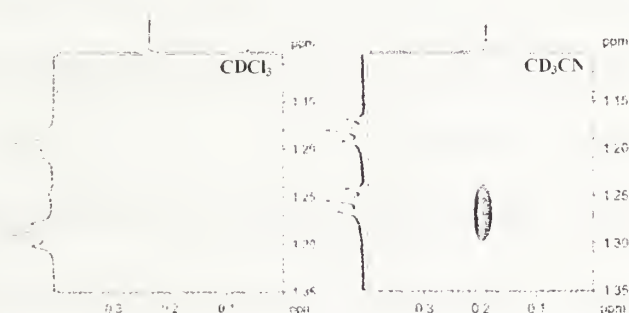


Figure 4.5: Partial ROESY spectra of **17**, Es₄ (1.25 mM, 600 MHz, 298 K, mixing time: 0.3 s) for the TMS and triazene region in CDCl₃ (left) and CD₃CN (right). No cross peak is observed in CDCl₃ while a strong NOE is present in CD₃CN.

Table 4.2 Calculated NOESY distances.

Molecule	A ₁	A ₂	r ₁ (known)	TMS to X distance (Å) (calculated r ₂)
			distance between proton a and proton c of any ring. Å	
22 (EsEt ₃)	1	1.47	2.44	2.29
17 (Es ₄)	1	0.14	2.44	3.36

X = Proton 3c for **22**, and methyl of triazene for **17**

When tetramer **11** was examined by NOESY, no NOE signal was observed. The lack of NOE peaks for tetramer **11** is most likely due to the presence of the two

electron rich rings which are not expected to promote folding as strongly and/or forces the two rings (1 and 4) further apart due to the higher electron density which consequently pushes the TMS protons out of NOE distance correlation range (4-5 Å). In addition to the crystal structure shown in Chapter 3 that has an extended conformation for an ether substituted oPE, recently published work by Bunz and coworkers shows a flat crystal structure for a di-methoxy substituted oPE pentamer with pyridine endgroups. The 1-D proton chemical shift values discussed in Figures 2 and 3 support folding of this oligomer, but are also consistent with the lack of NOE cross peaks since the Δppm is the smallest of all the three oligomers and the distance (measured by modeling) is the largest.

Other NOESY studies for folding oligomers(26) have indicated that low temperature is required to obtain an NOE cross peak. All of the work presented thus far was collected at room temperature. Taking into account this possible temperature dependence, we performed a limited temperature study to determine whether the NOE signals we observed for tetramer **22** were temperature dependent. Upon cooling tetramer **22**, Et_3Si , to 288K, a new NOE signal appears between the TMS protons and **3a** so that two NOE's are present (Figure 4.4c). These signals correspond to distances of 2.42 and 2.97 Å respectively for **3c** and **3a**. Conversely, when the temperature is increased to 310K (Figure 4.4d) the NOE for **3a** completely disappears and the original **3c** NOE is diminished by 95%. This temperature variation in NOE is consistent with a folding pathway in which rings 1 and 4 would interact more strongly with one another as the temperature is reduced, leading to the additional NOE signal. Conversely,

elevating the temperature reverses this effect resulting in the observed decrease in the two NOE signals and intensities.

4.5 Temperature study of Et₄, EsEt₃, and Es₄

A brief 1D study of tetramers **11**, **22**, and **17** is shown in Figure 4.6 over the same temperature range as the NOE study of **22**. This study reveals the expected downfield shift of the aromatic protons on rings 1 and 4 with increasing temperature and tetramer **17** shifts more than tetramers **22** and **11**. The larger observed shifts for the protons of tetramer **17** are likely due to the fact that **17** is stacked more closely than **22** and **11**. This is consistent with the data discussed above. In addition, since **17** is more closely packed, a small change in distance would influence the Δ ppm more. Another intriguing possibility is that **22** is more stable due to complimentary electrostatics. Iverson (27,28) showed that complimentary π -systems (π -rich and π -poor) associated more than two π -poor systems by one order of magnitude. His study formed a charge-transfer complex, unlike ours; however the trend is similar. Currently, we cannot distinguish these two possibilities: although, the first one in which **17** packs more tightly is most consistent with the data presented. What is clear is that the observations in the 1-D spectra agree (Figure 4.6) agree with the NOE variable temperature data. Additionally, when the data for **11** is examined, there is virtually no change for this particular system. Whether this lends credence to the possibility that these systems are not folded (as seen with other reported crystal structures) or that rings 1 and 4 are simply too far away from one another to influence the behavior of the other π systems, remains to be seen.

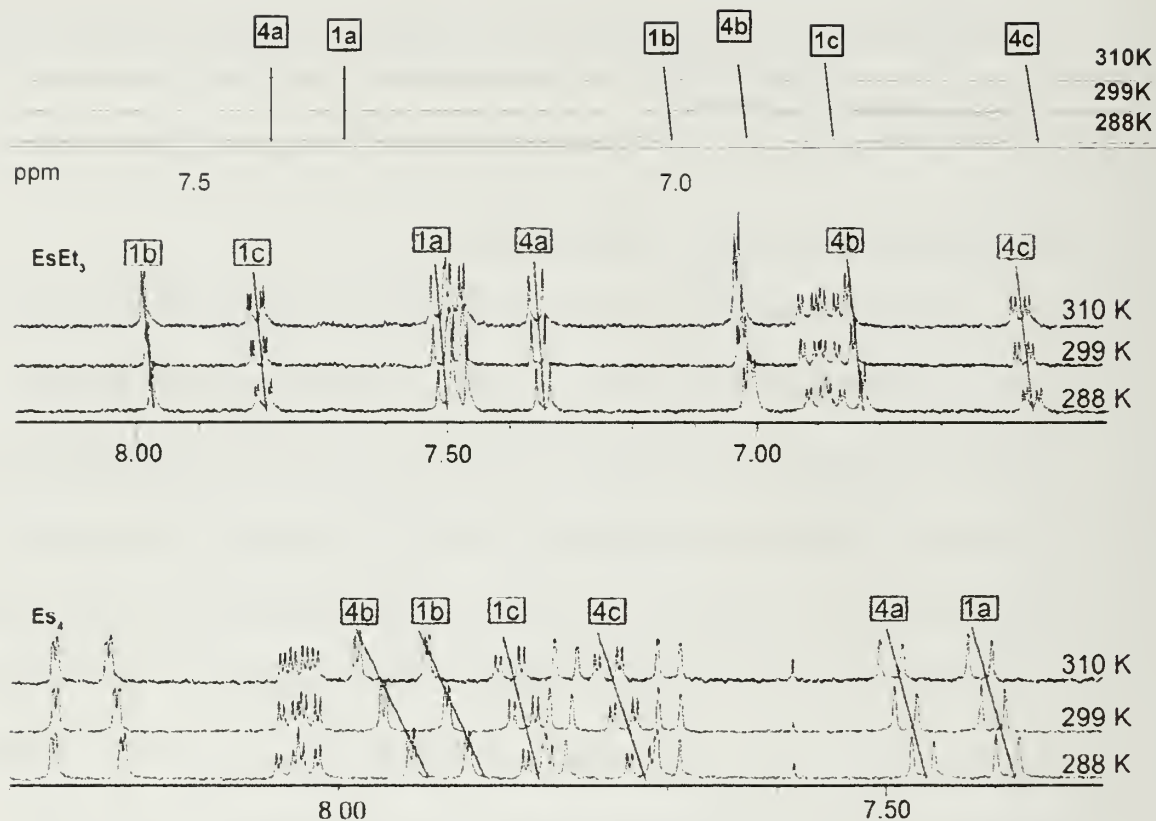


Figure 4.6: NMR traces in Acetonitrile (CD_3CN) for tetramers **11** Et_4 (top) **22** EsEt_3 (middle) and **17** Es_4 (bottom) at 288K, 299K, and 310K. Downfield shifting is evident as temperature is increased. Tetramethylsilane was used as an external reference for each spectra. Individual signals from rings **1** and **4** have been labeled and were assigned by a combination of COSY and HMBC 2D NMR experiments.

4.6 End group behavior

When the region for the TMS end group in Figures 4.4 and 4.5 is examined closely, it is evident that the signal for the TMS protons also shifts upfield in CD_3CN . The TMS end group of tetramer **17** (Es_4) is most affected, shifting upfield 0.06ppm. The magnitude of shifting, although small, is directly related to the tetramer studied and shows a larger shift going from **11** to **22** to **17** as shown in Table 4.3. This is additional support that the TMS end group lies over the plane of ring **3**.

Table 4.3: Δ ppm shifts for end group TMS

Molecule	Δ ppm
11 (Et ₄)	0.03
22 (EsEt ₃)	0.04
17 (Es ₄)	0.06

4.7 Conclusions

Very short novel oPE oligomers are reported and shown to fold at room temperature by 1D and 2D NMR. NOESY provides the first high resolution data on solvent driven PE oligomers and confirms oPE as a versatile and suitable scaffold to construct foldamers. Tetramers **22** and **17** appear to fold best with the potential to unfold at higher temperature indicating an additional route for denaturation. Additional studies to determine the structure most suitable for stable helix formation with the oPE systems is required. The 1-D chemical shifts appear to be more sensitive to aromatic stacking than NOE interactions. oPE oligomers will generate high aspect ratio objects when folded and are being studied for self assembly into larger, tertiary-like structures as well as for the display of chemical functions in 3-D space.

CHAPTER 5

CONFIRMING FOLDING IN LONGER OPE SYSTEMS

5.1 Introduction

Though folding was shown to be exhibited by an extremely short, electronically diverse set of oPE backbones in Chapter 4, the question remains whether these molecules will fold into compact helices at longer oligomer lengths. Other oPE systems reported in the literature either do not explore folding (40, 41, 44, 78) or report folding in longer systems with methods we have determined to be inconclusive at best (45).

Modeling using Molecular Mechanics Force Field (MMFF) simulations showed that at longer lengths these oPE oligomers have low energy helical conformations, this has yet to be proven experimentally.(79) Using the 1-D and 2-D NMR methods reported in Chapter 4 with the addition of temperature titration studies this Chapter will examine the longer folded structures of the Teg-Ester oPE system in detail. This chapter will include data to show that these oligomers 1) fold in acetonitrile, 2) are responsive to temperature in acetonitrile, 3) may have some folded character in chloroform as the oligomer length is extended and 4) exhibit peaks in the 2D spectra that definitively support folding. The sections will be broken into a discussion of 4 oligomers, tetramer Es₄ (17), pentamer Es₅ (18), hexamer Es₆ (19), and nonamer Es₉ (20).

5.2 Methodology

Our prior success using 1-D NMR methods as a characterization technique continues to hold at longer lengths for these oPEs. Comparing ¹H NMR traces of oPE

with meta PEs containing two turns, each in CD₃CN at similar concentration (Figure 5.1). It is very clear that the detailed NMR analysis reported here would be impossible with the ambiguous unresolved mPE systems. Clearly resolved and deconvolutable spectra are found even at lengths of 9 units (3 turns of a helix) or 27 different aromatic protons.

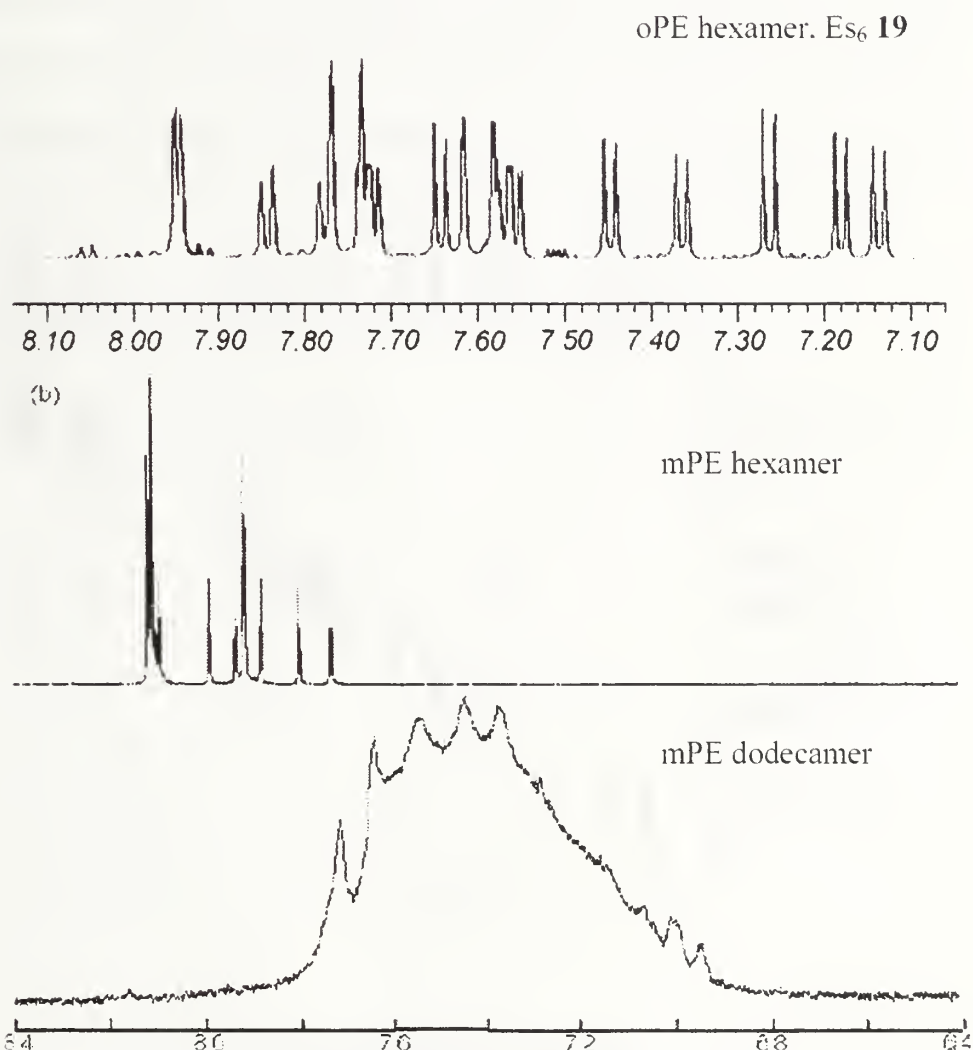


Figure 5.1 Comparison of oPE hexamer with two turns (top) and mPE oligomers with one (middle) and two turns (bottom). Bottom two spectra from Jason Nelson's thesis- <http://sulfur.uiuc.edu>.

To unambiguously assign all of the aryl protons and ring systems, a combination of J-coupled correlation spectroscopy (COSY) and Heteronuclear Multiple Bond Correlation (HMBC) spectroscopy were used (80). COSY (Figure 5.2) was utilized to identify particular ring systems for which each *a* (8.4Hz, d), *b* (2.1Hz, d) and *c* (8.4 Hz, 2.1 Hz, dd) proton were associated. HMBC (Figure 5.3) was used to walk along the structure, identifying each ring position starting with the two termini. The TMS acetylene terminus as ring 1 (R₁). Using strong, medium, and weak correlations, we were able to identify which acetylenic carbons (92 – 103 ppm for ¹³C NMR) are correlated with the *a* or *b* protons on the ester substituted rings, and thus assign all the ring systems. Figure 5.4 shows the assignments for 17, 18, and 19 as made by HMBC and COSY in CD₃CN.

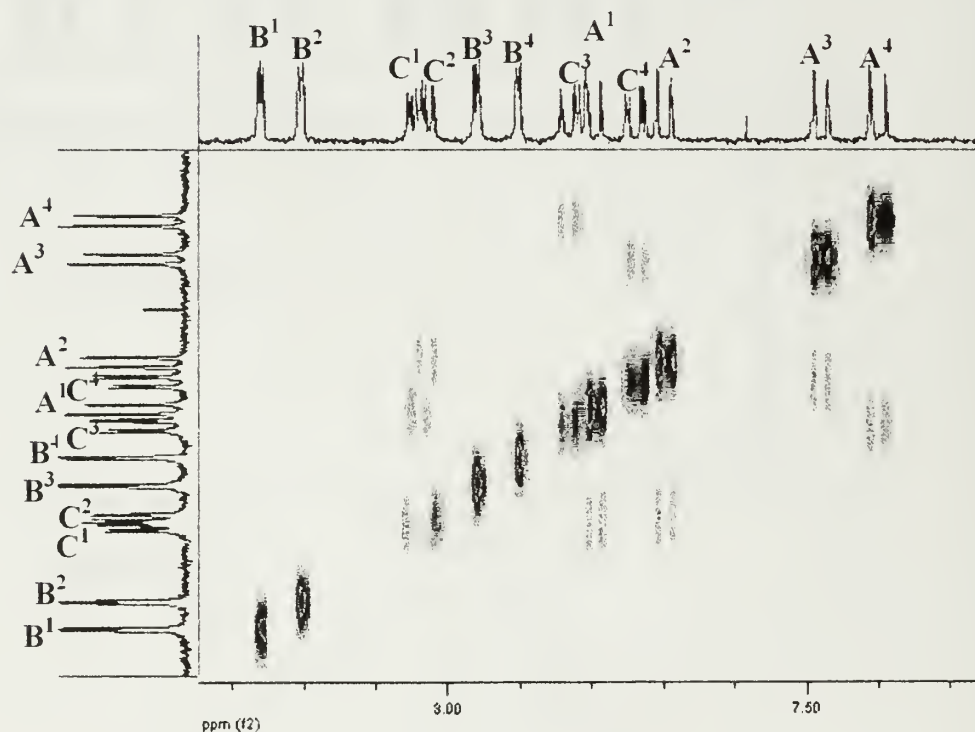


Figure 5.2 COSY spectra for Es₄.

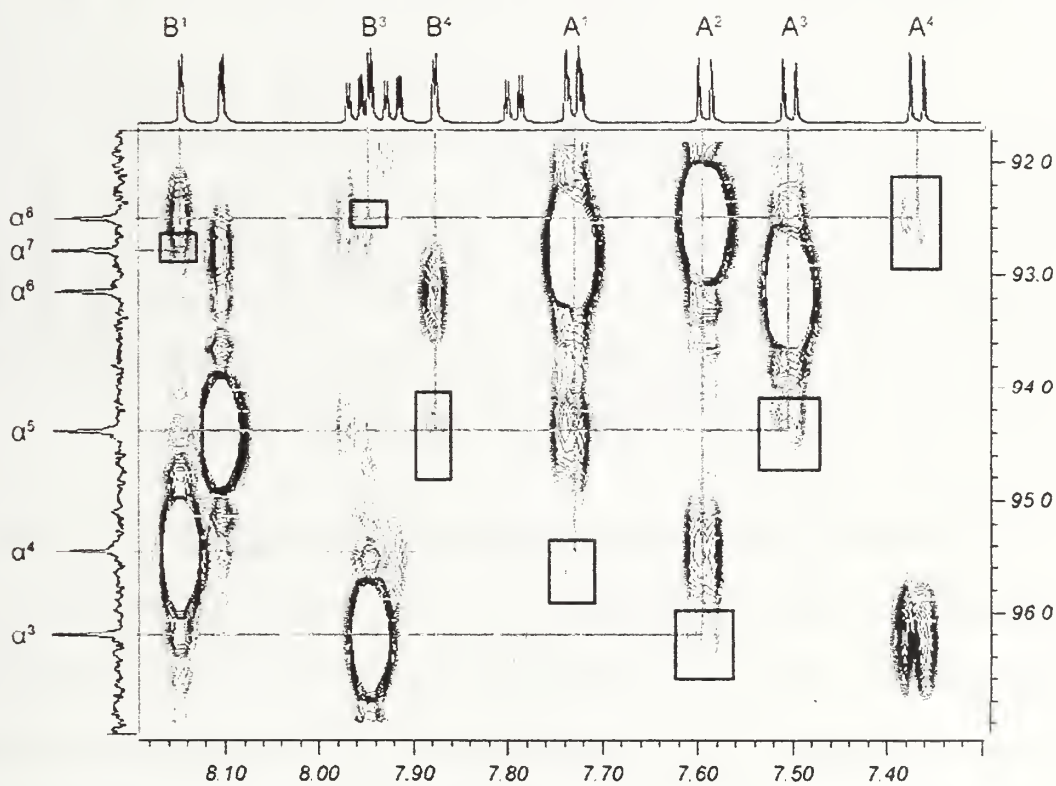
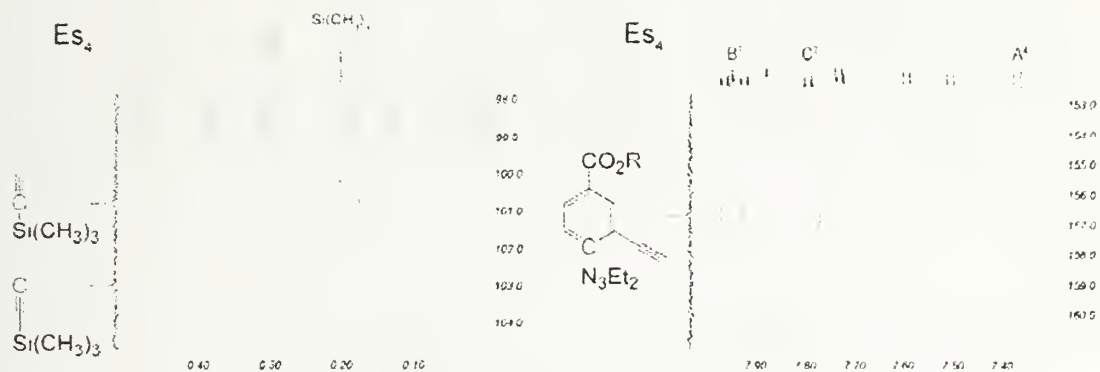


Figure 5.3 HMBC page identifying Es_4 .

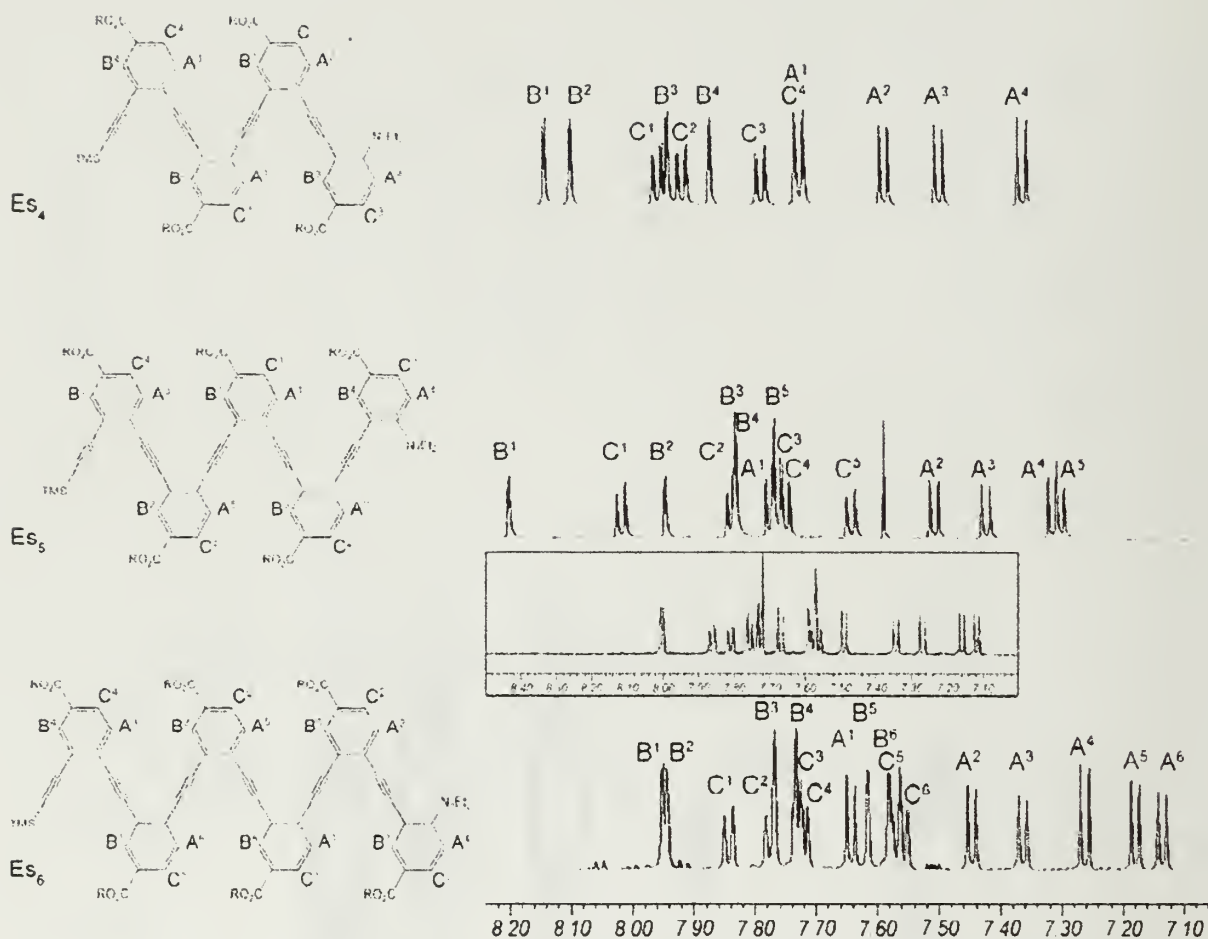


Figure 5.4 Assignments and protons for Es_4 - Es_6 .

For this study, each oligomer was examined at a concentration of 1.25 mM, a concentration at which it was determined there was no large scale aggregation by UV and fluorescence spectroscopy. Solvents used in this study were the same as those in Chapter 4, chloroform (CDCl_3), the "unfolded" solvent, and acetonitrile (CD_3CN) as the solvent that would preferentially solvate the side chain thus promoting folding of the oligomer into a helix. A solvent titration was performed from CDCl_3 to CD_3CN in increments of 10% volume CD_3CN , keeping the concentration constant. The presence of π - π stacking in longer oligomers would result in upfield shifting in the ^1H NMR for the aromatic protons on rings thought to be associated with folding. If these oPE

oligomers fold in a manner that is consistent with helix formation, it is expected that, in the case of tetramer **17**, the shifted rings involved in the study would be R_1 and R_4 . For pentamer **18**, the shifted rings would be $R_{1,2,4,5}$ and for hexamer **19** and nonamer **20**, all rings R_{1-6} and R_{1-9} would be involved in folding.

Given molecular modeling studies that indicating that the helically folded oPE hexamer is more energetically favorable than the extended conformation ($\Delta H_{\text{helix}} = -18$ kcal/mol), one could imagine a variety of misfolded states between these two extremes as seen below in Figure 5.5. Figure 5.5 (a) is the extended state and (e) is the folded state, endpoints of the conformational possibilities, while (b-d) represent some of the many potential conformers: (b) $R_{1,4}$ stacked, (c) $R_{1,4}$ and $R_{3,6}$ stacked, and (d) $R_{1,4}$ and $R_{2,5}$ stacked.

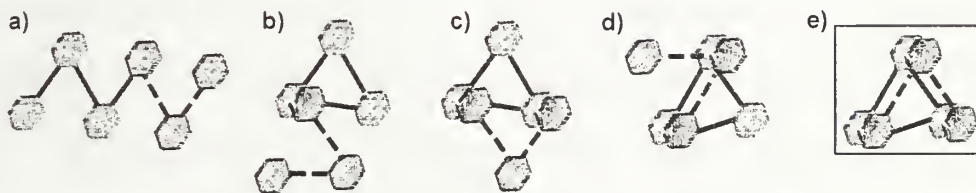


Figure 5.5 Potential conformers of oPE hexamer.

The calculated models do not take solvent into account thus the energy between the conformers stems from torsional differences. The confidence in the models, even though solvent is not taken into account, stems from the consistency they provide with respect to the 1-D and 2-D NMR data that has been obtained. It is thought that the mechanism of folding involves preferential solvation(72) showing the sidechains to the solvent and hiding the hydrophobic backbone in the presence of a high dielectric solvent. Given this premise it would be possible to have a structure like (c) with $R_{1,4}$

and R_{3,6} stacked with R₂ and R₅ on opposite sides of the molecule extending the Teg sidechains into the solvent.

Table 5.1 shows the energies for conformations as calculated by Spartan for hexamer **19** (series 1) and a series of previously published hexameric conformers (series 2). (79) It should be noted that series 2 conformers are disubstituted oPE oligomers in contrast to the mono substituted Teg-ester hexamer of series **1**. It is interesting to note that the ΔH_{helix} is identical between the extended and folded conformations of each series is identical even though they vary in electronic, side chain, and end group composition. Their similarity could be a result of balancing the off-set of the rings with electrostatics, dipole, or steric crowding which could be a factor in the disubstituted version.. It can be seen that the ΔH_{helix} of the "misfolded" conformers (b-d) is at most ~10kcal/mol. It is interesting that for series 1 (b) and series 2 (c) that the ΔH_{helix} is on the order of the rotation about an ethane carbon bond (3kcal). Though models provide some insight as to the character of these oPE helices they are not definitive.

Conformer	H _{series 1} (kcal/mol)	- ΔH_{helix} (Series 1) (kcal/mol)	H _{series 2} (kcal/mol)	- ΔH_{helix} (Series 2) (kcal/mol)
a) Extended	516.9	17.2	152.9	17.2
b)R ₁ over R ₄	504.7	5.0	145.6	9.9
c) R ₁ over R ₄ R ₃ over R ₆	508.5	7.8	143.7	8.0
d) R ₁ over R ₄ R ₂ over R ₅	504.0	4.3	140.6	4.9
e)fully Helical	499.7	0	135.7	0

Table 5.1 Energies for conformers of hexameric oPE as determined by MMFF in Spartan. The H is the energy of the conformer as given by modeling program while the ΔH is calculated as the difference between the helical and the other conformers

Experimentally, examination of the aryl region of the NMR should provide insight into the fully or partially folded conformer of longer oligomers with changing solvent. In addition to solvent, a variety of temperatures for both CD₃CN and CDCl₃ were examined to probe the stability of the structures formed. It has been shown that for longer oligomer lengths in other foldameric helices, the longer the structure the more stable the helix is (32, 81) even at high temperature in high dielectric solvent (81). This would be expected due to the stabilizing influence of the non-covalent interactions promoted by a helical conformation. A temperature range of -26°C to 77°C was explored here to determine if a) the structures are denaturable in CD₃CN or b) the structures are completely unfolded in CDCl₃. The low point of this temperature range was chosen due to instrument limitations though the freezing point of CD₃CN is -45°C and CDCl₃ is -63.5°C. Boiling points for CD₃CN (81-82°C) and CDCl₃ (62°C) were taken into account for the upper limit of the temperature study.

Though the 1-D NMR evidence of folding is compelling, additional data in the form of 2-D NMR showing intramolecular interactions in the folded structure would be of tremendous support. As it was shown in Chapter 4, Nuclear Overhauser Effect Spectroscopy (NOESY) is a very useful tool for investigating secondary structure. The beauty of the method is that it can be used to observe intramolecular proton-proton interactions of less than 5Å through space to elucidate solution conformations.(71) There are, unfortunately a few drawbacks to NOESY that made this work challenging. First, there is a molecular weight dependence (shown in Figure 5.6) that can make the NOE cross peak disappear as the intensity of the peak passes through zero. This was

remedied by using a slightly different form of NOESY- Rotating Frame Overhauser Spectroscopy (ROESY). This method is always positive and does not have a region where the NOESY signal could possibly be zero. Drawbacks to this method include a loss in sensitivity as molecular weight increases.

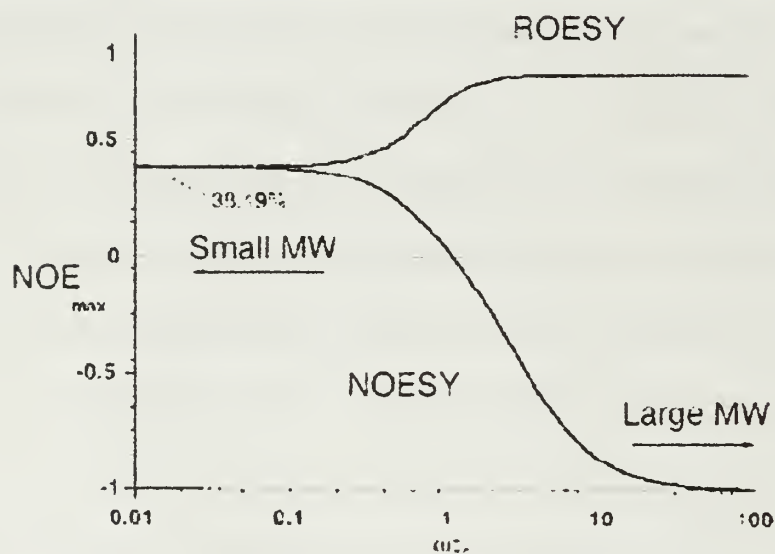


Figure 5.6: Depiction of molecular weight dependence for NOE experiments

The second challenge is the time frame over which these experiments were carried out. Unfortunately for a high resolution spectra with the spectral width that we wanted to observe (~ 8.5 ppm), many hours are required. Each of the ROESY experiments required over 20 hours on the 600 MHz, where we were limited for time.

Distance data can be approximated by the following relation between the intensities of the cross peaks and known distances and were calculated as such in this chapter.

$$\frac{A_1}{A_2} \propto \frac{r_1^6}{r_2^6}$$

Figure 5.7: Simple relation between intensities and distances for NOESY/ROESY experiments.

What follows is a detailed discussion of each oligomer for the solvent titration, temperature study in CD₃CN and CDCl₃, and ROESY measurements taken at 270K for the Teg-ester oPE oligomers.

5.3 Es₄ Oligomer Solvent and Temperature Effects

Figure 5.8 (a) shows an extended chemical structure and a folded molecular model of tetramer **17** with R₁ and R₄ stacked on top of one another. The raw data for this oligomer was presented in Chapter 4 but is added here for perspective with the longer oligomers. In (b) the raw data for solvent titration performed from 0% CD₃CN (100% CDCl₃) to 100% CD₃CN. Each peak for each proton has been labeled: 1a = the a proton on R₁. Lines to follow the paths of protons 1a-1c and 4a-4c have been added for clarity. It is very evident that all of the protons 1a-1c and 4a-4c shift upfield with the addition of CD₃CN while 2a-2c and 3a-3c shift downfield as the percentage of CD₃CN increases. It was previously discussed that the reason for this marked difference in the behavior of protons in the ester series may be due to two things: 1) the potential closeness of the ring system as it stacks and packs compactly, and 2) the overall spectral sensitivity of ester substituted phenyl rings (75). While this second possibility has yet to be fully explored, if the commentary put forth by Hunter and

Sanders (82) holds then electron acceptors, or electron poor rings would be more attractive to one another due to their ability to overcome the π -electron repulsion with electron deficiency which would then explain the remarkable upfield shifts that we observe in these systems. If the impact that the ring current has on neighboring protons varies widely with distance away from the ring then even a 0.5 Å difference in the distance between the rings would change the overall impact of the phenyl ring dramatically. In Figure 5.8 (c) we have compressed the data from the solvent titration for tetramer **17**, showing the Δ ppm values for each ring of oligomer **17**. Each value was calculated by averaging the a, b, and c protons of each ring, and corrected for the addition of CD₃CN. The values have been normalized to a Δ ppm value of zero at 0% CD₃CN for clarity. R₁ and R₄ both shift upfield (to negative values) dramatically while R₂ and R₃ clearly do not shift upfield with increasing CD₃CN concentration. Thus, the short tetramer **17** has been shown to fold in CD₃CN.

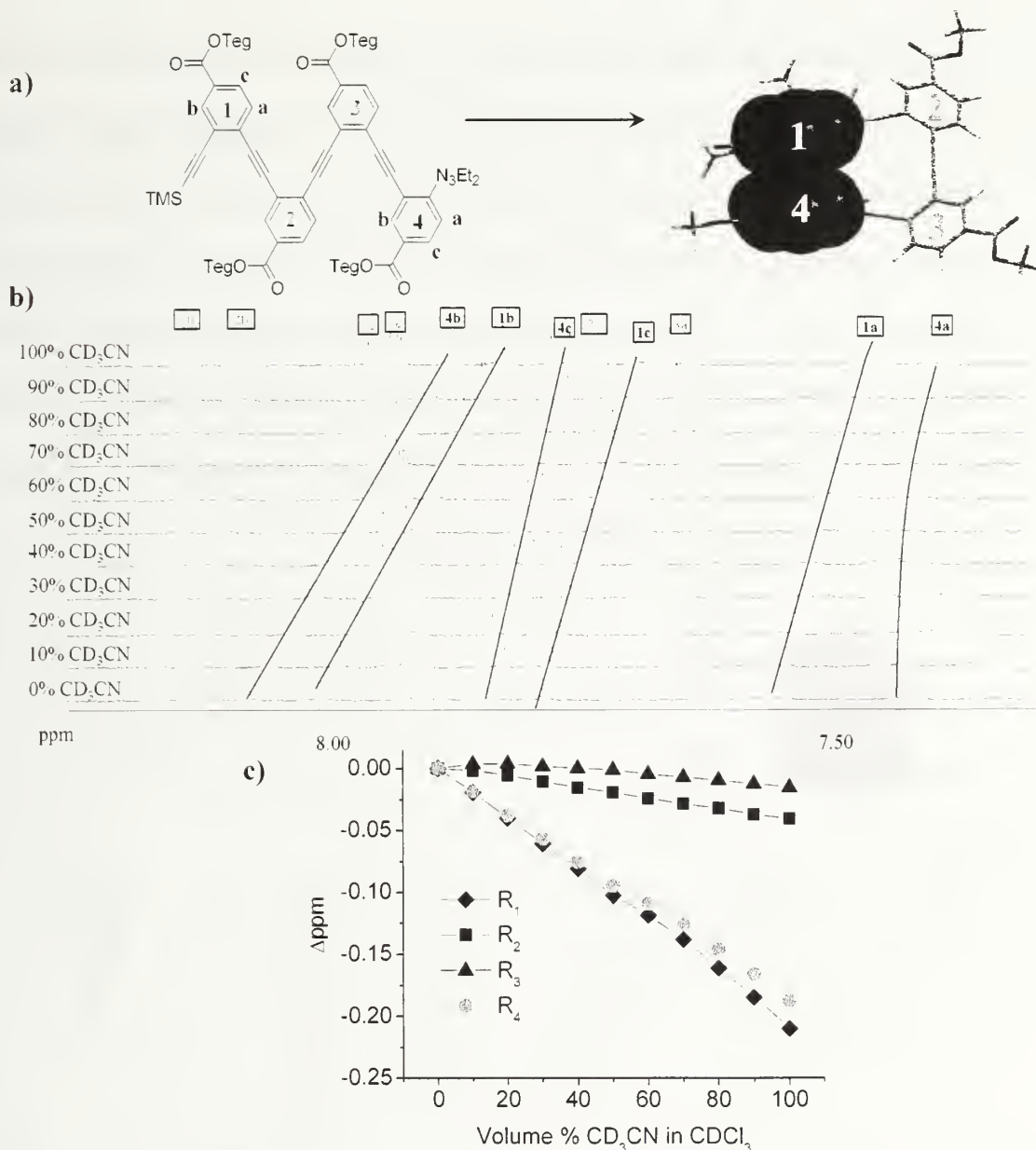


Figure 5.8: (a) Chemical structure and molecular model of tetramer 17 extended and folded. (b) Raw data for solvent titration of 17. (c) Compressed data showing the Δ ppm for each ring.

Figure 5.9 shows a temperature study in CD₃CN for tetramer 17. In (a), the folded molecular model is shown with R₁ and R₄ stacked on top of one another with the extended chemical structure of 17. In (b) the raw data for the temperature study performed from 247K (-26°C) to 350K (77°C) in CD₃CN is shown. Each peak for each proton has been labeled: 1a = the a proton on R₁. Lines to follow the paths of protons

1a-1c and 4a-4c have been added for clarity. In (c) compressed data of the temperature study for oligomer **17** in CD₃CN, showing the Δ ppm values for each ring of oligomer **17** are calculated by averaging the a, b, and c protons of each ring. The values have been normalized to a Δ ppm value of zero at 247K (-26°C) for clarity. It is very clear that R₁ and R₄ both shift downfield dramatically with increasing temperature while R₂ and R₃ clearly do not shift downfield during a 100°C temperature change. This change for R₁ and R₄ is due to the disruption of π - π stacking in the folded solvent which allows the protons on R₁ and R₄ to shift back downfield.

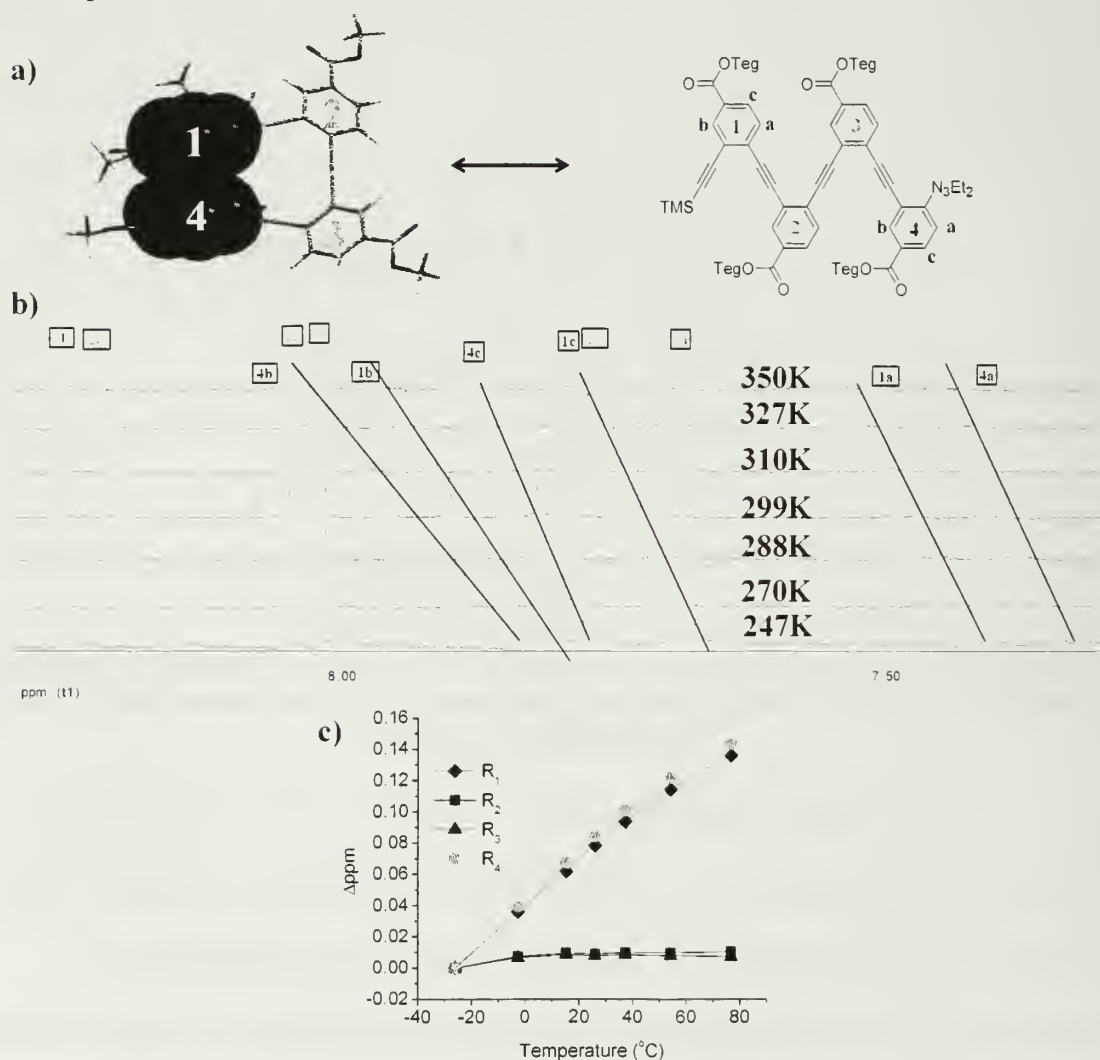


Figure 5.9: (a) Molecular model of tetramer **17** folded. (b) Raw data for temperature study of **17** (c) compressed data showing Δ ppm for each ring (R₁-R₄)

Moving to a temperature study in CDCl_3 , compressed and plotted data is shown in Figure 5.10. It is clear that any residual effect that R_1 and R_4 may have had on one another is absent. The scales of the x and y axes for Figures 5.9 and 5.10 are identical thus indicating that the impact of temperature on any possible secondary structure in CDCl_3 is absent. There is no substantive temperature dependence for any ring R_1 - R_4 . If anything there is a slight *upfield* shift as the temperature is increased in CDCl_3 counter to any residual π - π interactions that would be disrupted due to increased temperature. If it is assumed, therefore, that tetramer **17** is completely unfolded in CDCl_3 this lack of temperature dependence is perfectly reasonable, given that the shorter oligomers not capable of folding exhibit no temperature dependence as well.

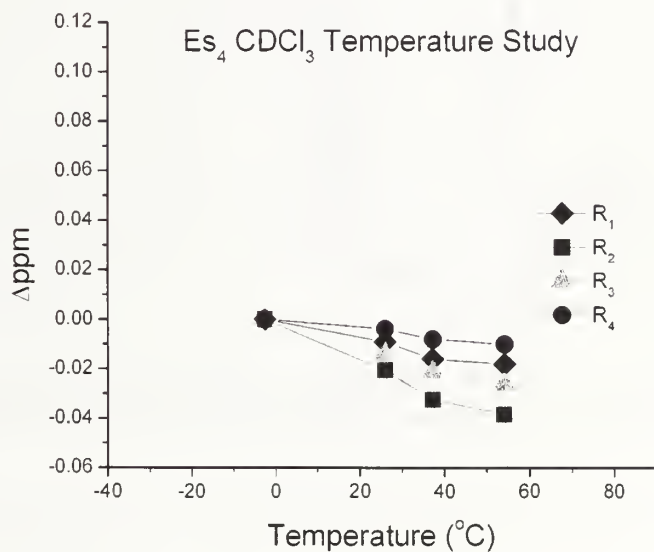


Figure 5.10: Δppm vs. Temperature in CDCl_3 for tetramer **17**

The preceding solvent and temperature data can be summarized on a single plot in Figure 5.11, where only the average of R_2 and R_3 are plotted (a) and the average of R_1 and R_4 are plotted (b) the shifts, trends, and sensitivity of this oPE oligomer are very clear. In Figure 5.11, average ppm is plotted on the x-axis while on the left y-axis.

volume % CD_3CN in CDCl_3 is plotted. On the two right y-axes temperature in CD_3CN is the first (red) axis and temperature in CDCl_3 is plotted on the second (blue) axis. It is evident in 5.11 (a) that there is little to no dependence of R_2 and R_3 ppm shifts on solvent or temperature in CDCl_3 or CD_3CN . These rings simply cannot be involved in folding or intermolecular associations for this tetrameric Teg-ester oPE. In (b) it is clear that R_1 and R_4 are impacted dramatically for both solvent and temperature studies but that these rings are unaffected in CDCl_3 . thus we believe that at this short length that tetramer **17** is completely unfolded.

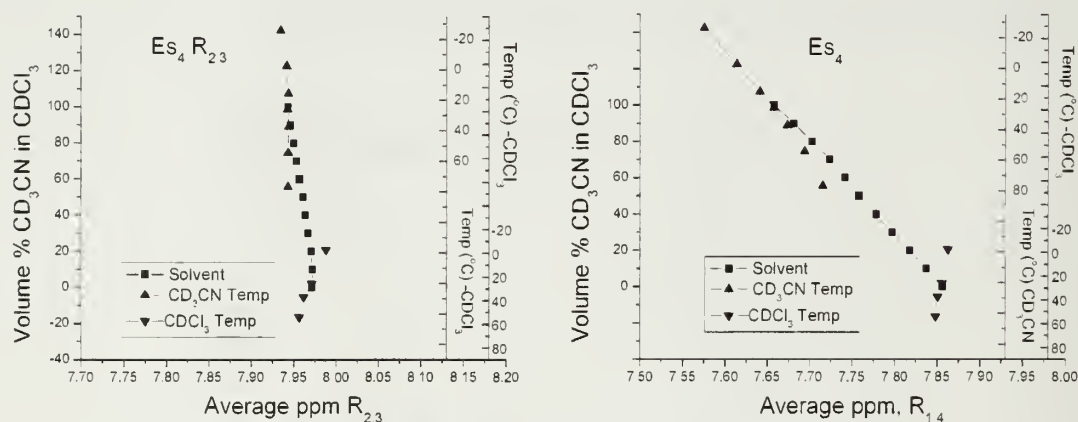


Figure 5.11: (a) Solvent and temperature plots for rings not involved in folding ($R_{2,3}$). (b) Solvent and temperature plots for rings involved in folding ($R_{1,4}$).

The linearity of the plots in CD_3CN (red) and the solvent plot (black) is probably due to the dynamic nature of these systems. In section 5.7, the dynamic nature of these systems will be explored in detail. Briefly, there is evidence of 2 conformers and thus substantiating that the NMR data taken is an average of the conformers that exist in solution but that the dominant form is a folded conformer where R_1 associates with R_4 .

The continued decrease in average ppm for R_1 and R_4 indicates that a plateau has not been reached for the total association of these rings. Given the opportunity to go to lower temperatures it is possible that a plateau may be reached, but as shown the slope of this plot below $\sim 20^\circ\text{C}$ is nearly identical to the solvent trace which is also linear. However, the increase in slope for the CD_3CN trace that occurs above $\sim 25^\circ\text{C}$ may indicate that there is an abrupt change/disruption in the association of these rings that is pushing them more quickly towards an unfolded conformation.

Clearly the conformation of tetramer **17** is highly solvent and temperature dependent, with a low average ppm (R_1 , R_4) of 7.55 ppm and a high of 7.85 which holds through heating in CDCl_3 indicating that the structure is completely unfolded in CDCl_3 .

5.4 Es_5 Oligomer Solvent and Temperature Effects

With the addition of 1 ring to the tetrameric oPE system, if the system is folding and rings are associating with one another, we would expect that this new ring (R_5) would fold in as well and associate with R_2 to form a helix where only R_3 is unaffected by changes in solvent and temperature. This is precisely what is observed. Figure 5.12 shows (a) the structure and folded model of pentamer **18**, (b) the raw data for the solvent titration, and (c) the compressed corrected data for the solvent titration.

In (b) each peak for each proton has been labeled: 1a = the a proton on R_1 . Lines to follow the paths of protons 1, 2, 4, and 5b, 2 and 3c, as well as 2 and 3a have been added. For (c) the plotted values have been normalized to a Δppm value of zero at 0% CD_3CN for clarity. R_1 , R_2 , R_4 , and R_5 all shift upfield due to π - π stacking dramatically while R_3 clearly does not shift upfield with increasing CD_3CN concentration. This is clear evidence that pentamer **18** is associated in CD_3CN into a conformation where R_3 is

not impacted by the presence of a nearby π system unless there is some strange stacking event that avoids the middle of pentamer **18**. The only possible conformation would be a helix.

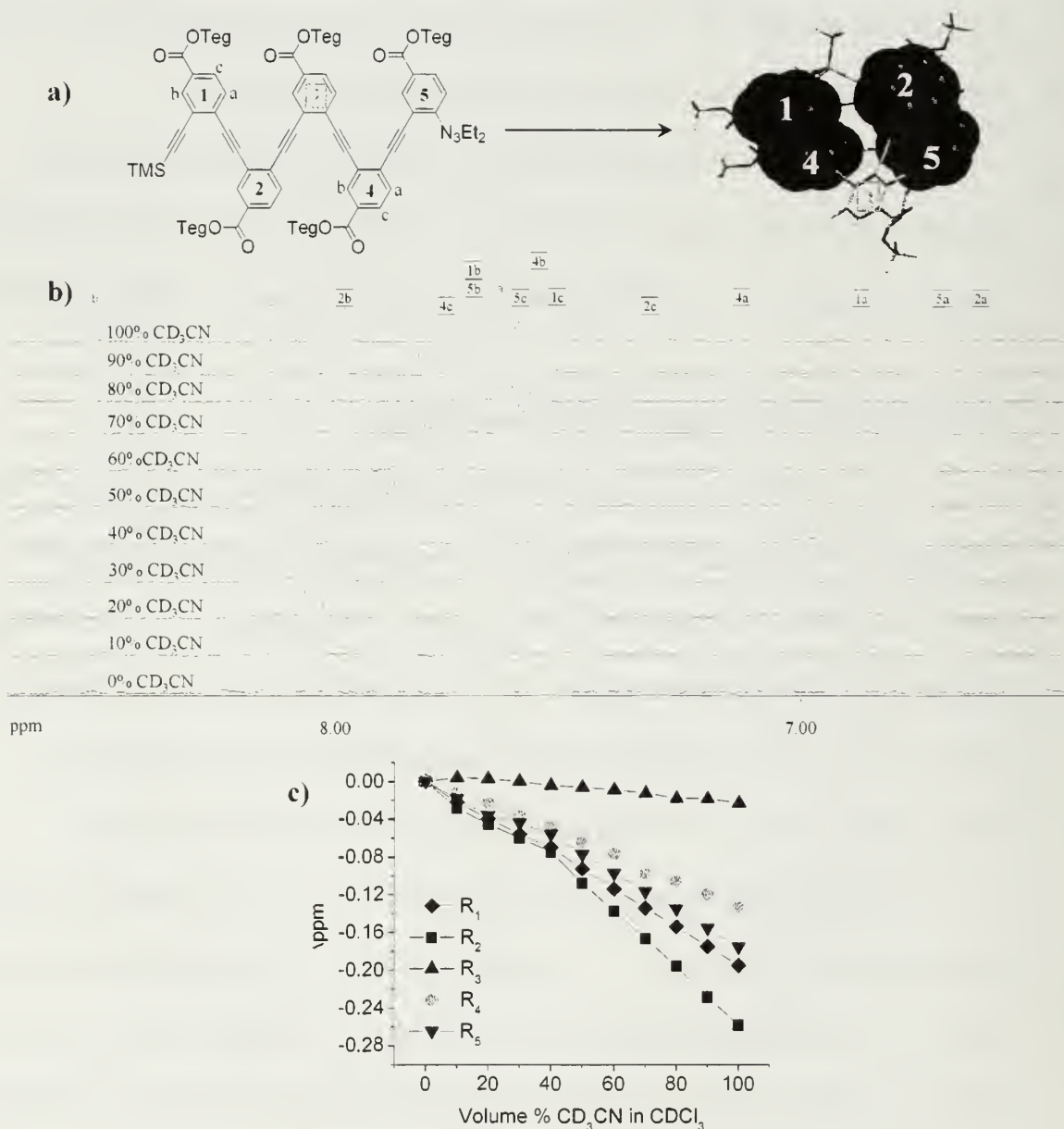


Figure 5.12: (a) Chemical structure of pentamer **18 extended and a folded molecular model. (b) Raw data of solvent titration of **18**. (c) Compressed data for solvent titration.**

What is interesting about this plot is the slope change that occurs at 30% CD₃CN for R_{1,2,4,5}. It is possible that there is some folded conformer in CDCl₃ that transitions to a different and better associated conformer at 40% CD₃CN. It may also be possible to have a rapid association of R_{1,4} or R_{2,5} and the sequential association of the other unassociated ring system. Either way, there are 2 clean slopes in Figure 5.12 (c). The explanation for the temperature study in CDCl₃ may further explain this phenomena.

Moving to the temperature exploration of pentamer **18** in CD₃CN, Figure 5.13 (a) shows the molecular model of pentamer **18** folded with R₁ stacked over R₄ and R₂ stacked over R₅ and the extended chemical structure. In (b) raw data for the temperature study performed from 247K (-26°C) to 350K (77°C) in CD₃CN. Each peak for each proton has been labeled: 1a = the a proton on R₁. Lines to follow the paths of protons 1, 2, 4, and 5b, 2 and 3c, as well as 2 and 3a have been added. Shown in (c)

Compressed data of the temperature study for oligomer **18**, showing the Δppm values for each ring of oligomer **2** calculated by averaging the a, b, and c protons of each ring. The values have been normalized to a Δppm value of zero at 247K (-26°C) for clarity. It is again clear from the data in 5.13 (c) that R₃ does not shift downfield with a temperature change of 100°C. R_{1,2,4,5} all shift downfield dramatically with increasing temperature due to the disruption of π-π stacking. The only possible way for this to occur is for the structure to have been in a folded conformation that would allow for the R_{1,2,4,5} to be associated.

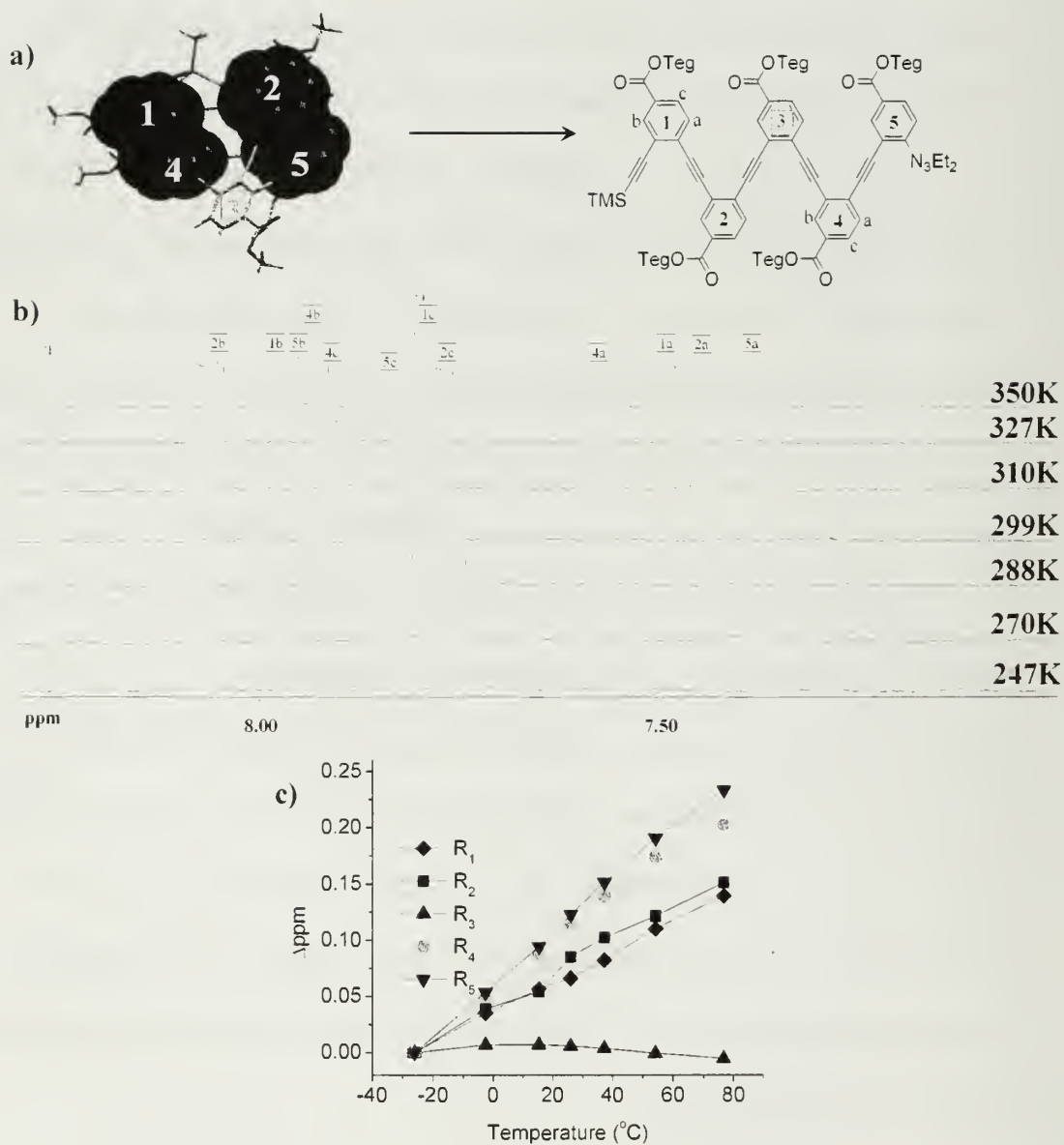


Figure 5.13: (a) Molecular model of pentamer 18 and extended chemical structure. (b) Raw data for temperature titration. (c) Compressed data.

Moving to the CDCl_3 temperature study in Figure 5.14, it is evident that the protons of $R_{1,2,4,5}$ continue to move downfield with the introduction of heat but appear to plateau at $\sim 50^\circ\text{C}$ indicating a possible endpoint of the unfolded/extended conformation in CDCl_3 that for tetramer **17** was present in CDCl_3 at 25°C . This 25°C increase could indicate that pentamer **18** is not fully dissociated in CDCl_3 and that there may be vestiges of partially folded conformers in CDCl_3 at room temperature. As we recall from the modeling studies, the ΔH_{helix} between a conformer with a single folded residue was with R_1 over R_4 was small, 5kcal/mol, so it would not be unreasonable to believe that as these oligomers extend in length, the addition of 1 phenyl unit would begin to push these oPE systems towards a folded, lower energy conformation regardless of the solvent.

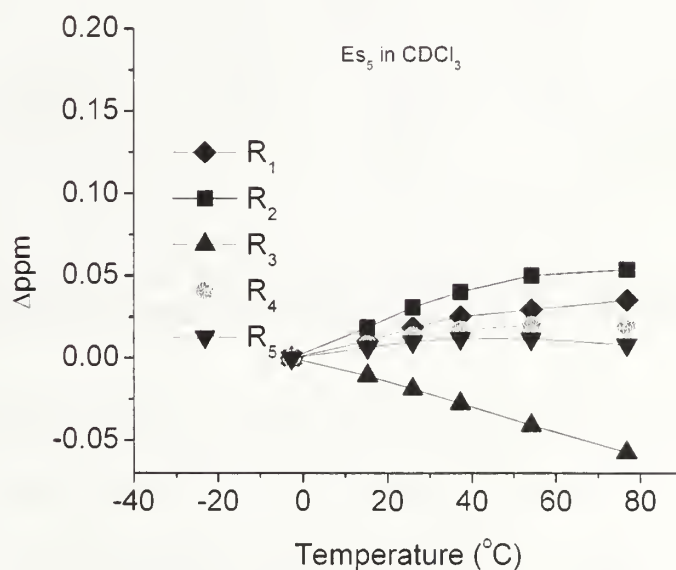


Figure 5.14: Compressed data for temperature study of pentamer **18** in CDCl_3 .

Examining all of the solvent and temperature data together in Figure 5.15 (a) shows the average ppm of only R_3 while (b) shows the average ppm for $R_{1,2,4,5}$ in a variety of conditions. It is apparent in (a) that R_3 is unaffected by the surrounding environment while $R_{1,2,4,5}$ are very sensitive due to their interactions with one another. In (b) it is interesting that the linearity of the solvent vs. ppm shift is continued with nearly exactly the same slope in the region below average ppm = 7.7 showing that the structure doesn't fully settle into a fully folded conformer. However, the near linearity of the $CDCl_3$ temperature vs. average ppm line indicates that an equilibrium extended conformation (or a conformation where the rings are far enough out of range to affect one another) has been reached.

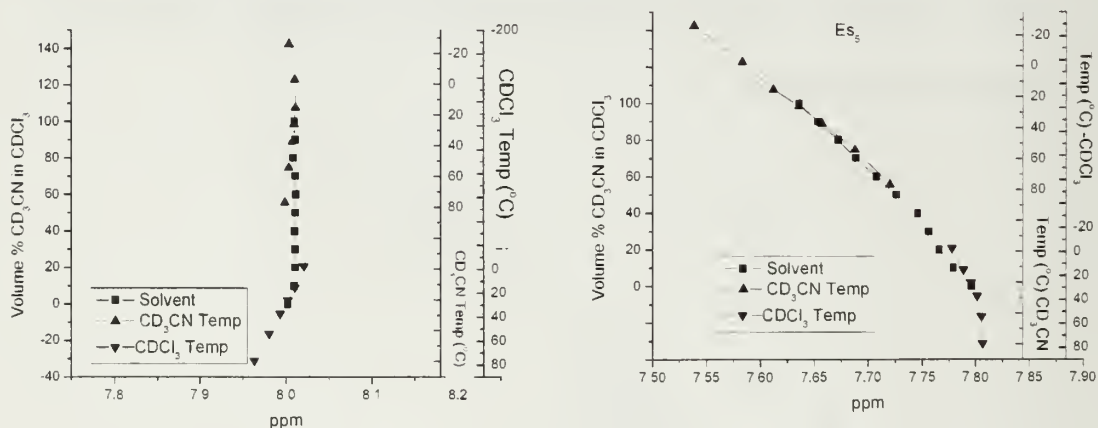


Figure 5.15: (a) Solvent and temperature plots for rings not involved in folding (R_3). (b) Solvent and temperature plots for rings involved in folding ($R_{1,2,4,5}$).

Clearly the conformation of oligomer **18** is highly solvent and temperature dependent with a low average ppm ($R_{1,2,4,5}$) of 7.53 and a high of 7.80 which is reached only above $50^{\circ}C$ in $CDCl_3$ indicating a highly dynamic structure.

5.5 Es₆ Oligomer Solvent and Temperature Effects

With the addition of two rings to the tetrameric oPE system to make hexamer **19** we complete what should be two full turns of a helix. If indeed this structure folds and associates into a compact 2 turn helix, we expect that all of the rings of this system would be π - π stacked, and that the protons of all of these rings, R₁-R₆, would shift upfield with the introduction of CD₃CN, the folding solvent. Examining Figure 5.16 in (a) hexamer **19** is pictured with its chemical structure extended and with a molecular model folded with R₁ stacked over R₄, R₂ stacked over R₅, and R₃ stacked over R₆. In (b) is raw data for solvent titration performed from 0% CD₃CN (100% CDCl₃) to 100% CD₃CN. Each peak for each proton has been labeled: 1a = the a proton on R₁. Lines to follow the paths of protons all b protons, and 2 and 3a have been added for clarity. Figure 5.16 (c) shows the compressed data of the solvent titration for hexamer **19**, showing the Δ ppm values for each ring (R₁ – R₆) calculated by averaging the a, b, and c protons of each ring, and correcting for the addition of CD₃CN. The values have been normalized to a Δ ppm value of zero at 0% CD₃CN for clarity. It is clear from (c) that All rings R₁ – R₆ shift upfield (to negative values) dramatically, which is indicative of π - π stacking.

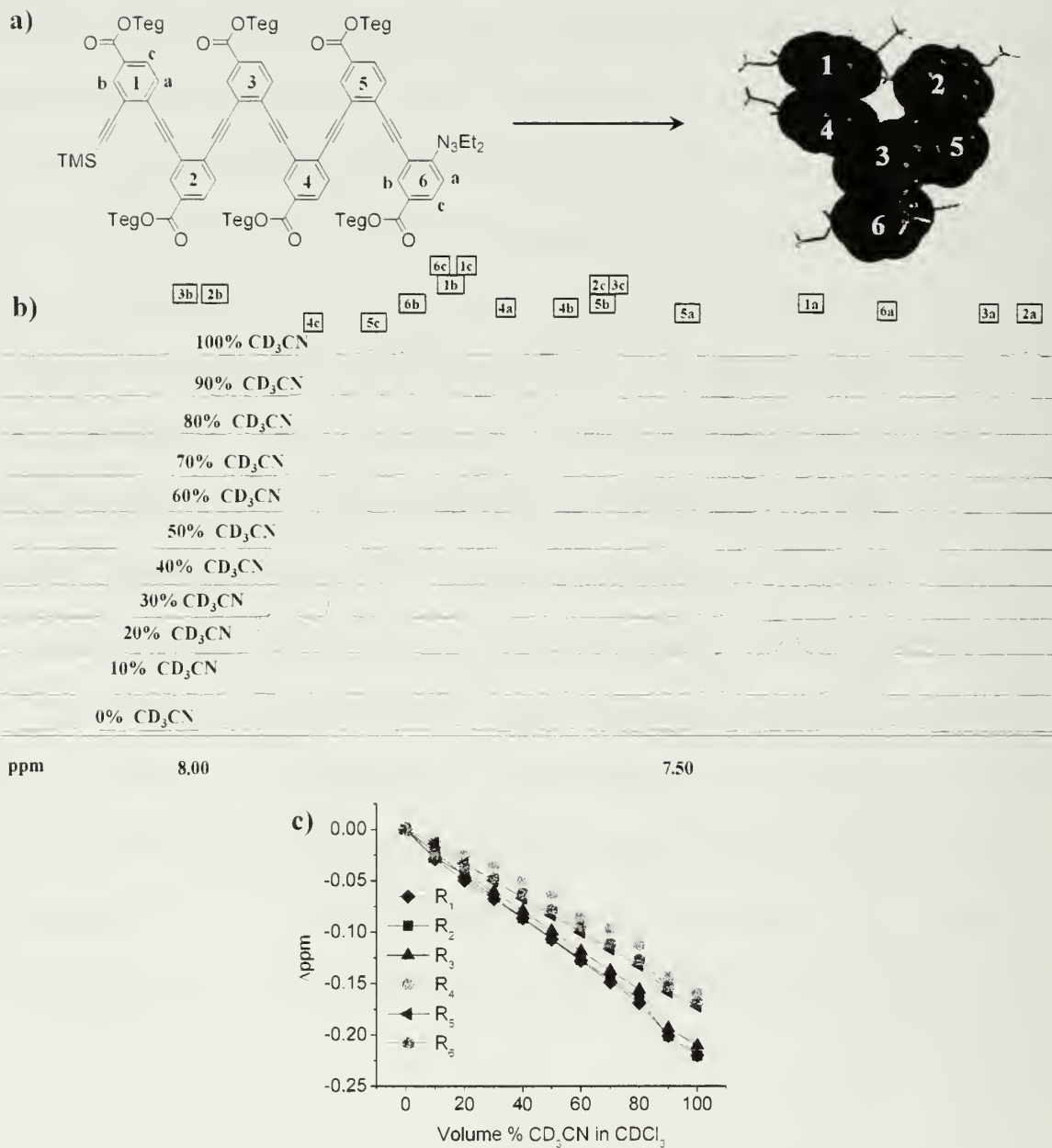


Figure 5.16: (a) Chemical structure for the extended hexamer 19 and molecular model of folded structure (b) Raw data for solvent titration (c) Compressed data.

Interestingly, going back to the raw data in (b) the 4a and 5a protons shift *downfield* while 6a shifts upfield minimally. This could be explained by the slip stacking of the helix, shown from a top down view in Figure 5.17, which would place these protons away from the π -electron cloud. As these rings find a suitably stable helical conformation now every ring must be off-set because there are 2 full levels of π electron clouds to accommodate. As the helix compacts there may also be a transition between 80-90% CD₃CN given the change in slope in this region. Unfortunately we cannot go past 100% CD₃CN to determine if the next point has the same slope.

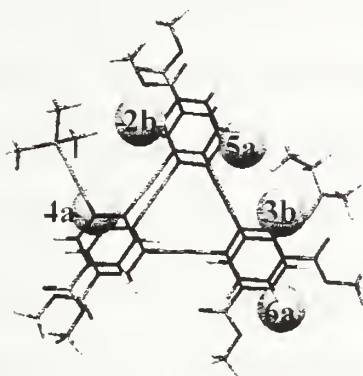


Figure 5.17: Top down view of a model for hexamer 19

Temperature studies in CD₃CN for hexamer **19** are, however, very different from previous temperature studies of tetramer **17** and pentamer **18**. Figure 5.18 (a) shows the folded molecular model and the extended chemical structure. Figure 5.18 (b) shows the raw data for the temperature study performed from 247K (-26°C) to 350K (77°C) in CD₃CN. Each peak for each proton has been labeled: 1a = the a proton on R₁. Lines to follow the paths of protons 3b, 2b, 6b, 5b, and 3a have been added. (c) Compressed data of the temperature study for oligomer **19**, showing the Δ ppm values for each ring of calculated by averaging the a, b, and c protons of each ring. The values

have been normalized to a Δppm value of zero at 247K (26°C) for clarity. It is clear that *all rings* R₁-R₆ clearly shift downfield with increasing temperature due to a disruption in π - π stacking. The raw data in (b) however shows a remarkable shift downfield with temperature from 308K-310K. This experiment was repeated in this range and the same shift occurs.

One possible interpretation of this shift is that the structure is "unlocking" from a low energy conformer with rings that are fairly compact. If that were the case then we would expect that the Δppm below 299K would remain constant, but it does not as the slope from -26°C to 15°C is the same as the slope from 34°C to 77°C. It is also possible that the system binds a solvent molecule which is released at room temperature which could also explain some of the erratic behavior that is observed for the hexamer by UV and fluorescence. The continued absence of shifting for protons 4a-6a supports the earlier notion of slipstacked rings with these protons to the "outside" of the helix. Protons 2b and 3b shift the least of the b protons so that they would also be on the "outside" of the helix in the top level: 1b would not be included because, as it will be shown in the 2-D NMR data (5.7), there may be some "flipping" about the R₁-R₂ axis.

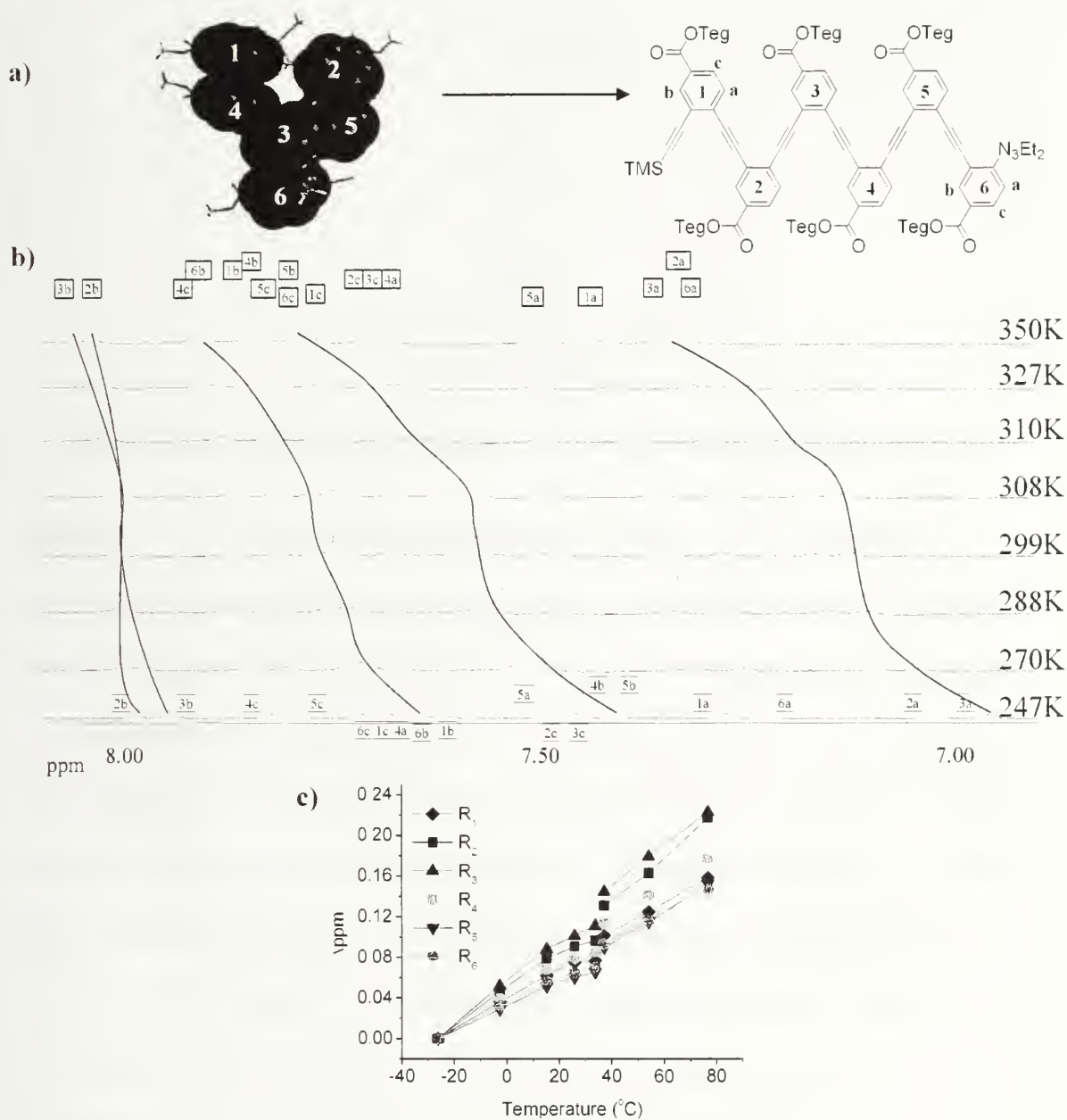


Figure 5.18: (a) Folded molecular model and extended chemical structure of hexamer 19. (b) Raw data for temperature study (c) Compressed data.

Turning briefly to the CDCl_3 temperature data in Figure 5.19, there is no plateau indicating that, contrary to what is observed in pentamer **18**, there is no endpoint to indicate a fully extended structure. The line is still increasing as the temperature is elevated.

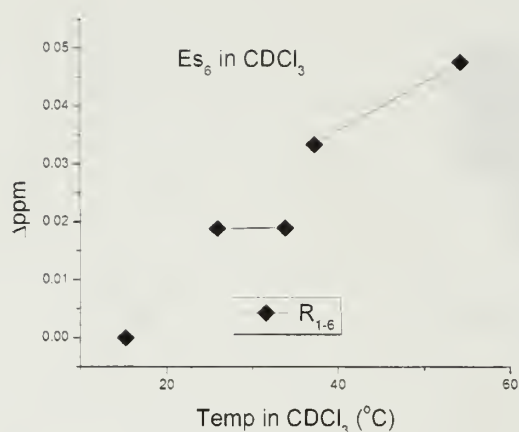


Figure 5.19: Plot of Δ ppm versus Temperature study of hexamer 19 in CDCl_3 .

Assembling all of the solvent and temperature data in Figure 5.20, the sensitivity of hexamer **19** holds, however there are short plateaus in all three sets of data not found in tetramer **17** or pentamer **18**. Given that the position of the CD_3CN temperature line is the same for all of the previous plots, for hexamer **19** this line, for the first time, is slightly above the solvent line. This change could be an indication of a change in the nature of the association of the helix. It is possible that the system could be “breathing” rather than unfolding, as there are no defined endpoints for either of the titrations. This will be discussed further in section 6.5. The added inflections marked with a (*) in Figure 5.20 could be an indication that the conformers slide into a more preferred conformation at low temperature in CD_3CN or 90% CD_3CN , one in which all of the rings are more consistently in contact with one another as opposed to vacillating between the fully folded conformer and its partially folded cousins.

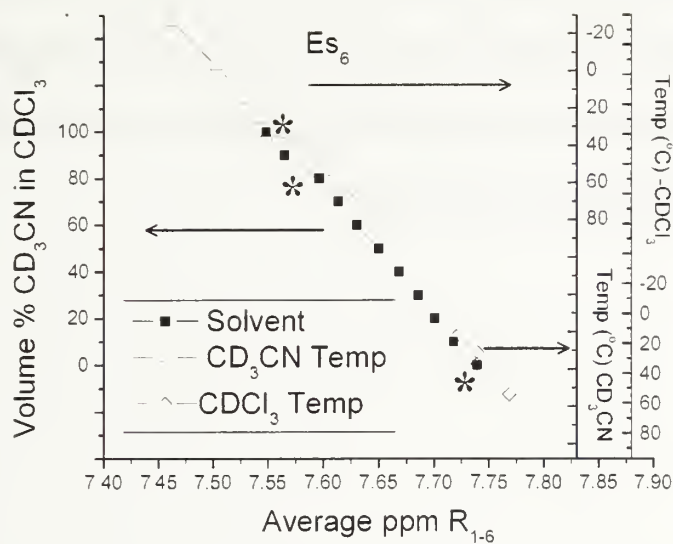


Figure 5.20: Solvent and temperature plots for hexamer 19 R₁₋₆

5.6 Es₉ Solvent and Temperature Studies

Though full assignments could not be made due to a poor ¹³C sample for HMBC experiments, the data could be deconvoluted to decipher the 9 different ring systems of nonamer **20**. As it assumed that all rings would be involved in folding much like they are for the hexamer **19**, a similar approach was taken for this particular set of data.

Averaging all of the points for both the solvent and respective temperature studies that were performed, the results are presented in Figures 5.21-5.23. Figure 5.21 showcases the end points of the raw data, CDCl₃ at 350K (77°C), CDCl₃ at 298K (25°C), CD₃CN at 298K (25°C) and CD₃CN at 247K (-26°C) for comparison. It is clearly evident from this data that the oligomer is dynamic even in Chloroform, much as was found for pentamer **18** and hexamer **19**, possibly even more so. Combining the data into a simple plot, it is evident that there are a few transitions in this data that were not originally seen in the linearity of the Es₄ and Es₅ system. This could possibly be explained by the

association of the rings and compacting of the system at as layers 1, 2, and 3, associate with one another. Synthesis of the macrocycles of this Ester system was attempted but at present remains unsuccessful, thus no association data exists with which to compare this data, unlike for the ether system.

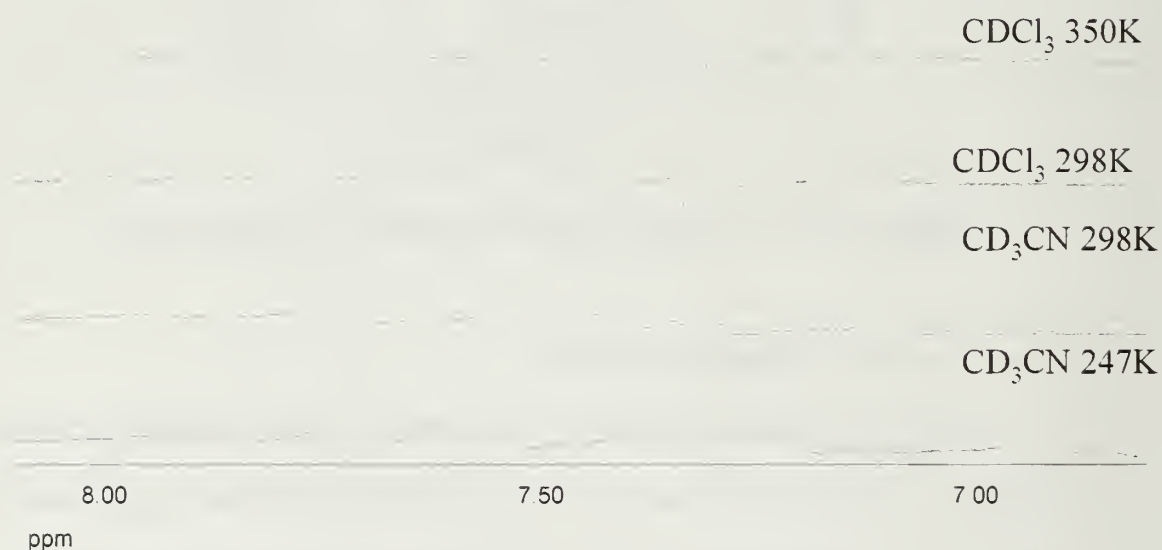


Figure 5.21: ¹H NMR data for nonamer **20** in CDCl₃ and CD₃CN.

First is the data for the solvent titration curve from CDCl₃ to CD₃CN at 298K in Figure 5.23(a). It is clearly evident from this aggregated curve that the rings for nonamer **20** move upfield on the same order as the other oligomers, a Δ ppm of -0.21 ppm. As shown in Table 5.2, this falls directly inline with the other Δ ppm data for shorter oligomers, which may indicate that this is the largest shift possible through solvent change given the nature of these systems.

Table 5.2 Δ ppm and length for folded oPE rings

Oligomer	Length	Average Δ ppm for folded rings
17	4	-0.20
18	5	-0.16
19	6	-0.19
20	9	-0.21

Similar to hexamer **19** for the solvent curve shown in Figure 5.22 (a) has an inflection point but it occurs between 20-30% CD_3CN as opposed to 80-90% CD_3CN . Additionally this data lacks the linearity of the shorter systems as there is a second inflection between 40-50 % CD_3CN . There appear to be two brief regions with the same slope while from 60%-100% CD_3CN the line trails off at a different slope than the other two. Dotted red lines have been added to aid in discerning these transitions.

The Δ ppm versus temperature data for both solvents is shown in 5.22 (b) and (c) for CD_3CN and CDCl_3 respectively. If not for the labels these plots are remarkably similar with the overall Δ ppm/ 10°C of 0.029 (CDCl_3) and 0.025 (CD_3CN) in contrast to the plots of the other oligomers examined here. Table 5.3 shows the Δ ppm/ 10°C for all oligomers. Neither of the plots in (b) and (c) are linear, standard curve fitting in Origin shows that sigmoidal lines fit both of these plots best which may indicate some cooperativity within this nonamer. The question of course remains what *kind* of cooperativity, especially since there are sigmoidal lines in both shown CDCl_3 and CD_3CN with changing temperature.

Table 5.3 $\Delta\text{ppm}/10^\circ\text{C}$ data for all ester oligomers

Oligomer	Length	$\Delta\text{ppm}/10^\circ\text{C}$ CD_3CN	$\Delta\text{ppm}/10^\circ\text{C}$ CDCl_3
17	4	0.014	-0.0050
18	5	0.018	0.00037
19	6	0.014	0.012
20	9	0.025	0.029

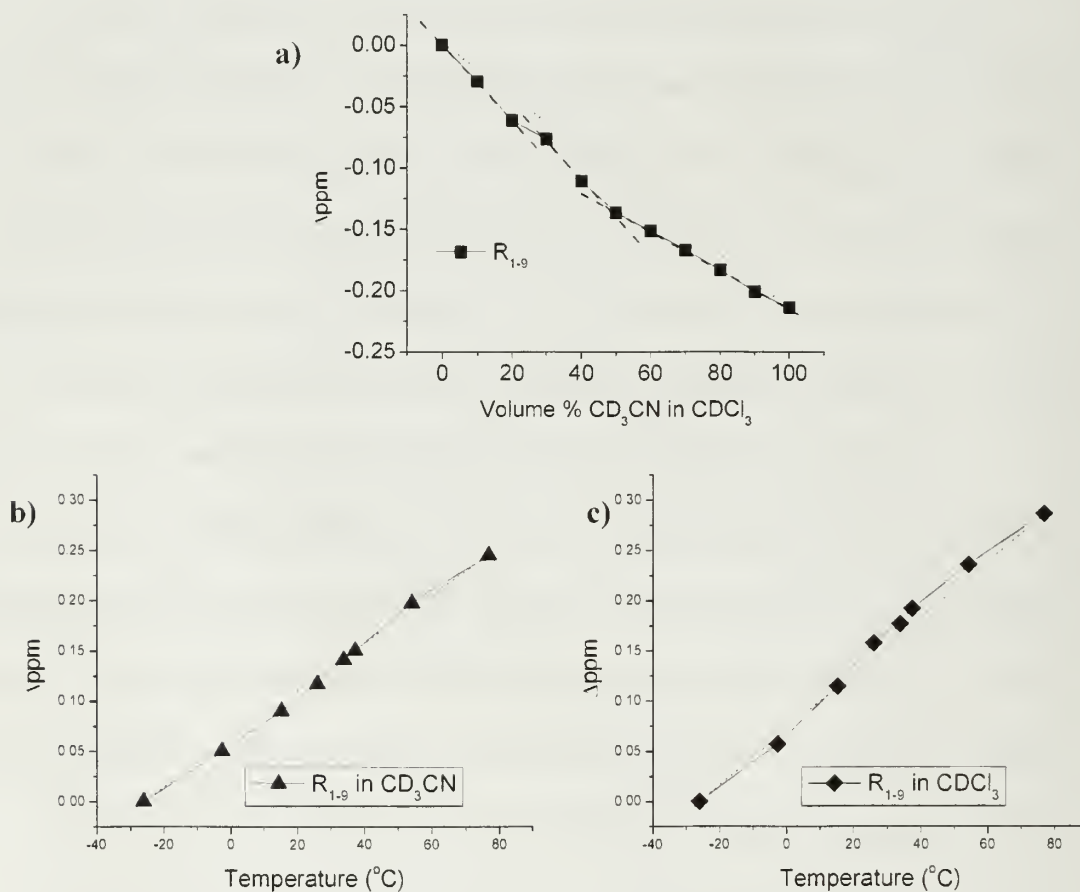


Figure 5.22: Nonamer 20 solvent and temperature studies (a) Δppm vs. Volume % CD_3CN (b) Δppm vs. Temperature in CD_3CN (c) Δppm vs. Temperature in CDCl_3 .

Bringing all of this data together on one plot in Figure 5.23, a very different picture for nonamer 20 emerges than for the other shorter oligomers. The overall range of the average ppm for nonamer 20 from -26°C in CD_3CN to 77°C in CDCl_3 is 7.22-7.7ppm which is larger than the ranges for the other oligomers. Given the range of

conformation possibilities it is reasonable to believe that some vestiges of helical conformations are present in CDCl_3 at a range of temperatures, and this would explain the high level of sensitivity of this oligomer in CDCl_3 . It should be noted that when tracking protons individually, even though they cannot be assigned, the same sets of protons that do not shift with solvent also do not shift with temperature. Given the previous data that appears to show that the layers of the helix are distinguishable from one another due to the nature of the slip-stacking and off-set, the same could be observed here with the sets of protons differentiated by layers.

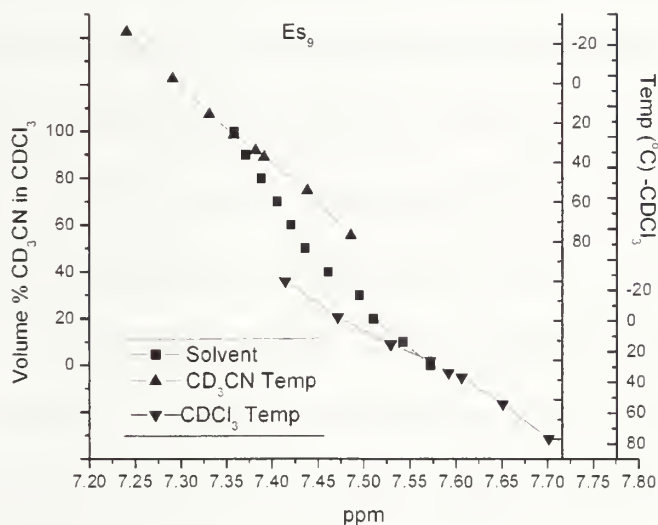


Figure 5.23 Solvent and temperature plots for nonamer 20 R_{1.9}.

5.7 2-D NMR studies for Teg-ester oligomers

As it was shown for all of the 1D data the π - π stacking sensitivity of these oPE systems to solvent and temperature change and the reflection of these changes paints a convincing picture for folding in oPE systems. To further this understanding, a series of ROESY experiment at low temperature were performed to determine whether the

aromatic protons or the terminal TMS protons are close enough to detect a through space interaction of less than 5Å.

Figure 5.24 (a) and (b) show ROESY spectra of tetramer **17** in CD₃CN at 270K (a) and 298K (b) showing the entire aryl region of the oligomer plotted versus the terminal trimethylsilyl (TMS) off of R₁. Given the 1D ¹H NMR data that indicated folding through the observation of π-π stacking for R₁ and R₄ this new ROESY data supports the existence of 2 conformers in solution. At 270K there are 2 cross peaks between the TMS and protons 2b and 3b as they are highlighted in the helical models shown in (c) and (d). Some elements of the models have been eliminated for clarity. These two cross peaks support the possibility of a dynamic folded system, as the only way for these two cross peaks to exist is for the oligomer to vacillate between conformers that have the TMS both in the progression of the helix and flipped outside of it as shown in (c) and (d). Prior ROESY data lacking any interactions between the terminal TMS and the triazene on R₄ in CDCl₃ (e) shows a very clear peak in CD₃CN (f), the folded solvent, at room temperature. The only possible way for this interaction to occur is through the folding of tetramer **17**. Otherwise, as shown in (g), the TMS is out of the 5Å range of allowable interactions for ROESY behavior. Table 5.4 shows the calculations and model estimations for the observed cross peaks in (a) and (b) for tetramer **17**.

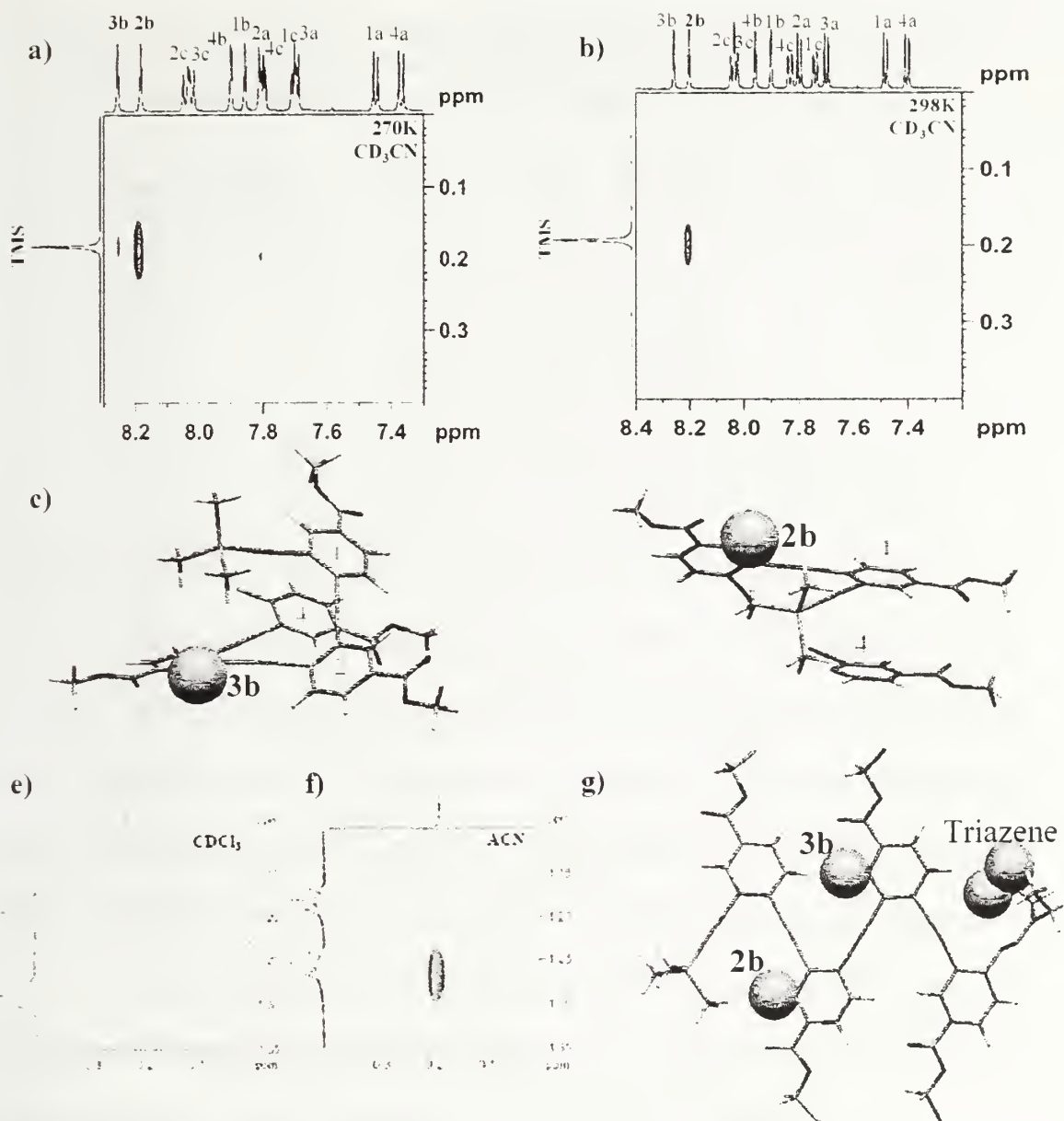


Figure 5.24 ROESY spectra and models for tetramer 17 (a) ROESY spectra in CD₃CN 270K (b) ROESY spectra in CD₃CN 298K (c) Helical model showing TMS to proton 3b interaction (d) Helical model showing TMS to proton 2b interaction (e) and (f) ROESY spectra showing TMS and triazene regions in CDCl₃ (e) and CD₃CN (f). (g) Extended model of tetramer 17.

Table 5.4 Calculations comparing ROESY data with model predictions for tetramer 17. The reference peak taken for the calculation is the peak corresponding to protons 2a and 2c which has a calculated distance of 2.44Å

Figure	Temp (K)	Observed Peak (A ₂)	Intensity (A ₁)	Intensity (A ₂)	Calculated Distance (r ₂)	Model Distance (r ₁)
5.24 (a)	270	TMS to 2b	361631	54125	3.35	3.49
5.24 (a)	270	TMS to 3b	361631	6513	4.77	4.10
not shown	270	TMS to Triazene	361631	88448	2.99	2.72
5.24 (b)	298	TMS to 2b	562371	51925	3.63	3.49
5.24 (f)	298	TMS to Triazene	562371	903545	2.25	2.72

In Figure 5.25. ROESY spectra of pentamer 18 in CDCl₃ (a) and CD₃CN (b) at 270K. Selected protons are labeled for the aryl region. Only one cross-peak is observed in the CDCl₃ between the TMS and the aryl region, peak 2b on R₂. This is reasonable because even in an extended conformation (c) with the rings relatively flat, the TMS and 2b can be ~ 3 Å away from one another. Keeping in mind that the system is dynamic, in an unfolded conformation this is the only reasonable explanation for this cross peak in CDCl₃. In CD₃CN however, a number of cross peaks are observed between the terminal TMS and the aryl region. All peaks are highlighted by model (d). It is clear that a peak between 3b and the TMS would occur only if the TMS terminus was in the progression of the helix over R₃. The distance calculated for this structure is 4.47 Å which is in line with the model prediction of 3.43Å. Though the calculated value is larger than the model prediction it is reasonable if the structure is dynamic and the TMS is flipping back and forth with R₁ in solution. The other more interesting possible position for the TMS would be for it to assume a position nestled in the hydrophobic pocket created near the stacked rings of this system. R_{1,4} and R_{2,5} shown in

(e). This option would put the TMS in very close proximity to protons 2b, 5b, and 4a. This is precisely what is observed in (b). The dynamic nature of this structure as folded provides for peaks with each of these protons. Table 5.5 gives distances calculated from the cross peak interactions for each interaction and values for the distances as predicted by the models. Though the calculated distances for these interactions are large as compared with the model predictions for a compact and folded structure, it should again be noted that these structures are dynamic in solution. It should be noted that it would be impossible for the TMS to have cross peaks with either 4a or 5b if the structure were extended as shown in (c) as the model approximated distances between these atoms are 13.0 Å and 12.9 Å respectively. Again, only one peak is present in CDCl_3 the one with proton 2b.

Table 5.5: ROESY distance calculations for pentamer 18. The reference peak taken for the calculation is the peak corresponding to protons 3a and 3c which has a calculated distance of 2.44 Å

Figure	Temp (K)/ Solvent	Observed Peak (A_2)	Intensity (A_1)	Intensity (A_2)	Calculated Distance (r_2)	Model Distance (r_1)
5.25 (a)	270 CDCl_3	TMS to 2b	528313	91704	3.27	2.94
5.25 (b)	270 CD_3CN	TMS to 2b	766360	124138	3.30	3.29
5.25 (b)	270 CD_3CN	TMS to 3b	766360	20032	4.48	3.43
5.25 (b)	270 CD_3CN	TMS to 4a	766360	13904	4.76	2.97
5.25 (b)	270 CD_3CN	TMS to 5b	766360	10923	4.96	2.70

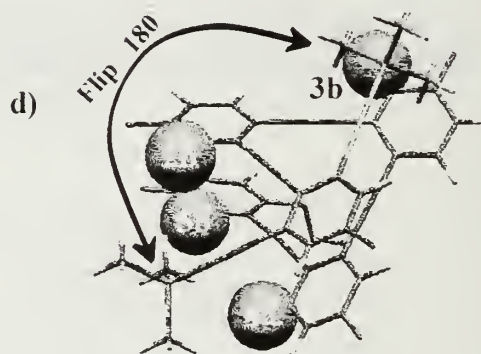
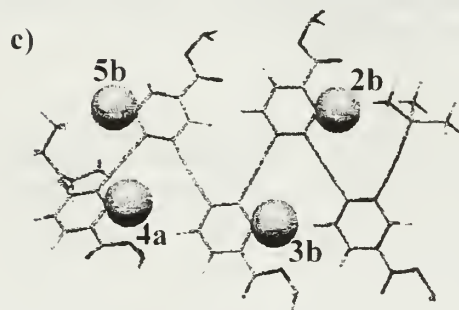
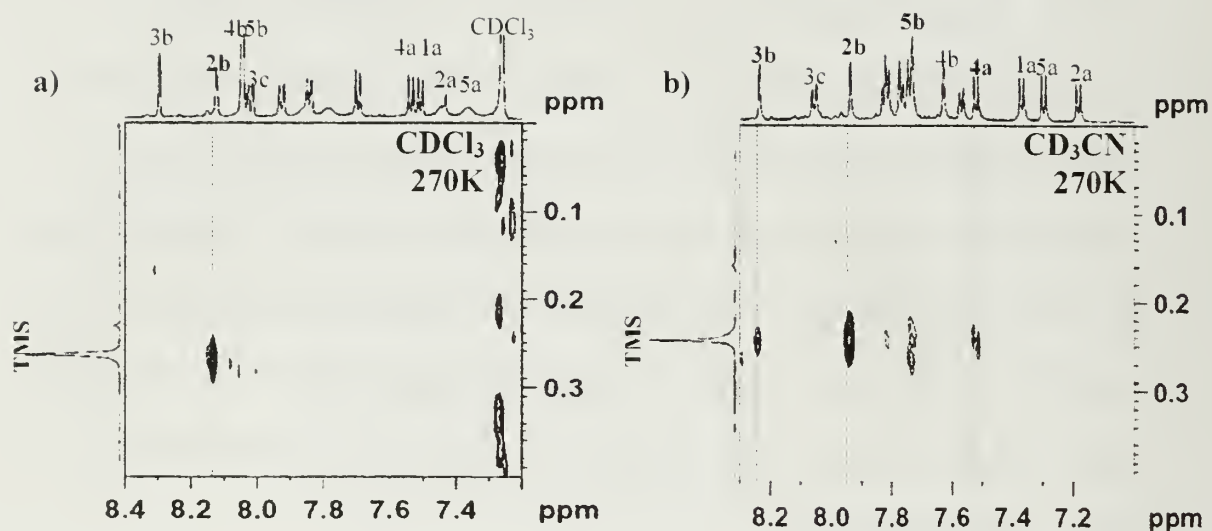


Figure 5.25 ROESY spectra and models for pentamer 18 (a) ROESY spectra in CDCl₃ at 270K (b) ROESY spectra in CD₃CN 270K (c) Extended model showing TMS and all potential interactions (d) Helical model showing TMS to proton 2b,4a, 5b, and 3b interaction with the TMS 'flipping' from one side of the molecule to the other shown.

In Figure 5.26 the ROESY spectra of hexamer **19** in CDCl₃ (a) and CD₃CN (b) at 270K are shown. In (c) the model of **19** is fully extended prominently showing protons 2b and 5b for overall reference. Shown in (d) is the helical conformation of **19** showing TMS nestled in hydrophobic region near R₁-R₄ and R₂-R₅. The only cross peak observed in CDCl₃ is reasonable because it could be exhibited even with an extended structure as shown in (c). In figure (b), two cross peaks are visible in CD₃CN with protons 2b and 5b. This is inline with all previous data: the π - π stacking shown in CD₃CN vs. CDCl₃ supports a folded structure. The ROESY data shown here fully supports folding. Table 5.6 shows the calculated versus the measured model distances for the TMS versus protons 2b and 5b. It should be noted that for (c) the shortest distance between the TMS and proton 5b was 12.4 Å which would be well out of range for NOE interactions.

Table 5.6: ROESY distance calculations for hexamer 19. The reference peak taken for the calculation is the peak corresponding to protons 2a and 2c for the peaks in CD₃CN and 6a to 6c in CDCl₃ which has a calculated distance of 2.44Å.

Figure	Temp (K)/ Solvent	Observed Peak (A ₂)	Intensity (A ₁)	Intensity (A ₂)	Calculated Distance (r ₂)	Model Distance (r ₁)
5.26 (a)	270 CDCl ₃	TMS to 2b	161090	91704	3.27	2.76
5.26 (b)	270 CD ₃ CN	TMS to 2b	161090	23525	3.37	3.48
5.26 (b)	270 CD ₃ CN	TMS to 5b	161090	18508	3.50	3.01

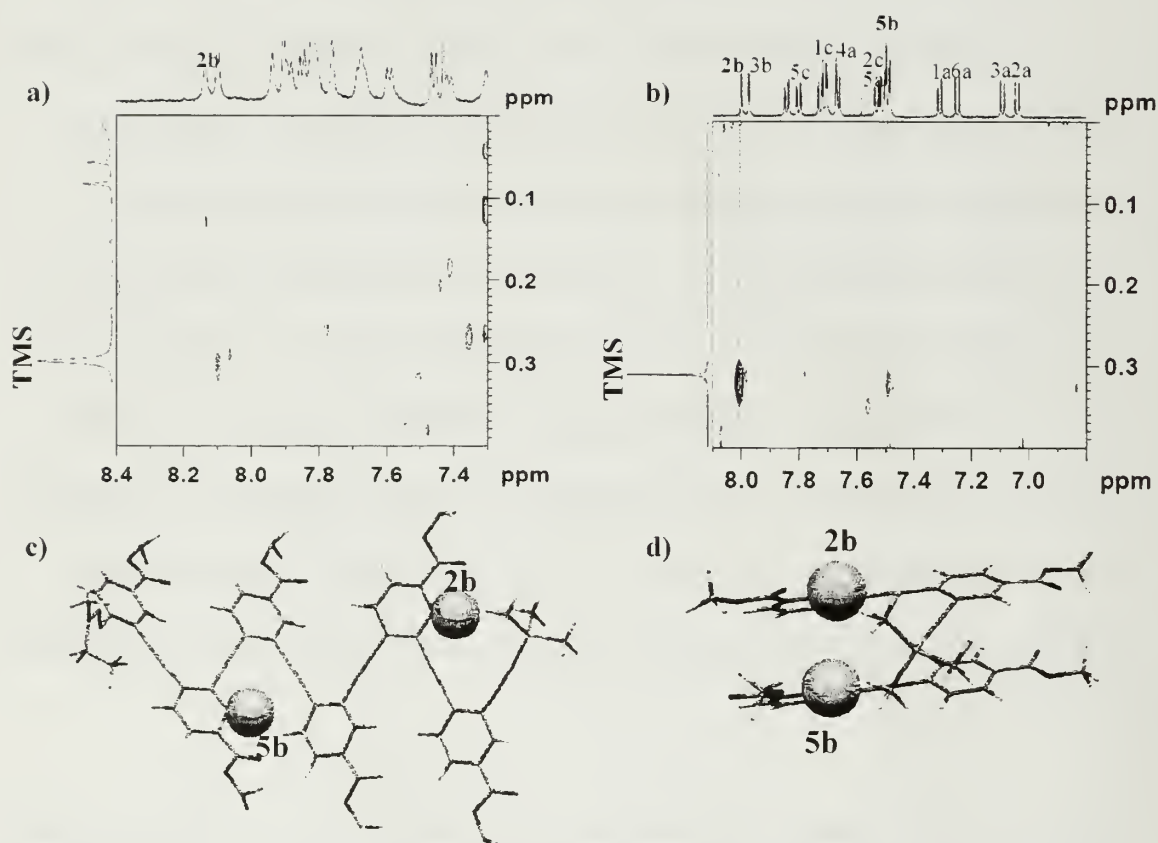


Figure 5.26 ROESY spectra and models for hexamer **19** (a) ROESY spectra in CDCl₃ at 270K (b) ROESY spectra in CD₃CN 270K (c) Extended model showing TMS and all potential interactions (d) Helical model showing TMS to proton **2b**, and **5b** interaction

Though ROESY experiments were run for nonamer **20**, no precise conformation assignments could be made for the cross peaks due to the lack of definitive aromatic proton assignments. However, there is more than a single cross peak present within this spectra, lending support to the folded structure as it has been observed in shorter oligomers.

5.8 Conclusions

The sensitivity and precision with which we can track the aromatic protons of this ester substituted oPE oligomer with 1-D ^1H NMR, even at longer lengths with many aromatic protons, provides striking evidence of a helical secondary conformation characterized by π - π stacking. These oligomers fold into helices in CD_3CN , maintain much of that folded character through temperature changes in CD_3CN , and, at longer lengths, exhibit the some folded character even in CDCl_3 . ROESY measurements confirm this secondary conformation indicating cross peaks for all three oligomers that could only exist if the oligomers were in a fully folded and helical conformation. These ROE correlations place three groups (TMS, R_2 , and R_5) together locally in space which is completely consistent with a compact helical structure. Due to the presence of R_5 in these longer oligomers, which is absent in tetramer **17**, it appears that a hydrophobic binding pocket is created for the TMS by the stacking of $\text{R}_{1,4}$ and $\text{R}_{2,5}$. Pentamer **18** has similar ROE correlations between the TMS and 2b, 5b, 4a consistent with a helical conformation and the formation of a hydrophobic pocket. It also has a new cross peak between the TMS and 3b, suggesting that the TMS can 'flip' to the other side by a 180° rotation around the $\text{R}_{1,2}$ linkage. Similar cross peaks between the TMS and 2b as well as 3b are observed for tetramer **17** in addition to those originally reported in Chapter 4 between the TMS and triazene. These additional correlations observed for **17** and **18** are consistent with the expected dynamic nature of short helices.

CHAPTER 6

EXPLORING THE INFLUENCE OF BACKBONE ELECTRONICS ON THE OPE SYSTEM

6.1 Introduction

Chapters 4 and 5 describe data that prove the existence of secondary helical structures for *ortho* Phenylene Ethynylene backbones using 1-D and 2-D NMR methods. Chapter 5 examined only the π -poor Teg-ester backbones in the exploration of whether oPEs formed helices at lengths longer than 4 units. As it was shown in Chapter 4, 4-unit oligomers display an electronic dependence on the upfield shifting of the aryl region of the NMR due to π - π stacking.

Other foldameric systems in the literature with a π - π stacking component vary in the electronic composition of their backbones. The Aedamer systems studied by Iverson (83-87) utilize the electrostatic complementarity of π -rich and π -poor systems to create stably folded structures. The mPE work cited previously explored a combination of backbone electronics that included π -rich, π -poor, and π poor/rich systems, but π -poor systems proved to be most favorable.(32) Modeling studies of mPE supported ΔG_{helix} calculations that found the π -poor helix to be most energetically favorable (77).

This chapter seeks to explore the effect of backbone electronics in oPEs at longer lengths for π -rich and π -poor/rich systems in comparison to the π -poor series profiled in Chapter 5. The question of whether complementarity of electrostatics in a π -poor/rich system or a homogeneous π -poor system contribute to the stability of a helical oPE backbone will be explored.

6.2 Methods

The synthesis of π -rich (Et_x) tetramer **11**, pentamer **12**, hexamer **13**, π -poor/rich (Es_xEt_y) tetramer **22**, pentamer **23**, hexamer **24**, and π -poor (Es_x) tetramer **22**, pentamer **23**, hexamer **24**, were described in Chapter 2. Details of this synthesis can be found in Chapter 7.

As described in section 5.2, the protons from the aryl ring are assigned by a combination of ^1H NMR, J coupled correlation spectroscopy (COSY) and Heteronuclear Multiple Bond Correlation (HMBC). 1-D methods varying solvent composition and temperature will be explored similar to those described in Chapter 5.

6.3 Effect of solvent and temperature on π - π stacking of π -rich, π -poor/rich and π -poor systems

6.3.1 Solvent effects

Given the previous study of tetramers in Chapter 4, there is a marked impact of π -electronics on upfield shifting in the aryl region due to π - π stacking as the solvent changes from CDCl_3 to CD_3CN . Table 6.1 shows the progression of the impact for the average Δppm of each ring 1-4.

Table 6.1: Average Δppm (CDCl_3 - CD_3CN) shifts for aryl protons of **11, **22**, and **17**.**

Ring Number	11 (Et_x) π -rich	22 (EsEt_x) π -poor rich	17 (Es_x) π -poor
1	-0.09	-0.13	-0.21
2	0.01	0.00	-0.04
3	0.02	0.00	-0.02
4	-0.05	-0.10	-0.19

While it is evident that the π -poor system is most responsive to the change in solvent, clearly rings 2 and 3 are not involved in π - π stacking for any of the tetramers. The Δppm of the π -rich system is 60% less than the Δppm of the π -poor system and

30% less than the Δ ppm of the π poor/rich system. Modeling indicated that the distances and the angles of offset could explain the differences observed in these experimental values. The π -poor system had the closest distance between the centers of the stacked rings R_1 and R_4 (3.8 Å) and the smallest angle between the centers of R_1 and R_4 . Table 6.2 illustrates this electronic dependence on a) distance measured between centers of the stacked rings x and y ($D_{x,y}$), b) the angle between the rings measured using a perpendicular line through the center of ring y and $D_{x,y}$ ($\theta_{x,y}$) and c) the offset between the centers of rings x and y ($O_{x,y}$) which can be found by calculating the following relation:

$$O_{x,y} = D_{x,y} * \sin(\theta_{x,y})$$

Table 6.2: Model Calculations for Tetramers

	11 (Et ₄) π -rich	22 (EsEt ₂) π -poor/rich	17 (Es ₄) π -poor
Distance $D_{1,4}$ (Å)	4.3	4.1	3.8
Angle $\theta_{1,4}$	35°	20°	11°
Offset $O_{1,4}$ (Å)	2.46	1.40	0.73

The impact of the π -system as seen through the model calculations is clear for the tetramers. The system that experiences the largest Δ ppm shift upfield with changing solvent is also the system that has the smallest D, θ , and O values, π -poor **17**. The question of whether or not the longer versions of these oligomers with a variety of electronic compositions will exhibit similar behavior both experimentally and in correlation with model studies is still open.

As pentamers **12**, **23**, and **18** are examined in Figure 6.1 (a) by solvent titration, the electronically dependent trend that was shown experimentally in the tetramers holds here as well. Each point on each plot represents the average a, b, and c for each protons

as shown in 6.1 (b). For each system the Δppm of R_3 remains at ~ 0 indicating that it is not involved in π - π stacking. $R_{1,2,4,5}$ all shift upfield in each system which is what was found for π -poor **18** in Chapter 5. Similar to the data for the tetrameric systems, the π -rich system appears to be the least impacted by the solvent change compared to the complementary poor/rich and the π -poor system. The Δppm values for the π -rich rings of **23** involved in folding ($R_{4,5}$) have higher Δppm values than π -rich **12**. This difference could be attributed to a stronger interaction of the complementary rings over the repulsion of the π -rich systems.

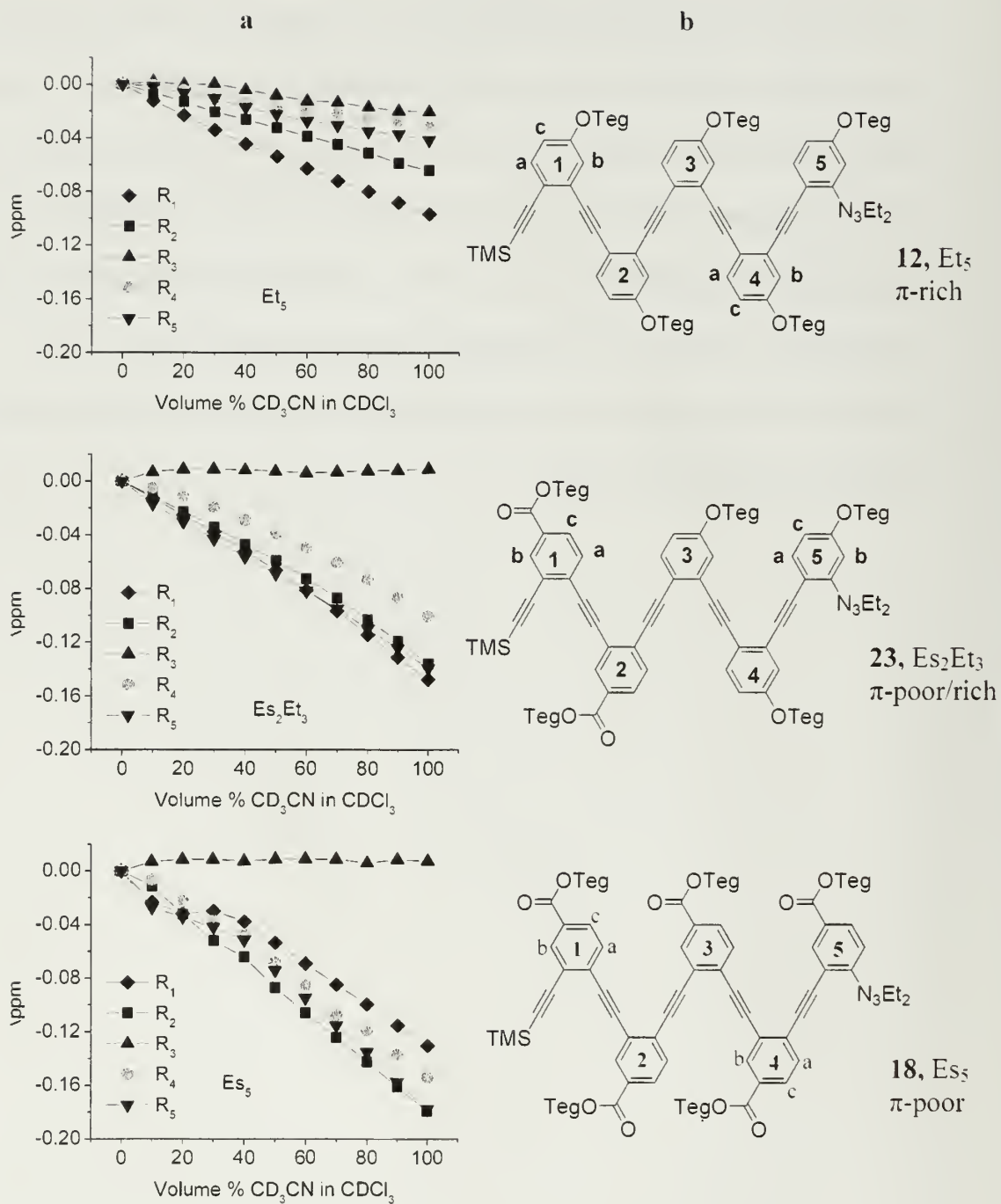


Figure 6.1 (a) Δ ppm vs. Solvent composition and (b) chemical structures for pentamers 12 (π -rich), 23 (π -poor/rich), and 18 (π -poor).

For hexamers **13**, **24**, and **19** the difference among the systems is very similar. Figure 6.2 plots Δppm vs solvent composition for the solvent titration of R_{1-6} for each oligomer shown in (b). Again the overall electronic trend observed for the tetramers and pentamers is also seen as rings 1-6 are combined: $\Delta\text{ppm } \pi\text{-rich} < \Delta\text{ppm } \pi\text{-poor/rich} < \Delta\text{ppm } \pi\text{-poor}$. Extracting the sets of π -rich and π -poor rings from the overall plot for **24** a phenomena similar to that seen with the pentamers is observed. The π -poor rings R_{1-3} have slightly smaller Δppm values than all π -poor **19** at -0.18 and 0.19 respectively. The π -rich rings R_{4-6} of **24** exhibit Δppm values more than twice those of R_{1-6} of π -rich **13** again a potential effect of complementarity at -0.15 and -0.06 respectively. Overall the π -poor have a Δppm of -0.19, while the mixed system stands at -0.17 and the π -rich system shows an overall Δppm of -0.06.

The linearity of the plots for the π -rich and π -poor/rich is similar to that seen in the tetramers. The initial curve at the start of the π -poor lines of pentamer **18** seem to indicate the presence of a remnant folded structure in CDCl_3 as shown in Chapter 5. As shown before with the tetramers, there continues to be remarkable sensitivity in the π -poor oligomers.

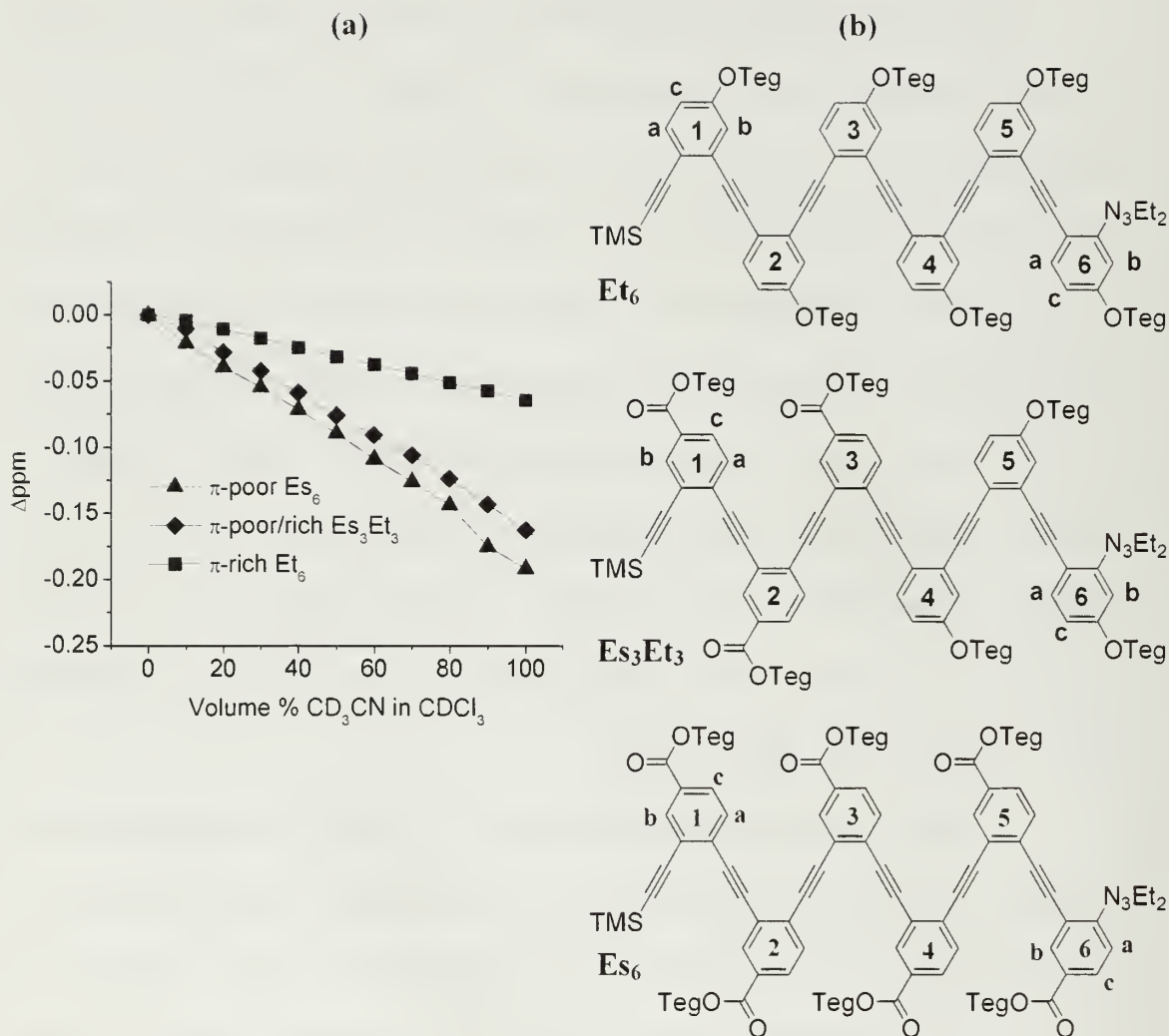


Figure 6.2 (a) Δppm vs. Solvent composition and (b) chemical structures for hexamers 13 (π -rich), 24 (π -poor/rich), and 19 (π -poor).

6.3.2 Temperature studies in CD_3CN

To determine the relative stability of these folded oligomers as a function of temperature in CD_3CN , Δppm versus $^\circ\text{C}$ is plotted for the tetramers in Figure 6.3, the pentamers in Figure 6.4, and the hexamers in Figure 6.5. Increasing temperature should result in downfield shifting of the aromatic protons involved in folding due to a disruption of π - π stacking much like it was shown in Chapter 5.

For the tetramers in Figure 6.3 an extended plot beyond the 3 data points shown in Chapter 4.3 is given. It is apparent that only the π -poor oligomer **17** (c) shows data that is easily interpretable for these systems, with only rings R_1 and R_4 shifting downfield with R_2 and R_3 remaining constant at $\Delta\text{ppm} = 0$. For the π -rich oligomer **11** and π -poor/rich **22** the trend is not clear. All rings R_{1-4} appear to move downfield slightly but not on the same order and lacking the same clear distinction between the inner rings $R_{2,3}$ and the folded ring $R_{1,4}$. Given the exhibited solvent sensitivity of the π -poor systems it is interesting to note that the π -poor ring 1 of the π -poor/rich system **22** does not appear to move as far downfield as the π -poor rings of **17** ($\Delta\text{ppm} = 0.05$ vs. $\Delta\text{ppm} = 0.15$). This could be due to an increased stability of the π -poor/rich systems and their potential ability to stabilize or counteract the energy added to the system by an increase in temperature.

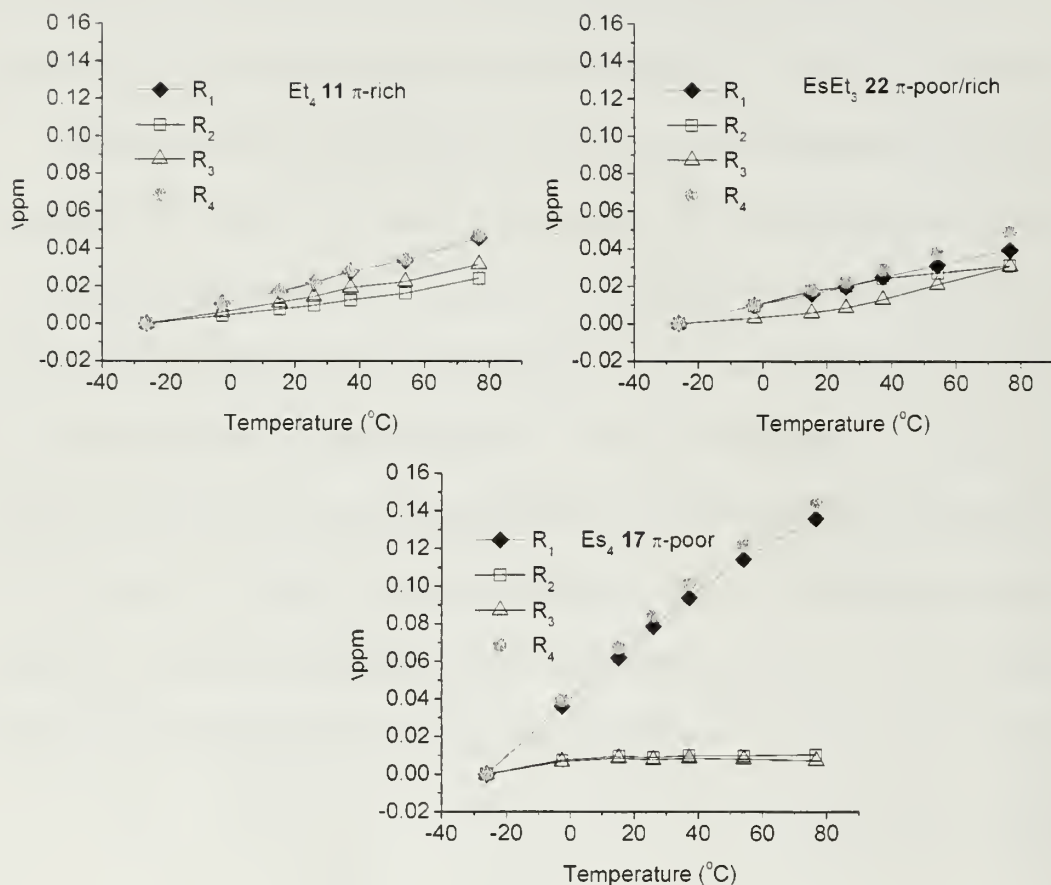


Figure 6.3 Δppm vs. Temperature ($^{\circ}\text{C}$) in CD_3CN for tetramers 11, 22, and 17.

Figure 6.4 shows the data for Δppm vs. temperature of the pentamers. As before, the π -poor system (**18**) provides the clearest indication of downfield shifting with increasing temperature for rings $R_{1,2,4,5}$ while R_3 remains constant. With the increase in oligomer length there is slightly more clarity for **23**, the π -poor/rich system and the π -rich system. **12** also shows R_3 at slightly lower values than $R_{1,2,4,5}$ but all of the Δppm values for the π -rich system are less than 0.05. In contrast, the π -poor **18** consistently exhibits differences between the Δppm of $R_{1,2,4,5}$ and R_3 of greater than 0.10ppm. Looking once again to determine whether the π -poor rings of **23** show the same sensitivity that the completely π -poor system exhibit, again, the Δppm values for

$R_{1,2}$ of **23** are approximately half the values of $R_{1,2}$ of **18** lending credence to the argument that the π -poor/rich systems may exhibit higher temperature stability than the π -poor systems overall. Another possible argument is that the π -poor/rich system simply is not stacked tightly enough in CD_3CN to exhibit high degrees of downfield shifting. However, the Δ ppm values for the solvent titration of **23** are in the range of 0.10-0.16 ppm above the maximum Δ ppm of 0.08 ppm shown for the temperature study, again, supporting overall stability. The maximum Δ ppm for the π -poor **18** systems for solvent and temperature are more closely related, between 0.12 and 0.25 for both experiments.

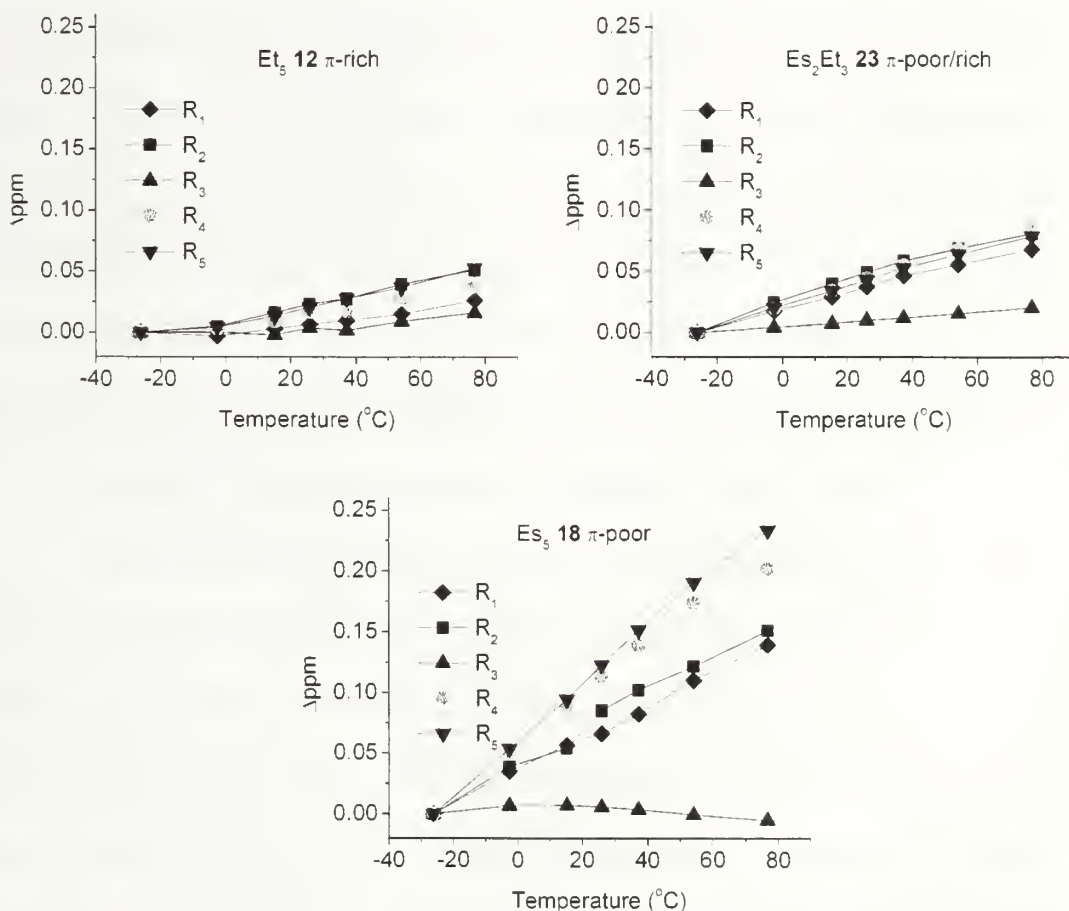


Figure 6.4 Δ ppm vs. Temperature ($^{\circ}C$) in CD_3CN for pentamers **12**, **23**, and **18**.

Finally, Figure 6.5 brings together the data for hexamers **13** (π -rich), **24** (π -poor/rich) and **19** (π -poor) showing the Δppm vs. temperature in CD_3CN . Again, hexamers **13** and **24** demonstrate the least sensitivity for these hexameric systems. Separating out the π -rich and poor halves of **24** and plotting them with the homogeneous π -rich and π -poor oligomers the comparison is shown in Figure 6.6. For each plot, only the portion of the **24** that is similar to the homogeneous oligomer is plotted. R_{1-6} of **24** is plotted with the averaged data of R_{1-6} of **13**, and R_{1-3} of **24** is plotted with R_{1-6} of π -poor **19**. For the π -rich systems there is only a small difference between the π -rich portion of **24** and **13** which indicates that the π -rich portions of **24** are slightly more impacted by neighboring π -systems and the temperature range that was explored. However, the marked differences between the behavior of the π -poor systems and the π -poor rings of hexamer **24** support the previous observation that in fact, the π -poor/rich systems may be more stable in CD_3CN in the face of a ΔT of 100°C given the relative temperature insensitivity of the π -poor rings of oligomer **24** relative to **19** despite the similarity of the Δppm values for solvent titration. This temperature stability of the π -poor/ π -rich coupled with the dynamic nature shown by the π -poor systems may lead to being able to tune the temperature responsiveness of oPE helices in future applications by introducing a variety of electronic elements.

As an added comparison of the π -poor components of the hetero oligomers, a plot of Δppm vs. temperature for the ester rings of **22**, **23**, and **24** is shown in Figure 6.7. The addition of 3 rings to the hetero-oligomers appears to have a slightly larger impact on the stability of the system as determined by Δppm as the value is reduced from slightly which would indicate higher stability.

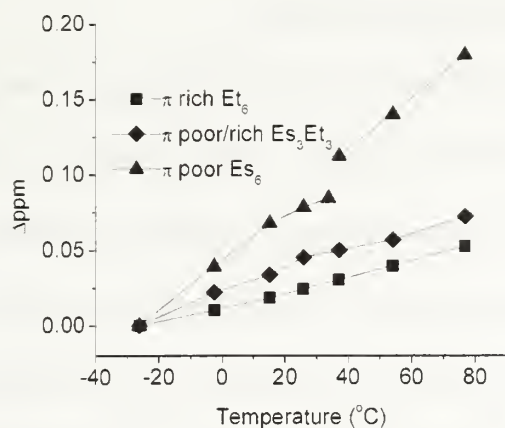


Figure 6.5 Δ ppm vs Temperature ($^{\circ}\text{C}$) in CD_3CN for hexamers 13, 24, and 19.

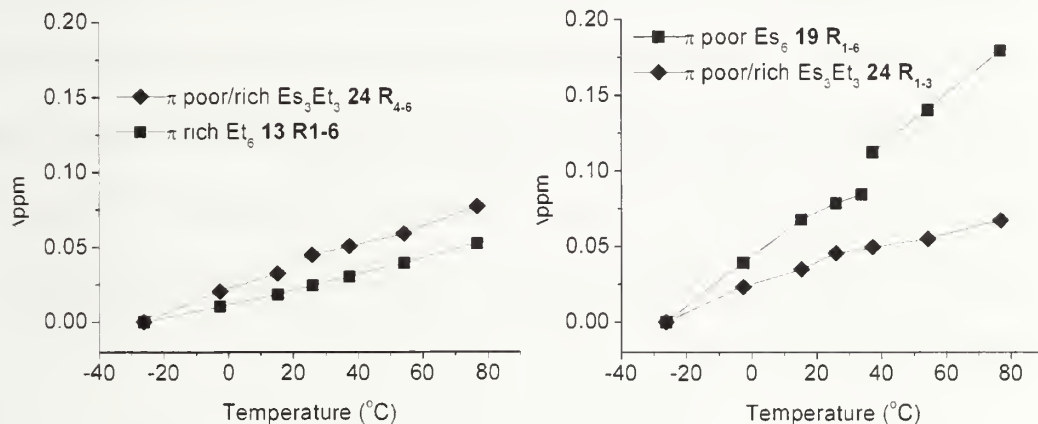


Figure 6.6 Δ ppm vs. Temperature in CD_3CN extracting π -rich (a) and π -poor (b) portions of oligomer 24 compared with oligomers 13 and 19.

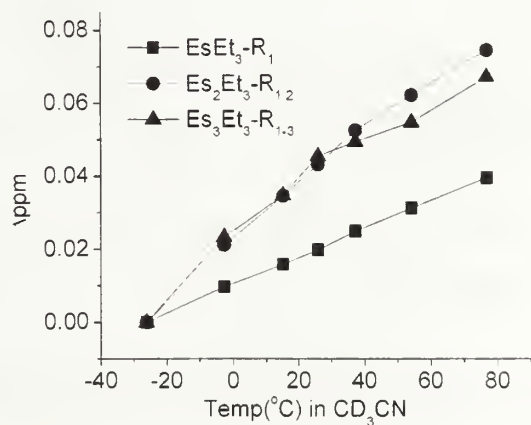


Figure 6.7 Δ ppm vs Temperature ($^{\circ}\text{C}$) in CD_3CN for the ester rings of 22-24.

6.3.3 Temperature studies in CDCl₃

Because the tetrameric π -poor systems were found to be unaffected by temperature in CDCl₃ in Chapter 5, there is no further exploration of the temperature sensitivity of the remaining tetramers in CDCl₃. Examining Δ ppm versus temperature data in CDCl₃ for pentamers **23** and **18**. Figure 6.8 (a) shows the continued influence of temperature on the π -poor systems **18** while there is absolutely no dependence of Δ ppm on temperature in CDCl₃ in the π -poor/rich system **23** (b). This could indicate that pentamer **23** is completely unfolded in CDCl₃ as opposed to the partially folded and still downfield shifting **18**. Figure 6.9 shows a similar result for the π -poor/rich (**24**) and π -poor (**19**) hexamers, showing the lack of temperature sensitivity in CDCl₃ for the π -poor/rich systems as opposed to the continued downfield shifting of the aryl region of the π -poor systems. For **19** the Δ ppm changes by 0.05 ppm over 40°C while **24** shows a change similar to that found in **23** which indicates an absence of π -interactions over a 100°C temperature change.

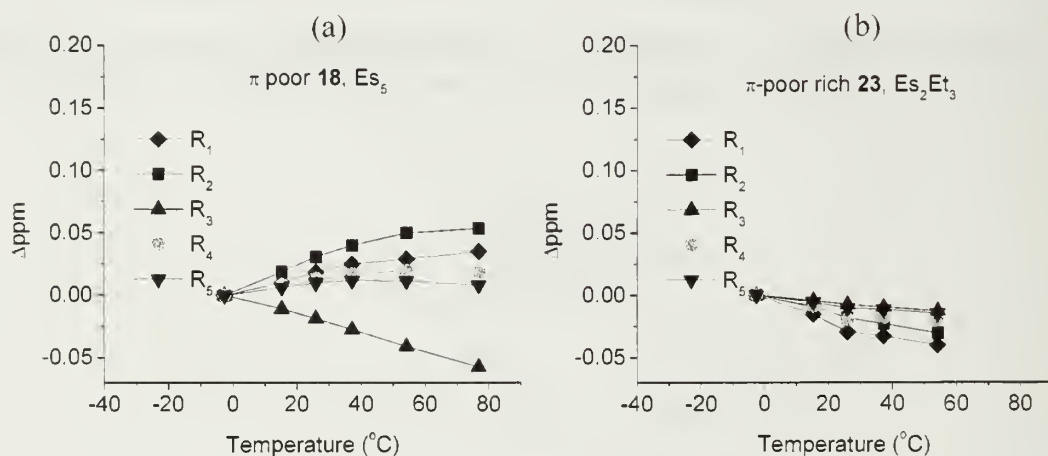


Figure 6.8 Δ ppm vs Temperature (°C) in CDCl₃ for pentamers **18** (a) and **23** (b).

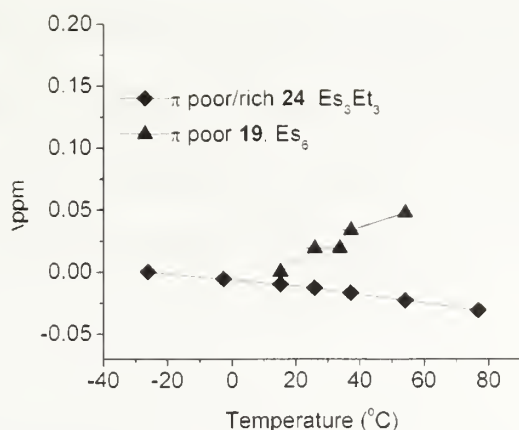


Figure 6.9 Δ ppm vs Temperature ($^{\circ}$ C) in CDCl_3 for hexamers **24** and **18**.

6.4 Modeling and the overall impact of solvent and temperature

Taking all of the previous measurements and plotting them so that solvent and temperature are shown together. Figure 6.10 shows each pentamer simply showing the average ppm value for $R_{1,2,4,5}$ plotted on the x axis, volume % CD_3CN in CDCl_3 is plotted on the left y-axis, (black), on the right y-axis (red) is plotted temperature in CD_3CN and on the farther most right y-axis (blue) is plotted temperature in CDCl_3 . The slopes of the lines as they are shown on these plots are indicative of the secondary state of the oligomer. Nearly vertical slopes for $^{\circ}\text{C}$ vs. average ppm in CDCl_3 as shown specifically in 6.10 (b) for **23** and 6.11 (b) for **24**, seem to indicate endpoints where either the spectroscopic sensitivity of NMR has been surpassed, or preferably where the systems are completely unfolded in CDCl_3 . Given that premise, the spectroscopic insensitivity of the π -rich alone (6.10 and 6.11 (a)) does not, unfortunately, provide a proper basis useful for extrapolating such endpoints. However, because the trends in Δ ppm shifting experience due to changes in solvent and temperature are similar to those shown for the other systems, it is highly likely that these π -rich scaffolds fold.

The π -poor/rich systems do appear to have an endpoint as observed in CDCl_3 that renders the system relatively insensitive to temperature for both the pentamer and hexamer thus indicating an endpoint for unfolded oPE. However the π -poor systems have slopes for both sets of temperature data that fall inline with the solvent data as plotted.

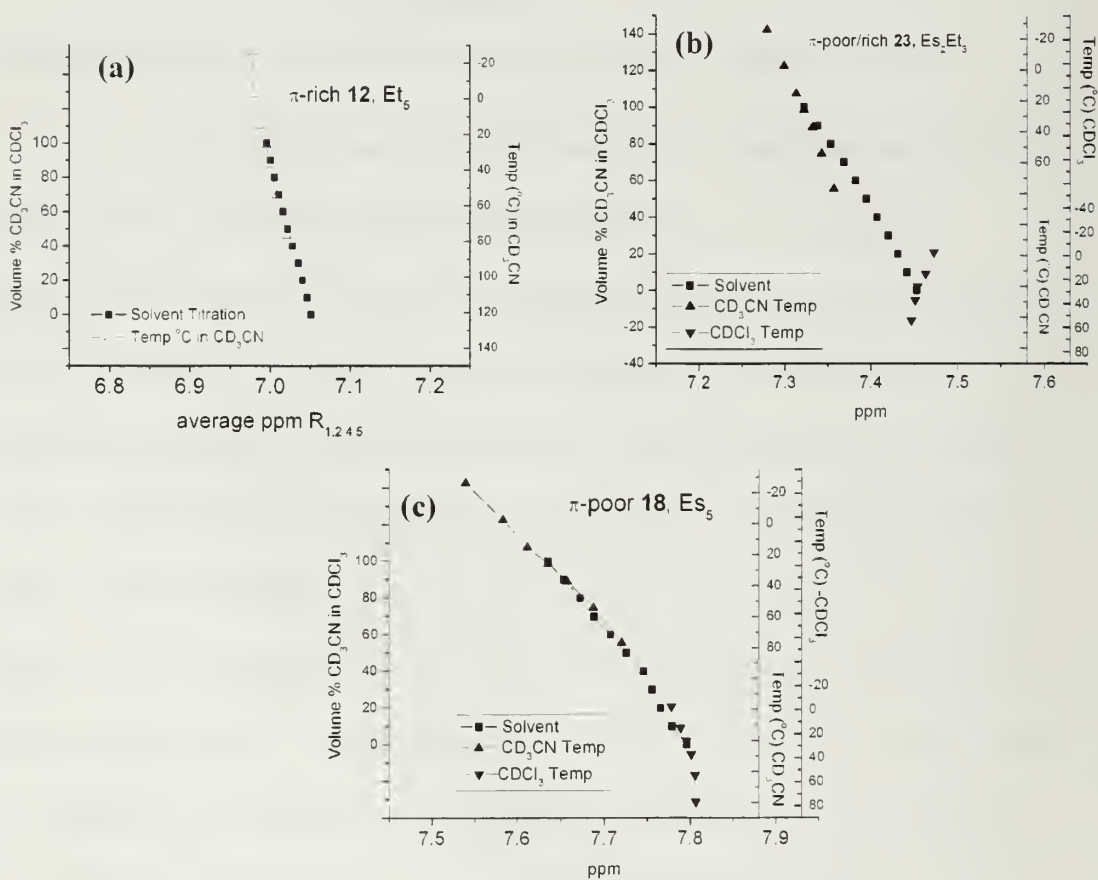


Figure 6.10: Combined solvent and temperature plots for all pentamers (a) π -rich 12 (b) π -poor/rich 23 (c) π -poor 18

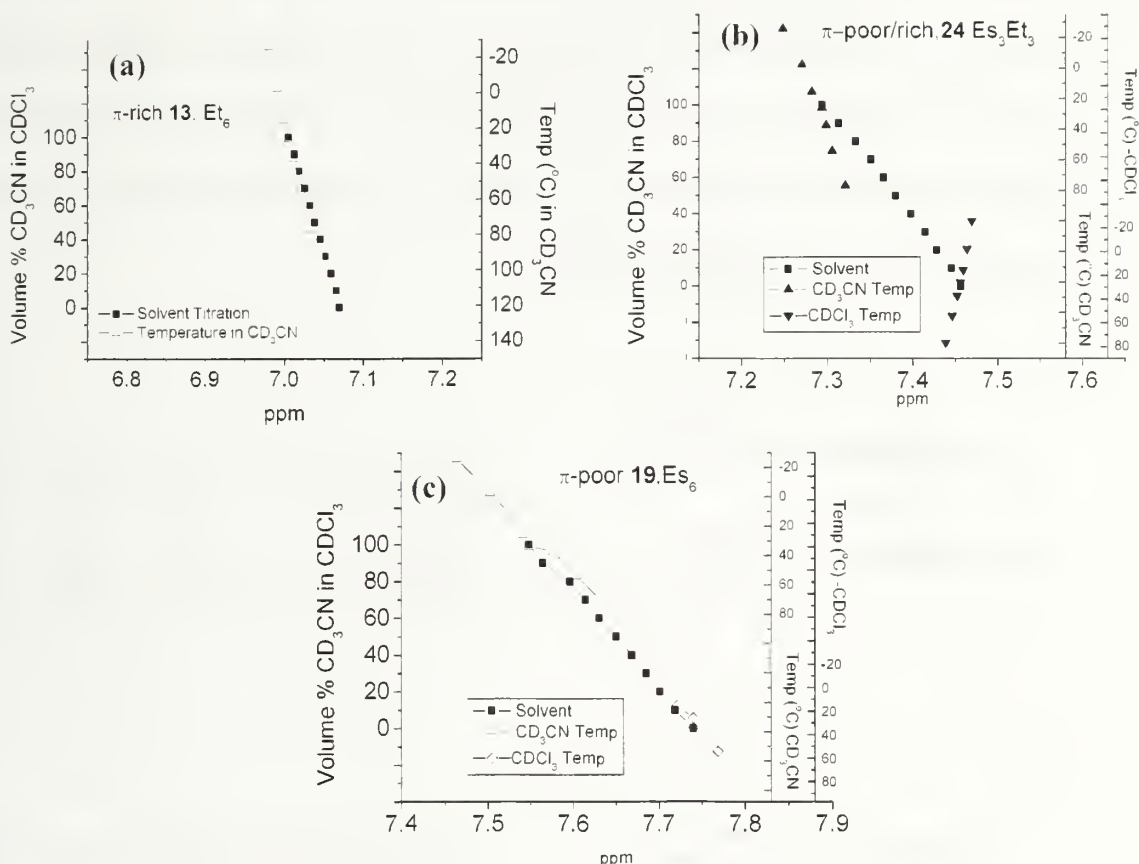


Figure 6.11: Combined solvent and temperature plots for all hexamers. (a) π -rich 13 (b) π -poor/rich 24 (c) π -poor 19

All of the data sets indicate that the π -poor systems are most affected by π - π stacking in solvent and temperature. The energy minimized MMFF models shown in Figures 6.12 (pentamers) and 6.13 (hexamers) however, differ in their predictions. Next to each model is a table containing the measured distance between the stacked rings ($D_{x,y}$), the angle between the rings measured using a perpendicular line through the center of ring y and $D_{x,y}$ ($\theta_{x,y}$) and the offset $O_{x,y}$ as calculated previously. The sidechains have been eliminated for clarity. For the pentamers, the π -poor/rich system **23** forms the most compact helix with the smallest distance between stacked rings and

offset between the stacked rings, followed closely by the π -poor then the π -rich. The measurements of course, are approximations and in general are very close, varying by less than 1 Å. In the hexamers, the prediction now places the π -rich slightly closer than the π -poor but by an even smaller margin than before. Unfortunately, with increasing oligomer length, the models do not capture the solvent dipole details and do not provide nuanced details as we had initially hoped.

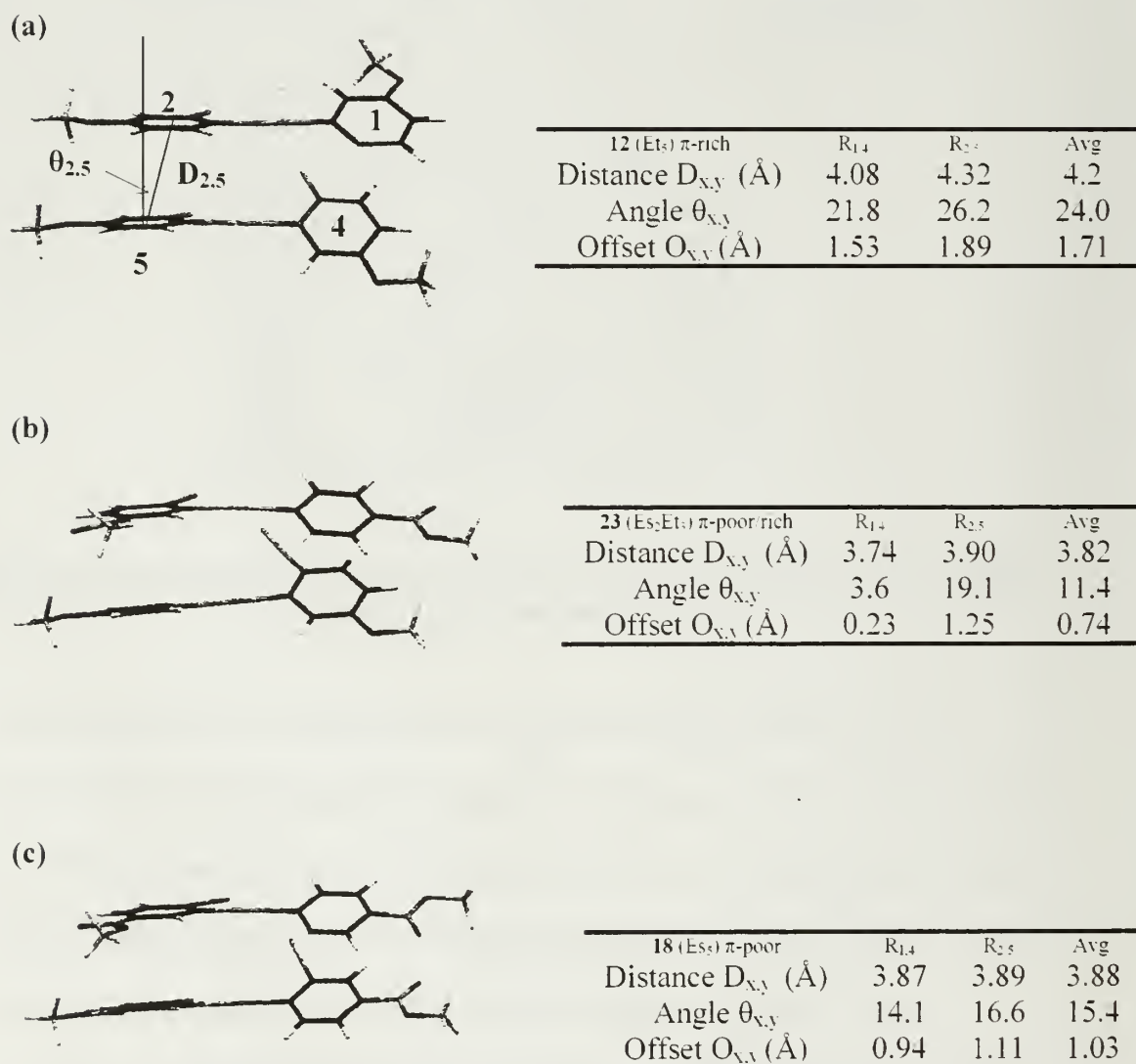
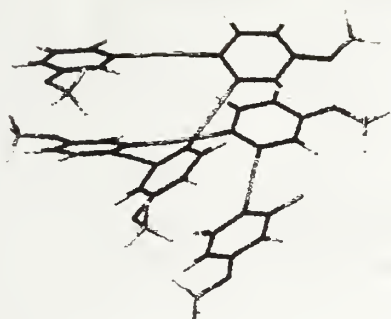


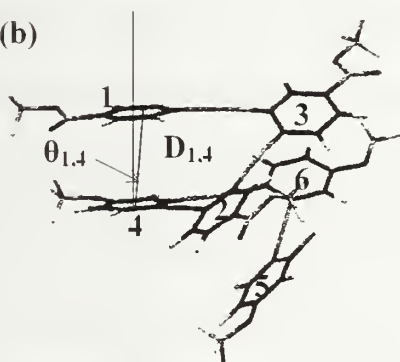
Figure 6.12: MMFF energy minimized models for all pentamers (a) π -rich 12 (b) π -poor/rich 23 (c) π -poor 18

(a)



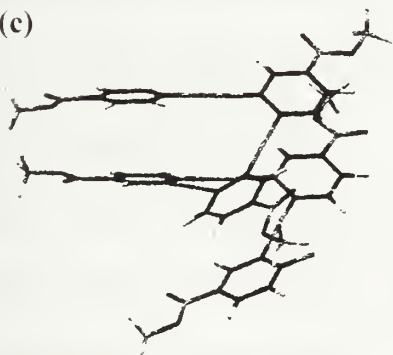
13 (Et ₂) π-rich	R _{1,4}	R _{2,5}	R _{3,6}	Avg
Distance D _{X,Y} (Å)	4.02	3.87	3.91	3.93
Angle θ _{X,Y}	23.1	8.8	11.2	14.4
Offset O _{X,Y} (Å)	1.58	0.59	0.76	0.98

(b)



24 (Es:Et) π-poor rich	R _{1,4}	R _{2,5}	R _{3,6}	Avg.
Distance D _{X,Y} (Å)	3.77	3.81	3.83	3.8
Angle θ _{X,Y}	6.8	6.2	13.3	8.8
Offset O _{X,Y} (Å)	0.44	0.41	0.88	0.58

(c)



18 (Es ₆) π-poor	R _{1,4}	R _{2,5}	R _{3,6}	Avg
Distance D _{X,Y} (Å)	3.88	3.97	3.96	3.94
Angle θ _{X,Y}	16.2	14.5	21.1	17.3
Offset O _{X,Y} (Å)	1.08	1.00	1.43	1.17

Figure 6.13: MMFF energy minimized models for all hexamer (a) π-rich 13 (b) π-poor/rich 24 (c) π-poor 19.

Calculating the formation energies (ΔH_{helix}) from the full models for each of these systems, the following values can be found in Table 6.3.

Table 6.3 ΔH_{helix} (kcal/mol) calculations for all oligomers

Oligomer length	π -rich	π -poor rich	π -poor
4	4.0	9.7	3
5	9.0	12.4	6.0
6	25.1	19.0	18.0
Simple oPE Models from reference 77			
6	13.7	21.0	16.2

In stark contrast to the simple models utilized previously with either alkoxy methyl or ester methyl side chains, the dramatic impact of the Teg side chain is evident. In this case, the compound with the lowest ΔH_{helix} is now the π -rich system as opposed to the π -poor/rich systems previously published (77). Unfortunately this has not been proven experimentally due to the relative insensitivity of the π -rich aromatic protons in our NMR studies. Comparing the formation energies of ΔH_{helix} versus oligomer length as shown in Figure 6.14 (a), the linearity that was previously observed for completely unsubstituted systems (b) is absent for the π -rich and π -poor Teg- substituted oligomers. However, the dramatic change in energy as the oligomer goes from a 1 and 2/3 system to a 2 layer helix is evidenced in the data. Figure 6.15 shows the average Δppm from CDCl_3 to CD_3CN as a function of oligomer length for the π -rich and π -poor oligomers profiled here. The only step change evident by this method is for the π -poor systems, while the π -rich systems appear to hold at the same Δppm between oligomer lengths of 5 and 6.

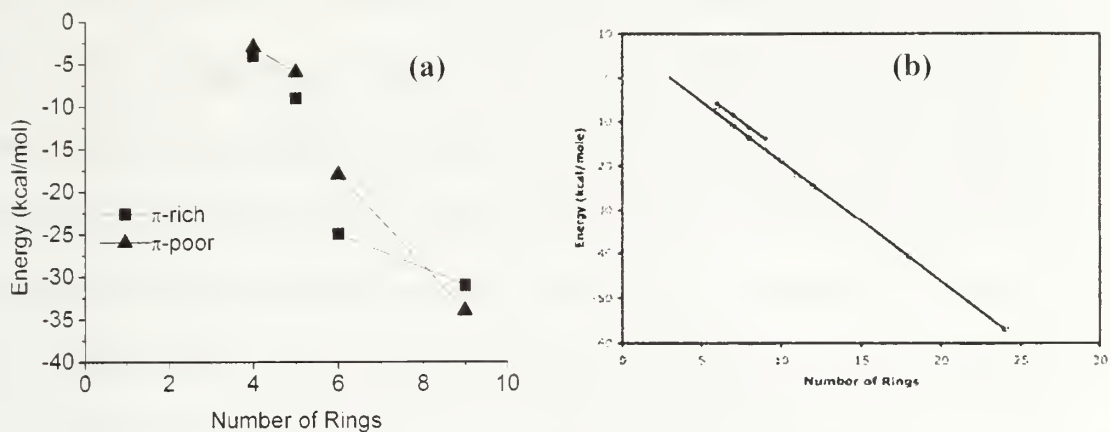


Figure 6.14: Plots of Energy vs. Number of Rings for (a) π -rich and π -poor systems as synthesized and (b) unsubstituted oligomers using MMFF energy minimization.

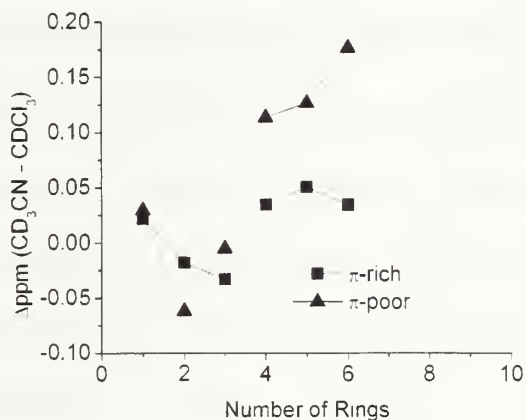


Figure 6.15: Plot of Δ ppm ($\text{CD}_3\text{CN} - \text{CDCl}_3$) vs. number of rings for π -rich and π -poor systems.

6.5 “Breathing” of the oPE system

In the end, the wide range of Δ ppm values for the π -poor systems may mean that the observations for these systems mean that a “breathing” macromolecular spring like entity could exist. This “breathing” would not cause the system to fully unravel, but rather dynamically stretch and contract like a macromolecular spring. Evidence for this macromolecular spring concept would be similar slopes for individual protons that

would be most impacted by the π -electrons in the system. As it was shown in section 5.5, the Δppm of individual protons could be extracted to two layers in the π -poor hexameric helix. The offset of the layers required to stabilize the π - π interaction allows for slip stacking that would selectively influence one set of protons over the other. Figure 6.16 examines two sets of protons that would be influenced differently based on their position within the layer. Protons 4a and 5a, would be on the "outside" of the helical structure, away from the influence of π -systems of adjacent layers and, as it was shown would be impacted less by a folded structure. Protons 2a and 3a would be located on the "inside" of the helical structure, close to adjacent layers of the helix and thus to the influence of the π -systems. If the oPE helix is "breathing" rather than unfolding, the "inside" protons would maintain similar Δppm slope measurements, rather than one selectively moving out of the range of the closest π -system at a time. The "outside" protons would consistently remain un-impacted by neighboring π -systems. Figure 6.17 plots the individual ppm tracks of these protons 2a, 3a, 4a, and 5a and this is exactly what is observed. Over this 100° temperature range, the $\Delta\text{ppm}/^\circ\text{C}$ of 4a and 5a remains flat while the $\Delta\text{ppm}/^\circ\text{C}$ of 2a and 3a are identical up between -26°C and 55°C evidence that the π -poor oPE helix is not unfolding with increasing temperature in CD_3CN , rather that it is "breathing". Figure 6.18 illustrates the concept of breathing (a) unfolding (b) and twisting (c). All of the data for the π -poor oligomeric systems seems to indicate that breathing is the most likely option.

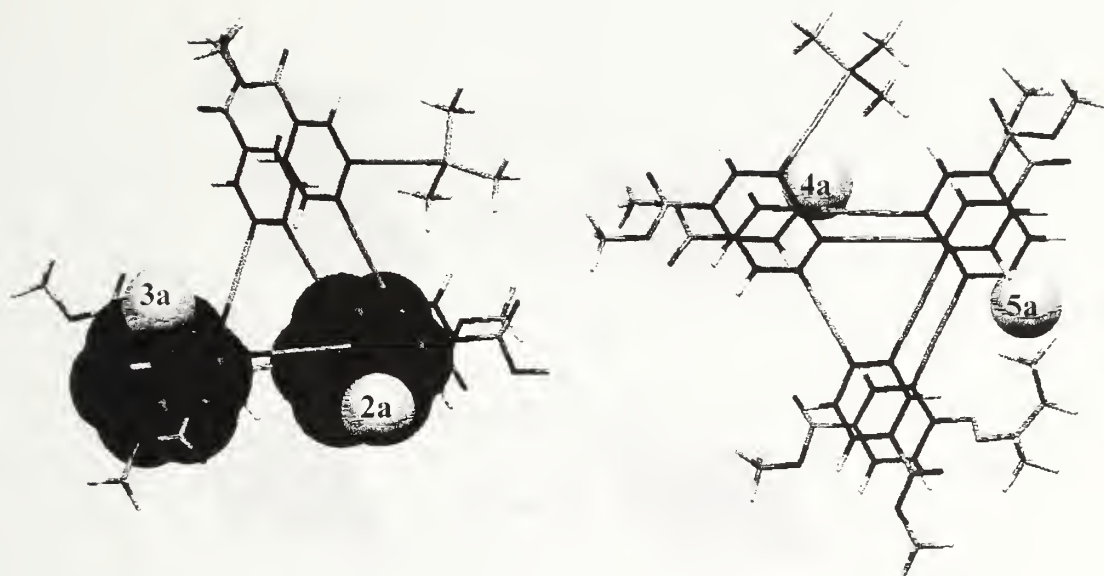


Figure 6.16: Models showing (a) “inside” protons 2a and 3a and (b) “outside” protons 4a and 5a for π -poor hexamer 19.

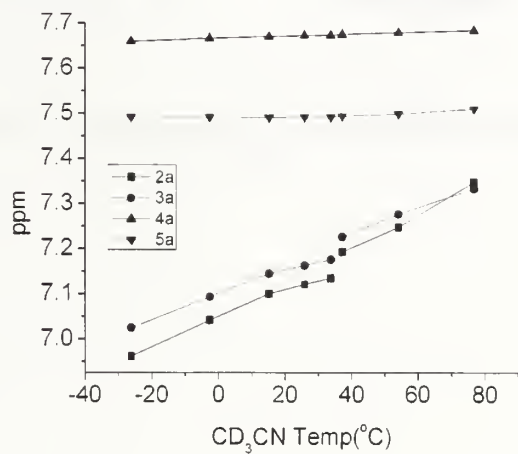


Figure 6.17: Plot of ppm vs. Temperature in CD₃CN for “inside” protons 2a and 3a and “outside” protons 4a and 5a.

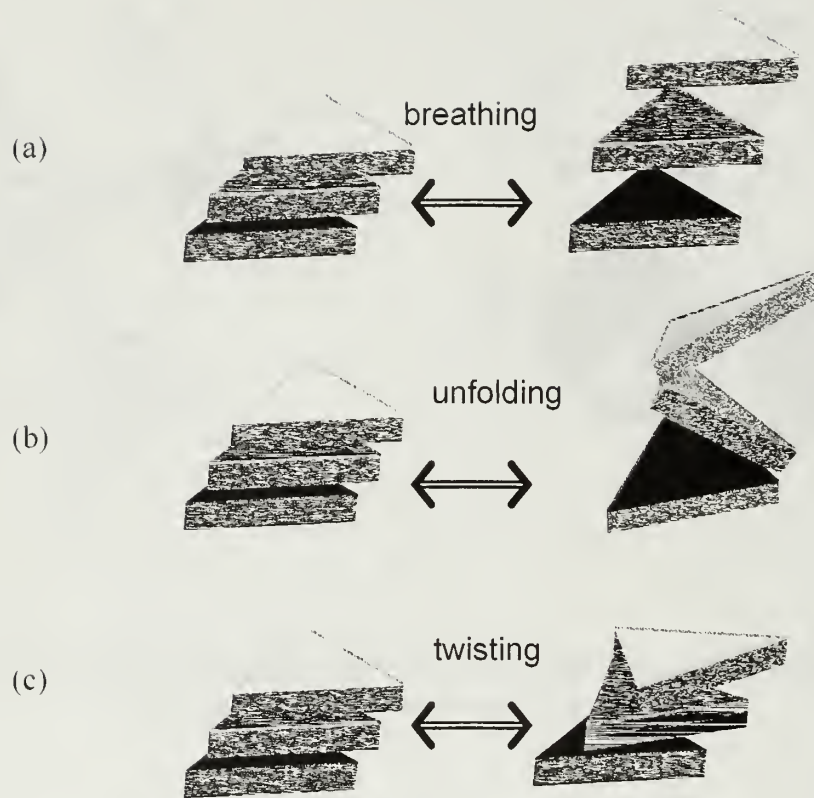


Figure 6.18: Representations of (a) breathing, (b) unfolding and (c) twisting for oPE systems

6.6 Conclusions

In conclusion, the electronic character of the oPE backbone has a significant impact on the stability and folded character of the oPE helix at longer lengths. Though π -rich and π -poor/rich systems exhibit the same basic 1-D ^1H NMR shifts in the aryl regions as the π -poor systems characterized in Chapter 5, the magnitude of these overall shifts can vary by factors of 2 or 3. Though the π -rich systems may be folding, the minimal changes in the aryl region of the NMR make it a poor candidate for further study. The potential stability that was sought through the complementarity of the π -poor/rich system does prove to be a better candidate for stable helix formation as the models might suggest due to the small $\Delta\text{ppm}/^\circ\text{C}$ changes the system experiences in CD_3CN . Overall, the models probed to be of smaller utility as oligomer lengths increased, predicting closer interactions for the complementary π -poor/rich systems, than the π -poor, then finally the π -rich contrary to what was shown in Chapter 4 with the short tetrameric sequences.

The dynamic nature of the π -poor oPEs at a variety of temperatures is not necessarily due to unfolding, but potentially to "breathing" that expand and contract the helix like a macromolecular spring. Ultimately, the π -poor systems, similar to findings for the mPEs show the most potential for future synthesis and study as a secondary helical structure that increases in stability with length. However, if future work requires more completely unfolded and folded states, the complementary systems may have some utility due to their temperature and solvent sensitivity.

CHAPTER 7

MATERIALS AND METHODS

7.1 Measurements

For basic monomer synthesis of the non-polar oligomers ^1H and ^{13}C NMR spectra were obtained at 300 MHz with a Bruker DPX-300 NMR spectrometer and ^{13}C NMR spectra were obtained at 100 MHz on a JEOL Eclipse spectrometer.. UV-visible spectra were recorded on a Hewlett-Packard 8453. Emission and excitation spectra were taken on a Perkin-Elmer LS 50B spectrometer with a xenon lamp light source. The maximum absorbivities of the solutions were 0.1 or less. Mass spectral data were obtained at the University of Massachusetts Amherst mass spec facility, which is supported in part by the National Science Foundation.

For oligomers ^1H , and ^{13}C NMR spectra were obtained at 400 MHz with a Bruker DPX-400 NMR spectrometer and analyzed with the Bruker XWIN NMR program.

High resolution 1-D and 2-D data for oligomers Oligomers **17-20**, were taken on a 600MHz Bruker spectrometer using both XWIN NMR and TOPSPIN software to analyze data.

7.2 Materials

Reagent grade tetrahydrofuran (THF) was distilled under nitrogen from sodium benzophenone. All other solvents were used as received. 3-nitro-4-iodophenol was purchased from Aldrich and used without further purification. Trans dichlorobis (triphenylphosphine) palladium ($\text{Pd}(\phi_3\text{P})_2\text{Cl}_2$) was purchased from Strem Chemical. S(-)-

2-methyl-1-butanol was purchased from Fluka Chemika. Tri-ethylene glycol monomethyl ether was purchased from Aldrich and used after solvation in dichloromethane, and passing through a pipette of silica and subsequent evaporation. The compound was then evaporated and dried under vacuum. Trimethylsilyl acetylene was purchased from GFS chemicals. Methyl iodide was purchased from Alfa Aesar and distilled into an airfree flask for subsequent use. All other reagents were purchased from Alfa Aesar or Aldrich Chemical Co. and all were used as received. All column chromatography was performed with 80-230 mesh silica from VWR.

Purification. All column chromatography was performed on an ISCO Companion using solvent gradients as indicated.

Abbreviations used: DCM (dichloromethane), TEA (triethylamine), TMS (trimethylsilyl) DMF (Dimethyl Formamide), DEA (Diethyl Amine).

7.3 General Synthetic Procedures

7.3.1 General Sonogashira Coupling Procedure

A schlenk flask with stirbar was flame dried under vacuum and backfilled with N₂ three times. To this flask were added 0.05-0.1 equivalents (based on the acetylene compound) of Pd(PPh₃)₂Cl₂ and 0.1-0.2 equivalents of CuI. The 1-1.1 equivalents of the acetylene compound to 1 equivalent iodide were dissolved in separate flasks in TEA and transferred via syringe to the schlenk flask under N₂. The schlenk flask was gently degassed for 30 seconds then backfilled with N₂. The flask sealed and placed in an oil

bath at 45°C for at least 6-18 hours and checked by TLC for completeness. A precipitate should form. Once done, the reaction solution was diluted with ether, filtered through a pad of Celite and concentrated. The residue was then purified using flash chromatography (Silica, eluent combination of hexanes and dichloromethane).

7.3.2 General TMS Deprotection Procedure 1 (K₂CO₃).

One equivalent of the TMS protected compound and 2.5 molar equivalents of K₂CO₃ with 5-10 mL of methanol (and 5-10 mL THF if necessary for solubility) were stirred in a nitrogen-flushed vial for 0.5 to 3 hours. Reaction was monitored by TLC. Upon completion the solution was diluted with ethyl acetate and water and washed twice with water. After drying the ethyl acetate layer over MgSO₄ and evaporation of solvent, the residue was purified by flash chromatography if necessary.

7.3.3 General TMS Deprotection Procedure 2 (TBAF).

One equivalent of the TMS protected compound was dissolved in dry THF and cooled to 0°C in a round bottom flask with stirbar. 1.2 equivalents of TBAF in 1 M THF solution with 5% H₂O content were added, and the reaction was stirred for 5 minutes. Enough hexane was then added to bring the reaction to a 1:1 THF/hexane ratio, precipitating most excess TBAF and t-butyl ammonium hydroxide, and the reaction was stirred for an additional 10 minutes. The reaction mixture was injected directly, without evaporation, onto either a silica-packed pipette or a flash chromatography column for purification.

7.3.4 General Sonogashira Coupling Procedure.

A schlenk flask with stirbar was flame dried under vacuum and backfilled with N₂ three times. To this flask were added 0.05-0.1 equivalents (based on the acetylene compound) of Pd(Pφ₃)₂Cl₂ and 0.1-0.2 equivalents of CuI. The 1-1.1 equivalents of the acetylene compound to 1 equivalent iodide were dissolved in separate flasks in TEA and transferred via syringe to the schlenk flask under N₂. The schlenk flask was gently degassed for 30 seconds then backfilled with N₂. The flask sealed and placed in an oil bath at 45°C for at least 6-18 hours and checked by TLC for completeness. A precipitate should form. Once done, the reaction solution was diluted with ether, filtered through a pad of Celite and concentrated. The residue was then purified using Silica flash chromatography using the solvents indicated.

7.3.5 General Triazene Activation Procedure

A schlenk flask with stirbar was flame dried under vacuum and backfilled with N₂ three times. The triazene compound was dissolved in enough distilled methyl iodide to make a 0.1M solution and transferred to the schlenk flask. The schlenk flask was then gently degassed for 30 seconds then backfilled with N₂ and closed. The reaction vessel was placed in a 110°C oil bath for 6-18 hours, and monitored by TLC. A precipitate should form. Upon completion the reaction mixture was diluted with hexanes, filtered over Celite and concentrated and purified by flash chromatography.

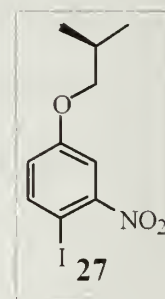
7.3.6 General Microwave Triazene Activation Procedure

This procedure was performed by microwave synthesis in Biotage 2-5 mL vials. Each vial was filled with 250 mg of triazene protected compound 0.05 eq of I₂ and of

MeI \approx 130 eq, a stirbar was added, and a septum crimped on. Microwave heat was applied to each tube, at a temperature of 150°C for a time of one hour. After all reactions had completed, the tubes were opened, combined, filtered through a Celite pad and washed with ethyl ether, and evaporated under a N₂ stream, and purified by flash chromatography.

7.4 Synthesis of Non-Polar Alkoxy Compounds

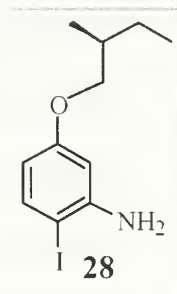
1-Iodo-4-((S)-2-methyl-butoxy)-2-nitro-benzene (27) Following the procedure for a Mitsunobu alkylation of an alcohol, a flame-dried and N₂ filled 100 mL sidearm flask with magnetic stirbar was charged with 3-nitro-4-iodo phenol (2 g, 7.54 mmol, 1 mol eq.), S-2-methyl butanol (0.97 mL, 1.2 mol eq) and triphenylphosphine (2.969 g, 11.32 mmol,



1.5 mol eq.) in 50 mL dry THF. The solution was cooled to 0°C in an ice bath and diisopropylazodicarboxylate (DIAD) (2.23 mL, 1.5 mol eq.) was slowly added to the stirring solution. The reaction was then removed from the ice bath and allowed to warm to room temperature. The reaction was complete after a half hour at room temperature as determined by TLC (15%DCM:Hexanes). The solvent was removed under reduced pressure yielding an orange oil that was purified by flash chromatography (Silica, 10%DCM:Hexanes) to afford **2** as a yellow oil (2.37 g) in 94% yield. ¹H NMR (CDCl₃): δ 7.85 (d, 1H, phenyl H J = 8.65 Hz), 7.40 (d, 1H, phenyl H, J = 2.85 Hz), 6.85 (dd, 1H, phenyl H, J₁ = 2.91, J₂ = 8.83), 3.73-3.86(m, 2H, CH₂), 1.82-1.93 (m, 1H, CH) 1.48-1.62 (m, 1H, CH₂), 1.20-1.35 (m, 1H, CH₂), 1.01 (d, 3H, CH₃ J = 6.8 Hz),

0.95 (t, 3H, CH₃ J = 7.4 Hz) ppm. ¹³C NMR (CDCl₃): δ 159.9, 153.48, 142.07, 120.98, 111.82, 74.04, 73.75, 34.75, 26.06, 16.50, 11.35 ppm MS: *m/z* 335.

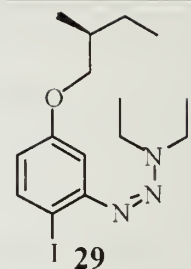
2-Iodo-5-((S)-2-methyl-butoxy)-aniline (28) 2.371 g (7.074 mmol, 1 mol eq) of **26**, FeCl₃•6H₂O (0.1146 g, 0.06 mol eq.), and Carbon Black (0.280 g, 3.3 mol eq.) were dissolved/suspended in 120 mL of Methanol in a 250 mL flask with magnetic stirbar. The solution was



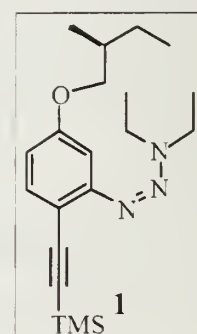
heated to 70°C. After 15 minutes, hydrazine (1.37 mL, 4 mol eq.) was slowly added to the stirring solution. The reaction was complete after a 2 hours at 70°C as determined by TLC (50%DCM: Hexanes). The reaction solution was filtered through a pad of Celite to remove the carbon black and the solvent was removed under reduced pressure yielding a clear oil and a small amount of a second phase. This residue was diluted with water and ethyl acetate, extracted 3 times with ethyl acetate, dried over MgSO₄ and filtered through a pad of silica gel to afford 2.01 g of product (94%) which was used without further purification. ¹H NMR (CDCl₃): δ 7.46 (d, 1H, phenyl H J = 8.65 Hz), 6.33 (d, 1H, phenyl H, J = 2.57 Hz), 6.13 (dd, 1H, phenyl H, J₁ = 2.59 J₂ = 8.66), 4.04 (s, 2H, NH₂) 3.63-3.77(m, 2H, CH₂), 1.77-1.88 (m, 1H, CH) 1.47-1.61 (m, 1H, CH₂), 1.19-1.31 (m, 1H, CH₂), 0.98 (d, 3H, CH₃ J = 6.7 Hz), 0.93 (t, 3H, CH₃ J = 7.4 Hz) ppm. ¹³C NMR (CDCl₃): δ 160.9, 147.63, 139.15, 107.35, 101.23, 73.2, 72.99, 34.72, 26.20, 16.6, 11.39 ppm MS: *m/z* 305.

N,N-Diethyl-N'-(2-Iodo-5-((S)-2-methyl-butoxy) phenyl)triazene (29) A solution of **28** (1.77 g, 5.85 mmol, 1mol eq.) in 120 mL acetonitrile, 20 mL of water, and 2.73 mL

(5.6 mol eq) hydrochloric acid in a 250 mL flask was cooled in an ice-acetone bath to -5°C . A cold solution of NaNO_2 (0.908 g, 13.16 mmol, 2.25 mol eq) in 15 mL water was added dropwise over 10 minutes. This was allowed to react for 30 minutes taking care to maintain vigorous stirring and low temperature (below 0°C). This mixture was transferred into a cold (-5°C) solution of K_2CO_3 (4.85 g, 35.1 mmol, 6 mol eq.), diethylamine (1.82 mL, 17.55 mmol, 3 mol eq.) and 20 mL water using a cannula. The reaction was allowed to warm to room temperature and stirred vigorously for an additional 15 minutes. The solution was extracted 3 times with ether; the organic phase was washed twice with brine, dried over MgSO_4 and evaporated to give a red oil. The residue was loaded on a silica gel column and eluted with 15% DCM:Hexanes to afford 1.50 g of the product (65%) as an orange oil. ^1H NMR (CDCl_3): δ 7.66 (d, 1H, phenyl H $J = 8.68$ Hz), 6.95 (d, 1H, phenyl H, $J = 2.94$ Hz), 6.49 (dd, 1H, phenyl H, $J_1 = 2.95$ $J_2 = 8.66$), 3.69-3.84(m, 6H, CH_2), 1.81-1.88 (m, 1H, CH) 1.51-1.60 (m, 1H, CH_2), 1.18-1.34 (m, 7H, CH_2 , CH_3), 1.00 (d, 3H, CH_3 $J = 6.8$ Hz), 0.94 (t, 3H, CH_3 $J = 7.4$ Hz) ppm. ^{13}C NMR (CDCl_3): δ 160.36, 151.14, 139.02, 103.59, 85.53, 77.38, 73.05, 49.02 34.72, 26.20, 16.6, 11.39 ppm MS: m/z 389.



***N,N*-Diethyl-*N'*-[2-trimethylsilylethynyl-5-((*S*)-2-methylbutoxy)phenyl]triazene (1)** The general Sonogashira coupling procedure described above was used to prepare this compound. 0.3793 g of **29** (0.974 mmol, 1 eq), 68 mg of $\text{Pd}(\text{P}\phi_3)_2\text{Cl}_2$ (97.4 μmol , 0.1 mol eq.), and 0.2 equivalents of CuI (37 mg, 0.1948

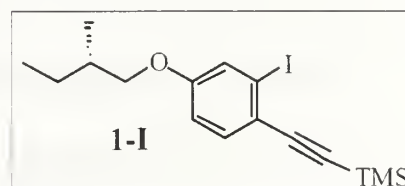


mmol) were combined in a schlenk flask with 10 mL TEA. TMS acetylene (0.165 mL, 0.1148 mmol, 1.2 mol eq.) was added to the solution. Once done, the reaction solution was diluted with ether, filtered through a pad of Celite and concentrated. The oil was then purified using flash chromatography in 25% DCM: hexanes to afford the product (0.3146 g, 90%) as an orange oil. ^1H NMR (CDCl_3): δ 7.37 (d, 1H, phenyl H $J = 8.53$ Hz), 6.91 (d, 1H, phenyl H, $J = 2.68$ Hz), 6.60 (dd, 1H, phenyl H, $J_1 = 2.62$ $J_2 = 8.63$), 3.71-3.85(m, 6H, CH_2), 1.79-1.90 (m, 1H, CH) 1.49-1.63 (m, 1H, CH_2), 1.18-1.34 (m, 8H, CH_2 , CH_3), 1.00 (d, 3H, CH_3 $J = 6.8$ Hz), 0.94 (t, 3H, CH_3 $J = 7.6$ Hz), 0.22(s, 9H, CH_3) ppm. ^{13}C NMR (CDCl_3): δ 160.21, 154.22, 134.24, 111.93, 110.65, 103.96, 101.98, 95.96, 76.87, 72.84, 49.11, 41.92, 34.82, 29.80, 26.22, 16.64, 11.43, 0.30 ppm MS: m/z 359.

[2-Iodo-4-((S)-2-methyl-butoxy)-phenylethynyl]-

trimethyl-silane (1-I) The general triazene

activation procedure was followed for this reaction.



dissolving 98.1 mg of **5** (0.2727 mmol, 1 mol eq.) in 3 mL CH_3I . After 12 hours, the

reaction mixture was diluted with hexanes, filtered over Celite, concentrated and

purified by column chromatography (hexanes) to afford the product as a beige oil (75.4

mg, 72%). ^1H NMR (CDCl_3): δ 7.36 (d, 1H, phenyl H $J = 4.55$ Hz), 7.34 (d, 1H, phenyl

H, $J = 1.47$ Hz), 6.80 (dd, 1H, phenyl H, $J_1 = 2.71$ $J_2 = 8.67$), 3.67-3.80(m, 2H, CH_2),

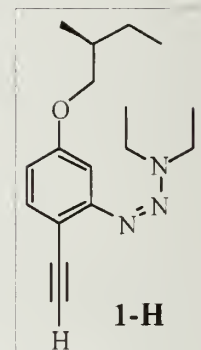
1.78-1.89 (m, 1H, CH) 1.47-1.61 (m, 1H, CH_2), 1.18-1.32 (m, 1H, CH_2 , CH_3), 1.01 (d,

3H, CH_3 $J = 6.77$ Hz), 0.95 (t, 3H, CH_3 $J = 7.6$ Hz), 0.27 (s, 9H, CH_3) ppm. ^{13}C NMR

(CDCl₃): δ values 159.38, 133.32, 124.63, 121.80, 114.58, 106.77, 101.89, 96.65, 77.42, 76.79, 73.21, 34.70, 26.12, 16.54, 11.38, 0.03 ppm MS: m/z 386.

***N,N*-Diethyl-*N'*-(2-ethynyl 5-((*S*)-2-methyl-butoxy**

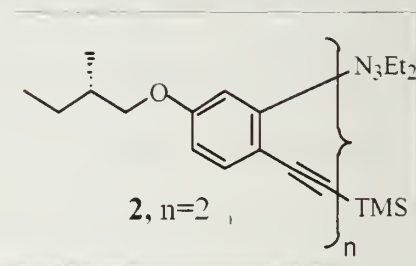
phenyl)triazene (1-H) The general TMS deprotection procedure was used to deprotect 0.100 g (0.278 mmol, 1 mol eq) of **1**. Flash chromatography (10%DCM:Hexanes) gave an orange oil (0.064 g, 80%). ¹H NMR (CDCl₃): δ 7.39 (d, 1H, phenyl H $J = 8.17$ Hz),



6.92 (d, 1H, phenyl H, $J = 2.57$ Hz), 6.63 (dd, 1H, phenyl H, $J_1 = 2.44$, $J_2 = 8.36$), 3.72-3.86(m, 6H, CH₂), 3.165 (s, 1H, CH), 1.80-1.91 (m, 1H, CH) 1.46-1.63 (m, 1H, CH₂), 1.19-1.33 (m, 7H, CH₂, CH₃), 1.01 (d, 3H, CH₃ $J = 6.8$ Hz), 0.94 (t, 3H, CH₃ $J = 7.3$ Hz) ppm.

TMS-Dimer-Triazene (2) The general procedure

for Sonogashira coupling was performed using 97.3 mg of **1-I** (0.252 mmol, 1 mol eq), and 79.8 mg of **1-H** (0.277 mmol, 1.1 mol eq.), 8.8 mg Pd(PPh₃)Cl₂

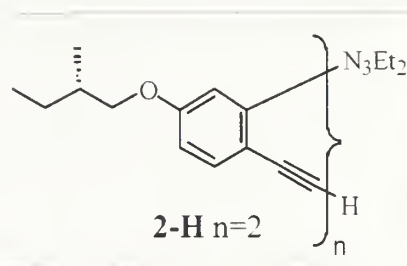


(12.6 μ mol, 0.05 mol eq.) and 4.8 mg CuI (25.2 μ mol, 0.1 mol eq.). After purification by flash chromatography (30% DCM: hexanes) a beige solid was produced (88.6 mg, 65%). ¹H NMR (CDCl₃): δ 7.47 (d, 1H, phenyl H $J = 8.40$ Hz), 7.37 (d, 1H phenyl H, $J = 8.69$), 6.96 (d, 1H, phenyl H, $J = 0.9$ Hz), 6.95 (d, 1H, phenyl H, $J = 0.9$ Hz), 6.75 (dd, 1H, phenyl H, $J_1 = 2.64$ $J_2 = 8.69$), 6.75 (dd, 1H, phenyl H, $J_1 = 2.59$ $J_2 = 8.66$), 3.67-3.88(m, 8H, CH₂), 1.82-1.90 (m, 2H, CH) 1.46-1.64 (m, 2H, CH₂), 1.23-1.38 (m,

8H. CH₂. CH₃). 0.88-1.029 (m. 6H. CH₃), 0.24 (s. 9H. CH₃) ppm. ¹³C APT NMR (CDCl₃): δ values 160.38, 159.14, 159.04, 153.95, 153.78, 134.26, 133.65, 133.89, 128.80, 128.29, 117.91, 117.55, 117.28, 116.70, 115.93, 114.77, 112.17, 110.88, 104.26, 104.15, 102.22, 96.76, 96.34, 96.20, 95.64, 92.93, 92.70, 90.86, 77.65, 76.80, 72.95, 34.92, 34.74, 29.88, 26.32, 26.26, 16.76, 16.63, 11.53, 11.45, 0.34 ppm.

H-Dimer-Triazene (2-H) The general TMS

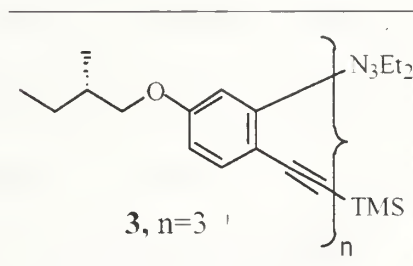
deprotection procedure was used to deprotect 36.7 mg (67.2 μmol, 1 mol eq) of **2** to give a beige oil (26 mg, 82%). ¹H NMR (CDCl₃): δ 7.48 (d, 1H, phenyl



H J = 8.67 Hz), 7.4 (d, 1H phenyl H, J = 8.49), 7.00 (d, 1H, phenyl H, J = 2.49 Hz), 6.96 (d, 1H, phenyl H, J = 2.47 Hz), 6.77 (dd, 1H, phenyl H, J₁ = 2.64 J₂ = 8.72), 6.67 (dd, 1H, phenyl H, J₁ = 2.54 J₂ = 8.65), 3.69-3.88 (m, 8H, CH₂), 3.21 (s, 1H, CH), 1.81-1.98 (m, 2H, CH) 1.48-1.62 (m, 2H, CH₂), 1.20-1.34 (m, 8H, CH₂, CH₃), 0.84-1.03 (m, 6H, CH₃) ppm.

TMS-Trimer-Triazene (3) The general procedure

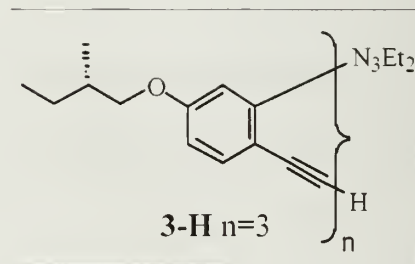
for Sonogashira coupling was performed using 21 mg **1-I** (54.9 μmol, 1 mol eq), and 26 mg **2-H** (54.9 μmol, 1 mol eq.), 1.9 mg Pd(PPh₃)Cl₂ (2.7 μmol,



0.05 mol eq.) and 1.0 mg CuI (5.5 μmol, 0.1 mol eq.) overnight. After purification by flash chromatography (15% DCM: hexanes) a beige solid was produced (24.1 mg, 60%). ¹H NMR (CDCl₃) δ 7.488 (1H, d, j=8.53), 7.440 (1H, d, j=8.62), 7.347 (1H, d,

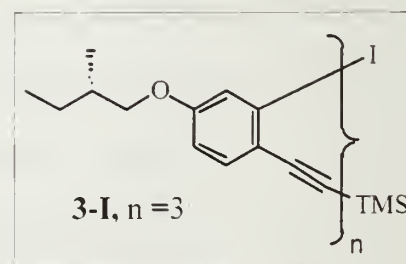
$j=8.63$). 7.012 (1H. d. $j=2.57$). 6.956 (1H. d. $j=2.60$). 6.936 (1H. d. $j=2.51$). 6.803 (1H. dd. $j=8.6$. 2.6). 6.736 (1H. dd. $j=8.6$. 2.6). 6.614 (1H. dd. $j=8.54$. 2.56). 3.87-3.68 (8H. m). 3.63-3.50 (2H. m). 1.93-1.68 (4H. m). 1.63-1.37 (4H. m). 1.34-1.10 (12H. m). 1.04-0.84 (21H. m). 0.24 (9H. s) ppm. MS: m/z 732.

H-Trimer-Triazene (3-H) The general procedure for TMS deprotection was followed with 14.6 mg of **3** in THF and methanol overnight to afford, after purification on silica gel (25% DCM: hexanes)



quantitative yield of **3-H**. ¹H NMR (CDCl₃) δ 7.496 (1H. d. $j=8.69$), 7.467 (1H. d. $j=8.85$), 7.374 (1H. d. $j=8.61$), 7.020 (1H. d. $j=2.59$), 6.989 (1H. d. $j=2.62$), 6.945 (1H. d. $j=2.55$), 6.804 (1H. dd. $j=8.6$. 2.6), 6.766 (1H. dd. $j=8.6$. 2.64), 6.632 (1H. dd. $j=8.55$. 2.56), 3.9-3.5 (10H. m), 3.158 (1H. s), 1.95-1.7 (3H. m), 1.65-1.4 (3H. m), 1.363-1.084 (9H. m), 1.010 (3H. d. $j=6.74$), 1.004 (3H. d. $j=6.73$), 0.941 (3H. d. $j=6.74$), 0.942 (6H. t. $j=7.6$), 0.89 (3H. t. $j=7.6$) ppm.

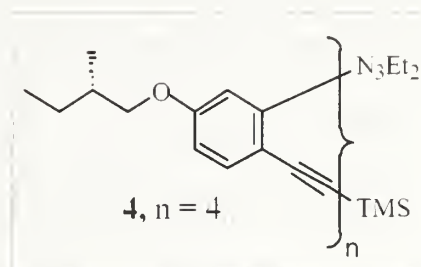
TMS-Trimer-I (3-I) The general procedure for triazene activation was performed on 30 mg of triazene **3** to afford 27.5 mg (88%) of **3-I** as a beige oil/solid after purification in 10% DCM:hexanes. ¹H



NMR (CDCl₃) δ 7.478 (2H. d. $j=8.62$), 7.380 (1H. d. $j=8.6$), 7.370 (1H. d. $j=2.47$), 7.103 (1H. d. $j=2.46$), 7.031 (1H. d. $j=2.51$), 6.893-6.697 (3H. m), 3.904-3.587 (6H. m).

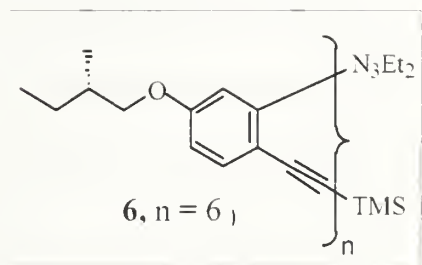
1.954-1.716 (3H, m), 1.658-1.416 (3H, m), 1.362-1.117 (3H, m), 1.073-0.835 (18H, m), 0.211 (9H, s) ppm.

Triazene-Tetramer-TMS (4) The general procedure for Sonogashira coupling was performed using 10.6 mg of **1-I** (27.5 μmol , 1.05 mol eq), and 1.73 mg **3-H** (26.2 μmol , 1 mol eq),



1.8 mg $\text{Pd}(\text{P}\phi_3)\text{Cl}_2$ (2.6 μmol , 0.1 mol eq.) and 0.9 mg CuI (5.2 μmol , 0.2 mol eq.) overnight. After purification by flash chromatography (25% DCM: Hexanes) a beige solid was produced (11 mg, 45%). ^1H NMR (CDCl_3): δ 7.51 (d, 1H, phenyl H $J = 8.7$), 7.50 (d, 1H, phenyl H $J = 8.7$), 7.45 (d, 1H, phenyl H, $J = 8.4$), 7.37 (d, 1H, phenyl H $J = 8.7$), 7.06 (d, 1H, phenyl H $J = 2.7$), 7.02 (d, 1H, phenyl, $J = ca. 1.8$), 7.01 (d, 1H, phenyl H, $J = 2.7$), 6.94 (d, 1H, phenyl H, $J = 2.4$), 6.82 (dd, 1H, phenyl H, $J_1 = 2.76$, $J_2 = 8.56$), 6.79-6.73 (m, 2H, phenyl H), 6.61 (dd, 1H, phenyl H $J_1 = 2.55$, $J_2 = 8.56$), 3.96-3.54 (m, 12H, CH_2), 1.90-1.68 (m, 4H, CH), 1.63-1.46 (m, 4H, CH_2), 1.36-1.18 (m, 10H, CH_2 , CH_3), 1.03-0.83 (m, 24H, CH_3), 0.235 (s, 9H, CH_3) ppm. MS: m/z 918.

Triazene-Hexamer-TMS (6) The general procedure for Sonogashira coupling was performed using 18.7mg **3-I** (24.6 μmol , 1 mol eq), and 16.5 mg **3-H** (246 μmol , 1 mol eq.), 0.4 mg $\text{Pd}(\text{P}\phi_3)\text{Cl}_2$

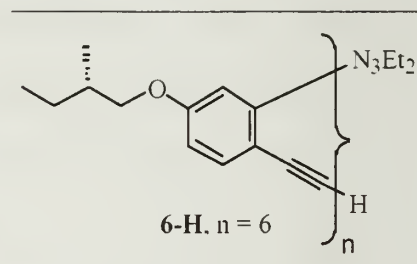


(0.6 μmol , 0.025 mol eq.) and 0.2 mg CuI (1.2 μmol , 0.05 mol eq.) overnight. After purification by flash chromatography (25-40% DCM:hexanes) a beige solid was

produced (16.5 mg, 52%). $^1\text{H NMR}$ (CDCl_3) δ 7.527 (2H, d, $j=8.59$), 7.517 (1H, d, $j=8.63$), 7.503 (1H, d, $j=8.57$), 7.457 (1H, d, $j=8.63$), 7.357 (1H, d, $j=8.65$), 7.119 (1H, d, $j=2.77$), 7.110 (1H, d, $j=2.84$), 7.059 (2H, d, $j=2.56$), 6.997 (1H, d, $j=2.56$), 6.949 (1H, d, $j=2.51$), 6.84-6.72 (5 H, m), 6.633 (1H, dd, $j=8.6, 2.6$), 3.894-3.516 (m, 15.822H), 1.975-1.679 (6.042H, m), 1.663-1.408 (8.763H, m), 1.393-1.081 (16.834H, m), 1.078-0.748 (40.351H, m), 0.264 (9H, s). MS $m/z = 1290$.

H-Hexamer-Triazene (6-H) The general K_2CO_3

procedure for TMS deprotection was followed with 19.1 mg of **6** in THF and methanol (1:1) for 3 hours to afford, after the addition of water and extraction



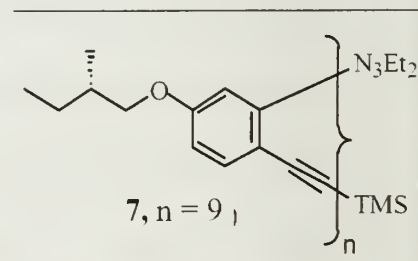
into EtOAc, a quantitative yield of **6-H**. $^1\text{H NMR}$ (CDCl_3) δ 7.496 (1H, d, $j=8.69$),

7.467 (1H, d, $j=8.85$), 7.374 (1H, d, $j=8.61$), 7.020 (1H, d, $j=2.59$), 6.989 (1H, d, $j=2.62$), 6.945 (1H, d, $j=2.55$), 6.804 (1H, dd, $j=8.6, 2.6$), 6.766 (1H, dd, $j=8.6, 2.64$),

6.632 (1H, dd, $j=8.55, 2.56$), 3.9-3.5 (10H, m), 3.158 (1H, s), 1.95-1.7 (3H, m), 1.65-1.4 (3H, m), 1.363-1.084 (9H, m), 1.010 (3H, d, $j=6.74$), 1.004 (3H, d, $j=6.73$), 0.941 (3H, d, $j=6.74$), 0.942 (6H, t, $j=7.6$), 0.89 (3H, t, $j=7.6$) ppm.

Triazene-Nonamer-TMS (7) The general procedure

for Sonogashira coupling was performed using 112 mg **3-I** (24.6 μmol , 1 mol eq), and 180 mg **6-H** (148 μmol , 1 mol eq), 3 mg $\text{Pd}(\text{P}\phi_3)_2\text{Cl}_2$ (0.4 μmol , 0.025

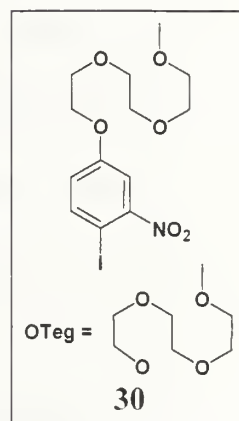


mol eq.) and 2 mg CuI (0.8 μmol , 0.05 mol eq.) overnight. After purification by flash chromatography (25-40% DCM :hexanes) a beige solid was produced (140 mg, 49%).

$^1\text{H NMR}$ (CDCl_3) δ 7.527 (2H, d, $j=8.59$), 7.517 (1H, d, $j=8.63$), 7.503 (1H, d, $j=8.57$), 7.457 (1H, d, $j=8.63$), 7.357 (1H, d, $j=8.65$), 7.119 (1H, d, $j=2.77$), 7.110 (1H, d, $j=2.84$), 7.059 (2H, d, $j=2.56$), 6.997 (1H, d, $j=2.56$), 6.949 (1H, d, $j=2.51$), 6.84-6.72 (5 H, m), 6.633 (1H, dd, $j=8.6, 2.6$), 3.894-3.516 (m, 15.822H), 1.975-1.679 (6.042H, m), 1.663-1.408 (8.763H, m), 1.393-1.081 (16.834H, m), 1.078-0.748 (40.351H, m), 0.264 (9H, s). MS $m/z = 1850$

7.5 Synthesis of Teg Alkoxy Compounds

1-Iodo-4-{2-[2-(2-methoxy-ethoxy)-ethoxy]-ethoxy}-2-nitrobenzene (30) Following the procedure for a Mitsunobu alkylation of an alcohol, a flame-dried and N_2 filled 250 mL sidearm flask with magnetic stirbar was charged with 3-nitro-4-iodo phenol (7 g, 26.41 mmol, 1.0 mol eq.). Tri-ethylene glycol monomethyl ether (5.07 mL, 1.2 mol eq) and triphenylphosphine (10.39 g, 39.62

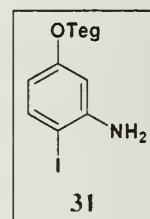


mmol, 1.5 mol eq.) in 150 mL dry THF. The solution was cooled to 0°C in an ice bath and diisopropylazodicarboxylate (DIAD) (7.79 mL, 1.5 mol eq.) was slowly added to the stirring solution. The reaction was then removed from the ice bath and allowed to warm to room temperature. The reaction was complete after a half hour at room temperature as determined by TLC (50%EtOAc:Hexanes). The solvent was removed under reduced pressure yielding an orange oil. The orange oil was taken up in 100ml of diethyl ether and chilled for 1 hour to precipitate triphenylphosphine-oxide as a white solid. The solution was filtered to remove the triphenylphosphine-oxide and the remaining solution was evaporated under reduced pressure and was purified by flash chromatography (Silica, 330g ISCO column, 30%-70% EtOAc:Hexane gradient) to

afford **30** as a yellow oil (10.86 g) in 95% yield. ^1H NMR (CDCl_3): δ 7.85 (d, 1H, phenyl H, $J = 8.78$ Hz), 7.44 (d, 1H, phenyl H, $J = 2.92$ Hz), 6.88 (dd, 1H, phenyl H, $J_1 = 2.92$, $J_2 = 8.78$), 4.16 (t, 2H, CH_2 , $J = 4.66$ Hz), 3.86 (t, 2H, CH_2 , $J = 4.65$ Hz), 3.70-3.72 (m, 2H, CH_2), 3.62-3.68 (m, 4H, CH_2), 3.52-3.55 (m, 2H, CH_2), 3.37 (s, 3H, CH_3). ^{13}C NMR (CDCl_3): δ 159.378, 142.03, 120.938, 111.757, 74.598, 71.874, 70.884, 70.61, 70.563, 69.351, 68.311, 59.023 ppm MS: m/z 434.1. ($m + \text{Na}^+$)

2-Iodo-5-{2-[2-(2-methoxy-ethoxy)-ethoxy]-ethoxy}-phenylamine (**31**)

8.32 g (20.233 mmol, 1.0 mol eq.) of **30**, $\text{FeCl}_3 \cdot 6\text{H}_2\text{O}$ (0.327 g, 0.06 mol eq.), and Carbon Black (0.802 g, 3.3 mol eq.) were dissolved/suspended in 350 mL of Methanol in a 500 mL flask with magnetic stirbar. The

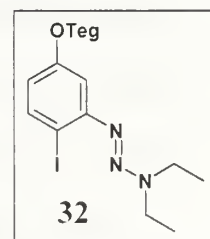


solution was heated to 70°C . After 15 minutes, 64% hydrazine (12.2 mL, 8 mol eq.) was slowly added to the stirring solution. The reaction was complete after 2 hours at 70°C as determined by TLC (50%EtOAc: Hexanes). The reaction solution was filtered through a pad of Celite to remove the carbon black and the solvent was removed under reduced pressure yielding a clear oil and a small amount of a second phase. This residue was diluted with water and ethyl acetate, extracted 3 times with ethyl acetate, dried over MgSO_4 , and concentrated to a clear oil. This oil was then purified by flash chromatography (Silica, 120g ISCO column, 30%-70% EtOAc:Hexane gradient) to afford **31** as a clear oil (7.17g) in 93% yield as a white waxy solid. ^1H NMR (CDCl_3): δ 7.45 (d, 1H, phenyl H, $J = 8.68$ Hz), 6.34 (d, 1H, phenyl H, $J = 2.79$ Hz), 6.12 (dd, 1H, phenyl H, $J_1 = 2.81$, $J_2 = 8.71$), 4.10 (s, 2H, NH_2), 4.05 (t, 2H, CH_2 , $J = 4.88$ Hz), 3.81 (t, 2H, CH_2 , $J = 4.87$ Hz), 3.70-3.72 (m, 2H, CH_2), 3.63-3.68 (m, 4H, CH_2), 3.53-

3.55 (m, 2H, CH₂), 3.37 (s, 3H, CH₃). ¹³C NMR (CDCl₃): δ 160.19, 147.534, 139.023, 107.139, 101.206, 73.573, 71.857, 70.739, 70.585, 70.498, 69.59, 67.402, 58.99 ppm.
MS: *m/z* 382.1. (*m* + H⁺)

***N,N*-Diethyl-*N'*-2-Iodo-5-{2-[2-(2-methoxy-ethoxy)-ethoxy]-ethoxy}-phenyl triazene (32)**

A solution of **31** (9.31 g, 24.42 mmol, 1 mol eq.) in 100 mL acetonitrile, 200 mL of water, and 10.18 mL (5 mol eq) hydrochloric acid in a 500 mL flask was



cooled in an ice-acetone bath to -5°C. A cold solution of NaNO₂ (3.37 g, 48.84 mmol, 2 mol eq) in 50 mL water was added dropwise with an addition funnel over 20 minutes.

This was allowed to react for 30 minutes taking care to maintain vigorous stirring and low temperature (below 0°C). This mixture was transferred into a cold (-5°C) solution

of K₂CO₃ (10.13 g, 73.27 mmol, 3 mol eq.), diethylamine (5.05 mL, 48.84 mmol, 2 mol eq.) and 50 mL water using a cannula. The reaction was allowed to warm to room

temperature and stirred vigorously for an additional 2 hours. The solution was extracted 3 times with ether: the organic phase was washed three times with brine, dried over

MgSO₄, filtered through a 2 inch pad of silica and evaporated to give a red oil. This oil was then purified by flash chromatography (Silica, 120g ISCO column, 30%-70%

EtOAc:Hexane gradient) to afford **6** as an orange oil (9.20g, 81%). ¹H NMR (CDCl₃):

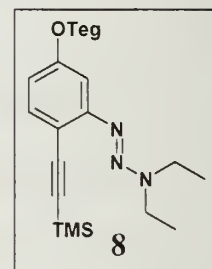
δ 7.66 (d, 1H, phenyl H, *J* = 8.64 Hz), 6.98 (d, 1H, phenyl H, *J* = 2.94 Hz), 6.50 (dd,

1H, phenyl H, *J*₁ = 2.95 *J*₂ = 8.66), 4.12 (t, 2H, CH₂, *J* = 4.95 Hz), 3.64-3.85 (m, 14H,

CH₂), 3.53-3.55 (m, 2H, CH₂), 3.37 (s, 3H, CH₃), 1.32 (broad s, 6H, CH₃). ¹³C NMR

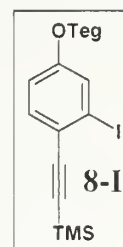
(CDCl₃): δ 159.711, 151.073, 139.006, 114.095, 103.466, 85.983, 77.251, 71.955, 70.851, 70.688, 70.608, 69.693, 67.497, 59.083 ppm. MS: m/z 488.1. ($m + Na^+$)

***N,N*-Diethyl-*N'*-[2-trimethylsilylethynyl-5-{2-[2-(2-methoxy-ethoxy)-ethoxy]-ethoxy}-phenyl]triazene (**8**)**



The general Sonogashira coupling procedure described above was used to prepare this compound. 8.86 g of **32** (19.03 mmol, 1 eq), .668 g of Pd(P ϕ ₃)₂Cl₂ (.9515 mmol, 0.05 mol eq.), and 0.1 equivalents of CuI (.362 g, 1.90 mmol) were combined in a schlenk flask with 190 mL TEA. TMS acetylene (4.03 mL, 28.56 mmol, 1.5 mol eq.) was added to the solution. Once done, the reaction solution was diluted with ether, filtered through a pad of Celite and concentrated. This oil was then purified by flash chromatography (Silica, 120g ISCO column, 30%-70% EtOAc:Hexane gradient) to afford **8** as an orange oil (5.24 g, 63%). ¹H NMR (CDCl₃): δ 7.37 (d, 1H, phenyl H, J = 8.54 Hz), 6.95 (d, 1H, phenyl H, J = 2.57 Hz), 6.62 (dd, 1H, phenyl H, H, J₁ = 2.58 J₂ = 8.55), 4.14 (t, 2H, CH₂, J = 4.92 Hz), 3.64-3.86 (m, 14H, CH₂), 3.53-3.56 (m, 2H, CH₂), 3.38 (s, 3H, CH₃), 1.31 (broad s, 6H, CH₃), 0.22 (s, 9H, Si-CH₃). ¹³C NMR (CDCl₃): δ 159.535, 154.154, 134.216, 112.049, 110.931, 103.635, 101.874, 96.219, 77.248, 71.954, 70.862, 70.687, 70.602, 69.694, 67.344, 59.082, 0.212 ppm. MS: m/z 458.3. ($m + Na^+$)

(2-Iodo-4-{2-[2-(2-methoxy-ethoxy)-ethoxy]-ethoxy}-phenylethynyl)-trimethyl-silane (8-I)



The general triazene activation procedure was followed for this reaction, dissolving 3.79 g of **8** (8.7 mmol, 1.0 mol eq..) in 30 mL CH₃I. After 12 hours, the reaction mixture was diluted with

ether, filtered over Celite, concentrated. (Silica, 40g ISCO column, 30%-70%

EtOAc:Hexane gradient) to afford **8-I** as a yellow oil (3.62 g, 90%). ¹H NMR

(CDCl₃): δ 7.38 (d, 1H, phenyl H, J = 2.53 Hz), 7.36 (d, 1H, phenyl H, J = 8.66 Hz),

6.83 (dd, 1H, phenyl H, J₁ = 2.53 J₂ = 8.62), 4.10 (t, 2H, CH₂, J = 4.88 Hz), 3.83 (t, 2H,

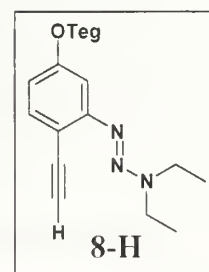
CH₂, J = 4.74 Hz), 3.71-3.73 (m, 2H, CH₂), 3.64-3.68 (m, 4H, CH₂), 3.53-3.56 (m, 2H,

CH₂), 3.38 (s, 3H, CH₃), 0.27 (s, 9H, Si-CH₃), ¹³C NMR (CDCl₃): δ values 158.699,

133.231, 124.646, 122.111, 114.596, 106.48, 101.709, 96.792, 71.903, 70.866, 70.638,

70.578, 69.486, 67.729, 59.052, -0.116 ppm. MS: *m/z* 485.4. (*m* + Na⁺)

***N,N*-Diethyl-*N'*-(2-ethynyl 5-{2-[2-(2-methoxy-ethoxy)-ethoxy]-ethoxy}-phenyl) triazene (8-H)**



The K₂CO₃ TMS deprotection procedure was used to deprotect 1.20 g (2.75 mmol, 1.0 mol eq.) of **7** and gave an orange oil (0.833 g, 83%) which was used without

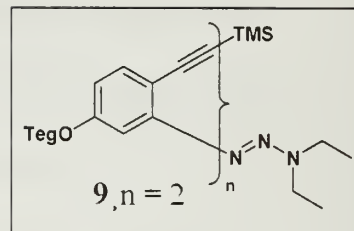
further purification for compound **8-H**. ¹H NMR (CDCl₃): δ 7.30 (d, 1H, phenyl H, J =

8.53 Hz), 6.89 (d, 1H, phenyl H, J = 2.52 Hz), 6.55 (dd, 1H, phenyl H, J₁ = 2.51, J₂ =

8.53), 4.03 (t, 2H, CH₂, J = 4.83 Hz), 3.51-3.74 (m, 12H, CH₂), 3.41-3.44 (m, 2H, CH₂),

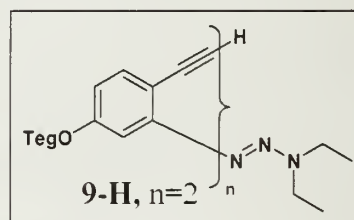
3.26 (s, 3H, CH₃), 3.13 (s, 1H, CH).

TMS-Et₂-Triazene (9) The general procedure for Sonogashira coupling was performed using .832 g of **8-H** (2.29 mmol, 1.0 mol eq.), and 1.17 g of **8-I** (2.52 mmol, 1.1.0 mol eq.), 40.2 mg Pd(PPh₃)Cl₂ (57.3 μmol, 0.025



mol eq.) and 21.8 mg CuI (114.6 μmol, 0.05 mol eq.). After purification by flash chromatography (Silica, 40g ISCO column, 0-10% Acetone:DCM gradient) a orange-brown oil was produced (1.40 g, 87%). ¹H NMR (CDCl₃): δ 7.47 (d, 1H, phenyl H, J = 8.54 Hz), 7.38 (d, 1H phenyl H, J = 8.63), 6.99 (d, 1H, phenyl H, J = 2.52 Hz), 6.95 (d, 1H, phenyl H, J = 2.58 Hz), 6.78 (dd, 1H, phenyl H, J₁ = 2.65 J₂ = 8.65), 6.68 (dd, 1H, phenyl H, J₁ = 2.58 J₂ = 8.56), 4.17 (t, 2H, CH₂, J = 4.66, 5.13 Hz), 4.09 (t, 2H, CH₂, J = 4.49, 4.99 Hz), 3.63-3.88 (m, 20 H, CH₂), 3.53-3.57 (m, 4 H, CH₂), 3.38 (s, 3H, CH₃), 3.37 (s, 3H, CH₃), 1.32 (t, 6H, CH₃, J = 7.00, 7.07 Hz), 0.23 (s, 9H, Si-CH₃). ¹³C NMR (CDCl₃): δ 159.62, 158.34, 153.75, 134.08, 133.30, 128.09, 117.60, 116.50, 115.09, 113.93, 111.08, 102.02, 94.22, 92.58, 90.65, 77.23, 71.93, 70.86, 70.67, 70.60, 70.57, 69.70, 59.07, 0.14 ppm. MS: *m/z* 721. (m + Na⁺)

H-Et₂-Triazene (9-H) The general K₂CO₃ TMS deprotection procedure was used to deprotect 1.40 g (2.00 mmol, 1mol eq) of **9** to give a orange-brown oil (1.22 g 97%). ¹H NMR (CDCl₃): δ 7.48 (d, 1H, phenyl H,



J = 8.53 Hz), 7.41 (d, 1H phenyl H, J = 8.61), 7.00 (d, 2H, phenyl H, J = 2.56 Hz), 6.81 (dd, 1H, phenyl H, J₁ = 2.63 J₂ = 8.63), 6.70 (dd, 1H, phenyl H, J₁ = 2.59 J₂ = 8.57), 4.18 (t, 2H, CH₂, J = 4.63, 5.21 Hz), 4.12 (t, 2H, CH₂, J = 4.60, 5.00 Hz), 3.65-3.89 (m,

20 H. CH₂). 3.54-3.58 (m. 4 H. CH₂). 3.39 (s. 3H. CH₃). 3.38 (s. 3H. CH₃). 3.22 (s. H. CH). 1.32 (t. 6H. CH₃, J = 6.89, 7.13 Hz).

TMS- Et₃-Triazene (10) The general procedure for

Sonogashira coupling was performed using .989 g **8-I**

(2.14 mmol, 1.1.0 mol eq.), and 1.22 mg **9-H** (1.94 mmol,

1.0 mol eq..), 34.1 mg Pd(PPh₃)Cl₂ (48.6 μmol, 0.025 mol

eq.) and 18.5 mg CuI (97.1 μmol, 0.05 mol eq.) overnight. After purification by flash

chromatography (Silica, 40g ISCO column, 0-20% Acetone:DCM gradient) a brown oil

was produced (1.18 g, 63%). ¹H NMR (CDCl₃) δ 7.48 (d, 1H, phenyl H, J = 8.54 Hz),

7.45 (d, 1H phenyl H, J = 8.64), 7.36 (d, 1H phenyl H, J = 8.64), 7.03 (d, 1H, phenyl H,

J = 2.59 Hz), 6.97 (d, 1H, phenyl H, J = 2.52 Hz), 6.94 (d, 1H, phenyl H, J = 2.62 Hz),

6.84 (dd, 1H, phenyl H, J₁ = 2.65 J₂ = 8.64), 6.79 (dd, 1H, phenyl H, J₁ = 2.64 J₂ =

8.61), 6.65 (dd, 1H, phenyl H, J₁ = 2.60 J₂ = 8.53), 4.13-4.16 (m, 4H, CH₂), 3.51-3.91

(m, 34H, CH₂), 3.38 (s, 6H, CH₃), 3.36 (s, 3H, CH₃), 1.26 (broad singlet, 6H, CH₃),

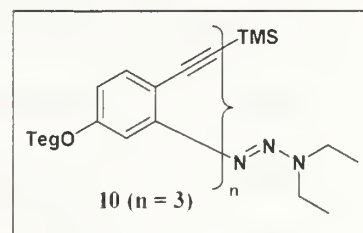
0.23 (s, 9H, Si-CH₃). ¹³C NMR (CDCl₃): δ 159.63, 158.46, 158.40, 153.81, 134.14,

133.36, 133.13, 128.41, 128.03, 118.17, 117.66, 116.60, 116.17, 116.09, 114.93,

112.09, 111.01, 103.74, 102.12, 96.53, 92.62, 90.74, 71.94, 70.91, 70.84, 70.81, 70.68,

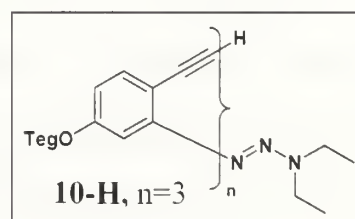
70.60, 70.57, 69.68, 69.53, 67.57, 67.37, 59.07, 59.05, 0.12 ppm. MS: m/z 983.4. (m +

Na⁺)



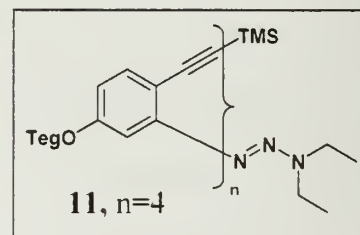
H- Et₃-Triazene (10-H) The general K₂CO₃

procedure for TMS deprotection was followed with



1.18 g of **10** in 1:1 THF and methanol to afford, **10-H** (1.06 g, 97%). $^1\text{H NMR}$ (CDCl_3) δ 7.49 (d, 1H, phenyl H, $J = 8.54$ Hz), 7.47 (d, 1H phenyl H, $J = 8.67$), 7.38 (d, 1H phenyl H, $J = 8.63$), 7.03 (d, 1H, phenyl H, $J = 2.59$ Hz), 6.98 (d, 2H, phenyl H, $J = 2.43$ Hz), 6.85 (dd, 1H, phenyl H, $J_1 = 2.68$, $J_2 = 8.62$), 6.81 (dd, 1H, phenyl H, $J_1 = 2.65$, $J_2 = 8.62$), 6.66 (dd, 1H, phenyl H, $J_1 = 2.53$, $J_2 = 8.56$), 4.12-4.17 (m, 4H, CH_2), 3.96 (t, 2H, $J_1 = 4.26$, $J_2 = 4.92$), 3.86 (t, 4H, $J_1 = 5.04$, $J_2 = 4.62$), 3.63-3.78 (m, 22H, CH_2), 3.52-3.57 (m, 8H, CH_2), 3.38 (s, 6H, CH_3), 3.37 (s, 3H, CH_3), 3.13 (s, 1H, CH), 1.26 (broad singlet, 6H, CH_3).

TMS-Et₄-Triazene (11) The general procedure for Sonogashira coupling was performed using 235 mg of **10-H** (509 μmol , 1.1.0 mol eq.), and 411 mg **8-I** (463 μmol , 1.0 mol eq.), 8.4 mg $\text{Pd}(\text{P}\phi_3)\text{Cl}_2$ (12 μmol , 0.025



mol eq.) and 4.4 mg CuI (23 μmol , 0.05 mol eq.) in 3:5 TEA:THF mixture overnight.

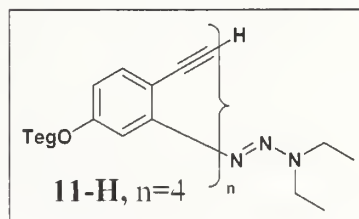
After purification by flash chromatography (Silica, 12g ISCO column, 0-30%

Acetone:DCM gradient) a brown oil was produced (333 mg, 58%). $^1\text{H NMR}$ (CDCl_3):

δ 7.48 (d, 1H, phenyl H, $J = 8.54$ Hz), 7.48 (d, 1H phenyl H, $J = 8.65$), 7.45 (d, 1H phenyl H, $J = 8.65$), 7.36 (d, 1H phenyl H, $J = 8.65$), 7.02 (d, 1H, phenyl H, $J = 2.66$ Hz), 7.00 (d, 1H, phenyl H, $J = 2.66$ Hz), 6.95 (d, 1H, phenyl H, $J = 2.55$ Hz), 6.84 (dd, 1H, phenyl H, $J_1 = 2.64$, $J_2 = 8.65$), 6.80 (dd, 1H, phenyl H, $J_1 = 2.63$, $J_2 = 8.66$), 6.78 (dd, 1H, phenyl H, $J_1 = 2.46$, $J_2 = 8.56$), 6.62 (dd, 1H, phenyl H, $J_1 = 2.59$, $J_2 = 8.56$), 4.10-4.15 (m, 4H, CH_2), 3.94-4.01 (m, 4H, CH_2), 3.61-3.78 (m, 36H, CH_2), 3.50-3.55 (m, 8H, CH_2), 3.37 (s, 6H, CH_3), 3.36 (s, 3H, CH_3), 3.35 (s, 3H, CH_3), 1.25 (broad

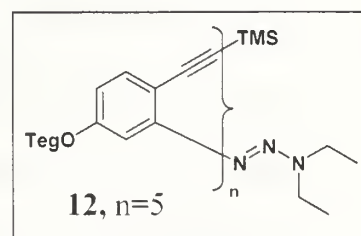
singlet, 6H, CH₃). 0.21 (s, 9H, Si-CH₃). ¹³C NMR (CDCl₃): δ 159.62, 158.48, 158.38, 153.74, 134.17, 133.46, 133.23, 128.33, 127.87, 127.69, 118.13, 117.92, 117.82, 116.60, 116.38, 116.15, 115.87, 114.94, 112.08, 110.94, 103.72, 102.09, 96.61, 92.85, 92.74, 92.37, 90.82, 90.71, 71.93, 70.88, 70.83, 70.66, 70.60, 70.57, 69.67, 69.62, 69.57, 67.50, 67.36, 59.06, 0.11 ppm. MS: *m/z* 1245.5. (m + Na⁺)

H- Et₄-Triazene (11-H) The general K₂CO₃ procedure for TMS deprotection was followed with 106mg of **11** in 1:1 THF and methanol to afford **11-H** (100 mg, 97%). ¹H NMR (CDCl₃) δ 7.49 (d, 1H, phenyl H, J =



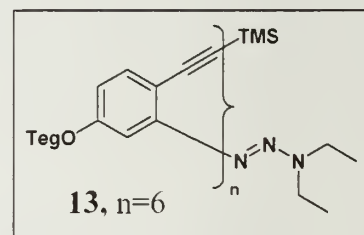
8.54 Hz), 7.47 (d, 1H phenyl H, J = 8.67), 7.38 (d, 1H phenyl H, J = 8.63), 7.03 (d, 1H, phenyl H, J = 2.59 Hz), 6.98 (d, 2H, phenyl H, J = 2.43 Hz), 6.85 (dd, 1H, phenyl H, J₁ = 2.68, J₂ = 8.62), 6.81 (dd, 1H, phenyl H, J₁ = 2.65, J₂ = 8.62), 6.66 (dd, 1H, phenyl H, J₁ = 2.53, J₂ = 8.56), 4.12-4.17 (m, 4H, CH₂), 3.96 (t, 2H, J₁ = 4.26, J₂ = 4.92), 3.86 (t, 4H, J₁ = 5.04, J₂ = 4.62), 3.63-3.78 (m, 22H, CH₂), 3.52-3.57 (m, 8H, CH₂), 3.38 (s, 6H, CH₃), 3.37 (s, 3H, CH₃), 3.13 (s, 1H, CH), 1.26 (broad singlet, 6H, CH₃).

TMS- Et₅- Triazene (12) The general procedure for Sonogashira coupling was performed using 100 mg of **10-H** (1.0 mol eq.), and 89.8 mg **9-I** (1.1 mol eq.), 2.0 mg Pd(PPh₃)Cl₂ (0.025 mol eq.) and 1.1 mg CuI (0.05 mol eq.) in 3:5 TEA:THF mixture overnight. After purification by flash chromatography (Silica, 12g ISCO column, 0-20% Acetone:DCM gradient) a brown oil was produced (100 mg, 58%). ¹H NMR (CDCl₃): δ 7.48 (d, 1H, phenyl H, J = 8.54 Hz), 7.48 (d, 1H



phenyl H, $J = 8.65$). 7.45 (d, 1H phenyl H, $J = 8.65$). 7.36 (d, 1H phenyl H, $J = 8.65$). 7.02 (d, 1H, phenyl H, $J = 2.66$ Hz), 7.00 (d, 1H, phenyl H, $J = 2.66$ Hz), 6.95 (d, 1H, phenyl H, $J = 2.55$ Hz), 6.84 (dd, 1H, phenyl H, $J_1 = 2.64$ $J_2 = 8.65$), 6.80 (dd, 1H, phenyl H, $J_1 = 2.63$ $J_2 = 8.66$), 6.78 (dd, 1H, phenyl H, $J_1 = 2.46$, $J_2 = 8.56$), 6.62 (dd, 1H, phenyl H, $J_1 = 2.59$ $J_2 = 8.56$), 4.10-4.15 (m, 4H, CH₂), 3.94-4.01 (m, 4H, CH₂), 3.61-3.78 (m, 36H, CH₂), 3.50-3.55 (m, 8H, CH₂), 3.37 (s, 6H, CH₃), 3.36 (s, 3H, CH₃), 3.35 (s, 3H, CH₃), 1.25 (broad singlet, 6H, CH₃), 0.21 (s, 9H, Si-CH₃). ¹³C NMR (CDCl₃): δ 159.62, 158.48, 158.38, 153.74, 134.17, 133.46, 133.23, 128.33, 127.87, 127.69, 118.13, 117.92, 117.82, 116.60, 116.38, 116.15, 115.87, 114.94, 112.08, 110.94, 103.72, 102.09, 96.61, 92.85, 92.74, 92.37, 90.82, 90.71, 71.93, 70.88, 70.83, 70.66, 70.60, 70.57, 69.67, 69.62, 69.57, 67.50, 67.36, 59.06, 0.11 ppm. MS: m/z 1508 ($m + \text{Na}^+$)

TMS- Et₆- Triazene (13) The general procedure for Sonogashira coupling was performed using 100 mg of **11-H** (1.0 mol eq.), and 69.3 mg **9-I** (1.1 mol eq.), 1.6 mg Pd(PPh₃)Cl₂ (0.025 mol eq.) and 0.8 mg CuI (0.05 mol

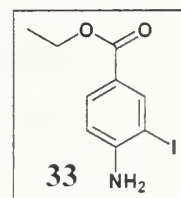


eq.) in 3:5 TEA:THF mixture overnight. After purification by flash chromatography (Silica, 12g ISCO column, 0-30% Acetone:DCM gradient) a brown oil was produced (123 mg, 58%). ¹H NMR (CDCl₃): δ 7.48 (d, 1H, phenyl H, $J = 8.54$ Hz), 7.48 (d, 1H phenyl H, $J = 8.65$), 7.45 (d, 1H phenyl H, $J = 8.65$), 7.36 (d, 1H phenyl H, $J = 8.65$), 7.02 (d, 1H, phenyl H, $J = 2.66$ Hz), 7.00 (d, 1H, phenyl H, $J = 2.66$ Hz), 6.95 (d, 1H, phenyl H, $J = 2.55$ Hz), 6.84 (dd, 1H, phenyl H, $J_1 = 2.6$ $J_2 = 8.7$), 6.80 (dd, 1H, phenyl

H, $J_1 = 2.63$ $J_2 = 8.66$). 6.78 (dd, 1H, phenyl H, $J_1 = 2.4$, $J_2 = 8.6$), 6.62 (dd, 1H, phenyl H, $J_1 = 2.59$ $J_2 = 8.56$), 4.10-4.15 (m, 4H, CH₂), 3.94-4.01 (m, 4H, CH₂), 3.61-3.78 (m, 36H, CH₂), 3.50-3.55 (m, 8H, CH₂), 3.37 (s, 6H, CH₃), 3.36 (s, 3H, CH₃), 3.35 (s, 3H, CH₃), 1.25 (broad singlet, 6H, CH₃), 0.21 (s, 9H, Si-CH₃). ¹³C NMR (CDCl₃): δ 159.62, 158.48, 158.38, 153.74, 134.17, 133.46, 133.23, 128.33, 127.87, 127.69, 118.13, 117.92, 117.82, 116.60, 116.38, 116.15, 115.87, 114.94, 112.08, 110.94, 103.72, 102.09, 96.61, 92.85, 92.74, 92.37, 90.82, 90.71, 71.93, 70.88, 70.83, 70.66, 70.60, 70.57, 69.67, 69.62, 69.57, 67.50, 67.36, 59.06, 0.11 ppm. MS: m/z 1770 ($m + \text{Na}^+$)

7.6 Synthesis of Teg-Ester Compounds

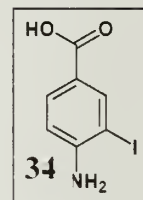
4-Amino-3-iodo-benzoic acid ethyl ester (33) 13.8 g of I₂ (54.5 μmol , 1.0 mol eq.), and 17.0 g of Ag₂SO₄ (54.5 μmol , 1.0 mol eq.) were added to 300 mL of 95% EtOH with rapid stirring. 9.00 g of 4-amino



benzoic acid ethyl ester (54.5 μmol , 1.0 mol eq.) was dissolved in another 100 mL EtOH and added to the reaction, which was stirred at room temperature for 30 minutes. Mixture was filtered through frit to remove salts and the EtOH was removed by rotary evaporation. Residue was partitioned between 300 mL DCM and 150 mL 5% aqueous NaOH. The organic layer was washed again with another 150 mL 5% aqueous NaOH, followed by washes with 2 150 mL portions of 5% aqueous Na₂SO₃, dried over MgSO₄, and evaporated. After purification by flash chromatography (85->100% DCM: Hexanes) a tan solid was obtained (13.6 g, 86%). ¹H NMR (DMSO-d₆): δ 8.102 (d, 1H, phenyl H, $J = 2.0$), 7.652 (dd, 1H, phenyl H, $J_1 = 2.0$, $J_2 = 8.4$), 6.743 (d, 1H, phenyl H,

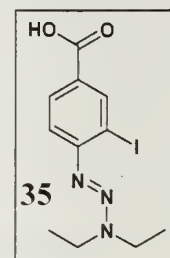
$J = 8.4$), 6.065 (s, 2H, NH_2), 4.207 (q, 2H, $J = 7.2$, CH_2), 1.267 (t, 3H, $J = 7.2$, CH_3) ppm. ^{13}C NMR (DMSO-d_6): δ 164.53, 152.94, 140.25, 130.50, 118.45, 112.92, 81.07, 60.00, 14.29 ppm. MS $m/z = 291$ ($m + \text{H}^+$).

4-Amino-3-iodo-benzoic acid (34) A solution of 13.0 g KOH (232 mmol, 5.0 eq) in 700 mL 3:1 MeOH/ H_2O was made, and 13.6 g of **33** (46.7 mmol, 1.0 eq) was added. The mixture was stirred at 50°C



overnight. Methanol was removed by rotary evaporation, and the mixture was brought to pH 3.0 by careful addition of concentrated H_2SO_4 . The product was obtained as a white precipitate and was isolated by filtration (11.42 g, 93%). ^1H NMR (DMSO-d_6): δ 8.091 (d, 1H, phenyl H, $J = 2.0$), 7.631 (dd, 1H, phenyl H, $J_1 = 2.0$, $J_2 = 8.4$), 6.731 (d, 1H, phenyl H, $J = 8.4$), 5.97 (br, 2H, NH_2) ^{13}C NMR (DMSO-d_6): δ 166.14, 152.63, 140.54, 130.71, 119.40, 112.89, 81.10 ppm. MS $m/z = 263$ ($m + \text{H}^+$).

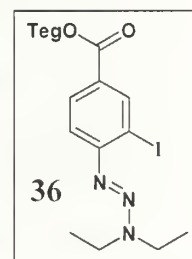
***N,N*-Diethyl-*N'*-(2-iodo-4-benzoic acid) triazene (35)** A solution of 5.81 g of **34** (22.1 mmol, 1.0 eq) in 380 mL of acetonitrile, 80 mL of water, and 11 mL concentrated HCl in a 1000 mL round bottom flask with stirbar was covered with aluminum foil to protect contents from



light, and cooled in a -5°C ice/acetone bath. A solution of 3.35 g NaNO_2 (48.6 mmol, 2.2 eq) in 50 mL of ice/water was slowly added through an addition funnel. After the addition was complete the mixture was cannulated into a 2000 mL round bottom flask with stirbar containing a solution of 4.85 g diethylamine (6.93 mL, 66.3 mmol, 3.0 eq) and 9.16 g K_2CO_3 (66.3 mmol, 3.0 eq) in 80 mL water in a -5°C ice/acetone bath.

Reaction was stirred for 90 minutes, and then allowed to warm up to room temperature. Concentrated HCl was added to bring pH to 4.5, and mixture was then extracted with 3 300mL portions of ethyl ether. The extract was dried over MgSO₄ and evaporated to obtain crude product as an orange/red solid. After purification by flash chromatography (0->15% EtOAc/DCM) a light yellow solid was obtained (5.83g, 76%). δ 8.591 (d, 1H, phenyl H, J = 2), 8.003 (dd, 1H, phenyl H, J₁ = 2 J₂ = 8.4), 7.423 (d, 1H, phenyl H, J = 8.4), 3.829-3.882 (m, 4H, CH₂), 1.313-1.397 (m, 6H, CH₂) ppm. ¹³C NMR(CDCl₃): δ 171.05, 154.74, 141.58, 130.87, 126.66, 116.82, 95.92, 49.87, 42.93, 14.59, 11.02. MS *m/z* = 347 (*m* + H⁺).

***N,N*-Diethyl-*N'* {2-Iodo-benzoic acid 2-[2-(2-methoxy-ethoxy)-ethoxy]-ethyl ester} triazene (36)** 7.03 g of **35** (20.3 mmol, 1.05 eq) was dissolved in 200 mL of dry DCM to which 3.79 g of



dimethylaminopyridine (30.9 mmol, 1.6 eq) was added. Mixture was cooled to 0°C, and 5.92 g of 1-ethyl-3-(3-dimethylaminopropyl)-carbodiimide (EDC) (30.9 mmol, 1.6 eq) in 100 mL dry DCM was added. After 20 minutes, 3.17 g triethylene glycol monomethyl ether (19.3 mmol, 1.0 eq) was added in 50 mL DCM.

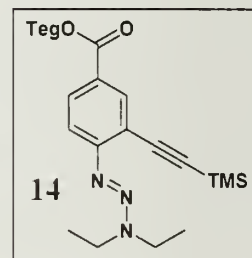
The reaction was stirred overnight, during which time the ice was allowed to melt. The mixture was evaporated and the residue partitioned between 60 mL water and 2 800 mL portions of EtOAc. The organic layer was washed with brine, dried over MgSO₄, and evaporated to give crude product. Purification by flash chromatography in 30->50% EtOAc/Hexanes gave a light yellow oil (8.70 g, 91%). ¹H NMR(CDCl₃): δ 8.490 (d, 1H, phenyl H, J = 1.6), 7.921 (dd, 1H, phenyl H, J₁ = 1.6 J₂ = 8.4), 7.361 (d, 1H, phenyl

H, $J = 8.4$), 4.430 (m, 2H, CO_2CH_2), 3.80 (m, 6H, CH_2), 3.65 (m, 6H, CH_2), 3.52 (m, 2H, CH_2), 3.341 (s, 3H, OCH_3), 1.309 (m, 6H, CH_3) ppm. ^{13}C NMR(CDCl_3): δ 165.33, 153.92, 140.71, 130.24, 127.47, 116.61, 95.79, 71.95, 70.72, 70.64, 70.62, 69.23, 64.15, 59.07, 49.66, 42.70 ppm. MS $m/z = 493$ ($m + \text{H}^+$).

***N,N*-Diethyl-*N'* {2- trimethylsilanylethynyl benzoic acid 2-[2-**

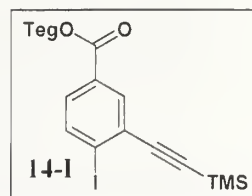
(2-methoxy-ethoxy)-ethoxy]-ethyl ester} triazene (14**)** The

general Sonogashira coupling procedure described above was used to prepare this compound. 8.70 g of **36** (17.6 mmol, 1.0 eq), 440



mg of $\text{Pd}(\text{P}\phi_3)_2\text{Cl}_2$ (0.63 mmol, 0.04 eq), and 34 mg CuI (0.176 mmol, 0.01 eq) were combined in a 330 mL schlenk flask with 180 mL TEA. TMS acetylene (3.73 mL/2.60 g, 26.5 mmol, 1.5 eq) was added to the solution. Reaction was stirred overnight at room temperature. After completion, the reaction solution was filtered through Celite with ether to wash, evaporated, and purified with flash chromatography in 20% \rightarrow 40% EtOAc/hexanes to give a light yellow oil (8.11 g, 99%). ^1H NMR (CDCl_3): δ 8.162 (d, 1H, phenyl H, $J = 2.0$), 7.902 (dd, 1H, phenyl H, $J_1 = 2.0$ $J_2 = 8.8$), 7.441 (d, 1H, phenyl H, $J = 8.8$), 4.459 (m, 2H, CO_2CH_2), 3.84 (m, 6H, CH_2), 3.69 (m, 6H, CH_2), 3.53 (m, 2H, CH_2), 3.365 (s, 3H, OCH_3), 1.31 (m, 6H, CH_3), 0.248 (s, 9H, $\text{Si}(\text{CH}_3)_3$) ppm. ^{13}C NMR(CDCl_3): δ 166.15, 156.24, 135.31, 130.58, 125.94, 118.03, 116.53, 102.64, 98.83, 72.07, 70.83, 70.79, 70.75, 69.41, 64.15, 59.19, 49.69, 42.40, 14.62, 11.09, 0.16 ppm MS $m/z = 464$ ($m + \text{H}^+$).

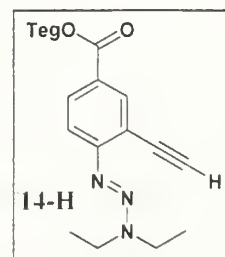
4-Iodo-3-trimethylsilanylethynyl-benzoic acid 2-[2-(2-methoxy-ethoxy)-ethoxy]-ethyl ester (14-I) This compound was prepared by microwave synthesis in 8 Biotage 2-5 mL vials.



Each vial was filled with 250 mg of **36** (0.54 mmol, 1.0 eq), 6.8 mg of I₂ (27 μmol, 0.05 eq), and 10 g of MeI (4.4 mL, 71 mmol, ≈130 eq), a stirbar was added, and a septum crimped on. Microwave heat was applied to each tube, at a temperature of 150°C for a time of one hour. After all reactions had completed, the tubes were opened, combined, filtered through a Celite pad and washed with ethyl ether, and evaporated under a N₂ stream. The residue was dissolved in 100 mL EtOAc, washed with 20 mL of 5% aqueous Na₂SO₃, dried over MgSO₄, and evaporated to yield crude product as a brown oil. Purification by flash chromatography in 20->40% EtOAc/Hexanes gave a yellow oil (2.12 g, 86%). ¹H NMR(CDCl₃): δ 8.093 (d, 1H, phenyl H, J = 2.0), 7.926 (d, 1H, phenyl H, J = 8.4), 7.622 (dd, 1H, phenyl J₁ = 2.0 J₂ = 8.4), 4.471 (m, 2H, CO₂CH₂), 3.83 (m, 2H, CH₂), 3.67 (m, 6H, CH₂), 3.52 (m, 2H, CH₂), 3.367 (s, 3H, OCH₃), 0.260 (s, 9H, Si(CH₃)₃) ppm. ¹³C NMR(CDCl₃): δ 165.63, 139.12, 133.57, 130.32, 130.15, 130.12, 107.58, 105.69, 100.20, 72.06, 70.81, 70.78, 70.76, 69.23, 64.60, 59.21, -0.13 ppm MS *m/z* = 490 (*m* + H⁺).

***N,N*-Diethyl-*N'*{2-ethynyl benzoic acid 2-[2-(2-methoxy-ethoxy)-ethoxy]-ethyl ester} triazene (14-H)**

The general TMS deprotection procedure 2, listed above, was used to prepare this compound. 640 mg of **14** (1.40 mmol, 1.0 eq) was dissolved in 5.4 mL THF, and the solution was cooled to 0°C. 1.67 mL of 1M



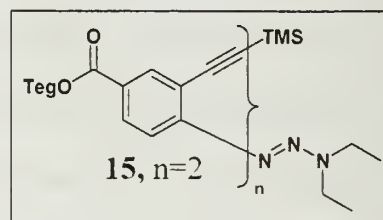
TBAF/THF with 5% water content was added to the mixture. After 5 minutes stirring, 5.4 mL hexane was added and the reaction stirred another 10 minutes. Purification was performed by filtration of the reaction mixture through silica gel-packed pipettes. elution of absorbed produce with 1:1 EtOAc/Hexanes, and evaporation to give a light yellow oil (445 mg, 81%).

TMS-Es₂-Triazene (15) 1.05 g of **14** (2.26 mmol,

1.0 eq) was converted to **14-H** with the procedure

described above. The product was not fully

characterized, but was taken directly through



Sonogashira coupling using the general procedure described above. The **14-H**, 1.53 g of **14-I** (3.69 mmol, 1.6 eq), 78 mg of Pd(PPh₃)₂Cl₂ (111 μmol, 0.05 eq), and 7 mg CuI (37 μmol, 0.016 eq) were added to a schlenk flask with 60 mL of TEA and 60 mL of THF. The reaction was heated at 55°C overnight, worked up as described in the general procedure, and purified by flash chromatography in 0->10% acetone/CHCl₃ to obtain a yellow oil (1.38 g, 81%). ¹H NMR(CDCl₃): δ 8.249 (d, 1H, phenyl H, J = 1.6), 8.171 (d, 1H, phenyl H, J = 1.6), 7.967 (dd, 1H, phenyl H, J₁ = 1.6 J₂ = 8.8), 7.934 (dd, 1H, phenyl H, J₁ = 1.6 J₂ = 8.0), 7.516 (d, 1H, phenyl H, J = 8.0), 7.508 (d, 1H, phenyl H, J = 8.8), 4.48 (m, 4H, CO₂CH₂), 3.83 (m, 8H, CH₂), 3.67 (m, 12H, CH₂), 3.51 (m, 4H, CH₂), 3.369 (s, 3H, OCH₃), 3.351 (s, 3H, OCH₃), 1.30 (m, 6H, CH₃), 0.263 (s, 9H, Si(CH₃)₃) ppm. ¹³C NMR(CDCl₃): δ 165.98, 165.61, 155.99, 134.99, 133.53, 131.68, 131.13, 131.04, 129.17, 129.11, 126.16, 125.82, 117.73, 116.69, 102.65, 99.99, 94.76,

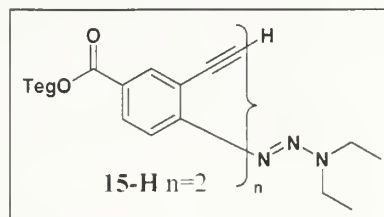
92.00, 76.86, 72.06, 70.84, 70.81, 70.79, 70.76, 69.34, 69.30, 64.51, 64.05, 59.19,

59.17, 49.80, 42.56, 14.63, 11.04, 0.05 ppm MS $m/z = 754$ ($m + H^+$).

H-Es₂-Triazene (15-H) The general TMS deprotection

procedure 2, listed above, was used to prepare this

compound. 422 mg of **15** (560 μ mol, 1.0 eq) was



dissolved in 4.0 mL THF, cooled to 0°C, and reacted with 0.671 mL (1.6 eq) of 1M

TBAF/THF + 5% H₂O. After 5 minutes, 4.0 mL of hexane was added to the reaction.

After another 10 minutes of stirring, reaction mixture was injected onto a silica-packed

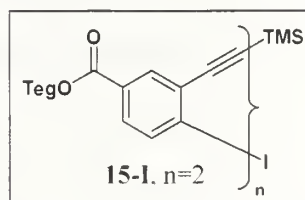
pipette and eluted with 150 mL 2:1 EtOAc/Hexanes. Evaporation gave a yellow-orange

oil (317 mg, 83%).

TMS-Es₂-Iodide (15-I) This compound was prepared by the

general triazene activation procedure described above, with a

longer reaction time and the addition of catalytic I₂. 274 mg



of **15** (363 μ mol, 1.0 eq), 2.4 mL MeI (5.5g, 0.15M in **15**) and 2.1 mg I₂ (18 μ mol, 0.05

eq) were reacted in a schlenk flask under N₂ at 110°C for 2 weeks. Reaction was

filtered through a Celite pad, washed with ethyl ether, and evaporated under a N₂

stream. The residue was dissolved in 15 mL EtOAc, washed with 3 mL of 5% aqueous

Na₂SO₃, dried over MgSO₄, and evaporated to yield crude product as a brown oil.

Purification by flash chromatography in a 40%->80% EtOAc/Hexanes gradient gave a

dark yellow oil (212 mg, 75%). ¹H NMR (CDCl₃): δ 8.20 (m, 2H, phenyl H), 7.97 (m,

2H, phenyl H), 7.69 (m, 2H, phenyl H), 4.49 (m, 4H, CO₂CH₂), 3.84 (m, 4H, CH₂), 3.68

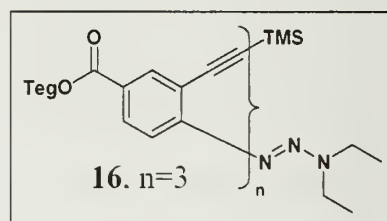
(m, 12H, CH₂), 3.54 (m, 4H, CH₂), 3.377 (s, 3H, OCH₃), 3.357 (s, 3H, OCH₃), 0.283 (s, 9H, Si(CH₃)₃) ppm. ¹³C NMR (CDCl₃): δ 165.46, 139.30, 133.77, 133.74, 132.30, 130.59, 130.38, 130.05, 129.60, 129.21, 125.95, 107.16, 102.37, 100.47, 97.00, 91.88, 72.07, 72.06, 70.82, 70.80, 70.77, 69.27, 69.18, 64.63, 64.57, 59.21, 59.19, 0.10 ppm
MS *m z* = 781 (*m* + H⁺).

TMS-Es₃-Triazene (16) This compound was prepared by the general Sonogashira

procedure described above. 317 mg of **14-I** (465 μmol,

1.2 eq), 190 mg of **15-H** (387 μmol, 1.0 eq), 8.1 mg of

Pd(Pφ₃)₂Cl₂ (12 μmol, 0.03 eq), and 0.8 mg CuI (4



μmol, 0.01 eq) were added to a schlenk flask in 15 mL TEA and 30 mL THF. The

reaction was heated at 55°C overnight, worked up as described in the general procedure,

and purified by flash chromatography in 0->20% acetone/CHCl₃ to obtain an orange oil

(350 mg, 87%). ¹H NMR (CDCl₃): δ 8.284 (d, 1H, phenyl H, J = 2.0), 8.265 (d, 1H,

phenyl H, J = 2.0), 8.169 (d, 1H, phenyl H, J = 2.0), 8.01 (dd, 1H, phenyl H, J₁ = 2.0 J₂

= 8.4), 7.98 (dd, 1H, phenyl H, J₁ = 2.0 J₂ = 8.4), 7.90 (dd, 1H, phenyl H, J₁ = 2.0 J₂ =

8.4), 7.607 (d, 1H, phenyl H, J = 8.4), 7.575 (d, 1H, phenyl H, J = 8.4), 7.511 (d, 1H,

phenyl H, J = 8.4), 4.49 (m, 6H, CO₂CH₂), 3.6-3.9 (m, 30H, CH₂), 3.53 (m, 4H, CH₂),

3.360 (s, 1H, OCH₃), 3.341 (s, 1H, OCH₃), 1.2-1.3 (m, 6H, CH₃), 0.285 (s, 9H,

Si(CH₃)₃) ppm. ¹³C NMR(CDCl₃): δ values 165.82, 165.37, 165.31, 155.98, 135.03,

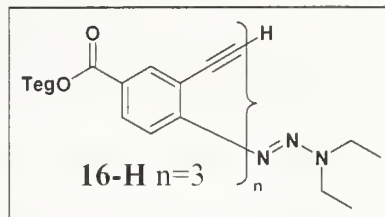
133.29, 132.37, 131.79, 131.00, 130.93, 130.07, 129.57, 129.49, 129.33, 129.16,

126.08, 125.80, 125.36, 117.40, 116.80, 102.29, 100.16, 95.21, 94.35, 92.24, 91.80.

71.94, 70.68, 70.64, 70.60, 69.22, 69.14, 69.12, 64.42, 64.33, 64.04, 59.06, 59.03.

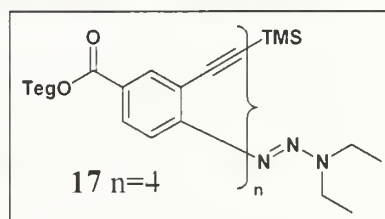
49.54, 14.42, 10.91, 0.11 ppm MS $m/z = 1044$ ($m + H^+$).

H-Es₃-Triazene (16-H) This compound was prepared by the general TMS deprotection procedure 2 described above. 350 mg of **16** (335 μ mol, 1.0 eq) was dissolved in 14 mL THF, cooled to 0°C, and



reacted with 0.402 mL (1.2 eq) of 1M TBAF/THF + 5% H₂O. After 5 minutes, 14 mL hexane was added and the reaction was stirred for another 10 minutes. The reaction mixture was filtered through silica gel-packed pipettes and eluted with 2:1 EtOAc/Hexanes. Evaporation gave a yellow oil (305 mg, 94%).

TMS-Es₄-Triazene (17) This compound was prepared by the general Sonogashira procedure described above. 256 mg of **16-H** (263 μ mol, 1.0 eq).



194 mg of **14-I** (395 μ mol, 1.5 eq), 5.5 mg of Pd(PPh₃)₂Cl₂ (8 μ mol, 0.03 eq), and 0.5 mg of CuI (3 μ mol, 0.01 eq) were added to a schlenk flask in 15 mL TEA and 30 mL THF. The reaction was heated at 55°C overnight, worked up as described in the general procedure, and purified by flash chromatography in 0->40% acetone/CHCl₃ to obtain a light yellow oil (284 mg, 77%).

¹H NMR(CDCl₃): δ 8.299 (d, 1H, phenyl H, J = 2.0), 8.253 (d, 1H, phenyl H, J = 2.0), 8.196 (d, 1H, phenyl H, J = 2.0), 8.110 (d, 1H, phenyl H, J = 2.0), 8.011 (dd, 1H, phenyl H, J₁ = 2.0 J₂ = 8.4), 7.983 (dd, 1H, phenyl H, J₁ = 2.0 J₂ = 8.4), 7.926 (dd, 1H, phenyl H, J₁ = 2.0 J₂ = 8.4), 7.866 (dd, 1H, phenyl H, J₁ = 2.0 J₂ = 8.4), 7.668 (d, 1H, phenyl H,

J = 8.4), 7.615 (d, 1H, phenyl H, J = 8.4), 7.593 (d, 1H, phenyl H, J = 8.4), 7.451 (d, 1H, phenyl H, J = 8.4), 4.43-4.56 (m, 8H, CO₂CH₂), 3.6-3.9 (m, 36H, CH₂), 3.48-3.58 (m, 8H, CH₂), 3.32-3.38 (m, 12H, OCH₃), 1.18-1.27 (m, 6H, CH₃), 0.280 (s, 9H, Si(CH₃)₃) ppm. ¹³C NMR(CDCl₃): δ 165.73, 165.30, 165.25, 165.20, 155.82, 135.02, 133.61, 133.25, 132.51, 132.17, 131.95, 130.94, 130.81, 129.90, 129.81, 129.74, 129.55, 129.36, 129.10, 125.93, 125.82, 125.53, 125.17, 117.32, 116.68, 102.29, 100.00, 95.37, 94.87, 93.75, 92.51, 92.14, 91.70, 71.92, 70.68, 70.64, 70.60, 69.22, 69.15, 69.11, 69.08, 64.38, 64.01, 59.05, 59.03, 49.50, 42.27, 14.42, 10.93, -0.11 ppm. MS *m/z* = 1335 (*m* + H⁺).

TMS-Es₅-Triazene (18) This compound was prepared

by the general Sonogashira procedure described above.

234 mg of **16-H** (241 μmol, 1.0 eq), 207 mg of **15-I**

(265 μmol, 1.1 eq), 8.5 mg of Pd(PPh₃)₂Cl₂ (12 μmol,

0.05 eq), and 0.5 mg of CuI (2.4 μmol, 0.01 eq) were added to a schlenk flask in 50 mL

TEA and 100 mL THF. The reaction was heated at 55°C overnight, worked up as

described in the general procedure, and purified by flash chromatography in 0->30%

acetone/CHCl₃ to obtain an orange oil (269 mg, 69%). ¹H NMR (CD₃CN): δ 8.203 (d,

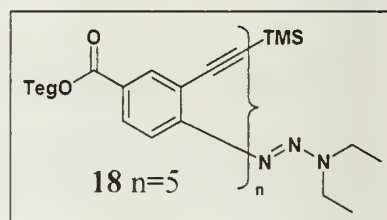
1H, phenyl H, J = 2.0), 8.019 (dd, 1H, phenyl H, J₁ = 2.0 J₂ = 8.4), 7.948 (d, 1H, phenyl

H, J = 2.0), 7.843 (dd, 1H, phenyl H, J₁ = 2.0 J₂ = 8.4), 7.835 (d, 1H, phenyl H, J = 2.0),

7.832 (d, 1H, phenyl H, J = 2.0), 7.779 (d, 1H, phenyl H, J = 8.4), 7.771 (d, 1H, phenyl

H, J = 2.0), 7.766 (dd, 1H, phenyl H, J₁ = 2.0 J₂ = 8.4), 7.753 (dd, 1H, phenyl H, J₁ =

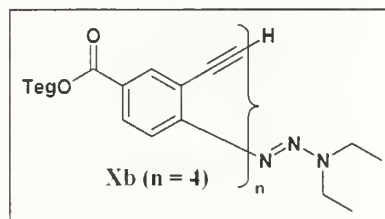
2.0 J₂ = 8.4), 7.645 (dd, 1H, phenyl H, J₁ = 2.0 J₂ = 8.4), 7.510 (d, 1H, phenyl H, J =



8.4).7.426 (d, 1H, phenyl H, J = 8.4).7.318 (d, 1H, phenyl H, J = 8.4).7.304 (d, 1H, phenyl H, J = 8.4). 4.35-4.48 (m, 10H, CO₂CH₂). 3.35-3.80 (m, 54H, CH₂). 3.20-3.28 (m, 15H, OCH₃). 1.10-1.30 (m, 6H, CH₃). 0.235 (s, 9H, Si(CH₃)₃) ppm. ¹³C NMR(CD₃CN): δ 166.56, 166.26, 166.16, 166.08, 166.05, 157.03, 136.21, 134.41, 134.14, 133.95, 133.82, 133.76, 133.42, 131.89, 131.84, 131.70, 131.19, 131.18, 130.93, 130.92, 130.75, 130.64, 130.53, 130.52, 130.42, 130.16, 127.01, 126.87, 126.70, 126.45, 126.04, 118.46, 117.63, 103.47, 101.25, 96.39, 96.06, 95.29, 95.21, 93.81, 93.17, 93.15, 93.00, 73.00, 72.96, 71.73, 71.72, 71.69, 71.66, 71.48, 71.46, 71.44, 71.40, 71.39, 70.02, 69.99, 69.97, 65.99, 65.91, 65.86, 65.82, 65.29, 59.31, 59.27, 50.78, 47.98, 43.54, 15.06, 11.72, 0.45 ppm.

H-Es₄-Triazene (17-H) This compound was prepared

by the general TMS deprotection procedure 2 described above. 146 mg of **17** (109 μmol, 1.0 eq) was dissolved in 6 mL THF, cooled to 0°C, and

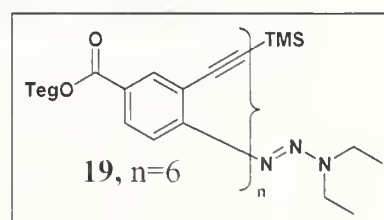


reacted with 0.120 mL (120 μmol, 1.1 eq) of 1M TBAF/THF + 5% H₂O. After 5 minutes, 6 mL hexane was added and the reaction was stirred for another 10 minutes.

The reaction mixture was injected onto a dry 12g ISCO silica cartridge and eluted with a 0->20% acetone/CHCl₃ gradient to obtain a light yellow oil (101 mg, 73%).

TMS-Es₆-Triazene This compound was prepared by the general Sonogashira procedure described above.

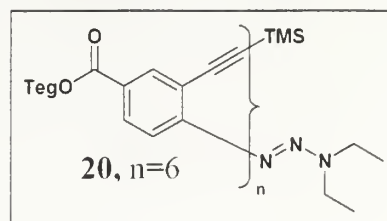
101 mg of **17-H** (75.7 μmol, 1.0 eq), 64.9 mg of **15-I**



(83.2 μmol , 1.1 eq), 1.6 mg of $\text{Pd}(\text{P}\phi_3)_2\text{Cl}_2$ (2.3 μmol , 0.03 eq), and 0.2 mg of CuI (0.7 μmol , 0.01 eq) were added to a schlenk flask in 5.5 mL TEA and 11 mL THF. The reaction was heated at 55°C overnight, worked up as described in the general procedure, and purified by flash chromatography in 0-35% acetone/ CHCl_3 to obtain an orange oil (117 mg, 81%). ^1H NMR (CD_3CN): δ 7.934 (d, 1H, phenyl H, $J = 2.0$), 7.926 (d, 1H, phenyl H, $J = 2.0$), 7.827 (dd, 1H, phenyl H, $J_1 = 2.0$ $J_2 = 8.4$), 7.759 (dd, 1H, phenyl H, $J_1 = 2.0$ $J_2 = 8.4$), 7.752 (d, 1H, phenyl H, $J = 2.0$), 7.717 (d, 1H, phenyl H, $J = 2.0$), 7.713 (dd, 1H, phenyl H, $J_1 = 2.0$ $J_2 = 8.4$), 7.703 (dd, 1H, phenyl H, $J_1 = 2.0$ $J_2 = 8.4$), 7.626 (d, 1H, phenyl H, $J = 8.4$), 7.598 (d, 1H, phenyl H, $J = 2.0$), 7.564 (d, 1H, phenyl H, $J = 2.0$), 7.551 (dd, 1H, phenyl H, $J_1 = 2.0$ $J_2 = 8.4$), 7.540 (dd, 1H, phenyl H, $J_1 = 2.0$ $J_2 = 8.4$), 7.430 (d, 1H, phenyl H, $J = 8.4$), 7.346 (d, 1H, phenyl H, $J = 8.4$), 7.245 (d, 1H, phenyl H, $J = 8.4$), 7.162 (d, 1H, phenyl H, $J = 8.4$), 7.117 (d, 1H, phenyl H, $J = 8.4$), 4.25-4.45 (m, 12H, CO_2CH_2), 3.35-3.80 (m, 64H, CH_2), 3.20-3.30 (m, 18H, OCH_3), 1.15-1.25 (m, 6H, CH_3), 0.283 (s, 9H, $\text{Si}(\text{CH}_3)_3$) ppm. ^{13}C NMR(CDCl_3): δ 166.65, 166.16, 166.09, 166.03, 165.95, 165.91, 156.83, 136.04, 133.98, 133.86, 133.63, 133.61, 133.53, 133.50, 133.45, 133.29, 131.68, 131.65, 130.95, 130.82, 130.79, 130.75, 130.74, 130.66, 130.59, 130.35, 130.32, 130.28, 130.23, 130.18, 130.03, 126.83, 126.62, 126.60, 126.48, 126.25, 126.06, 118.49, 117.40, 103.57, 101.40, 96.15, 95.79, 95.52, 95.42, 95.18, 93.47, 93.35, 93.31, 93.10, 92.98, 72.97, 72.96, 72.91, 71.72, 71.70, 71.69, 71.66, 71.60, 71.47, 71.42, 71.40, 71.38, 71.35, 70.09, 70.08, 70.05, 70.02, 65.93, 65.92, 65.88, 65.77, 65.75, 65.29, 59.39, 59.37, 59.36, 59.35, 59.34, 59.32, 50.81, 47.75, 43.57, 15.05, 11.71, 0.57 ppm.

TMS-Es₉-Triazene This compound was prepared by the general Sonogashira procedure described above.

101 mg of **19-H** (75.7 μ mol, 1.0 eq), 64.9 mg of **16-I** (83.2 μ mol, 1.1 eq), 1.6 mg of Pd(P ϕ ₃)₂Cl₂ (2.3 μ mol,



0.03 eq), and 0.2 mg of CuI (0.7 μ mol, 0.01 eq) were added to a schlenk flask in 5.5 mL TEA and 11 mL THF. The reaction was heated at 55°C overnight, worked up as

described in the general procedure, and purified by flash chromatography in 0->35%

acetone/CHCl₃ to obtain an orange oil (117 mg, 81%). ¹H NMR (CD₃CN): δ 7.934 (d,

1H, phenyl H, J = 2.0), 7.926 (d, 1H, phenyl H, J = 2.0), 7.827 (dd, 1H, phenyl H, J₁ =

2.0 J₂ = 8.4), 7.759 (dd, 1H, phenyl H, J₁ = 2.0 J₂ = 8.4), 7.752 (d, 1H, phenyl H, J =

2.0), 7.717 (d, 1H, phenyl H, J = 2.0), 7.713 (dd, 1H, phenyl H, J₁ = 2.0 J₂ = 8.4), 7.703

(dd, 1H, phenyl H, J₁ = 2.0 J₂ = 8.4), 7.626 (d, 1H, phenyl H, J = 8.4), 7.598 (d, 1H,

phenyl H, J = 2.0), 7.564 (d, 1H, phenyl H, J = 2.0), 7.551 (dd, 1H, phenyl H, J₁ = 2.0 J₂

= 8.4), 7.540 (dd, 1H, phenyl H, J₁ = 2.0 J₂ = 8.4), 7.430 (d, 1H, phenyl H, J = 8.4),

7.346 (d, 1H, phenyl H, J = 8.4), 7.245 (d, 1H, phenyl H, J = 8.4), 7.162 (d, 1H, phenyl

H, J = 8.4), 7.117 (d, 1H, phenyl H, J = 8.4), 4.25-4.45 (m, 12H, CO₂CH₂), 3.35-3.80

(m, 64H, CH₂), 3.20-3.30 (m, 18H, OCH₃), 1.15-1.25 (m, 6H, CH₃), 0.283 (s, 9H,

Si(CH₃)₃) ppm. ¹³C NMR(CDCl₃): δ 166.65, 166.16, 166.09, 166.03, 165.95, 165.91,

156.83, 136.04, 133.98, 133.86, 133.63, 133.61, 133.53, 133.50, 133.45, 133.29,

131.68, 131.65, 130.95, 130.82, 130.79, 130.75, 130.74, 130.66, 130.59, 130.35,

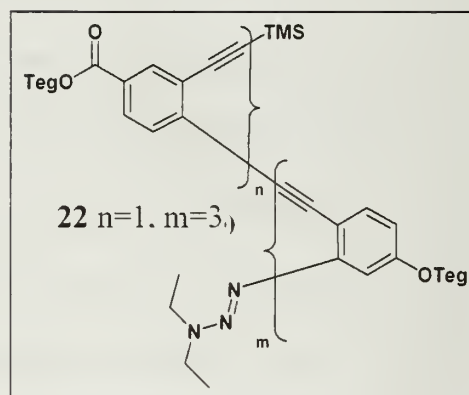
130.32, 130.28, 130.23, 130.18, 130.03, 126.83, 126.62, 126.60, 126.48, 126.25,

126.06, 118.49, 117.40, 103.57, 101.40, 96.15, 95.79, 95.52, 95.42, 95.18, 93.47, 93.35.

93.31, 93.10, 92.98, 72.97, 72.96, 72.91, 71.72, 71.70, 71.69, 71.66, 71.60, 71.47, 71.42, 71.40, 71.38, 71.35, 70.09, 70.08, 70.05, 70.02, 65.93, 65.92, 65.88, 65.77, 65.75, 65.29, 59.39, 59.37, 59.36, 59.35, 59.34, 59.32, 50.81, 47.75, 43.57, 15.05, 11.71, 0.57 ppm.

7.7 Synthesis of Teg-Alkoxy/Ester Compounds

TMS-Es-Et₃-Triazene (22) The general procedure for Sonogashira coupling was performed using 183 mg **14-I** (374 μ mol, 1.1.0 mol eq.), and 302 mg **10-H** (340 μ mol, 1.0 mol eq.), 6 mg Pd(PPh₃)Cl₂ (8.5 μ mol, 0.025 mol eq.) and 3.2 mg CuI (1.7 μ mol, 0.05 mol eq.)



overnight in 1:1 TEA:THF. After purification by flash chromatography (Silica, 12g ISCO column, 0-20% Acetone:DCM gradient) a beige solid was produced (291 mg, 68%). ¹H NMR (CDCl₃): δ 8.12 (d, 1H, phenyl H, $J = 1.66$ Hz), 7.85 (dd, 1H phenyl H, $J_1 = 1.75, J_2 = 8.17$), 7.54 (d, 1H phenyl H, $J = 8.19$), 7.45 (d, 3H phenyl H, $J = 8.50$), 7.03 (d, 1H, phenyl H, $J = 2.61$ Hz), 7.00 (d, 1H, phenyl H, $J = 2.61$ Hz), 6.93 (d, 1H, phenyl H, $J = 2.55$ Hz), 6.85 (dd, 1H, phenyl H, $J_1 = 2.63, J_2 = 8.78$), 6.82 (dd, 1H, phenyl H, $J_1 = 2.63, J_2 = 8.78$), 6.61 (dd, 1H, phenyl H, $J_1 = 2.56, J_2 = 8.55$), 4.46 (t, 2H, CH₂, $J = 4.67, 5.00$ Hz), 4.12 (t, 4H, CH₂, $J = 4.57, 5.09$ Hz), 3.94 (t, 2H, CH₂, $J = 4.14, 4.95$ Hz), 3.81-3.86 (m, 6H, CH₂), 3.61-3.77 (m, 34H, CH₂), 3.50-3.54 (m, 8H, CH₂), 3.36 (s, 6H, CH₃), 3.35 (s, 3H, CH₃), 3.34 (s, 3H, CH₃), 1.23 (broad singlet, 6H, CH₃), 0.23 (s, 9H, Si-CH₃). ¹³C NMR (CDCl₃): δ 165.51, 159.61, 158.85, 158.58, 153.37.

134.06, 133.60, 133.41, 133.35, 131.82, 129.02, 128.86, 128.82, 128.54, 128.43,
 127.98, 125.36, 124.30, 117.93, 117.25, 117.00, 116.76, 116.39, 116.22, 114.99,
 112.08, 110.94, 110.90, 102.69, 102.05, 99.44, 95.83, 93.24, 93.18, 92.79, 92.72, 90.76,
 90.64, 90.28, 71.93, 70.68, 70.67, 70.63, 70.59, 69.67, 69.62, 69.53, 69.16, 67.60,
 67.52, 67.35, 64.38, 64.31, 59.06, 0.01 ppm. MS: m/z 1273.0 ($m + Na^+$)

TMS-Es₂-Et₃-Triazene (23) The general

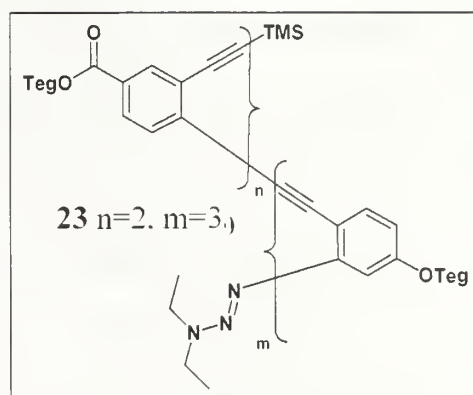
procedure for Sonogashira coupling was

performed using 183 mg **15-I** (374 μ mol, 1.1.0

mol eq.), and 302 mg **10-H** (340 μ mol, 1.0 mol

eq.), 6 mg Pd(PPh₃)Cl₂ (8.5 μ mol, 0.025 mol

eq.) and 3.2 mg CuI (1.7 μ mol, 0.05 mol eq.)



overnight in 1:1 TEA:THF. After purification by flash chromatography (Silica, 12g

ISCO column, 0-20% Acetone:DCM gradient) a beige solid was produced (291 mg,

68%). ¹H NMR (CDCl₃): δ 8.12 (d, 1H, phenyl H, J = 1.66 Hz), 7.85 (dd, 1H phenyl H,

J_1 = 1.75, J_2 = 8.17), 7.54 (d, 1H phenyl H, J = 8.19), 7.45 (d, 3H phenyl H, J = 8.50),

7.03 (d, 1H, phenyl H, J = 2.61 Hz), 7.00 (d, 1H, phenyl H, J = 2.61 Hz), 6.93 (d, 1H,

phenyl H, J = 2.55 Hz), 6.85 (dd, 1H, phenyl H, J_1 = 2.63 J_2 = 8.78), 6.82 (dd, 1H,

phenyl H, J_1 = 2.63 J_2 = 8.78), 6.61 (dd, 1H, phenyl H, J_1 = 2.56, J_2 = 8.55), 4.46 (t, 2H,

CH₂, J = 4.67, 5.00 Hz), 4.12 (t, 4H, CH₂, J = 4.57, 5.09 Hz), 3.94 (t, 2H, CH₂, J = 4.14,

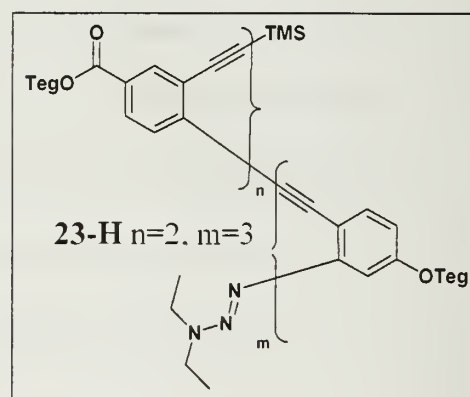
4.95 Hz), 3.81-3.86 (m, 6H, CH₂), 3.61-3.77 (m, 34H, CH₂), 3.50-3.54 (m, 8H, CH₂),

3.36 (s, 6H, CH₃), 3.35 (s, 3H, CH₃), 3.34 (s, 3H, CH₃), 1.23 (broad singlet, 6H, CH₃),

0.23 (s, 9H, Si-CH₃). ¹³C NMR (CDCl₃): δ 165.51, 159.61, 158.85, 158.58, 153.37,

134.06, 133.60, 133.41, 133.35, 131.82, 129.02, 128.86, 128.82, 128.54, 128.43,
 127.98, 125.36, 124.30, 117.93, 117.25, 117.00, 116.76, 116.39, 116.22, 114.99,
 112.08, 110.94, 110.90, 102.69, 102.05, 99.44, 95.83, 93.24, 93.18, 92.79, 92.72, 90.76,
 90.64, 90.28, 71.93, 70.68, 70.67, 70.63, 70.59, 69.67, 69.62, 69.53, 69.16, 67.60,
 67.52, 67.35, 64.38, 64.31, 59.06, 0.01 ppm. MS: m/z 1273.0 ($m + Na^+$)

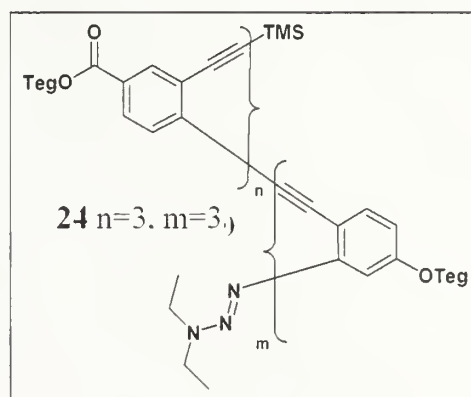
H-Es₂-Et₃-Triazene (23-H) The general procedure for Sonogashira coupling was performed using 183 mg **14-I** (374 μ mol, 1.1.0 mol eq.), and 302 mg **10-H** (340 μ mol, 1.0 mol eq.), 6 mg Pd(P ϕ ₃)Cl₂ (8.5 μ mol, 0.025 mol eq.) and 3.2 mg CuI (1.7 μ mol, 0.05 mol eq.)



overnight in 1:1 TEA:THF. After purification by flash chromatography (Silica, 12g ISCO column, 0-20% Acetone:DCM gradient) a beige solid was produced (291 mg, 68%). ¹H NMR (CDCl₃): δ 8.12 (d, 1H, phenyl H, $J = 1.66$ Hz), 7.85 (dd, 1H phenyl H, $J_1 = 1.75, J_2 = 8.17$), 7.54 (d, 1H phenyl H, $J = 8.19$), 7.45 (d, 3H phenyl H, $J = 8.50$), 7.03 (d, 1H, phenyl H, $J = 2.61$ Hz), 7.00 (d, 1H, phenyl H, $J = 2.61$ Hz), 6.93 (d, 1H, phenyl H, $J = 2.55$ Hz), 6.85 (dd, 1H, phenyl H, $J_1 = 2.63, J_2 = 8.78$), 6.82 (dd, 1H, phenyl H, $J_1 = 2.63, J_2 = 8.78$), 6.61 (dd, 1H, phenyl H, $J_1 = 2.56, J_2 = 8.55$), 4.46 (t, 2H, CH₂, $J = 4.67, 5.00$ Hz), 4.12 (t, 4H, CH₂, $J = 4.57, 5.09$ Hz), 3.94 (t, 2H, CH₂, $J = 4.14, 4.95$ Hz), 3.81-3.86 (m, 6H, CH₂), 3.61-3.77 (m, 34H, CH₂), 3.50-3.54 (m, 8H, CH₂), 3.36 (s, 6H, CH₃), 3.35 (s, 3H, CH₃), 3.34 (s, 3H, CH₃), 1.23 (broad singlet, 6H, CH₃), 0.23 (s, 9H, Si-CH₃). ¹³C NMR (CDCl₃): δ 165.51, 159.61, 158.85, 158.58, 153.37,

134.06, 133.60, 133.41, 133.35, 131.82, 129.02, 128.86, 128.82, 128.54, 128.43,
 127.98, 125.36, 124.30, 117.93, 117.25, 117.00, 116.76, 116.39, 116.22, 114.99,
 112.08, 110.94, 110.90, 102.69, 102.05, 99.44, 95.83, 93.24, 93.18, 92.79, 92.72, 90.76,
 90.64, 90.28, 71.93, 70.68, 70.67, 70.63, 70.59, 69.67, 69.62, 69.53, 69.16, 67.60,
 67.52, 67.35, 64.38, 64.31, 59.06, 0.01 ppm. MS: m/z 1273.0 ($m + Na^+$)

TMS-Es₃-Et₃-Triazene (24) The general procedure for Sonogashira coupling was performed using 183 mg **14-I** (374 μ mol, 1.1.0 mol eq.), and 302 mg **23-H** (340 μ mol, 1.0 mol eq.), 6 mg Pd(PPh₃)Cl₂ (8.5 μ mol, 0.025 mol eq.) and 3.2 mg CuI (1.7 μ mol, 0.05 mol eq.)



overnight in 1:1 TEA:THF. After purification by flash chromatography (Silica, 12g ISCO column, 0-20% Acetone:DCM gradient) a beige solid was produced (291 mg, 68%). ¹H NMR (CDCl₃): δ 8.12 (d, 1H, phenyl H, $J = 1.66$ Hz), 7.85 (dd, 1H phenyl H, $J_1 = 1.75$, $J_2 = 8.17$), 7.54 (d, 1H phenyl H, $J = 8.19$), 7.45 (d, 3H phenyl H, $J = 8.50$), 7.03 (d, 1H, phenyl H, $J = 2.61$ Hz), 7.00 (d, 1H, phenyl H, $J = 2.61$ Hz), 6.93 (d, 1H, phenyl H, $J = 2.55$ Hz), 6.85 (dd, 1H, phenyl H, $J_1 = 2.63$, $J_2 = 8.78$), 6.82 (dd, 1H, phenyl H, $J_1 = 2.63$, $J_2 = 8.78$), 6.61 (dd, 1H, phenyl H, $J_1 = 2.56$, $J_2 = 8.55$), 4.46 (t, 2H, CH₂, $J = 4.67, 5.00$ Hz), 4.12 (t, 4H, CH₂, $J = 4.57, 5.09$ Hz), 3.94 (t, 2H, CH₂, $J = 4.14, 4.95$ Hz), 3.81-3.86 (m, 6H, CH₂), 3.61-3.77 (m, 34H, CH₂), 3.50-3.54 (m, 8H, CH₂), 3.36 (s, 6H, CH₃), 3.35 (s, 3H, CH₃), 3.34 (s, 3H, CH₃), 1.23 (broad singlet, 6H, CH₃), 0.23 (s, 9H, Si-CH₃). ¹³C NMR (CDCl₃): δ 165.51, 159.61, 158.85, 158.58, 153.37,

134.06, 133.60, 133.41, 133.35, 131.82, 129.02, 128.86, 128.82, 128.54, 128.43,
127.98, 125.36, 124.30, 117.93, 117.25, 117.00, 116.76, 116.39, 116.22, 114.99,
112.08, 110.94, 110.90, 102.69, 102.05, 99.44, 95.83, 93.24, 93.18, 92.79, 92.72, 90.76,
90.64, 90.28, 71.93, 70.68, 70.67, 70.63, 70.59, 69.67, 69.62, 69.53, 69.16, 67.60,
67.52, 67.35, 64.38, 64.31, 59.06, 0.01 ppm. MS: m/z 1273.0 ($m + \text{Na}^+$)

BIBLIOGRAPHY

1. Gellman, S. H.. Foldamers: A manifesto. *Acc. Chem. Res.* **1998**, 31. (4). 173-180.
2. Hill, D. J.; Mio, M. J.; Prince, R. B.; Hughes, T. S.; Moore, J. S.. A field guide to foldamers. *Chemical Reviews* **2001**, 101. (12). 3893-4011.
3. Cheng, R. P.. Beyond de novo protein design - de novo design of non-natural folded oligomers. *Current Opinion in Structural Biology* **2004**, 14. (4). 512-520.
4. Burkoth, T. S.; Beausoleil, E.; Kaur, S.; Tang, D. Z.; Cohen, F. E.; Zuckermann, R. N.. Toward the synthesis of artificial proteins: The discovery of an amphiphilic helical peptoid assembly. *Chemistry & Biology* **2002**, 9. (5). 647-654.
5. Raguse, T. L.; Lai, J. R.; LePlae, P. R.; Gellman, S. H.. Toward beta-peptide tertiary structure: Self-association of an amphiphilic 14-helix in aqueous solution. *Organic Letters* **2001**, 3. (24). 3963-3966.
6. Cheng, R. P.; DeGrado, W. F.. Long-range interactions stabilize the fold of a non-natural oligomer. *Journal of the American Chemical Society* **2002**, 124. (39). 11564-11565.
7. Bruckner, A. M.; Chakraborty, P.; Gellman, S. H.; Diederichsen, U.. Molecular architecture with functionalized beta-peptide helices. *Angewandte Chemie-International Edition* **2003**, 42. (36). 4395-4399.
8. Hayen, A.; Schmitt, M. A.; Ngassa, F. N.; Thomasson, K. A.; Gellman, S. H.. Two helical conformations from a single foldamer backbone: "Split personality" in short alpha/beta-peptides. *Angewandte Chemie-International Edition* **2004**, 43. (4). 505-510.
9. De Pol, S.; Zorn, C.; Klein, C. D.; Zerbe, O.; Reiser, O.. Surprisingly stable helical conformations in alpha/beta-peptides by incorporation of cis-beta-aminocyclopropane carboxylic acids. *Angewandte Chemie-International Edition* **2004**, 43. (4). 511-514.
10. Gopi, H. N.; Roy, R. S.; Raghothama, S. R.; Karle, I. L.; Balaram, P.. beta-hairpins generated from hybrid peptide sequences containing both alpha- and beta-amino acids. *Helvetica Chimica Acta* **2002**, 85. (10). 3313-3330.
11. Wu, C. W.; Kirshenbaum, K.; Sanborn, T. J.; Patch, J. A.; Huang, K.; Dill, K. A.; Zuckermann, R. N.; Barron, A. E.. Structural and spectroscopic studies of peptoid

- oligomers with alpha-chiral aliphatic side chains. *Journal of the American Chemical Society* **2003**, 125, (44), 13525-13530.
12. Seebach, D.; Matthews, J. L.. beta-peptides: a surprise at every turn. *Chemical Communications* **1997**, (21), 2015-2022.
13. Cheng, R. P.; Gellman, S. H.; DeGrado, W. F.. beta-peptides: From structure to function. *Chemical Reviews* **2001**, 101, (10), 3219-3232.
14. Cheng, R. P.; DeGrado, W. F.. De novo design of a monomeric helical beta-peptide stabilized by electrostatic interactions. *Journal of the American Chemical Society* **2001**, 123, (21), 5162-5163.
15. Rueping, M.; Mahajan, Y. R.; Jaun, B.; Seebach, D.. Design, synthesis and structural investigations of a beta-peptide forming a 3(14)-helix stabilized by electrostatic interactions. *Chemistry-a European Journal* **2004**, 10, (7), 1607-1615.
16. Etezady-Esfarjani, T.; Hilty, C.; Wuthrich, K.; Rueping, M.; Schreiber, J.; Seebach, D.. NMR-structural investigations of a beta(3)-dodecapeptide with proteinogenic side chains in methanol and in aqueous solutions. *Helvetica Chimica Acta* **2002**, 85, (5), 1197-1209.
17. Seebach, D.; Brenner, M.; Rueping, M.; Jaun, B., gamma(2)-, gamma(3)-, and gamma(2,3,4)-amino acids, coupling to gamma-hexapeptides: CD spectra, NMR solution and X-ray crystal structures of gamma-peptides. *Chemistry-a European Journal* **2002**, 8, (3), 573-584.
18. Woll, M. G.; Lai, J. R.; Guzei, I. A.; Taylor, S. J. C.; Smith, M. E. B.; Gellman, S. H.. Parallel sheet secondary structure in gamma-peptides. *Journal of the American Chemical Society* **2001**, 123, (44), 11077-11078.
19. Semetey, V.; Rognan, D.; Hemmerlin, C.; Graff, R.; Briand, J. P.; Marraud, M.; Guichard, G.. Stable helical secondary structure in short-chain N,N'-linked oligoureas bearing proteinogenic side chains. *Angewandte Chemie-International Edition* **2002**, 41, (11), 1893-1895.
20. Kolomiets, E.; Berl, V.; Odriozola, I.; Stadler, A. M.; Kyritsakas, N.; Lehn, J. M.. Contraction/extension molecular motion by protonation/deprotonation induced structural switching of pyridine derived oligoamides. *Chemical Communications* **2003**, (23), 2868-2869.
21. Dolain, C.; Maurizot, V.; Huc, I.. Protonation-induced transition between two distinct helical conformations of a synthetic oligomer via a linear intermediate. *Angewandte Chemie-International Edition* **2003**, 42, (24), 2738-2740.

22. Berl, V.; Huc, I.; Khoury, R. G.; Krische, M. J.; Lehn, J. M., Interconversion of single and double helices formed from synthetic molecular strands. *Nature* **2000**, 407, (6805), 720-723.
23. Stadler, A. M.; Kyritsakas, N.; Lehn, J. M., Reversible folding/unfolding of linear molecular strands into helical channel-like complexes upon proton-modulated binding and release of metal ions. *Chemical Communications* **2004**, (18), 2024-2025.
24. Barboiu, M.; Lehn, J. M., Dynamic chemical devices: Modulation of contraction/extension molecular motion by coupled-ion binding/pH change-induced structural switching. *Proceedings of the National Academy of Sciences of the United States of America* **2002**, 99, (8), 5201-5206.
25. Jiang, H.; Leger, J. M.; Huc, I., Aromatic delta-peptides. *Journal of the American Chemical Society* **2003**, 125, (12), 3448-3449.
26. Gong, B.; Zeng, H. Q.; Zhu, J.; Yua, L. H.; Han, Y. H.; Cheng, S. Z.; Furukawa, M.; Parra, R. D.; Kovalevsky, A. Y.; Mills, J. L.; Skrzypczak-Jankun, E.; Martinovic, S.; Smith, R. D.; Zheng, C.; Szyperski, T.; Zeng, X. C., Creating nanocavities of tunable sizes: Hollow helices. *Proceedings of the National Academy of Sciences of the United States of America* **2002**, 99, (18), 11583-11588.
27. Nguyen, J. Q.; Iverson, B. L., An amphiphilic folding molecule that undergoes an irreversible conformational change. *Journal of the American Chemical Society* **1999**, 121, (11), 2639-2640.
28. Lokey, R. S.; Iverson, B. L., Synthetic Molecules That Fold into a Pleated Secondary Structure in Solution. *Nature* **1995**, 375, (6529), 303-305.
29. Nelson, J. C.; Saven, J. G.; Moore, J. S.; Wolynes, P. G., Solvophobic driven folding of nonbiological oligomers. *Science* **1997**, 277, (5333), 1793-1796.
30. Brunsveld, L.; Prince, R. B.; Meijer, E. W.; Moore, J. S., Conformational ordering of apolar, chiral m-phenylene ethynylene oligomers. *Organic Letters* **2000**, 2, (11), 1525-1528.
31. Prince, R. B.; Saven, J. G.; Wolynes, P. G.; Moore, J. S., Cooperative conformational transitions in phenylene ethynylene oligomers: Chain-length dependence. *Journal of the American Chemical Society* **1999**, 121, (13), 3114-3121.
32. Lahiri, S.; Thompson, J. L.; Moore, J. S., Solvophobic driven pi-stacking of phenylene ethynylene macrocycles and oligomers. *Journal of the American Chemical Society* **2000**, 122, (46), 11315-11319.

33. Matsuda, K.; Stone, M. T.; Moore, J. S.. Helical pitch of m-phenylene ethynylene foldamers by double spin labeling. *Journal of the American Chemical Society* **2002**, 124, (40), 11836-11837.
34. Cary, J. M.; Moore, J. S.. Hydrogen bond-stabilized helix formation of a m-phenylene ethynylene oligomer. *Organic Letters* **2002**, 4, (26), 4663-4666.
35. Yang, X. W.; Yuan, L. H.; Yamamoto, K.; Brown, A. L.; Feng, W.; Furukawa, M.; Zeng, X. C.; Gong, B.. Backbone-rigidified oligo(m-phenylene ethynylenes). *J. Am. Chem. Soc.* **2004**, 126, (10), 3148-3162.
36. Stone, M. T.; Moore, J. S.. A water-soluble m-phenylene ethynylene foldamer. *Organic Letters* **2004**, 6, (4), 469-472.
37. Goto, H.; Heemstra, J. M.; Hill, D. J.; Moore, J. S.. Single-site modifications and their effect on the folding stability of m-phenylene ethynylene oligomers. *Organic Letters* **2004**, 6, (6), 889-892.
38. Stone, M. T.; Fox, J. M.; Moore, J. S.. A helicene-containing foldamer displaying highly solvent-dependent CD spectra. *Organic Letters* **2004**, 6, (19), 3317-3320.
39. Grubbs, R. H.; Kratz, D.. Highly Unsaturated Oligomeric Hydrocarbons - Alpha- (Phenylethynyl)-Omega-Phenylpoly 1,2-Phenylene(2,1-Ethynediyl). *Chem. Ber., Recl.* **1993**, 126, (1), 149-157.
40. Orita, A.; Yoshioka, N.; Struwe, P.; Braier, A.; Beckmann, A.; Otera, J.. InTegrated chemical process: One-pot double elimination method for acetylenes. *Chem. Eur. J.* **1999**, 5, (4), 1355-1363.
41. Orita, A.; Alonso, E.; Yaruva, J.; Otera, J.. InTegrated chemical process. Convergent strategy for ortho-phenylene ethynylene skeleton by one-pot double elimination method. *Synlett* **2000**, (9), 1333-1335.
42. Jones, T. V.; Blatchly, R. A.; Tew, G. N.. Synthesis of alkoxy-substituted ortho-phenylene ethynylene oligomers. *Organic Letters* **2003**, 5, (18), 3297-3299.
43. Jones, T. V.; Slutsky, M. S.; Laos, R.; de Greef, T. F. A.; Tew, G. N.. Solution ¹H confirmation of folding in short o-Phenylene Ethynylene Oligomers. *Journal of the American Chemical Society* **2005**, 127, (49), 17235-17240.
44. Shotwell, S.; Windscheif, P. M.; Smith, M. D.; Bunz, U. H. F.. Pyridine-capped, oligomeric (o-phenyleneethynylene)s. *Organic Letters* **2004**, 6, (23), 4151-4154.

45. Khan, A.; Hecht, S. Poly(ortho-phenylene ethynylene)s: Synthetic accessibility and optical properties. *Journal of Polymer Science Part a-Polymer Chemistry* **2006**, *44*, (5), 1619-1627.
46. Jones, T. V.; Slutsky, M. S.; Tew, G. N.. Extending Helicity - Capturing the Helical Character of Longer *ortho* Phenylene Ethynylene Oligomers. *Journal of the American Chemical Society* **2006**, submitted.
47. Slutsky, M. S.; Jones, T. V.; Tew, G. N.. Spin System Assignment of homo-ortho-Phenylene Ethynylene Oligomers. *Journal of Organic Chemistry* **2006**, submitted.
48. Wong, M. S.; Nicoud, J.-F.. Synthesis and Computational Studies of Hyperpolarizable Zig-Zag Chromophores. *Tetrahedron Lett.* **1994**, *35*, (33), 6113-6116.
49. Zhang, S. W.; Swager, T. M.. Fluorescent detection of chemical warfare agents: Functional group specific ratiometric chemosensors. *Journal of the American Chemical Society* **2003**, *125*, (12), 3420-3421.
50. McQuade, D. T.; Hegedus, A. H.; Swager, T. M.. Signal amplification of a "turn-on" sensor: Harvesting the light captured by a conjugated polymer. *Journal of the American Chemical Society* **2000**, *122*, (49), 12389-12390.
51. Kimball, D. B.; Weakley, T. J. R.; Haley, M. M.. Cyclization of 1-(2-alkynylphenyl)-3,3-dialkyltriazenes: A convenient, high-yield synthesis of substituted cinnolines and isoindazoles. *Journal of Organic Chemistry* **2002**, *67*, (18), 6395-6405.
52. Kimball, D. B.; Hayes, A. G.; Haley, M. M.. Thermal cyclization of (2-ethynylphenyl)triazenes: Facile synthesis of substituted cinnolines and isoindazoles. *Organic Letters* **2000**, *2*, (24), 3825-3827.
53. Shirtcliff, L. D.; Hayes, A. G.; Haley, M. M.; Kohler, F.; Hess, K.; Herges, R.. Biscyclization Reactions in Butadiyne- and Ethyne-Linked Triazenes and Diazenes: Concerted versus Stepwise Coarctate Cyclizations. *Journal of the American Chemical Society* **2006**, online.
54. John, J. A.; Tour, J. M.. Synthesis of Polyphenylenes and Polynaphthalenes by Thermolysis of Eneidyne and Dialkynylbenzenes. *Journal of the American Chemical Society* **1994**, *116*, (11), 5011-5012.
55. Arnt, L.; Tew, G. N.. New Poly(phenyleneethynylene)s with Cationic, Facially Amphiphilic Structures. *J. Am. Chem. Soc.* **2002**, *124*, (26), 7664-7665.
56. Arnt, L.; Tew, G. N.. Cationic Facially Amphiphilic Poly(phenylene ethynylene)s Studied at the Air-Water Interface. *Langmuir* **2003**, *19*, (6), 2404-2408.

57. Schenning, A.; Jonkheijm, P.; Peeters, E.; Meijer, E. W.. Hierarchical order in supramolecular assemblies of hydrogen-bonded oligo(p-phenylene vinylene)s. *J. Am. Chem. Soc.* **2001**, *123*, (3), 409-416.
58. Clive, D. L. J.. Radical Spirocyclization: Synthesis of an Appropriately Oxygenated Spiro Compound Related to the Antitumor Antibiotic Fredericamycin A. *J. Org. Chem.* **1987**, *52*, 1339-1342.
59. Haley, M. M.. Carbon Networks Based on Dehydrobenzoannulenes. 3. Synthesis of Graphyne Substructures. *Org. Lett.* **2000**, *2*, (7), 969-972.
60. Haley, M. M.; Bell, M. L.; Brand, S. C.; Kimball, D. B.; Pak, J. J.; Wan, W. B.. One-pot desilylation/dimerization of ethynyl- and butadiynyltrimethylsilanes. Synthesis of tetrayne-linked dehydrobenzoannulenes. *Tetrahedron Lett.* **1997**, *38*, (43), 7483-7486.
61. Haley, M. M.; Bell, M. L.; English, J. J.; Johnson, C. A.; Weakley, T. J. R.. Versatile synthetic route to and DSC analysis of dehydrobenzoannulenes: Crystal structure of a heretofore inaccessible 20 annulene derivative. *J. Am. Chem. Soc.* **1997**, *119*, (12), 2956-2957.
62. Bell, M. L.; Chiechi, R. C.; Johnson, C. A.; Kimball, D. B.; Matzger, A. J.; Wan, W. B.; Weakley, T. J. R.; Haley, M. M.. A versatile synthetic route to dehydrobenzoannulenes via in situ generation of reactive alkynes. *Tetrahedron* **2001**, *57*, (17), 3507-3520.
63. Berl, V.; Huc, I.; Khoury, R. G.; Lehn, J. M.. Helical molecular programming: Supramolecular double helices by dimerization of helical oligopyridine-dicarboxamide strands. *Chemistry-a European Journal* **2001**, *7*, (13), 2810-2820.
64. Dolain, C.; Zhan, C. L.; Leger, J. M.; Daniels, L.; Huc, I.. Folding directed N-oxidation of oligopyridine-dicarboxamide strands and hybridization of oxidized oligomers. *Journal of the American Chemical Society* **2005**, *127*, (8), 2400-2401.
65. Prince, R. B.; Moore, J. S.; Brunsveld, L.; Meijer, E. W.. Cooperativity in the folding of helical m-phenylene ethynylene oligomers based upon the 'Sergeants-and-Soldiers' principle. *Chemistry-a European Journal* **2001**, *7*, (19), 4150-4154.
66. Prince, R. B.; Brunsveld, L.; Meijer, E. W.; Moore, J. S.. Twist sense bias induced by chiral side chains in helically folded oligomers. *Angew. Chem., Int. Ed.* **2000**, *39*, (1), 228-230.
67. Kilbinger, A. F. M.; Schenning, A.; Goldoni, F.; Feast, W. J.; Meijer, E. W.. Chiral aggregates of alpha.omega-disubstituted sexithiophenes in protic and aqueous media. *J. Am. Chem. Soc.* **2000**, *122*, (8), 1820-1821.

68. Inouye, M.; Waki, M.; Abe, H., Saccharide-dependent induction of chiral helicity in achiral synthetic hydrogen-bonding oligomers. *Journal of the American Chemical Society* **2004**, 126, (7), 2022-2027.
69. Prince, R. B.; Saven, J. G.; Wolynes, P. G.; Moore, J. S., Cooperative conformational transitions in phenylene ethynylene oligomers: Chain-length dependence. *J. Am. Chem. Soc* **1999**, 121, (13), 3114-3121.
70. Günther, H., *NMR Spectroscopy*, 2nd Edition ed.: John Wiley & Sons, Inc: New York, 1995.
71. Neuhaus, D.; Williamson, M., *The Nuclear Overhauser Effect in Structural and Conformational Analysis*, 2nd ed.: John Wiley & Sons, Inc: New York, 2000: p 619.
72. Hill, D. J.; Moore, J. S., Helicogenicity of solvents in the conformational equilibrium of oligo(m-phenylene ethynylene)s: Implications for foldamer research. *Proceedings of the National Academy of Sciences of the United States of America* **2002**, 99, (8), 5053-5057.
73. Pickholz, M.; Stafstrom, S., Theoretical investigation of the role of pi-pi interactions for the stability of phenylene ethynylene aggregates. *Chemical Physics* **2001**, 270, (2), 245-251.
74. The average ring ppm going from CDCl₃ to CD₃CN is ~0.05ppm based on model compounds like the trimer, which can not fold and rings that are not involved in p-p stacking in oligomers 1-3.
75. Ghosh, S.; Ramakrishnan, S., Structural fine-tuning of (-donor-spacer-acceptor-spacer)-n type foldamers. Effect of spacer segment length, temperature, and metal-ion complexation on the folding process. *Macromolecules* **2005**, 38, (3), 676-686.
76. Lee, M. K.; Shephard, M. J.; Risser, S. M.; Priyadarshy, S.; Paddon-Row, M. N.; Beratan, D. N., The nature of tunnel splitting mediated by stacked aromatics. *Journal of Physical Chemistry A* **2000**, 104, (32), 7593-7599.
77. Blatchly, R. A.; Tew, G. N., Theoretical study of helix formation in substituted phenylene ethynylene oligomers. *J. Org. Chem.* **2003**, 68, (23), 8780-8785.
78. Wong, M. S.; Nicoud, J. F., Synthesis and Computational Studies of Hyperpolarizable Zigzag Chromophores. *Tetrahedron Lett.* **1994**, 35, (33), 6113-6116.
79. Blatchly, R. A.; Tew, G. N., Theoretical study of helix formation in substituted phenylene ethynylene oligomers. *Journal of Organic Chemistry* **2003**, 68, (23), 8780-8785.

80. Dolain, C.; Grelard, A.; Laguerre, M.; Jiang, H.; Maurizot, V.; Huc, I. Solution structure of quinoline- and pyridine-derived oligoamide foldamers. *Chemistry-a European Journal* **2005**, 11. (21). 6135-6144.
81. Jiang, H.; Leger, J. M.; Dolain, C.; Guionneau, P.; Huc, I. Aromatic delta-peptides: design, synthesis and structural studies of helical, quinoline-derived oligoamide foldamers. *Tetrahedron* **2003**, 59. (42). 8365-8374.
82. Hunter, C. A.; Sanders, J. K. M.. The Nature of Pi-Pi Interactions. *Journal of the American Chemical Society* **1990**, 112. (14). 5525-5534.
83. Gabriel, G. J.; Iverson, B. L.. Aromatic oligomers that form hetero duplexes in aqueous solution. *Journal of the American Chemical Society* **2002**, 124. (51). 15174-15175.
84. Zych, A. J.; Iverson, B. L.. Conformational modularity of an abiotic secondary-structure motif in aqueous solution. *Helvetica Chimica Acta* **2002**, 85. (10). 3294-3300.
85. Cubberley, M. S.; Iverson, B. L.. Models of higher-order structure: foldamers and beyond. *Current Opinion in Chemical Biology* **2001**, 5. (6). 650-653.
86. Cubberley, M. S.; Iverson, B. L.. H-1 NMR investigation of solvent effects in aromatic stacking interactions. *Journal of the American Chemical Society* **2001**, 123. (31). 7560-7563.
87. Zych, A. J.; Iverson, B. L.. Synthesis and conformational characterization of tethered, self-complexing 1.5-dialkoxynaphthalene/1.4.5.8-naphthalenetetracarboxylic diimide systems. *Journal of the American Chemical Society* **2000**, 122. (37). 8898-8909.

